



TECHNISCHE  
UNIVERSITÄT  
WIEN

---

Dissertation

# Recovery of Platinum Group Metals from Spent Car Catalysts with the Aid of Ionic Liquids and Deep Eutectic Solvents

Ausgeführt zum Zwecke der Erlangung des akademischen Grades eines  
Doktors der technischen Wissenschaften unter der Leitung von

Univ. Prof. Dipl.-Ing. Dr.techn. Katharina Schröder  
Institut für Angewandte Synthesechemie

Eingereicht an der Technischen Universität Wien  
Chemische Fakultät

von

Dipl.-Ing. Olga Lanaridi

Matrikelnummer: 01128450



Wien, im November 2021

---

When you set out on your journey to Ithaca,  
pray that the road is long,  
full of adventure, full of knowledge.

**Constantine P. Cavafy**

# Table of Contents

<b>List of Tables</b> .....	X
<b>List of Abbreviations</b> .....	XI
<b>Acknowledgements</b> .....	XIV
<b>Acknowledgements of Scientific and Other Contributions</b> .....	XV
<b>Abstract</b> .....	XVI
<b>Kurzfassung</b> .....	XVII
<b>1 Introduction</b> .....	1
<b>1.1 Platinum group metals: significance and current status</b> .....	1
<b>1.2 Conventional approaches to platinum group metal recycling</b> .....	5
1.2.1 Hydrometallurgy.....	5
1.2.2 Pyrometallurgy.....	7
1.2.3 Challenges for separation and refining.....	9
<b>1.3 Alternative extraction processes for platinum group metal recovery</b> .....	11
<b>2 Ionic Liquids and Deep Eutectic Solvents: Properties and Applications</b> .....	13
<b>2.1 Ionic liquids</b> .....	13
<b>2.2 Deep eutectic solvents</b> .....	15
<b>2.3 Ionic liquids and deep eutectic solvents: similarities and differences</b> .....	17
<b>3 Ionic Liquids in Platinum Group Metal Recovery</b> .....	19
<b>3.1 Ionic liquids in liquid-liquid separations</b> .....	20
3.1.1 Extraction mechanisms of metals to ionic liquids.....	21
3.1.2 Analyte partitioning in liquid-liquid separations.....	23
3.1.3 Liquid-liquid separations.....	23
3.1.3.1 Ammonium-based ionic liquids.....	23
3.1.3.2 Imidazolium-based ionic liquids.....	34
3.1.3.3 Phosphonium-based ionic liquids.....	44
3.1.3.4 Pyridinium-based ionic liquids.....	56
3.1.3.5 Guanidinium-based ionic liquids.....	57
3.1.3.6 Task-specific ionic liquids.....	58
3.1.3.7 Thermomorphic ionic liquids.....	61
<b>3.2 Ionic liquids in solid-liquid separations</b> .....	65
3.2.1 Solid-supported ionic liquids as novel resins.....	67
3.2.2 Capsules.....	70
3.2.3 Membranes.....	71
3.2.4 Nanoparticles.....	73

<b>3.3</b>	<b>Experimental gaps and omissions in the literature</b> .....	75
<b>3.4</b>	<b>Environmental considerations</b> .....	78
<b>3.5</b>	<b>Financial considerations</b> .....	84
<b>3.6</b>	<b>Concluding remarks on ionic liquid-based separations</b> .....	85
<b>4</b>	<b>The Platirus Project</b> .....	86
<b>5</b>	<b>Research Goal</b> .....	87
<b>6</b>	<b>Results and Discussion</b> .....	88
<b>6.1</b>	<b>Development of analytical approaches</b> .....	88
6.1.1	Validation of selected method for PGM quantification in car catalyst sample.....	88
6.1.2	Analytical challenges associated with deep eutectic solvents .....	89
6.1.3	Development of analytics for quantification in deep eutectic solvents.....	90
6.1.4	Quality evaluation of the analytical results .....	91
6.1.4.1	Standard addition experiments .....	91
6.1.4.2	Spike-recovery experiments .....	92
<b>6.2</b>	<b>Characterization of the car catalyst sample</b> .....	93
6.2.1	Quantification of the car catalyst elemental matrix.....	93
6.2.2	XRD analysis of the car catalyst sample.....	94
<b>6.3</b>	<b>Leaching of platinum group metals from spent car catalyst</b> .....	95
6.3.1	Goals and objectives.....	95
6.3.2	Classification of selected ionic liquids and deep eutectic solvents for leaching studies....	95
6.3.3	Preliminary leaching experiments with selected ionic liquids and deep eutectic solvents	97
6.3.3.1	Leaching process.....	97
6.3.3.2	Evaluation of platinum group metal leaching with various ionic liquids and deep eutectic solvents.....	97
6.3.3.3	Pre-selection of leaching system .....	97
6.3.4	Optimization of selected leaching system.....	99
6.3.4.1	Amount and nature of oxidizing agent .....	99
6.3.4.2	Effect of solid:liquid ratio .....	100
6.3.4.3	Effect of leaching temperature.....	100
6.3.4.4	Effect of leaching duration .....	101
6.3.5	Preconcentration of platinum group metals in the leachate .....	102
6.3.6	Pre-treatment of the car catalyst material.....	103
6.3.7	Upscaling of selected and optimized leaching system .....	104
6.3.7.1	Upscaling with untreated car catalyst sample.....	104
6.3.7.2	Upscaling with pre-treated car catalyst sample .....	105



<b>6.4</b>	<b>Quality control of the deep eutectic solvent employed in leaching experiments</b>	106
6.4.1	Qualitative control via <sup>1</sup> H-NMR	106
6.4.2	Quantitative control via UHPLC	106
6.4.2.1	UHPLC-MS with ELS detector for the quality control of the deep eutectic solvent	106
6.4.2.2	Application of UHPLC-MS with ELS detector method to authentic catalyst leachate samples	107
<b>6.5</b>	<b>Liquid-liquid separation of platinum group metals leached in deep eutectic solvent</b>	108
6.5.1	Goals and objectives	108
6.5.2	Selection of hydrophobic ionic liquids for liquid-liquid separation studies	108
6.5.3	Preliminary liquid-liquid separation experiments	109
6.5.3.1	Liquid-liquid separation process	109
6.5.3.2	Evaluation of separation with selected hydrophobic ionic liquids	109
6.5.4	Optimization of liquid-liquid separation parameters	110
6.5.4.1	Effect of dilution of the hydrophilic DES phase	110
6.5.4.2	Effect of dilution of the hydrophobic phosphonium-IL phase	111
6.5.4.3	Effect of acidity of hydrophilic-IL phase	112
6.5.5	Application of optimized liquid-liquid separation system to authentic car catalyst leachate	113
6.5.6	Recycling of hydrophilic deep eutectic solvent after liquid-liquid separation	114
6.5.6.1	Leaching efficiency and DES recovery after L-L separation	114
6.5.6.2	Quality control of hydrophobic IL and hydrophilic DES stability in recycling	115
6.5.7	Upscaling of liquid-liquid separation system	116
<b>6.6</b>	<b>Solid-liquid separation of platinum group metals from acidic leachate</b>	117
6.6.1	Goals and objectives	117
6.6.2	Classification of solid sorbent materials for solid-liquid separation studies	117
6.6.3	Characterization of synthesized solid sorbent materials	119
6.6.3.1	Thermogravimetric analysis	119
6.6.3.2	DRIFT-IR and ATR-IR spectroscopy	120
6.6.3.3	Scanning electron microscopy	121
6.6.3.4	BET analysis	122
6.6.4	Evaluation of solid sorbent materials in solid-liquid separation experiments	123
6.6.4.1	Acidic leaching of car catalyst material	123
6.6.4.2	Solid-liquid separation process	123
6.6.5	Optimization of solid-liquid separation parameters	124
6.6.5.1	Effect of PGM solution acidity	124
6.6.5.2	Effect of PGM solution dilution level	126

6.6.5.3	Effect of IL loading on solid sorbent material.....	127
6.6.6	Application of optimized solid-liquid separation system to authentic car catalyst leachate 128	
6.6.7	Stripping of Pt and Pd from the polySILP material .....	128
6.6.8	Stability, capacity and recyclability of supported ionic liquid phases .....	130
<b>7</b>	<b>Summary and Conclusion</b> .....	<b>133</b>
<b>8</b>	<b>Outlook</b> .....	<b>135</b>
<b>9</b>	<b>Experimental Part</b> .....	<b>136</b>
<b>9.1</b>	<b>Materials and methods</b> .....	<b>136</b>
9.1.1	Chemicals and reagents.....	136
9.1.2	Instrumentation.....	136
<b>9.2</b>	<b>Experimental and analytical protocols</b> .....	<b>139</b>
9.2.1	Leaching procedures.....	139
9.2.1.1	Leaching in DES.....	139
9.2.1.2	Leaching in mineral acid .....	139
9.2.2	Separation procedures .....	139
9.2.2.1	Liquid-liquid separation procedure .....	139
9.2.2.2	Solid-liquid separation procedure .....	139
9.2.3	Stripping procedure.....	140
9.2.4	Measurement procedure .....	140
9.2.4.1	Measurements with ICP-MS .....	140
9.2.4.2	Measurements with ICP-OES.....	141
<b>9.3</b>	<b>Synthesis of ionic liquids and deep eutectic solvents</b> .....	<b>143</b>
9.3.1	Choline-based deep eutectic solvents.....	143
9.3.2	Brønsted acidic ionic liquids .....	143
9.3.3	Protic ionic liquids.....	144
9.3.4	Hydrophobic ionic liquids .....	144
<b>9.4</b>	<b>Synthesis of supported ionic liquid phases</b> .....	<b>146</b>
9.4.1	Synthesis of SILP P <sub>66614</sub> Cl 10% (w/w).....	146
9.4.2	Synthesis of polySILP 10% (w/w) .....	146
<b>9.5</b>	<b>Characterization of solid supported phases</b> .....	<b>147</b>
9.5.1	DRIFT-IR spectra of SILPs .....	147
9.5.2	SEM images of SILPs .....	147
<b>10</b>	<b>Appendix</b> .....	<b>148</b>
<b>10.1</b>	<b>Characterization of deep eutectic solvents and ionic liquids</b> .....	<b>148</b>
10.1.1	NMR spectra of deep eutectic solvents and ionic liquids.....	148

10.1.1.1	Deep eutectic solvents used in leaching.....	148
10.1.1.2	Ionic liquids used in leaching.....	149
10.1.1.3	Ionic liquids used in liquid-liquid separation.....	152
10.1.2	IR spectra of deep eutectic solvents and ionic liquids.....	156
10.1.2.1	Deep eutectic solvents used in leaching.....	156
10.1.2.2	Ionic liquids used in leaching.....	157
10.1.2.3	Ionic liquids used in liquid-liquid separation.....	158
<b>10.2</b>	<b>Characterization data of supported ionic liquid phases.....</b>	<b>160</b>
10.2.1	DRIFT-IR spectra of supported ionic liquid phases.....	160
<b>10.3</b>	<b>References.....</b>	<b>161</b>
<b>10.4</b>	<b>Curriculum Vitae.....</b>	<b>171</b>

## List of Figures

<b>Figure 1.</b> Platinum group metal consumption per metal and industry.....	2
<b>Figure 2.</b> Examples of metal and cordierite catalyst substrates and a catalytic converter with the outer shell cut to show the inner construction.....	2
<b>Figure 3.</b> Overview of PGM recycling technologies.....	5
<b>Figure 4.</b> Process flowsheet of <i>aqua regia</i> -based hydrometallurgical process.....	6
<b>Figure 5.</b> Process flowsheet of a pyrometallurgical process relying on a Cu collector .....	8
<b>Figure 6.</b> Rhodium-chloride speciation diagram at 25 °C.....	10
<b>Figure 7.</b> Packing of ions in molten salts and ionic liquids .....	13
<b>Figure 8.</b> Schematic representation of the comparison of the solid-liquid equilibria of a simple ideal eutectic mixture and a deep eutectic mixture .....	16
<b>Figure 9.</b> Similarities and differences of deep eutectic solvents and ionic liquids.....	17
<b>Figure 10.</b> Application of ionic liquids in platinum group metal recovery. ....	19
<b>Figure 11.</b> Categorization of ILs in liquid-based separations within the current chapter.....	20
<b>Figure 12.</b> Experimental data of distribution ratio for Pt(IV) at different concentrations.....	25
<b>Figure 13.</b> Distribution isotherms of Pd at 25 °C.....	26
<b>Figure 14.</b> Experimental data of distribution ratio for Rh at different Cl <sup>-</sup> concentrations.....	27
<b>Figure 15.</b> Experimental data of distribution ratio for Pd(II) at different HNO <sub>3</sub> concentrations .....	28
<b>Figure 16.</b> Loading capacity of Aliquat 336 .....	29
<b>Figure 17.</b> Flowsheet of the developed process for the separation and recovery of Pt and Pd from simulated spent car catalyst leach liquor .....	30
<b>Figure 18.</b> McCabe-Thiele plot for Pt extraction .....	30
<b>Figure 19.</b> Salting-out effect on the extraction of Rh.....	33
<b>Figure 20.</b> Proposed flowsheet for the separation of precious metals from the leachate of spent automotive catalyst by split-anion extraction, using water-saturated [N <sub>8881</sub> ]I .....	34
<b>Figure 21.</b> Simplified flowsheet of the two processes for Au(III) and Pt(IV) separation.....	37
<b>Figure 22.</b> Extraction/precipitation efficiencies of Pt(IV) with hydrophobic/hydrophilic ILs with varying side-chain lengths.....	38
<b>Figure 23.</b> The extraction-stripping-regeneration process of Pt(IV) with the mixed hydrophobic/hydrophilic ILs.....	39
<b>Figure 24.</b> Separation process for Pt(IV), Pd(II), Ru(III) and Rh(III).....	40
<b>Figure 25.</b> Selective extraction of Pt(IV) from multi-metal solutions obtained with [C <sub>14</sub> Pim]Br in [C <sub>8</sub> mim][PF <sub>6</sub> ] .....	40
<b>Figure 26.</b> Acidization and dimerization of BmimSe .....	42
<b>Figure 27.</b> Structures of amino moieties attached to the IL to enhance the extraction efficiency of [C <sub>4</sub> mim][NTf <sub>2</sub> ] .....	43
<b>Figure 28.</b> Effect of Cl <sup>-</sup> concentration in initial aqueous solutions on partition of Pt(IV), Pd(II) and Rh(III) in two-phase system [C <sub>4</sub> mim][PF <sub>6</sub> ]/H <sub>2</sub> O .....	44
<b>Figure 29.</b> Distribution ratio for Rh(III) as a function of HCl concentration .....	45
<b>Figure 30.</b> Speciation diagram of Rh constructed by Svecova et al. Concentration profile of [RhCl <sub>4</sub> (H <sub>2</sub> O)] <sup>-</sup> , [RhCl <sub>5</sub> (H <sub>2</sub> O)] <sup>2-</sup> and RhCl <sub>6</sub> <sup>3-</sup> . The data has been fitted using the extended Debye-Hückel expression.....	47
<b>Figure 31.</b> Extraction isotherms for Rh from fresh solutions and aged solutions, with NaCl and without NaCl.....	48
<b>Figure 32.</b> Effect of NaCl concentration on the distribution ratio of Rh, in P <sub>66614</sub> Cl and P <sub>66614</sub> DOP .....	49
<b>Figure 33.</b> Isotherms of Pd(II) extraction from 0.1 M HCl, 3.0 M HCl and 0.1 M HCl/0.5 M NaCl .....	49
<b>Figure 34.</b> Isotherms of Pd(II) extraction with Cyphos 102, with NaCl and without NaCl .....	50

<b>Figure 35.</b> Separation flowsheet of Pt(IV), Pt(II), Rh(III) and Ru(III) from their mixture with Cyphos 101.52	
<b>Figure 36.</b> Ionic liquid cation release to the aqueous phase after repeated contact with an aqueous phase	54
<b>Figure 37.</b> Effect of contact time on the extraction of metals from a model leach liquor	55
<b>Figure 38.</b> Flow chart summarizing the separation and recovery process of PGMs from an automotive catalyst leachate	55
<b>Figure 39.</b> Experimental schematic for the extraction of precious metals using the microemulsion P <sub>66614</sub> Cl/TX-100/H <sub>2</sub> O along with the simplified chemical structure of the extracted Pd species	56
<b>Figure 40.</b> Selective extraction of Pt(IV) with the guanidinium-based IL [diHTMG]Br	57
<b>Figure 41.</b> Distribution ratios and extraction percentages of Pd from aqueous solution, pH 2.8	58
<b>Figure 42.</b> Extraction of Pd(II) as a function of HCl, NaCl, NaNO <sub>3</sub> and H <sup>+</sup> concentration under different [C <sub>10</sub> (mim) <sub>2</sub> ] <sup>2+</sup> 2[MBT] <sup>-</sup> concentrations	60
<b>Figure 43.</b> Extraction behavior of Pd with IL1 and varying HCl concentration and structures of IL1 and IL2	61
<b>Figure 44.</b> Temperature-dependent behavior of a binary [Hbet][NTf <sub>2</sub> ]/H <sub>2</sub> O mixture	62
<b>Figure 45.</b> Extraction efficiency (%) for Pd, Rh and Ru with [Hbet][NTf <sub>2</sub> ] at various HNO <sub>3</sub> concentrations, at RT and under microwave irradiation	63
<b>Figure 46.</b> Phase diagrams at 24 and 50 °C and related snapshots taken after extraction of Co(II) using P <sub>44414</sub> Cl/HCl/H <sub>2</sub> O	64
<b>Figure 47.</b> Ionic liquids in solid-based separations are implemented in resins, capsules, membranes and nanoparticles	65
<b>Figure 48.</b> Microphotograph of Amberlite XAD-7/Cyphos 101, after Pt sorption and Pt desorption	67
<b>Figure 49.</b> Adsorption and desorption of PGMs from aqueous solution in CP-AMIN	69
<b>Figure 50.</b> SEM image of dry polymeric beads containing immobilized Cyphos 101	70
<b>Figure 51.</b> Transport of Rh(III), Pt(IV) and Pd(II) through the liquid membrane	72
<b>Figure 52.</b> Nanoparticle with attached magnetic task-specific polymeric IL	73
<b>Figure 53.</b> Recovery of Pt and Pd with Fe <sub>3</sub> O <sub>4</sub> magnetic nanoparticles coated with an IL-functionalized polymer	74
<b>Figure 54.</b> Distribution ratio of undissociated acetylacetonate between benzene and aqueous phase containing different inorganic salts	76
<b>Figure 55.</b> Relative toxicity of some commonly employed ILs expressed in EC <sub>50</sub> values	79
<b>Figure 56.</b> Overview of the Platirus project	86
<b>Figure 57.</b> Microwave oven (left) and digestion unit (right) where car catalyst digestion was performed	88
<b>Figure 58.</b> PGM concentrations provided by certificate versus PGM concentrations determined by ICP-MS	89
<b>Figure 59.</b> (a) Liquid sample introduction system consisting of (b) a spray chamber and (c) a nebulizer	89
<b>Figure 60.</b> Simplified drawing of ICP-MS system with Universal cell technology	90
<b>Figure 61.</b> Standard addition process graphic for the evaluation of interference with the quantification results	91
<b>Figure 62.</b> Concentration of elements present in the car catalyst material	93
<b>Figure 63.</b> X-Ray diffractogram of car catalyst material used in the present study	94
<b>Figure 64.</b> Classification of ILs and DESs evaluated in PGM leaching studies	95
<b>Figure 65.</b> Leachate before centrifugation and after centrifugation	97
<b>Figure 66.</b> PGM leaching efficiency (%) with different oxidizing agents, at 80 °C, 4 h, solid:liquid 1:5	99
<b>Figure 67.</b> PGM leaching efficiency (%) at different solid:liquid ratios, at 80 °C, 4 h	100
<b>Figure 68.</b> PGM leaching efficiency (%) at different temperatures, solid:liquid 1:5, 4 h	101

<b>Figure 69.</b> PGM leaching efficiency (%) at different leaching times, at 80 °C, solid:liquid 1:5 .....	101
<b>Figure 70.</b> DES reuse in the process flowsheet of PGM recovery .....	102
<b>Figure 71.</b> Effect of catalyst pre-treatment on the extraction efficiency of Rh .....	104
<b>Figure 72.</b> Upscaled leaching set-up on a 100 g catalyst scale.....	104
<b>Figure 73.</b> PGM extraction monitoring over a 24 h time frame .....	105
<b>Figure 74.</b> <sup>1</sup> H-NMR spectra of choline Cl/ <i>p</i> -TsOH recorded before and after leaching.....	106
<b>Figure 75.</b> Chromatogram of choline Cl/ <i>p</i> -TsOH recorded on a C4 column with an ELS detector .....	106
<b>Figure 76.</b> Mass spectroscopic assignment of choline Cl/ <i>p</i> -TsOH components in ESI +/- mode .....	107
<b>Figure 77.</b> Calibration curves obtained for choline Cl and <i>p</i> -TsOH .....	107
<b>Figure 78.</b> Position of liquid-liquid separation in the process flowsheet of PGM recovery.....	108
<b>Figure 79.</b> Hydrophobic ionic liquids evaluated for PGM separation .....	109
<b>Figure 80.</b> Extraction efficiencies (%) of PGMs from model solution with different phosphonium-based ILs .....	110
<b>Figure 81.</b> Extraction efficiencies (%) of PGMs from PGM model solution to phosphonium ILs with DES phase (a) diluted 1:1 with H <sub>2</sub> O, (b) diluted 1:5 with H <sub>2</sub> O, (c) diluted 1:5 with NaCl .....	111
<b>Figure 82.</b> Extraction efficiencies (%) of PGMs to pure (undiluted) phosphonium ILs .....	112
<b>Figure 83.</b> Extraction efficiencies (%) of PGMs to phosphonium ILs from PGM model solution, at 3.7 M HCl and at 9.7 M HCl .....	112
<b>Figure 84.</b> Extraction efficiency (%) of PGMs to P <sub>66614</sub> Cl from car catalyst DES-based leachate.....	113
<b>Figure 85.</b> Concentration (mg/kg) of elements in car catalyst with their respective extraction efficiencies to the DES phase and their respective extraction efficiencies to the phosphonium-IL phase .....	114
<b>Figure 86.</b> Extraction efficiency (%) of PGMs to P <sub>66614</sub> Cl with recycled DES.....	114
<b>Figure 87.</b> Hydrophilic DES appearance before leaching and after leaching/L-L separation.....	115
<b>Figure 88.</b> <sup>1</sup> H-NMR spectra of P <sub>66614</sub> Cl before and after L-L separation .....	115
<b>Figure 89.</b> Position of solid-liquid separation in the process flowsheet of PGM recovery .....	117
<b>Figure 90.</b> Classification of ionic liquid-based solid sorbent materials evaluated in PGM solid-liquid separation experiments.....	118
<b>Figure 91.</b> Concept and structure of SILP and polySILP materials as solid sorbents for PGM recovery ..	118
<b>Figure 92.</b> TGA curves of SILP (left) and polySILP (right) with loadings of 10, 20 and 50% (w/w) .....	119
<b>Figure 93.</b> DRIFT-IR spectra of S-grafted silica and pure silica and polySILP loadings of 10, 20 and 50% (w/w) .....	120
<b>Figure 94.</b> ATR-IR spectra of polySILP 20% (w/w) and PGM-loaded polySILP 20% (w/w) .....	120
<b>Figure 95.</b> SEM image of polySILP with a loading of 20% (w/w), (a) pure, (b) after retention of PGM-rich acidic solution, (c) after stripping step 1 and (d) after stripping step 2 .....	121
<b>Figure 96.</b> BET curve for dried silica and SILP and calcinated silica and polySILP with different loadings .....	122
<b>Figure 97.</b> Effect of HCl concentration on PGM leaching efficiency (%) .....	123
<b>Figure 98.</b> Retention behavior of PGMs from model solution of different HCl concentrations on SILP 20% (w/w) and polySILP 20% (w/w).....	124
<b>Figure 99.</b> Retention behavior of PGMs from model solution of different HCl concentrations on SILP 10% (w/w) and polySILP 10% (w/w).....	124
<b>Figure 100.</b> Retention behavior of PGMs from model solution of different HCl concentrations on SILP 50% (w/w) (left) and polySILP 50% (w/w) (right). .....	125
<b>Figure 101.</b> Effect of dilution on PGM retention from model solution on SILP 20% (w/w) and polySILP 20% (w/w) .....	126
<b>Figure 102.</b> Effect of dilution on PGM retention from model solution on SILP 10% (w/w) and polySILP 10% (w/w) .....	126



<b>Figure 103.</b> Effect of dilution on PGM retention from model solution on SILP 50% (w/w) and polySILP 50% (w/w) .....	127
<b>Figure 104.</b> Retention behavior of PGMs from model solution diluted 1:7 (w/w), on SILP and polySILP with different IL loadings (w/w) .....	127
<b>Figure 105.</b> Retention behavior of PGMs and accompanying elements from automotive catalyst leachate on SILP 20% (w/w) and polySILP 20% (w/w) .....	128
<b>Figure 106.</b> Flowsheet of PGM acidic leaching and S-L recovery process.....	129
<b>Figure 107.</b> Elemental composition (mg/L) of acidic leachate solution and recovered stripping solution after the 2 <sup>nd</sup> stripping step .....	130
<b>Figure 108.</b> Cumulative retention capacity for Pt and Pd on polySILP 20% (w/w) versus Amberlite IRA-400, short-term and complete breakthrough curves.....	131
<b>Figure 109.</b> Retention behavior on recycled polySILP 20% (w/w) .....	132
<b>Figure 110.</b> ATR-IR spectra of polySILP 20% (w/w) and stripped polySILP 20% (w/w) after washing with 0.1 M HCl .....	132
<b>Figure 111.</b> Summary of processes developed within the course of the work for PGM extraction and separation.....	134
<b>Figure 112.</b> Starting materials choline Cl, <i>p</i> -TsOH and the DES choline Cl/ <i>p</i> -TsOH .....	143
<b>Figure 113.</b> Polymerization of the monomer on the silica surface .....	146
<b>Figure 114.</b> DRIFT-IR spectra of pure silica and SILPs with P <sub>66614</sub> Cl loadings of 10, 20 and 50% (w/w) ...	147
<b>Figure 115.</b> SEM images of SILP with P <sub>66614</sub> Cl 20% (w/w) pure and loaded with PGMs.....	147
<b>Figure 116.</b> <sup>1</sup> H-NMR of choline Cl/ <i>p</i> -TsOH .....	148
<b>Figure 117.</b> <sup>13</sup> C-NMR of choline Cl/ <i>p</i> -TsOH.....	148
<b>Figure 118.</b> <sup>1</sup> H-NMR of [HSO <sub>3</sub> C <sub>4</sub> mim]Cl .....	149
<b>Figure 119.</b> <sup>13</sup> C-NMR of [HSO <sub>3</sub> C <sub>4</sub> mim]Cl .....	149
<b>Figure 120.</b> <sup>1</sup> H-NMR of [EtNH <sub>3</sub> ][NO <sub>3</sub> -Cl] .....	150
<b>Figure 121.</b> <sup>13</sup> C-NMR of [EtNH <sub>3</sub> ][NO <sub>3</sub> -Cl] .....	150
<b>Figure 122.</b> <sup>1</sup> H-NMR of P <sub>66614</sub> ·HSO <sub>4</sub> .....	151
<b>Figure 123.</b> <sup>13</sup> C-NMR of P <sub>66614</sub> Cl·HSO <sub>4</sub> .....	151
<b>Figure 124.</b> <sup>1</sup> H-NMR of P <sub>66614</sub> Cl .....	152
<b>Figure 125.</b> <sup>13</sup> C-NMR of P <sub>66614</sub> Cl .....	152
<b>Figure 126.</b> <sup>31</sup> P-NMR of P <sub>66614</sub> Cl .....	153
<b>Figure 127.</b> <sup>1</sup> H-NMR of P <sub>66614</sub> B2EHP .....	153
<b>Figure 128.</b> <sup>13</sup> C-NMR of P <sub>66614</sub> B2EHP .....	154
<b>Figure 129.</b> <sup>31</sup> P-NMR of P <sub>66614</sub> B2EHP.....	154
<b>Figure 130.</b> <sup>1</sup> H-NMR of P <sub>66614</sub> DOP .....	155
<b>Figure 131.</b> <sup>13</sup> C-NMR of P <sub>66614</sub> DOP .....	155
<b>Figure 132.</b> <sup>31</sup> P-NMR of P <sub>66614</sub> DOP .....	156
<b>Figure 133.</b> ATR-IR spectrum of choline Cl/ <i>p</i> -TsOH.....	156
<b>Figure 134.</b> ATR-IR spectrum of [HSO <sub>3</sub> C <sub>4</sub> mim]Cl .....	157
<b>Figure 135.</b> ATR-IR spectrum of [EtNH <sub>3</sub> ][NO <sub>3</sub> -Cl] .....	157
<b>Figure 136.</b> ATR-IR spectrum of P <sub>66614</sub> ·HSO <sub>4</sub> .....	158
<b>Figure 137.</b> ATR-IR spectrum of P <sub>66614</sub> Cl .....	158
<b>Figure 138.</b> ATR-IR spectrum of P <sub>66614</sub> B2EHP.....	159
<b>Figure 139.</b> ATR-IR spectrum of P <sub>66614</sub> DOP .....	159
<b>Figure 140.</b> DRIFT-IR spectra of pure silica and SILPs with P <sub>66614</sub> Cl loadings of 10, 20 and 50% (w/w) ...	160

## List of Tables

<b>Table 1.</b> Estimated EOL global recycling rates for precious metals for the main and end user sectors .....	4
<b>Table 2.</b> Classification and general formula of deep eutectic solvents.....	15
<b>Table 3.</b> Summary of PGM extraction conditions and results with ammonium-based ionic liquids.....	24
<b>Table 4.</b> Summary of PGM extraction conditions and results with imidazolium-based ionic liquids.....	35
<b>Table 5.</b> Summary of PGM extraction conditions and results with phosphonium-based ionic liquids .....	46
<b>Table 6.</b> Summary of PGM extraction conditions and results with pyridinium-, guanidinium-based and task-specific ionic liquids .....	59
<b>Table 7.</b> Summary of PGM extraction conditions and results with thermomorphic ionic liquids.....	62
<b>Table 8.</b> Summary of PGM extraction conditions and results with ionic liquid-impregnated resins and capsules .....	68
<b>Table 9.</b> Summary of PGM extraction conditions and results with ionic liquid-based membranes.....	73
<b>Table 10.</b> Toxicity of some common solvents and salts toward HeLa cells.....	79
<b>Table 11.</b> Stripping conditions used for the recovery of PGMs from ionic liquid phases .....	81
<b>Table 12.</b> Representative ionic liquids of all categories used in the leaching studies .....	96
<b>Table 13.</b> Platinum group metal extraction efficiencies with selected leaching systems.....	98
<b>Table 14.</b> Cumulative PGM leaching (ppm) and DES recovery (%) per leaching cycle .....	102
<b>Table 15.</b> Conditions of chemical and physical pre-treatment of the car catalyst material .....	103
<b>Table 16.</b> Quantification of DES components in DES before leaching and after leaching .....	107
<b>Table 17.</b> Structural parameters calculated for the N <sub>2</sub> absorption/desorption isotherms.....	122
<b>Table 18.</b> Stability of SILP and polySILP expressed in % leaching of ionic liquid .....	130
<b>Table 19.</b> ICP-MS instrumental measurement parameters .....	140
<b>Table 20.</b> ICP-OES instrumental measurement parameters .....	141
<b>Table 21.</b> Selected emission wavelengths for elemental quantification .....	142
<b>Table 22.</b> ICP-OES instrumental measurement parameters for phosphorus.....	142



## List of Abbreviations

AIBN	azobisisobutyronitrile
ATR-IR	attenuated total reflectance-infrared spectroscopy
BmimSe	1-butyl-3-methyl-imidazole-2-selone
[C <sub>4</sub> Bim]Br	1-butyl-3-benzimidazolium bromide
[C <sub>14</sub> Bim]Br	1-tetradecyl-3-butylimidazolium bromide
CH <sub>2</sub> Cl <sub>2</sub>	dichloromethane
CHCl <sub>3</sub>	chloroform
[(CH <sub>3</sub> ) <sub>3</sub> NCH <sub>2</sub> CH <sub>2</sub> OMe][NTf <sub>2</sub> ]	1-methoxy-2-tetramethylammoniummethane bis(trifluoromethylsulfonyl)imide
[C <sub>2</sub> mim][NTf <sub>2</sub> ]	1-ethyl-3-methylimidazolium bis(trifluoromethylsulfonyl)imide
[C <sub>4</sub> mim][NTf <sub>2</sub> ]	1-butyl-3-methylimidazolium bis(trifluoromethylsulfonyl)imide
[C <sub>4</sub> mim][PF <sub>6</sub> ]	1-butyl-3-methylimidazolium hexafluorophosphate
[C <sub>6</sub> mim]Cl	1-hexyl-3-methylimidazolium chloride
[C <sub>6</sub> mim][DDTC]	1-hexyl-3-methylimidazolium diethyldithiocarbamate
[C <sub>6</sub> mim][NTf <sub>2</sub> ]	1-hexyl-3-methylimidazolium bis(trifluoromethylsulfonyl)imide
[C <sub>8</sub> dmim][NTf <sub>2</sub> ]	1,2-dimethyl-3-octylimidazolium bis(trifluoromethylsulfonyl)imide
[C <sub>8</sub> mim]Cl	1-octyl-3-methylimidazolium chloride
[C <sub>8</sub> mim][NTf <sub>2</sub> ]	1-octyl-3-methylimidazolium bis(trifluoromethylsulfonyl)imide
[C <sub>8</sub> mim][PF <sub>6</sub> ]	1-octyl-3-methylimidazolium hexafluorophosphate
[C <sub>10</sub> (mim) <sub>2</sub> ] <sup>2+</sup> 2[MBT] <sup>-</sup>	2-mercaptobenzothiazolate
[C <sub>12</sub> (mim) <sub>2</sub> ][Br <sub>2</sub> ]	1,12-bis-(3-methylimidazolium-1-yl)dodecane bromide
[C <sub>12</sub> (mim) <sub>2</sub> ][NTf <sub>2</sub> ]	1,12-bis-(3-methylimidazolium-1-yl)dodecane bis(trifluoromethylsulfonyl)imide
[C <sub>16</sub> mim]Cl	1-hexadecyl-3-methylimidazolium chloride
[C <sub>12</sub> Pim]Br	1-dodecadecyl-3-propylimidazolium bromide
[C <sub>14</sub> Pim]Br	1-tetradecyl-3-propylimidazolium bromide
[C <sub>16</sub> Pim]Br	1-hexadecyl-3-propylimidazolium bromide
[C <sub>14</sub> PimNH <sub>2</sub> ]Br	1-tetradecyl-2-aminoethylimidazolium bromide
CMPO	octyl-phenyl- <i>N,N</i> -diisobutylcarbamoyl methylphosphine oxide
CP-AMIN	imidazolium-based task-specific ionic liquid on chloromethylated polystyrene beads
Cyanex 471	tri-isobutylphosphine sulfide
DCA	dicyanamide
DES	deep eutectic solvent
DHS	di- <i>n</i> -hexyl sulfide
[diHTMA]Br	2,2-diheptyl-1,1,3,3,-tetramethylguanidinium bromide
DSDMAC	distearyldimethylammonium chloride
EC <sub>50</sub>	half maximal effective concentration
EElmT	1,3-diethyl-imidazole-2-thione
ELS	evaporative light scattering
EOL	end of life
ESI	electrospray ionization
FT-IR	Fourier transform infrared spectroscopy
[HBBIm]Br	1-butyl-3-benzimidazolium bromide
[Hbet][NTf <sub>2</sub> ]	betainium bis(trifluoromethylsulfonyl)imide or protonated betaine bis(trifluoromethylsulfonyl)imide
HCl	hydrochloric acid
HClO <sub>4</sub>	perchloric acid
HES	hydrophobic eutectic solvents
HNO <sub>3</sub>	nitric acid
[Hpy]Cl	hexadecylpyridinium chloride
H <sub>2</sub> SO <sub>4</sub>	sulfuric acid
ICP-MS	inductively coupled plasma-mass spectrometry
ICP-OES	inductively coupled plasma-optimal emission spectroscopy
IL	ionic liquid
ISO	international organization for standardization
IXR	ion-exchange resin
KSCN	potassium thiocyanate

LCA	life-cycle assessment
LC <sub>50</sub>	median lethal concentration
LCD	liquid crystal display
LCI	life-cycle inventory
LCM	liquid surfactant membrane
LD <sub>50</sub>	median lethal dose
LIX 63 <sub>anti</sub>	anti-isomer of 5,8-diethyl-7-hydroxy-6-dodecanone oxime
LIX 65N	2-hydroxy-5-nonyl-benzophenone oxime
L-L	liquid-liquid
[MBCNPIP][NTf <sub>2</sub> ]	1-butyronitrile-1-methylpiperidinium bis(trifluoromethylsulfonyl)imide
[4MBCNPYR][NTf <sub>2</sub> ]	1-butyronitrile-4-methylpyridinium bis(trifluoromethylsulfonyl)imide
[MOPYRRO][NTf <sub>2</sub> ]	1-octyl-1-methylpyrrolidinium bis(trifluoromethylsulfonyl)imide
[MPIPCN][NTf <sub>2</sub> ]	1-methyl-1-butyronitrilepiperidinium bis(trifluoromethyl)sulfonylimide
[MPS <sub>2</sub> PIP][NTf <sub>2</sub> ]	1-methyl-1-[4,5-bis(methylsulfide)]pentylpiperidinium bis(trifluoromethylsulfonyl)imide
[MPTPIP][NTf <sub>2</sub> ]	1-methyl-1-pentenepiperidinium bis(trifluoromethylsulfonyl)imide
[MPTPYRRO][NTf <sub>2</sub> ]	1-methyl-1-pentenepyrrolidinium bis(trifluoromethylsulfonyl)imide
[4MPYRCN][NTf <sub>2</sub> ]	1-butyronitrile-4-methylpyridinium bis(trifluoromethyl)sulfonylimide
NaCl	sodium chloride
NADES	natural deep eutectic solvent
NaHSO <sub>3</sub>	sodium bisulfite
NaNO <sub>3</sub>	sodium nitrate
NaOH	sodium hydroxide
Na <sub>3</sub> PO <sub>4</sub> ·12H <sub>2</sub> O	sodium phosphate tribasic dodecahydrate
NaSCN	sodium thiocyanate
Na <sub>2</sub> S <sub>2</sub> O <sub>3</sub>	sodium thiosulfate
NH <sub>3</sub>	ammonia
NH <sub>4</sub> OH	ammonium hydroxide
NH <sub>4</sub> NO <sub>3</sub>	ammonium nitrate
(NH <sub>4</sub> ) <sub>2</sub> S	ammonium sulfide
NH <sub>4</sub> SCN	ammonium thiocyanate
NMR	nuclear magnetic resonance
N <sub>2</sub> SO <sub>3</sub>	sodium sulfite
N <sub>6666</sub> <sup>+</sup>	tetrahexylammonium cation
[N <sub>6666</sub> ][NTf <sub>2</sub> ]	tetrahexylammonium bis(trifluoromethylsulfonyl)imide
[N <sub>888</sub> ][HNO <sub>3</sub> ]	trioctylammonium hydrogen nitrate
[N <sub>888</sub> ][NO <sub>3</sub> ]	trioctylammonium nitrate
[N <sub>888</sub> ][NTf <sub>2</sub> ]	trioctylammonium bis(trifluoromethylsulfonyl)imide
[N <sub>888</sub> 1]Cl/Alquat 336	trioctylmethylammonium chloride
[N <sub>888</sub> 1][HSO <sub>4</sub> ]	trioctylmethylammonium hydrogen sulfate
[N <sub>888</sub> 1][NO <sub>3</sub> ]/Alquat 336N	trioctylmethylammonium nitrate
[N <sub>888</sub> 1][NTf <sub>2</sub> ]	trioctylmethylammonium bis(trifluoromethylsulfonyl)imide
[N <sub>888</sub> 1][SCN]	trioctylmethylammonium thiocyanate
N <sub>8888</sub> <sup>+</sup>	tetraoctylammonium cation
[N <sub>8888</sub> ][DCA]	tetraoctylammonium dicyanamide
[N <sub>8888</sub> ][NTf <sub>2</sub> ]	tetraoctylammonium bis(trifluoromethylsulfonyl)imide
PGM	platinum group metal
polySILP	polymerized supported ionic liquid phase
<i>p</i> -TsOH	<i>para</i> -toluenesulfonic acid
PVC	polyvinyl chloride
P <sub>44414</sub> Cl	tributyltetradecylphosphonium chloride
P <sub>66614</sub> Br/Cyphos 102	trihexyltetradecylphosphonium bromide
P <sub>66614</sub> Cl/Cyphos 101	trihexyltetradecylphosphonium chloride
P <sub>66614</sub> DCA/Cyphos 105	trihexyltetradecylphosphonium dicyanamide
P <sub>66614</sub> DOP/Cyphos 104	trihexyltetradecylphosphonium bis-(2,4,4-trimethylpentyl)phosphinate
P <sub>66614</sub> MTBA	trihexyltetradecylphosphonium 2-(methylthio)benzoate
P <sub>66614</sub> NO <sub>3</sub>	trihexyltetradecylphosphonium nitrate

P <sub>66614</sub> NTf <sub>2</sub> /Cyphos 109	trihexyltetradecylphosphonium bis(trifluoromethylsulfonyl)imide
P <sub>88812</sub> Cl	trioctyldodecylphosphonium chloride
RT	room temperature
SCN	thiocyanato
scCO <sub>2</sub>	supercritical carbon dioxide
SEM	scanning electron microscopy
SILP	supported ionic liquid phase
SnCl <sub>2</sub>	tin chloride
Span 80	polyoxyethylene (80) sorbitan monooleate
S-L	solid-liquid
[3-TPPy][NTf <sub>2</sub> ]	3-thiapentylpyridinium bis(trifluoromethylsulfonyl)imide
TOPO	trioctylphosphine oxide
Tris	2-amino-2-hydroxymethyl-1,3-propanediol
TSIL	task-specific ionic liquid
TX-100	triton X-100
UCST	upper-critical solution temperature
UV-Vis	ultraviolet-visible
WEEE	waste electrical and electronic equipment

## Acknowledgements

The first person to whom I would like to express my deepest and most sincere gratitude is my supervisor, Prof. Katharina Schröder; for putting her trust in me, for never giving up and constantly fighting to improve my work and my skills, for always preventing missteps, for supporting and guiding me until the very end.

I am forever thankful to Prof. Andreas Limbeck, my unofficial co-supervisor and problem solver, for painstakingly instilling his knowledge into my mind. Words cannot express my appreciation for his immense patience, persistence, unlimited help and collection of drawings!

My profound gratitude goes out to my interim supervisor, Prof. Michael Schnürch. His undoubtedly loaded schedule never prevented him from taking the time to listen to us and offer his support. Always serving with a smile and a joke!

It would be amiss not to mention Prof. Erwin Rosenberg. Although not in any way involved with the PhD itself, he was the person who reached out to me and brought me back to academia for this much desired endeavor. My heartfelt gratitude goes out to him for putting me in the path of my goals and dreams.

I am extremely grateful to and for my colleagues, Aitor, Apurba, Ádám and Fabian, with whom I spent the majority of my PhD journey, as well as the members most recently added to the group, Lisa, Connie, Julia, Jasmina, Philipp, Kristof, Prasad, Izzy; I could have never wished for a better group of people to accompany and support me to see this challenging path through. I am especially thankful for meeting Aitor in this journey; a true friend, hopefully for life, never taking himself too seriously, always seeing the lighter side of life. Together we made the much-needed comedy duo to see us through it all! I feel tremendously lucky to have crossed paths with Apurba; I want to thank him for always sharing his words of wisdom and for being someone I always look up to, both on a scientific and personal level. Many thanks to my regular coffee/tea buddies, Bletë and Michaela, for the much-needed shots of caffeine and motivation! Many thanks to all the students that joined our group throughout my stay for adding to the pleasant and cheerful atmosphere and unknowingly teaching me new things about myself, chemistry and life in general; Inga, Stefan, Nicole, Melanie, Magdalena, Johannes, Payam, Jakob, Elias, Dorka, Clemence...

I feel very lucky to have been blessed with an equally fun and supporting group of people in the analytics department; my second research base! Christopher, Lukas, Carina, Max, Felix, Maxi, Tobias, Jacob, Stefan; I want to deeply thank them all for their much-needed support and guidance as well as our entertaining exchanges! To my regular “analytics” coffee/tea buddies, Maria and Natalia, how would I have managed without you in the “darkest” hours?

I really want to thank all the people who unknowingly brought me on this journey. First and foremost, my boss in my first job in Austria, Rainer Bernert, for re-opening the Austrian “door” and its professional world to me. I want to thank him for believing in me, for introducing me to a unique international working experience under a variety of unexpected conditions, for pushing me to reach my full potential and for always supporting the idea of my further academic development. I owe a world of gratitude to my supervisor in my second job, Bernd Hoffmann, for putting his trust in me right from the start, for supporting me and motivating me to reach my full potential, for teaching me to stand my ground.

Last and most certainly not least, I owe my deepest gratitude to my parents. I would not be standing where I am today without their sacrifice, support, patience and faith. A big thank you to my brother and his skeptical and inquisitive nature for inspiring my love for science at a young age.



## Abstract

The platinum group metals, Pt, Pd, Rh, have been used in numerous applications, ranging from production of chemicals to dental material construction, while the extensive use of automotive vehicles accounts for the majority of the consumption of these precious metals. Unfortunately, their continuously increasing demand and the simultaneous gradual depletion of their natural resources paint a bleak picture with regard to the future satisfaction of said demand. Although recycling of these metals from secondary sources has become a common practice, which could bridge the gap between their supply and demand, it is plagued by significant shortcomings, i.e., incomplete metal recovery and significant environmental impact.

On the one hand, achieving complete metal recovery from end-of-life materials will further assist the conservation of natural resources, which are fairly limited and strictly localized. On the other hand, environmental impact of processes is nowadays, perhaps more than ever, a pressing issue that needs to be carefully evaluated and properly addressed. The scientific community has certainly developed, within the last decades, a heightened sensibility toward environmental protection, which is reflected in the strives it is making to minimize the detrimental effect of products and developed processes. In the same spirit, the following doctoral thesis was perceived and performed.

The thesis focuses on the recovery of platinum group metals (Pt, Pd, Rh) from spent materials, specifically car catalysts, with the aid of ionic liquids and deep eutectic solvents. The topic addressed in this thesis was perceived and performed within the frame of the EU Project Platirus; the multinational project aimed to investigate novel and alternative recovery processes for platinum group metals from secondary raw materials. Key focus of the project was the development of novel extraction and separation technologies with potential for industrial upscaling, aiming for a sustainable process with high metal recovery and minimized environmental impact.

Deep eutectic solvents based on the choline cation were investigated and successfully applied to the quantitative leaching/extraction of Pt and Pd and partial leaching (50%) of Rh, at mild process conditions. The possibility to increase Rh leachability was additionally explored, which was feasible (increase by approx. 20%) by pre-treatment of the car catalyst material at high temperature and inert gas atmosphere.

Further separation of the platinum group metals by co-extracted metals, which are present in the car catalyst matrix, was evaluated by two different approaches, namely, liquid-liquid and solid-liquid separation. Commercially available and in-house synthesized hydrophobic ionic liquids were employed for the liquid-liquid separation via bi-phasic system formation with  $P_{66614}Cl$ , yielding quantitative extraction of all three target metals and significant separation from the main interfering metal, i.e., Al. Although complete separation of platinum group metals was not achieved with this approach, it still offers two major advantages; recovery and reuse of the deep eutectic solvent for subsequent leaching cycles and a hydrophobic environment for platinum group metals which ideally serves for their recovery via electrodeposition. Direct recovery of the metals from the deep eutectic solvent with the aid of gas-diffusion electrocrystallization is also a distinct possibility, as demonstrated within the Platirus project.

Alternatively, the immobilization of an ionic liquid on silica support via polymerization (polymerized supported ionic liquid phase) allowed for the fast and simple separation of Pt and Pd, leached in an acidic liquor, from other interfering elements, whereas the removal of Rh from the sorbent material is a topic that still needs to be addressed.

## Kurzfassung

Die Platingruppenmetalle, Pt, Pd und Rh wurden schon in vielen Anwendungen verwendet, von Chemikalienproduktion bis zu zahnärztlichen Werkstoffen, wobei Kraftfahrzeuge den größten Teil des Konsums dieser Edelmetalle ausmachen. Ihre kontinuierlich steigende Nachfrage und die gleichzeitige graduelle Erschöpfung ihrer natürlichen Ressourcen werfen einen Schatten auf die Zukunft der Deckung ebener Nachfrage. Auch wenn das Recycling dieser Metalle inzwischen eine gängige Praxis geworden ist, die die Lücke zwischen Angebot und Nachfrage schließen könnte, leidet es unter bedeutenden Mängeln, wie zum Beispiel der unvollständigen Rückgewinnung der Metalle und der bedeutenden Umweltbelastung.

Einerseits unterstützt die vollständige Rückgewinnung von Platingruppenmetallen aus Altmaterialien die Konservierung natürlicher Ressourcen, welche limitiert und örtlich beschränkt sind. Andererseits ist heutzutage, vielleicht mehr denn je, die Umweltbelastung von Prozessen ein zunehmendes Problem, das evaluiert und entsprechend adressiert werden muss. Die Wissenschaft hat in den vergangenen Jahrzehnten eine erhöhte Sensibilität für Umweltschutz entwickelt, um zerstörerische Effekte von Produkten und entwickelten Prozessen zu minimieren. In diesem Sinne wurde auch die vorliegende Doktorarbeit wahrgenommen und ausgeführt.

Die Arbeit konzentriert sich auf die Rückgewinnung von Platingruppenmetallen (Pt, Pd, Rh) aus Endprodukten, vor allem Autokatalysatoren, mit Hilfe von ionischen Flüssigkeiten und tiefeutektischen Lösungsmitteln. Diese Arbeit wurde im Rahmen des EU-Projekts Platirus durchgeführt; einem multinationalen Projekt, das sich auf die Untersuchung von neuartigen und alternativen Rückgewinnungsprozessen für Platingruppenmetalle aus Sekundärrohstoffen widmet. Hauptschwerpunkt dieses Projekts war die Entwicklung und Bewertung umweltverträglicher Technologien, um einen nachhaltigen Prozess mit einer hohen Metallrückgewinnung und minimaler Umweltbelastung zu entwickeln.

Tiefeutektische Lösungsmittel basierend auf dem Cholin-Kation wurden untersucht und erfolgreich für das quantitative Extrahieren von Pt und Pd und teilweises Auslaugen von Rh unter milden Prozessbedingungen verwendet. Untersuchungen zur Erhöhung der Extrahierbarkeit von Rh wurde ebenfalls durchgeführt, was durch eine Vorbehandlung des Autokatalysatormaterials bei höheren Temperaturen unter Inertgasatmosphäre (Erhöhung um rund 20%) erreicht werden konnte.

Die weitere Abtrennung der Platingruppenmetalle von den mitextrahierten Metallen, welche ebenfalls in der Autokatalysatormatrix präsent sind, wurde durch zwei verschiedene Ansätze untersucht, nämlich Flüssig-Flüssig- und Fest-Flüssig-Trennung. Es wurden sowohl kommerziell verfügbare als auch hausintern synthetisierte ionische Flüssigkeiten für die Flüssig-Flüssig-Trennung mittels zweiphasiger Systeme eingesetzt, wobei die ionische Flüssigkeit  $P_{66614}Cl$  quantitative Extraktion von allen drei Zielmetallen und bedeutende Abtrennung der Hauptinterferenzmetalle, v.a. Al, erreicht. Auch wenn die komplette Trennung der Platingruppenmetalle durch diesen Ansatz nicht erreicht wurde, bietet er dennoch zwei bedeutende Vorteile; die Rückgewinnung und Wiederverwendung des tiefeutektischen Lösungsmittels für folgende Auslaugungszyklen und eine hydrophobe Umgebung für die Platingruppenmetalle, welche optimal für deren Rückgewinnung durch Elektroabscheidung ist. Direkte Rückgewinnung der Metalle aus dem tiefeutektischen Lösungsmittel mit Hilfe von Gasdiffusions-Elektrokristallisation ist ebenfalls eine Möglichkeit, die im Rahmen des Platirus-Projekts demonstriert wurde.

Alternativ erlaubte die Immobilisierung einer ionischen Flüssigkeit auf einem Kieselgelträger mittels Polymerisation eine schnelle und einfache Trennung von Pt und Pd, ausgelaugt in saurer Flüssigkeit, von anderen interferierenden Elementen.



# 1 Introduction

Recycling is an essential process in order to conserve the progressively depleting resources of platinum group metals (PGMs). Additionally, the environmental impact associated with their mining and their release in the environment through discarded end-of-life (EOL) products is an additional issue that should not be overlooked and further underlines the importance of recycling processes.<sup>1</sup> The present chapter will provide an introduction to the properties of PGMs, the state-of-the-art processes for their recycling from EOL materials, the chemical characteristics that pose a challenge for their recycling, as well as a brief overview of alternative technologies that are under investigation for their recovery.

## 1.1 Platinum group metals: significance and current status

Platinum group metals, comprising Ru, Rh, Pd, Os, Ir and Pt, are characterized by distinctive properties that have established them as imperative components in industrial applications. Besides possessing typical transition metal characteristics, such as catalytic activity, paramagnetism and tendency toward complex formation, they are further distinguished by their high melting point, low vapor pressure and resistance to corrosion.<sup>2</sup> Platinum group metals exhibit siderophilic and chalcophilic behavior, forming metallic bonds or covalent bonds with S, respectively. Although there are various mechanisms for PGM concentration on Earth's crust, formation of igneous intrusions (magma cools and solidifies before it reaches the surface) has chiefly contributed to the principal PGM deposits known to date. More than 120 primary and secondary PGM minerals have been thus far identified.<sup>3,4</sup> Specifically, PGMs are encountered in sulfide minerals and platinum-group minerals. Sulfide minerals contain, in addition to PGMs, S, Cu, Ni, Fe, Co, Cd, Ag and Au. Platinum-group minerals are alloys of Pt-Fe or Pt-Pd-Bi-Te.<sup>5</sup> The vast majority of PGMs is located in Africa, with the Bushveld complex being the largest deposit worldwide contributing more than 80% to the global PGM production. Russia is also a notable supplier, especially for Pd.<sup>6</sup>

From a financial perspective, PGM ores are classified in four categories, depending on their deposited amounts (1-23 g/t) and the concentration of accompanying Cu and Ni (0.1-5%). Coarse PGM deposits of mainly Pt exist but typically in very small scales.<sup>7</sup>

Platinum group metals constitute components of a broad array of applications, such as electrical and electronic equipment, fuel cells, dental materials, medication, jewelry and chemical and petroleum production. The automotive industry is the dominant consumer, where PGMs are used in vehicle catalysts.<sup>8</sup> Considerations for the environmental impact of vehicle exhaust emissions lead to the introduction of car catalysts. Incomplete combustion results to the introduction of pollutants in the exhaust and the main function of the car catalyst is the conversion of hydrocarbons (HCs), oxidation of carbon monoxide (CO) and reduction of nitrogen oxides (NO<sub>x</sub>) to less harmful products.<sup>9,10</sup> The tolerance of PGMs to sulfur compounds present in the exhaust and their high specific activity that allows construction of catalysts with small volumes, which is significant for rapid heating of the catalyst during operation and ease of packaging in the vehicle, makes them ideal for use in car catalysts.<sup>11</sup> An overview of PGM consumption per industry for 2020<sup>12</sup> is presented in Figure 1.

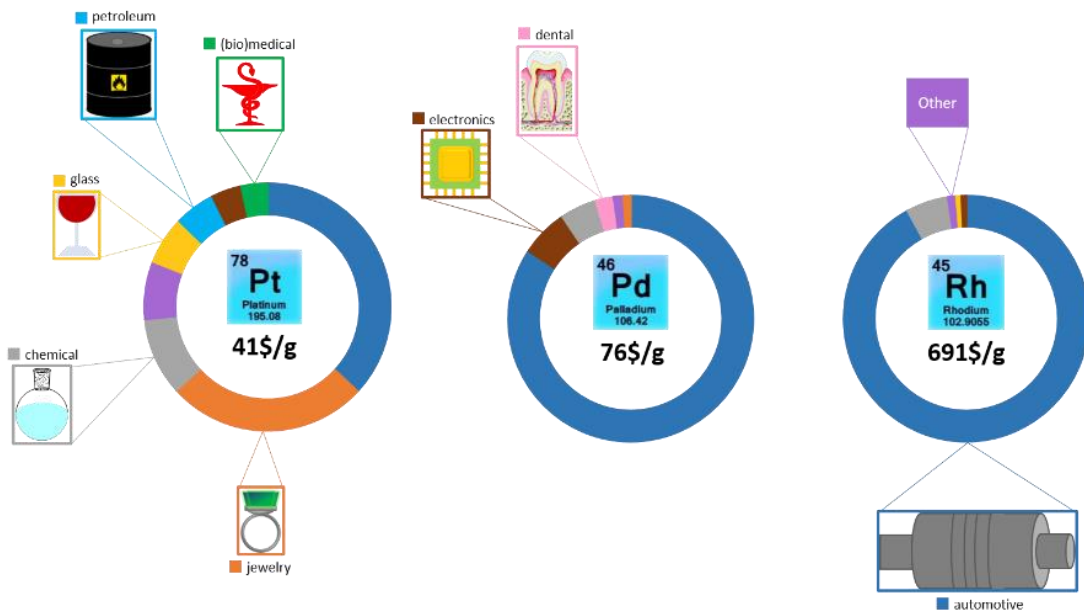


**Figure 1.** Platinum group metal consumption per metal and industry (PGM prices can fluctuate significantly, thus, the presented values are only indicative and valid at the time this thesis was written).

Catalytic converters mainly consist of a honeycomb structured ceramic (cordierite,  $2\text{MgO}\cdot 2\text{Al}_2\text{O}_3\cdot 5\text{SiO}_2$ ) or metal material coated largely with  $\gamma\text{-Al}_2\text{O}_3$  and additional chemical compounds, such as rare earth and alkaline earth oxides (Figure 2). The noble metals, which are located on the washcoat (alumina layer that contains the PGMs), are supported by  $\alpha\text{-Al}_2\text{O}_3$  or zirconia. Platinum group metals constitute only a small percentage of the washcoat (1-2%). A small percentage of other elements, which function as additives, is present in the catalyst. This structure is mounted inside a stainless-steel canister and the whole assembly comprises the catalytic converter.<sup>13,14,15</sup>

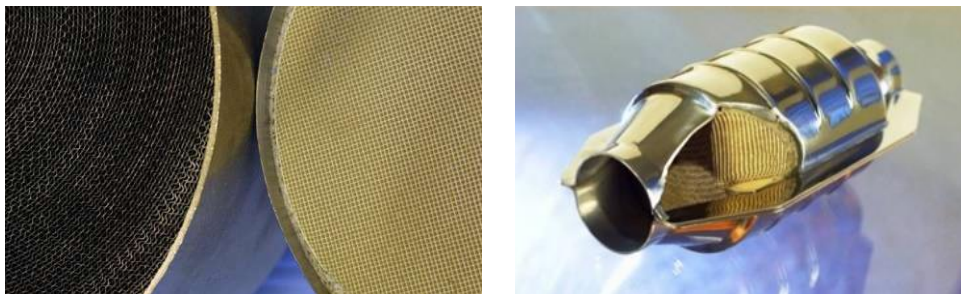


**Figure 2.** Examples of metal and cordierite catalyst substrates (left)<sup>10</sup> and a catalytic converter with the outer shell cut to show the inner construction (right).<sup>16</sup>

Observed historical trends and future projections indicate that demand for PGMs in the automotive industry has and will steadily increase. The driving forces of this trend are the spike in purchase of vehicles, implementation of stricter regulatory measures for exhaust emissions and a shift in Europe toward fuel-efficient diesel vehicles, whose catalytic converters require higher PGM amounts than gasoline ones.<sup>17</sup> Although growing environmental concerns have brought electric powered vehicles in focus, only 500 million out of 1.6 billion cars on the road are expected to be powered by electricity in 2040.<sup>18</sup> Therefore, the use of combustion engine cars is not foreseen to decline in the near future. Europe’s automotive industry accounts for the highest PGM consumption by far on a global level.<sup>19</sup> Within Europe, PGMs have been assigned a critical raw material (CRM) status due to their economic importance and high supply risk.<sup>20</sup> Additionally, they are classified by the United Nations Environment Program as critical metals because of their rapid demand growth, the risk in their supply and the restrictions in their

recycling.<sup>21</sup> Currently, there are three PGM sources; primary deposits, as by-products of Ni and Cu recovery, and recycling.<sup>17</sup>

The global demand for Pt has steadily exceeded the attainable supply and this tendency is expected to continue well into the future. Unfortunately, Pt is largely irreplaceable in industrial applications and, at the same time, geologists foresee that discovery of new resources is highly unlikely.<sup>22</sup> Immediate implications of this situation are gradual depletion of natural resources and increasing cost of PGMs, which will most probably get progressively higher. Extensive efforts to substitute the existing PGM-based car catalysts have been made,<sup>23,24,25</sup> but the efficiency of developed alternatives is not on par with the existing technology. Although the current PGM resources are expected to last for a few decades more, the increasing mining costs of their continuously depleting deposits can increase the vehicle prices substantially. Efficient PGM recycling can assist in maintaining the actual technology at affordable costs.<sup>26</sup> It is also a strategic approach to minimize Europe's dependency on imported PGMs.<sup>27</sup>

Apart from the financial aspect, the environmental impact of increasing PGM mining operations should be taken seriously into consideration. Mining of progressively depleting resources implies increasing energy consumption (related to increasing depth of mines) and generated greenhouse gas emissions have demonstrated a steady upward trend.<sup>28</sup> Employed mining and processing approaches induce the formation of trace amounts of dangerous and toxic compounds, such as furans, dioxins and polychlorinated biphenyls.<sup>29,30</sup> Ore extraction operations are associated with high water consumption and waste water production of unknown quality which is discarded to the environment. Additionally, generated solid wastes, namely tailings (solid waste remaining after metal extraction) and waste rock (rock excavated during mining but with no metals of economic importance), the amount of which is commonly not reported by mining companies, can have serious environmental and health repercussions.<sup>28</sup> Mining activities also have the potential to affect protected areas and pose a threat to endangered species, nevertheless, biodiversity data reported by mining companies are rather poor.<sup>31</sup>

Concentrations of PGMs found in the surrounding areas of mining and ore processing sites are elevated and it has been estimated that Pt and Pd emissions from smelting facilities globally could exceed 5% of the annual Pt and Pd production level.<sup>32</sup> Platinum group metals produced from anthropogenic activities bioaccumulate in living organisms and they have been detected in aquatic organisms, birds and humans. The mobility of Pt in soil though is only favored under acidic conditions and high levels of Cl.<sup>33</sup> The potential health effects that PGMs have on people who are occupationally exposed to them (smelting and processing facilities) should not be overlooked; exposure to Pt salts can lead to Platinosis, which is associated with cutaneous and respiratory allergy-like symptoms, such as dermatitis, eczema, dyspnea or asthma attacks.<sup>33,34</sup> It is noteworthy that only 1% of Pt can be absorbed by the human digestive system.<sup>35</sup> Additionally, it should be noted that metallic Pt is not biologically active and does not have allergenic potential; chlorinated PGM complexes, i.e.,  $H_2[PtCl_6]$ ,  $(NH_4)_2[PtCl_6]$ ,  $K_2[PtCl_4]$ ,  $Na[PtCl_4]$ , on the other hand, are associated with observed undesirable health effects.<sup>36</sup> Thus, the impact of PGMs on living organisms depends on their bioavailability.<sup>33</sup>

Secondary metal production through recycling can minimize the negative environmental impact of mining and contribute to substantial energy conservation.<sup>37</sup> This approach is also in line with the Sustainable Development Goals (Goal 12) that the United Nations have set to realize by 2030, aiming for a globally sustainable future.<sup>38</sup> Unfortunately, the overall recycling rates for PGMs reach a maximum of 70% (Table 1). As far as EOL car catalysts are concerned, only 50% of their PGMs is recycled, as is evident by the discrepancy between the number of annually deregistered automobiles and the number of collected EOL car catalysts. The losses can be attributed to the export of deregistered used cars or their use within

private sites but also to the illegal dumping of vehicles.<sup>39</sup> Significant amounts of EOL vehicles and waste electrical and electronic equipment (WEEE) are delivered to developing countries that lack the infrastructure for proper waste management, and follow environmentally non-sound practices, such as open dumping of EOL vehicles or open burning of tires and WEEE.<sup>40,41</sup>

**Table 1.** Estimated EOL global recycling rates for precious metals for the main and end user sectors.<sup>40</sup>

Overall EOL Recycling Rates per PGM (%) <sup>a</sup>		EOL Recycling Rates per Sector (%)					
		Vehicles	Electronics	Industrial Applications	Dental	Other	Jewelry, Coins
Pt	60-70	50-55	0-5	80-90	-	30-50	90-100
Pd	60-70	50-55	5-10	80-90	15-20	15-20	90-100
Rh	50-60	45-50	5-10	80-90	15-20	10-20	40-50

<sup>a</sup> Jewelry not included.

Open dumping of waste can lead to contamination of soil and water.<sup>37</sup> The implications can be more prominent in low- and middle-income countries, where waste is usually improperly disposed of in low-lying areas and areas adjacent to slums. Air contamination, emission of greenhouse gases and water pollution are the immediate effects of these waste practices on an environmental level, while the social and economic impacts should not be overlooked. In addition, the access of waste scavengers to the disposed waste possesses a direct health hazard. Alternatively, the waste is incinerated with minimal or non-existent emission monitoring. Open burning generates pollutants, which are harmful to the atmosphere but are also dangerous and toxic to humans.<sup>41,42</sup>

Evaluation of EOL vehicle recycling data from some developing countries revealed that the lack of a regulatory framework for their management and recycling as well as access to relevant information is a common problem.<sup>43</sup> Certain liquids that are present in vehicles (e.g., motor and brake oil, antifreeze) have to be treated before disposal for removal of hazardous pollutants. Additionally, heavy metals found in vehicles, such as Hg, Pb, Cd, Cr and Zn, need to be extracted properly to avoid soil and water contamination. Cars that are illegally dumped or abandoned in these countries are illegally collected by dealers for the recovery of re-usable parts. However, improper handling results in leakage of hazardous materials to the soil and water, thereby, contributing to environmental pollution.<sup>43</sup>

## 1.2 Conventional approaches to platinum group metal recycling

The state-of-the-art PGM recovery from PGM-containing EOL materials, such as car catalysts and WEEE, relies on hydrometallurgical and pyrometallurgical processes, which comprise thermal pre-treatment of the materials followed by leaching and selective PGM recovery via cementation, solvent extraction or adsorption on an ion-exchange resin. The selected approach is contingent upon the material composition. Prior to processing, the spent materials are segregated, crushed and ground. Efficient recovery and separation of PGMs is the desired objective from a financial perspective. A recovery rate of >90% is considered economically viable. The recyclability of PGMs from spent car catalysts is determined by three factors: the inherent value of the metal, the catalyst composition and the target field of application.<sup>44,45,46</sup> State-of-the-art processes yield recovery rates over 95%.<sup>47</sup> A brief overview of the employed recycling approaches is presented in Figure 3.

Even though PGM applications are manifold, the automotive industry is the most prominent consumer (i.e., 56% of the global PGM production in 2012).<sup>48</sup> Consequently, extracting PGMs from spent car catalysts has the potential of inserting back into the supply chain vast amounts of PGMs. An extensive interest in EOL car catalysts is also reflected in the available literature on PGM recovery processes. Therefore, in the following section, the practices of hydro- and pyro-metallurgy on the example of car catalyst recycling will be introduced.

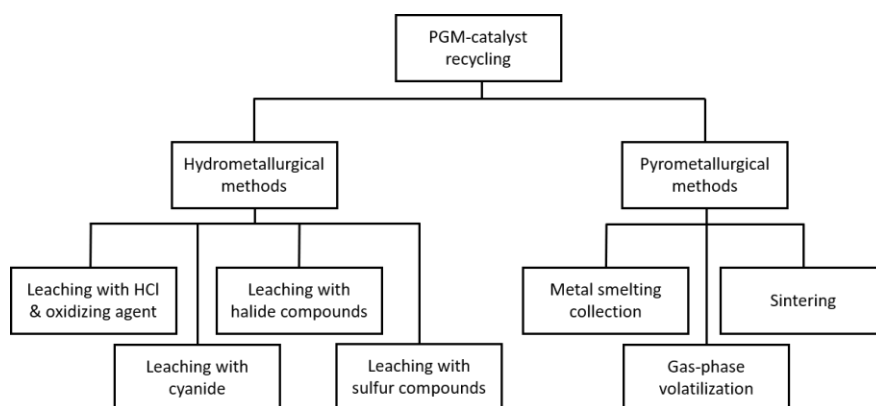


Figure 3. Overview of PGM recycling technologies.<sup>49,50,51</sup>

### 1.2.1 Hydrometallurgy

Hydrometallurgical approaches aim for the selective dissolution of the washcoat, where the PGMs are located. The steel shell is removed and recycled in a separate process, while the ceramic monolith is subjected to the PGM recovery process.<sup>44</sup> Dissolution relies on the use of *aqua regia* and mineral acids, such as HCl, HNO<sub>3</sub> and H<sub>2</sub>SO<sub>4</sub>, with the aid of oxidizing agents, such as oxygen, iodine, bromine, chlorine and hydrogen peroxide.<sup>46</sup> Alternatively, the ceramic material can be leached with NaOH or hot H<sub>2</sub>SO<sub>4</sub>, neither of which are capable of dissolving PGMs, thus, in this case they are recovered as solids.<sup>52</sup>

Prior to hydrometallurgical processing, pre-treatment of the catalyst, such as fine grinding, roasting, reduction, or pressure leaching, is necessary to attain maximum PGM leaching capacity which is otherwise hampered by organic substances deposited on the catalyst surface or by the form of the support material itself. After the pre-treatment, leaching is performed for PGM dissolution.<sup>53</sup>

The leaching systems typically used rely on the following agents:

- (i) Hydrochloric acid with an oxidizing agent

Leaching in HCl and oxidizing agents (e.g.,  $\text{HNO}_3$ ,  $\text{H}_2\text{O}_2$ ,  $\text{Cl}_2$ ,  $\text{NaClO}$ ,  $\text{NaClO}_3$ ) provides the necessary chemical environment (oxidation potential and  $\text{Cl}^-$  concentration) for the formation of soluble PGM-chlorocomplexes, whose chemistry is exploited for the separation of PGMs.<sup>46</sup>

#### (ii) Cyanide

Sodium cyanide has the ability to form stable cyanocomplexes with PGMs in alkaline pH under conditions of elevated temperature and pressure.<sup>45,50</sup>

#### (iii) Halide compounds

Halide salts have been employed due to their less hazardous nature compared to the previously mentioned approaches. Owing to their low potential, PGM-iodide complexes are more readily formed, thereby rendering  $\text{I}^-$  more promising than its counterparts.<sup>45,50</sup>

#### (iv) Sulfur compounds

Thiocompounds (e.g., thiocyanate, thiosulfate, thiourea) are alternative leaching agents for PGMs. The PGM-thiocyanate complexes exhibit higher stability than the halide ones. Despite the more environmentally benign nature of thiosulfate anions, large quantities are required for leaching which raises financial concerns.<sup>50</sup> A typical hydrometallurgical process scheme is depicted in Figure 4. A detailed discussion of available hydrometallurgical procedures can be found by referring to relevant comprehensive reviews by Jha et al.,<sup>45</sup> Dong et al.,<sup>46</sup> Padamata et al.<sup>54</sup> and Karim et al.<sup>50</sup>

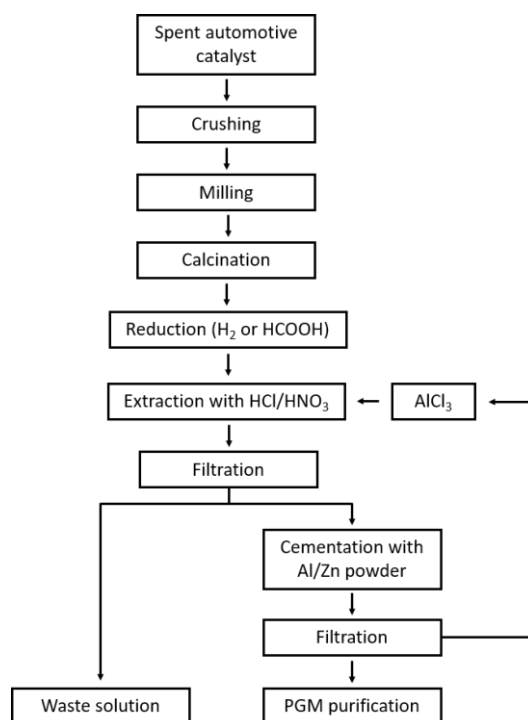


Figure 4. Process flowsheet of aqua regia-based hydrometallurgical process.<sup>55</sup>

The dissolution of PGMs in various acidic media is easier when they are encountered in their metallic form.<sup>56</sup> Even though they are originally deposited on the catalyst support as metallic particles, in the EOL catalysts they have been partly converted to their respective oxides.<sup>57</sup> Their chemical inertness renders their dissolution a challenging task. Excessive amounts of strong acids mixed with strong oxidants are usually required, which implies the generation of waste water that contains high acid and heavy metal amounts. For example, for the recovery of 1 g of Pt, approx. 7000 mL of 37% HCl or 1500 mL of hot concentrated  $\text{H}_2\text{SO}_4$  followed by treatment with 1000 mL of 37% HCl are required, depending on whether



the PGMs or the ceramic material is dissolved, respectively.<sup>58</sup> Use of *aqua regia* is a notable drawback of these processes, because mixing of HNO<sub>3</sub> and HCl for its generation, leads to formation of toxic gases, i.e., nitrosyl chloride and chlorine gas. Nitrosyl chloride can further decompose to chlorine gas and nitric oxide which is also highly toxic and can induce serious environmental repercussions, such as depletion of the ozone layer and acid rain formation.<sup>45</sup> Cyanide-based leaching produces considerable amounts of waste and calls for specialized equipment.<sup>59</sup> While it allows high PGM extraction efficiencies, its highly toxic nature is a major drawback.<sup>50</sup> Working conditions are negatively affected by the presence of harmful liquids and gases and as a consequence, costly protective measures need to be implemented for personnel protection.<sup>60</sup> A number of other technical challenges are associated with hydrometallurgical approaches, namely the presence of contaminant elements on the catalyst washcoat, the presence of refractory materials (alumina and additives), the use of highly aggressive and corrosive reagents and production of large amounts of solid waste in addition to the liquid waste.<sup>61</sup> Additionally, several hours are needed to attain maximum dissolution efficiency of PGMs,<sup>14</sup> while, at the same time, severe conditions of pressure (up to 6000 kPa) and temperature (up to 900 °C) are required.<sup>51</sup>

### 1.2.2 Pyrometallurgy

Pyrometallurgical treatment involves slagging of the catalyst support or the ceramic material in a reductive atmosphere, which takes place at high temperatures inside special furnaces.<sup>62</sup> The use of elevated temperatures, in a range below the melting point of PGMs (1500-1700 °C),<sup>63</sup> in the presence of fluxing agents is necessary.<sup>64</sup> The addition of fluxing agents reduces the metal compounds to their metallic form<sup>65</sup> and promotes the vitrification of ceramic materials at lower temperatures.<sup>66</sup> Platinum group metals are recovered from the support material slag in the form of particulate matter,<sup>63</sup> with the aid of collector metals, such as Cu, Fe, Ni or Pb, which are characterized by good affinity for PGMs, and then subjected to further wet-chemical processing.<sup>49,62</sup> This process, which allows the preconcentration of the precious metals and their separation from the slag phase, is called smelting.<sup>49</sup>

A typical pyrometallurgical process scheme employing a Cu collector is presented in Figure 5. The smelting process with a Cu collector (e.g., CuCO<sub>3</sub>, CuO, Cu) is performed at 1450-1600 °C, in an electric arc furnace, with the aid of fluxing agents (e.g., SiO<sub>2</sub>, CaO). Electrorefining of the PGM-containing Cu generates a slag with 20-25% PGMs while the Cu is recovered with high purity (99.99%). The overall PGM recovery of the process can reach 99%.<sup>51</sup> A detailed discussion of pyrometallurgical approaches is beyond the scope of this thesis. A good insight on the topic can be found in relevant comprehensive reviews by Liu et al.,<sup>49</sup> Peng et al.<sup>51</sup> and Dong et al.<sup>46</sup>

In addition to smelting, which is the most commonly employed pyrometallurgical approach, volatilization and sintering are also used. In gas-phase volatilization, PGMs are brought to the gas phase by selective chlorination and are subsequently separated based on the different vapor pressures that the metal chlorides possess.<sup>49</sup> Volatilization is not industrially favorable due to the use of toxic gases (CO and Cl<sub>2</sub>), which pose health and environmental hazards. Furthermore, the corrosive effect that the process has on the facilities, implies increased cost of production. Sintering takes place in a plasma atmosphere, whereby the oxidized PGMs present in the car catalyst are reduced in situ, at temperatures over 1200 °C. Overall, the temperatures employed in pyrometallurgical processes are significantly higher than in the case of hydrometallurgy, rendering them expensive and insufficient from an energy consumption perspective.<sup>51</sup>

As already discussed, both processes (hydro- and pyro-metallurgy) are associated with certain advantages and disadvantages, however, the selection of the employed recovery process is decisively affected by the

precious metal content of the EOL material that is to be recycled. High PGM contents (>30%) allow direct application of hydrometallurgy, whereas lower contents require preconcentration, which can be achieved by pyrometallurgical smelting or hydrometallurgical dissolution. Aside from the PGM content, the capabilities of the refining facility are a definitive factor of the final process selection.

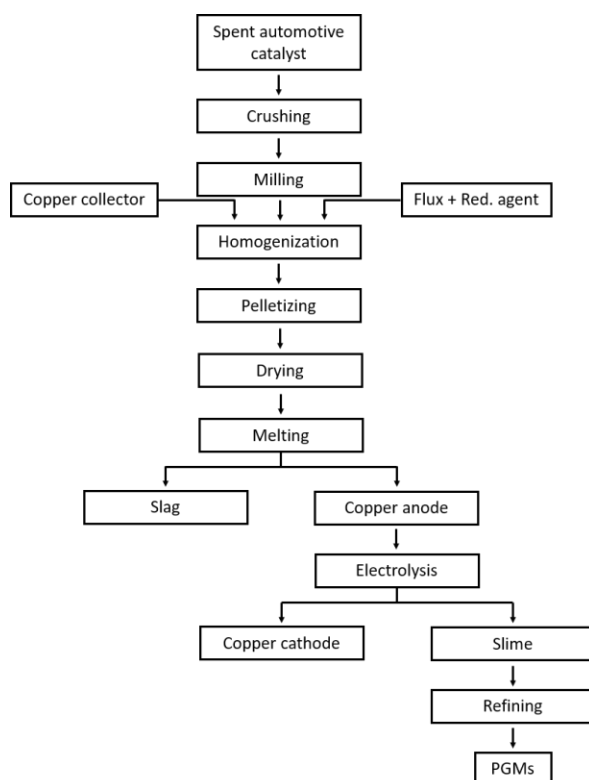


**Figure 5.** Process flowsheet of a pyrometallurgical process relying on a Cu collector.<sup>51</sup>

As already discussed, both processes (hydro- and pyro-metallurgy) are associated with certain advantages and disadvantages, however, the selection of the employed recovery process is decisively affected by the precious metal content of the EOL material that is to be recycled. High PGM contents (>30%) allow direct application of hydrometallurgy, whereas lower contents require preconcentration, which can be achieved by pyrometallurgical smelting or hydrometallurgical dissolution. Aside from the PGM content, the capabilities of the refining facility are a definitive factor of the final process selection.

In reality, the two processes are complementary, since most facilities integrate them, using pyrometallurgy for preconcentration of the precious metals, followed by hydrometallurgy in the subsequent refining steps. Nevertheless, pyrometallurgy is superior for the recovery of PGMs from complex materials, in which case hydrometallurgy encounters technical limitations.<sup>47</sup>

The pyrometallurgical smelting process seems to be the method of choice for a large number of industries involved in PGM recovery, such as Umicore, Johnson Matthey, BASF and Nippon.<sup>51,54</sup> This is, presumably, due to some quite notable advantages that it possesses in comparison to hydrometallurgy, which become more significant at industrial levels. Metal smelting is ideally applicable to refractory materials and secondary materials that contain small amounts of PGMs.<sup>46</sup> Particularly, the process employing a Cu collector allows for fast processing times, high recovery rates and higher recovery of Rh, contrary to hydrometallurgical approaches.<sup>49</sup> An overall PGM recovery of 99% is achieved, while the Cu collector can be recovered in highly pure form (99.99%) and reused. Additionally, if the car catalyst material is pretreated for the removal of contaminants, the energy consumption and environmental impact of the process can be significantly reduced.<sup>51</sup> Despite the many advantages Cu collection offers, the subsequent



PGM purification is a complex process which produces large volumes of waste water, thus, generating a secondary environmental impact.<sup>49</sup> It should be noted that Cu is a rather expensive collector metal.<sup>67</sup> Collection with Fe provides easy separation of PGMs from the slag, due to their considerable difference in density, while the low price of Fe makes this process more economical.<sup>51</sup> However, since higher temperatures are employed, there is the possibility of SiO<sub>2</sub> reduction to Si and subsequent formation of ferrosilicon alloys which impede PGM recovery, since these alloys are not susceptible to acid dissolution. Besides, hazardous compounds are produced in the process, meaning the generated waste has to be treated prior to its release to the environment.<sup>49</sup> Smelting with Pb collector is one of the oldest PGM recovery methods. Despite its low price and simple operation, low recovery of Rh (70-80%) and production of the hazardous PbO are the major drawbacks of this option.<sup>53</sup>

### 1.2.3 Challenges for separation and refining

The variety and strength of complexes that PGMs can form is one of their unparalleled features. PGMs are B-type metals and tend to form stable complexes with soft ( $\pi$ -bonding) ligands, such as chloride (Cl<sup>-</sup>). Platinum-group-metal chlorocomplexes are particularly important in their separation and refining processes, since in this form PGMs are soluble in acidic and oxidizing environments. The thermodynamic and kinetic differences between the metal ion species, is the fundamental parameter on which their effective separation is based.<sup>68,69,70</sup>

According to thermodynamic data, Pd has the highest solubility in its chloride form, followed by Pt and Rh.<sup>70</sup> Rhodium, particularly, is quite inert and not soluble or only slightly soluble in acids.<sup>56</sup> This is also the case for Rh<sub>2</sub>O<sub>3</sub>, which is less readily chlorinated than metallic Rh<sup>57</sup> and stable over a wide range of temperature and pressure.<sup>71</sup> The solubility and extractability of PGMs is also largely affected by the size and the charge of the complex present in solution, since those directly affect the selectivity of the extracting agent. Taking into account the decisive effect that these two parameters impart on the extraction, it comes as no surprise that Rh is only poorly extracted compared to Pt and Pd.<sup>68</sup> Pt is commonly encountered as PtCl<sub>4</sub><sup>2-</sup> and PtCl<sub>6</sub><sup>2-</sup> with oxidation numbers of +II and +IV, respectively. Similarly, the most common Pd species are PdCl<sub>4</sub><sup>2-</sup> and PdCl<sub>6</sub><sup>2-</sup> with oxidation numbers of +II and +IV, respectively.<sup>69</sup> The cationic and neutral Rh complexes are quite inert, while an oxidation number of +III is dominant in chloride solutions. Rh(III) has the tendency to form octahedral complexes which are particularly difficult to extract due to steric limitations.<sup>72</sup> This specific behavior of Rh and the challenges associated with its quantitative extraction is a topic consistently encountered in publications dealing with PGM extractions and separations. In Figure 6, a speciation diagram of Rh-chlorocomplexes is presented. Although there is a considerable number of Rh-species available, from a thermodynamic perspective, the highly charged octahedral complexes [RhCl<sub>5</sub>(H<sub>2</sub>O)]<sup>2-</sup> and RhCl<sub>6</sub><sup>3-</sup> are favored and are, thus, the most prominent over a wide range of Cl<sup>-</sup> concentrations. The different behavior of PGM chlorocomplexes is a major advantage that can be utilized in their refining processes. A comprehensive description of the refining and purification processes has been presented by Ramachandran et al.<sup>73</sup>

Following the extraction from the EOL material, the feed produced for the refining step contains 50-70% precious metals. Primary separation and secondary purification yield the precious metals in the form of metal salts, which are subsequently reduced to their metallic form to recover metals of high purity. The approaches used on an industrial level, are of hydrometallurgical nature and rely on selective precipitation via complex formation, solvent extraction and ion exchange.<sup>73,74</sup>

While precipitation processes are cheap, well established and can produce metals of the required purity, they are hampered by low efficiency in terms of release speed of the refined metals to the market, high costs, difficulty in automation and increased exposure risk of personnel to Pt.

Ion exchange has much higher selectivity in comparison and significantly faster kinetics, while the material handling and associated exposure to dangerous chemicals is effectively reduced. Nevertheless, the extent of dilution of the treated solutions, implies increased energy consumption since a considerable number of steps is required for the evaporation of excess solvents.<sup>73</sup>

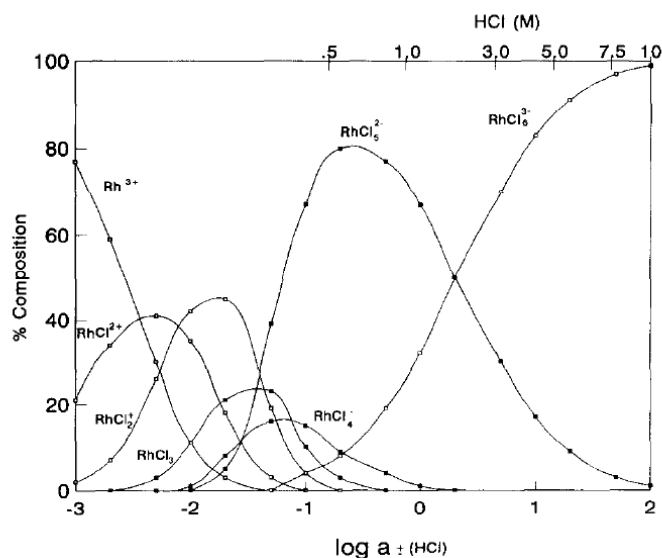


Figure 6. Rhodium-chloride speciation diagram at 25 °C.<sup>72</sup>

Typically, further refining and separation steps are based on solvent extraction in the presence of carefully refined ligands.<sup>75</sup> The widespread application of this approach for metal recovery on an industrial level is mainly attributed to the speed, simplicity and wide applicability of solvent-based extractions.<sup>76</sup> Nevertheless, their extensive use is not void of considerable drawbacks. The overall separation rate is determined by the kinetics of the chemical- and mass-transfer processes, while emulsion formation during mixing of the phases can further affect the rate. Additionally, the generated amount of the output organic waste is significant,<sup>77</sup> while the highly flammable nature of the solvents poses a significant fire risk.<sup>73</sup>

### 1.3 Alternative extraction processes for platinum group metal recovery

Apart from the industrial-level approaches of hydrometallurgy and pyrometallurgy, alternative processes for PGM recycling are under investigation within the scientific community. In this section, a brief overview is provided.

**Bioleaching.** It is the branch of biometallurgy that exploits the metabolic pathways of microorganisms for the extraction of PGMs from spent car catalysts and other waste material. It is considered to be an environmentally benign and economical alternative to the commonly employed processes.<sup>50,54</sup> Autotrophic bacteria, e.g., *Acidithiobacillus ferrooxidans*, can leach metallic ions in the presence of Fe or S species.<sup>78</sup> The cyanide produced by heterotrophic bacteria, e.g., *Chromobacterium violaceum*, *Pseudomonas fluorescens*, *Bacillus megaterium*, binds PGMs in the form of stable cyanocomplexes.<sup>79</sup> While the overall PGM extraction efficiency of the latter approach is usually lower than the conventional ones, the ability of these bacteria to convert toxic cyanide to the non-toxic  $\beta$ -cyanoalanine and bind PGMs at atmospheric pressure renders the process environmentally compatible and efficient in terms of energy consumption.<sup>54,79</sup> Shin et al. reported a bioleaching process, utilizing the cyanide-producing bacterium *Chromobacterium violaceum*, where comparable leaching efficiencies for Pt, Pd and Rh from a spent automotive catalyst were afforded with the chemical-based leaching process employing NaCN. In both cases, the leaching conditions were 1000 mg CN/L, at 150 °C, for 1 h; in the case of bioleaching, 92.1% Pt, 99.5% Pd and 96.5% Rh were leached, whereas in the chemical leaching the respective values of 100%, 99.9% and 100% were afforded.<sup>80</sup> Simultaneous significant removal of Cu and Ni, which compete with PGMs for cyanide binding, from the car catalyst matrix and increase of the PGM leaching efficiency is feasible by ultrasonication-assisted HNO<sub>3</sub> pre-treatment, as demonstrated when the bacteria *Pseudomonas fluorescens* and *Bacillus megaterium* were employed.<sup>81</sup>

**Supercritical carbon dioxide (scCO<sub>2</sub>).** The non-toxic and non-flammable nature of scCO<sub>2</sub>, its tunability and recyclability, as well as its low price, and easy separation from the extracted products, render it a highly versatile alternative solvent.<sup>82</sup> Selective extraction of Pd, from a solid matrix containing Pt, Pd and Rh, with the aid of scCO<sub>2</sub> and a chelating agent (tributyl phosphate in HNO<sub>3</sub>) has been reported. As expected, pure scCO<sub>2</sub> was unable to extract any PGMs without the addition of the selective ligand due to its low solvating power. The formation of a neutral complex between the metal and the employed ligand increases the metal solubility in scCO<sub>2</sub>. High pressure (20 MPa) and relatively mild temperature (60 °C) afforded high and selective Pd extraction (>96%) within 1 h, while Pt extraction remained below 5% and Rh could not be detected.<sup>83</sup> Selective removal of Pd from industrial aluminosilica catalysts simulating real spent car catalysts has been reported. The use of scCO<sub>2</sub>-soluble polymers with Pd-complexing pyridine units could extract 73% Pd at mild process conditions (25 MPa, 40 °C). Additionally, it was demonstrated that the extractability is dependent on the Pd species, with Na<sub>2</sub>PdCl<sub>4</sub> exhibiting the highest reactivity.<sup>84</sup> The recovery of PGMs with the aid of scCO<sub>2</sub> is still at a nascent stage.

**Magnetic separation.** Two different approaches have been reported for the magnetic recovery of PGMs. The surface of the catalyst is coated with electroless plating with a ferromagnetic metal, i.e., Ni, which forms alloys with PGMs at high temperature (800 °C). Following Ni deposition, the catalyst is pulverized and the ferromagnetic properties on Ni are exploited to achieve separation of the metals from the ceramic material powder with the aid of a neodymium magnet (Nd-Fe-B alloy). The PGMs can be recovered from the Ni alloy either by direct dissolution of the magnetic powder in an acidic medium or by a pyrometallurgical approach where Ni serves as the collector metal. Although the efficiency of this approach is not very high, since enrichment factors of 4-6 are achieved, it has potential to be further improved and it demonstrates the feasibility of the magnetic separation as a possible alternative to the currently employed preconcentration approaches.<sup>85</sup> Alternatively, treatment of the spent catalyst material with FeCl<sub>2</sub> vapor at 927 °C can be used to form the ferromagnetic Pt-Fe alloy, which can be

preconcentrated with the aid of a neodymium magnet. Subsequent exposure of the alloy to  $\text{FeCl}_3$  vapor at  $927^\circ\text{C}$  leads to dealloying, removal of Fe and loss of ferromagnetism.<sup>86</sup> This approach is also applicable for the recovery of Pd and Rh. Enrichment factors of 3-5 were achieved for the three PGMs, however, optimization of the pulverization and the magnetic separation processes is regarded as a potential approach to improve these factors. The feasibility of direct PGM recovery from the spent car catalyst material has been demonstrated.<sup>87</sup> Fast separation, low cost and limited environmental impact are the major advantages of the magnetic-based separation.

**Non-ionic hydrophobic eutectic solvents (HESs).** They are the most recently assigned subcategory of deep eutectic solvents (DESs), which will be presented in the following chapter. Typically, DESs are characterized by the presence of hydrogen bonding interactions arising from the presence of at least one ionic species in the mixture, which imparts on it its hydrophilic nature. Unlike DESs, HESs are solely composed on non-ionic species.<sup>88</sup> The lack of coulombic interactions in HESs results in higher potential for recovery of the HES and faster mass-transfer rates, due to limited solubility in water and decreased viscosity, respectively.<sup>89</sup> Systems comprising trioctylphosphine oxide (TOPO) have demonstrated selectivity, which can be tuned by selection of the other HES component (hydrogen bond donor), toward the recovery of Pt(IV), Pd(II) and Fe(III) from a metal mixture simulating catalyst leachates. Regardless of the employed hydrogen bond donor in the TOPO systems, maintaining the HCl concentration of the metal mixture below 1 M allows excellent extraction of Pt and Pd and their sufficient separation from other interfering metals (Cu, Co Ni, Cr, Fe). As the authors demonstrated on the example of Pd, the target metals can be recovered from the HES either by stripping or formation of Pd nanoparticles in the HES medium, in which case the HES is sacrificed since the TOPO functions as a capping agent (stabilizer that inhibits the overgrowth of the particles and prevents their aggregation)<sup>90</sup> in the particle synthesis.<sup>89</sup>

## 2 Ionic Liquids and Deep Eutectic Solvents: Properties and Applications

An emerging branch of extractive metallurgy, called solvometallurgy, employs low-water-content solvents, such as DESs, for metal recovery.<sup>91</sup> When the process makes use of ionic solvents, such as ILs, it is referred to as ionometallurgy.<sup>92</sup> The predominantly attractive features of solvometallurgical approaches pertain to processing at low temperatures, use of constituents with lower environmental impact and, most importantly, the ability to tailor the solvent properties to the target application.<sup>93</sup> Thus, ILs and DESs constitute ideal candidates for this field.

### 2.1 Ionic liquids

Ionic liquids (ILs) are salts with melting points below 100 °C, which consist entirely or almost entirely of ions.<sup>94</sup> Organic cations and organic or inorganic anions constitute their building blocks.<sup>95</sup> Early examples of ILs date back to 1888, when Gabriel reported ethanol-ammonium nitrate with a melting point of 55 °C, followed a few years later, in 1914, by a scientific publication, by Walden, that presented the synthesis of the room-temperature IL (RTIL), ethylammonium nitrate.<sup>94</sup>

When they are liquid at room temperature (RT) they are referred to as “room-temperature ionic liquids”. The term “molten salt” is sometimes used as synonymous, however, ILs possess many of the advantages that are characteristic of molten salts, while at the same time they circumvent disadvantages associated with their high melting points.<sup>96</sup> While, e.g., NaCl melts at 801 °C, ILs can be liquid at temperatures as low as -96 °C. Thus, it becomes immediately apparent, that unlike molten salts, ILs can be handled like ordinary solvents.<sup>96,97</sup>

Thermodynamic data provide an insight into the liquid state of ILs. Based on free energy calculations of the fusion of the ions, it is demonstrated that, under ambient conditions, the liquid state is thermodynamically favorable.<sup>98</sup> The asymmetry of the ions, usually present on the cation, disrupts the ordered lattice packing that normally leads to crystallization, hence imparting a wide liquid range to ILs (Figure 7).<sup>99,100</sup>

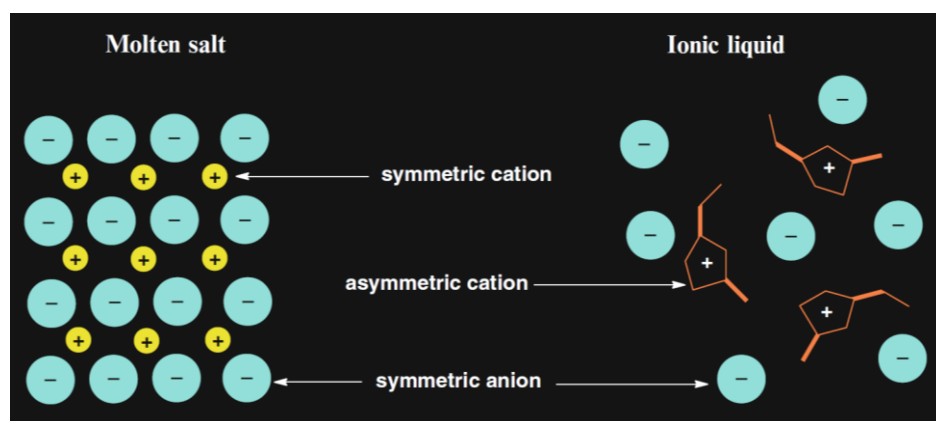


Figure 7. Packing of ions in molten salts and ionic liquids.<sup>101</sup>

Despite their ionic character and their dual organic and ionic nature, ILs can be likened more to organic solvents, in terms of certain behaviors they exhibit, such as retaining their liquid state at RT and possessing surface tensions in the range between dimethyl sulfoxide (DMSO) and toluene. Nevertheless, their low volatility and low flammability, which are typical undesirable traits of organic solvents, set them apart.<sup>102</sup>

Numerous unique properties distinguish them from common solvents; wide liquidus range that exceeds 400 °C, high thermal stability and conductivity, wide solvation range for a significant number of molecules, ability to prolong the lifetime of certain complex species, as well as the capability to suppress solvolysis phenomena and marked catalytic activity.<sup>95,102,103,104</sup> Most importantly, either variation in the building anion/cation or their functionalization by attaching a functional group, can impart desirable properties to ILs that are suitable for targeted applications.<sup>105,106</sup> The anion accounts for certain properties, such as thermal stability and miscibility, while viscosity, surface tension and density are determined by the length of the alkyl chain on the cation and/or its shape or symmetry.<sup>107</sup> Hence, the term “designer solvents” has been assigned to ILs to describe their distinctive tunable nature.<sup>105</sup>

From a historical standpoint, ILs are classified in three generations. The *first generation* comprises chloroaluminate (III) ILs, while ILs of more benign nature used in laboratory scale research constitute the *second generation*. The *third generation* includes task-specific ILs. It should be noted though, that this classification is broad and not strictly exclusive.<sup>108,94</sup>

Since 2000, there has been a steadily expanding interest of the scientific community in ILs as reflected by the number of annually peer-reviewed publications. This steady increase is largely in line with the growing effort to substitute conventionally used solvents with more environmentally benign alternatives.<sup>109</sup> Ionic liquids have been, perhaps optimistically, labelled “green solvents”, mainly due to their low volatility which implies a lesser degree of negative environmental impact and health hazards, low toxicity and non-flammability. Despite their unique and useful properties, it should be noted that the use of ILs does not automatically imply a “green” process. Contrary to widespread belief that they cannot evaporate, it has been proven that they can actually be distilled by selection of appropriate temperature and pressure conditions.<sup>110</sup> Additionally, even if ILs can be used in “green chemistry” processes and under certain conditions their non-volatility leads to reduction of emissions, it should still be pointed out that the “green” aspect of a process cannot simply be concluded based on the nature of the employed solvent, but rather by evaluation of the cumulative process. Potential toxicity cannot be excluded either; e.g., the commonly used anion  $\text{PF}_6^-$  can hydrolyze generating HF, which is both corrosive and extremely toxic.<sup>111</sup> Furthermore, the attractive feature of non-flammability (flash point below 37.8 °C) does not go hand in hand with inherent safety; many ILs are combustible (flash point above 37.8 °C) due to their oxygen content or decomposition products.<sup>112</sup>

That being said, it is evident that ILs have demonstrated superior performance in many applications compared to commonly used solvents and have introduced new frontiers to long standing research challenges. Their application in catalysis is particularly attractive, considering the increased reactivity and catalytic performance, ease of product separation, possibility of extensive recycling meaning mitigation of costs and reduction of down-stream processing. The remarkable improvements brought about by ILs have also been demonstrated in the extraction of various metals where not only can they assume the solvent role in the presence of an extracting agent, but in some cases, they also exhibit significantly enhanced extraction efficiencies compared to commonly used organic solvents.<sup>113,114</sup> Additionally, many limitations imposed by conventional solvents can be overcome with ILs, presumably because the formed extractable species and the respective extraction mechanisms differ between ILs and organic solvents. For example, a strong dependency exists between the extraction yield and the anionic counterion for extractions in organic solvents. This effect is considerably less explicit for ILs, since the extraction of PGMs in ILs does not seem to be susceptible to anion variation.<sup>114</sup> Additionally, tunability is one of the properties that comes in handy for extractions and separations, since, via modifications in the IL, the selectivity toward a certain metal can be adjusted.<sup>113,114</sup>



## 2.2 Deep eutectic solvents

Deep eutectic solvents, which are considered to be IL analogues, are eutectic mixtures formed by the combination of two or more components; specifically, Lewis or Brønsted acids and bases comprising a variety of anionic and/or cationic species. The building ions are large and non-symmetric with low lattice energies, thus, low melting points. Usually, they comprise a quaternary ammonium salt complexed with a metal salt or a hydrogen bond donor, which leads to charge delocalization and subsequent decrease in the melting point of the formed mixture.<sup>115</sup>

The general formula  $\text{Cat}^+\text{X}^- \cdot z\text{Y}$  can describe DESs, where  $\text{Cat}^+$  is an ammonium, phosphonium or sulfonium cation,  $\text{X}^-$  is a Lewis base, usually a halide anion, and  $\text{Y}$  is a Lewis or Brønsted acid. The complex anionic species are formed between  $\text{X}^-$  and  $\text{Y}$ , where  $z$  refers to the number of  $\text{Y}$  molecules that interact with the  $\text{X}^-$  anion.<sup>115</sup> Deep eutectic solvents are classified into five types, with the 5<sup>th</sup> one having recently been identified (Table 2).<sup>88</sup>

**Table 2.** Classification and general formula of deep eutectic solvents.

DES Classification	General Formula	Terms
Type I	$\text{Cat}^+\text{X}^- \cdot z\text{MCl}_x$	$\text{M} = \text{Zn, Sn, Fe, Al, Ga, In}$
Type II	$\text{Cat}^+\text{X}^- \cdot z\text{MCl}_x \cdot y\text{H}_2\text{O}$	$\text{M} = \text{Cr, Co, Cu, Ni, Fe}$
Type III	$\text{Cat}^+\text{X}^- \cdot z\text{RZ}$	$\text{Z} = \text{CONH}_2, \text{COOH, OH}$
Type IV	$\text{MCl}_x + \text{RZ} = \text{MCl}_{x-1}^+ \cdot \text{RZ} + \text{MCl}_{x+1}^-$	$\text{M} = \text{Al, Zn}; \text{Z} = \text{CONH}_2, \text{OH}$
Type V	Non ionic	-

The first three types contain a quaternary ammonium salt as one of the constituents of the DES. In the case of Type I, the salt is combined with anhydrous metal chloride and in the case of Type II, with a hydrated metal chloride. When the quaternary ammonium salt (hydrogen bond acceptor) is combined with a hydrogen bond donor, which is typically a small organic molecule, the formed DES is categorized as Type III. In Type III, a phosphonium salt can also serve as a hydrogen bond acceptor. Type IV DESs comprise a hydrated metal chloride and an organic hydrogen bond donor.<sup>116</sup> The most recently identified Type V is made up of non-ionic hydrogen bond donors and hydrogen bond acceptors.<sup>88</sup> When the DESs comprise natural compounds, i.e., primary metabolites, such as sugars, amino acids, organic acids and choline derivatives, the term natural DESs (NADESs) is sometimes used to characterize them. In fact, not only the building ingredients of the NADES but also their deep eutectic mixtures have been observed in plants.<sup>117</sup>

The characterization “deep” has been attributed in order to specifically describe eutectic mixtures that exhibit a eutectic temperature much lower than the thermodynamically predicted for an ideal liquid mixture; thus, a clear differentiation between eutectic mixtures and DESs should be made. The decline in temperature should be defined as the difference ( $\Delta T_2$ ) between the ideal ( $T_{e,\text{ideal}}$ ) and the real ( $T_E$ ) eutectic point and not as the difference ( $\Delta T_1$ ) between the linear combination of the melting points of the pure components and the real eutectic point ( $T_E$ ) (Figure 8).<sup>118</sup> A common misconception encountered in literature is that the DES composition is defined by the mixing ratio of the building components, pointing to the erroneous perception that the eutectic point composition is somehow connected to the formation of a complex. However, this is not the case; the intersection of the melting curves that are dominated by the fusion properties account for the eutectic composition and not the stoichiometry between the hydrogen bond donor and the hydrogen bond acceptor. By doing away with the stoichiometric notion for the DES formation and rather viewing it for what it is, i.e., a mixture and not a fixed composition complex, an extra degree of freedom is incorporated in the definition of DES; any mixture with compositions between  $x_1$  and  $x_2$  (Figure 8) can be considered as a DES, thereby relaxing the fixed stoichiometric proportions.<sup>118</sup>

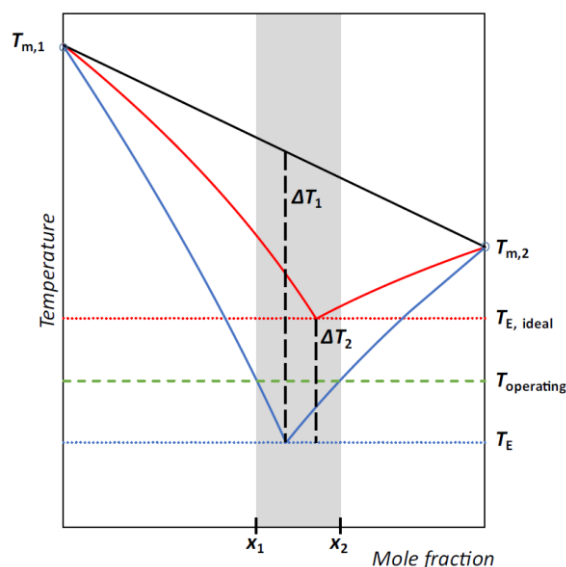


**Figure 8.** Schematic representation of the comparison of the solid-liquid equilibria of a simple ideal eutectic mixture (red line) and a deep eutectic mixture (blue line).<sup>118</sup>

Interestingly, apart from the depression in the melting point, a depression in the freezing point of the mixtures is also observed when an acid is used as hydrogen bond donor. Additionally, there seems to be a reverse correlation between the freezing point depression and the molecular weight of the employed acid, i.e., the lower the molecular weight the higher the depression of the freezing point. This phenomenon is dependent on the lattice energies of the individual DES components, which are related to the interaction of the anion with the hydrogen bond donor; therefore, the depression of the freezing point is a measure of the entropy change that results from the formation of the liquid.<sup>119</sup>

It is worth mentioning that the amount of H<sub>2</sub>O added to a DES can impact its structure; however, in choline-based DESs, it has been reported that the solvophobic sequestration of H<sub>2</sub>O into nanostructured domains around cholinium cations enables retention of the DES nanostructure at H<sub>2</sub>O content up to 50% (w/w). Any further dilution beyond this point leads to the formation of an aqueous solution that contains the free forms of the individual components.<sup>120</sup> Of note, is also the observation pertaining to choline-based DESs that working temperatures exceeding 80 °C are to be avoided to prevent the progressive degradation of the DES.<sup>121</sup>

Deep eutectic solvents have gained the attention of researchers due to their properties, such as low toxicity and low vapor pressure, which render them ideally suited to replace commonly used organic solvents, and simple tuning of their properties, by variation in their individual building components or their respective mixing ratio. Additionally, their comparably low price and biodegradable nature make them both financially desirable and environmentally compatible.<sup>122</sup> Specifically, DESs comprising the quaternary ammonium salt choline chloride and a hydrogen bond donor (DESs type III), have been employed in a wide range of applications due to their versatile nature. The simplicity of their preparation, low reactivity with water, biodegradability and low cost along with their wide solvation range and tunability of their properties, which is largely attributed to the large number of available hydrogen bond donors, render these DESs particularly interesting.<sup>115</sup> With respect to metal extraction, choline-based DES applications have, among others, been reported in the extraction of rare earth elements from magnets,<sup>123</sup> the selective extraction of transition metals from mixed metal oxide matrices,<sup>124</sup> and the extraction of metal traces from barley,<sup>125</sup> while *para*-toluenesulfonic acid-based DESs have demonstrated the ability to solubilize metal oxides.<sup>126</sup>



### 2.3 Ionic liquids and deep eutectic solvents: similarities and differences

Deep eutectic solvents are considered by many scientists to be simply a subclass of ILs; thus, the two terms are many times used interchangeably, albeit erroneously. Although it is a fact that many similarities between DESs and ILs can be detected, at the same time, there are many distinctive differences between the two types of compounds. An overview of the different as well as the common features that DESs and ILs share are presented in Figure 9.

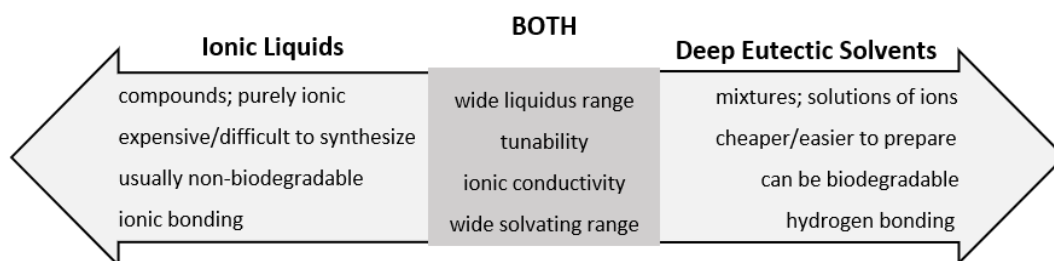


Figure 9. Similarities and differences of deep eutectic solvents and ionic liquids.<sup>127,128</sup>

A very distinctive way in which they differ is the nature of the starting materials as well as their formation. As it was already discussed in the previous paragraphs, ILs comprise organic cations and organic or inorganic anions, while DESs are made up of hydrogen bond donors and acceptors.

Since ILs are compounds and DESs are mixtures, it can be inferred that their preparation will be different, as is indeed the case. Ionic liquids are typically synthesized in a 2-step process; first, quaternization of the starting compound (e.g., imidazole, amine) with an alkyl halide which affords the respective cation and, second, formation of the IL, either by reaction with a Lewis acid or exchange of the halide anion for the desired one.<sup>129</sup> On the other hand, the formation of DESs is much simpler; the building components are mixed together and heated at mild temperature until complete liquefaction of the mixture is achieved.<sup>130</sup>

The synthetic procedure of ILs requires the use of several reagents and organic solvents, while by-products and waste are generated. The yields of the obtained ILs can vary and the product may require further purification steps. None of these problems is present in the case of DESs where 100% efficiency and 100% atom economy is achieved.<sup>128</sup>

The melting point of ILs is below 100 °C, whereas the melting point of DESs is defined more arbitrarily as being simply below the melting point of each individual constituent. Additionally, ILs are usually stable at larger temperature ranges than DESs. With respect to their financial aspect, DESs are usually cheaper to produce since the cost of their components is lower than those used in ILs.<sup>131</sup>

Generally, DESs are considered to be a better option than ILs with regard to environmental impact, since their components can be of natural origin, therefore are of higher biodegradability and lower toxicity. In contrast, ILs are made up of -onium salts which can be highly toxic,<sup>128</sup> as is discussed in detail in the next chapter. Nevertheless, arbitrary generalizations of this type should be avoided and only judgement for specific cases should be made with respective data to support it. Both ILs and DESs are highly tunable, meaning a number of different starting compounds can be combined and many different products/mixtures can be generated, which means that any unsustained claims about toxicity and biodegradability are completely senseless.

Most DESs are characterized by conductivities below 2 mS·cm<sup>-1</sup> at RT. This can be attributed to their highly viscous nature, thus, naturally, the conductivity increases with increasing temperature, since the viscosity

is reduced in this case. The conductivity can also be influenced by variation in the mixing ratio of the DES components.<sup>130</sup> For imidazolium-based ILs, it has been demonstrated that their aqueous solutions exhibit higher conductivities (92-98 mS-cm<sup>-1</sup> at RT) than their solutions with other molecular liquids (18-30 mS-cm<sup>-1</sup> at RT) and naturally their conductivity increases with increasing temperature, i.e., decrease in viscosity.<sup>132</sup>

Both ILs and DESs have the tendency to absorb water, which can act both as a hydrogen bond donor and a hydrogen bond acceptor owing to its high polarity.<sup>133,134</sup> The water added in DESs can be incorporated in their structure, thus, it is also possible to form DESs with the hydrated forms of their components. However, when the hydrated forms are used, they do not necessarily form a DES in the same range of molar composition as their anhydrous counterparts and the liquid range of the DES differs according to its water content.<sup>133</sup> When it comes to ILs, the interaction of the IL with water depends on the water content. It was demonstrated with the aid of three imidazolium-based ILs, that water molecules are dispersed within the IL and bind with its ions when the water concentration is very low. As the water concentration increases, the interaction between the water molecules is favored leading to formation of water aggregates. Interestingly, thermodynamic data indicate that the water-anion interactions have a very weak impact on the weakening of the ion-ion interactions of the IL.<sup>135</sup>

Numerous studies so far have addressed the recovery of PGMs with the aid of ionic liquids. On the contrary, no publication thus far has addressed their recovery by employing DESs, as literature search has revealed; the first application is reported in this thesis. In the following chapter, the existing literature data on PGM recovery with ILs will be discussed in detail.

### 3 Ionic Liquids in Platinum Group Metal Recovery

State-of-the-art recovery/recycling processes salvage a considerable amount of PGMs that would otherwise be discarded. Nevertheless, the demand outweighs the available supply. Additionally, there is still a significant detriment to the environment associated with the used chemicals and overall employed conditions, while, at the same time, maximum recovery efficiencies are not achieved. In addition, the processes themselves have major drawbacks that hamper their efficient application.<sup>46</sup> Regardless of the origin of the waste material, all PGMs and most notably Rh are extremely challenging to extract and to separate due to their inert nature coupled with their remarkably complicated chemistry and complexation behavior in solutions, which up to date has not been fully explored and understood, as can be deduced by conflicting literature data.<sup>2,72</sup> Specifically, in the vast majority of reported research, PGMs are encountered in HCl solutions, where they form a number of chlorocomplexes that vary depending on the solution composition.<sup>69</sup>

Ionic liquids face the same recovery challenges with commonly used solvents due to the complexity of PGMs, but they have the potential for extraction and separation under significantly milder process conditions, thus, the probability to contribute to the reduction of the negative environmental impact and conservation of energy resources.<sup>136</sup> Consequently, a broad pool of opportunities exists for the application of ILs for the recovery of PGMs. In the following chapter, different strategies for the recovery of PGMs employing ILs are discussed. While liquid-based separations typically involve the use of ILs as solvents or selective extractants, solid-based separations may include materials, such as (i) resins, (ii) capsules, (iii) membranes, and (iv) nanoparticles as support, as summarized in Figure 10.

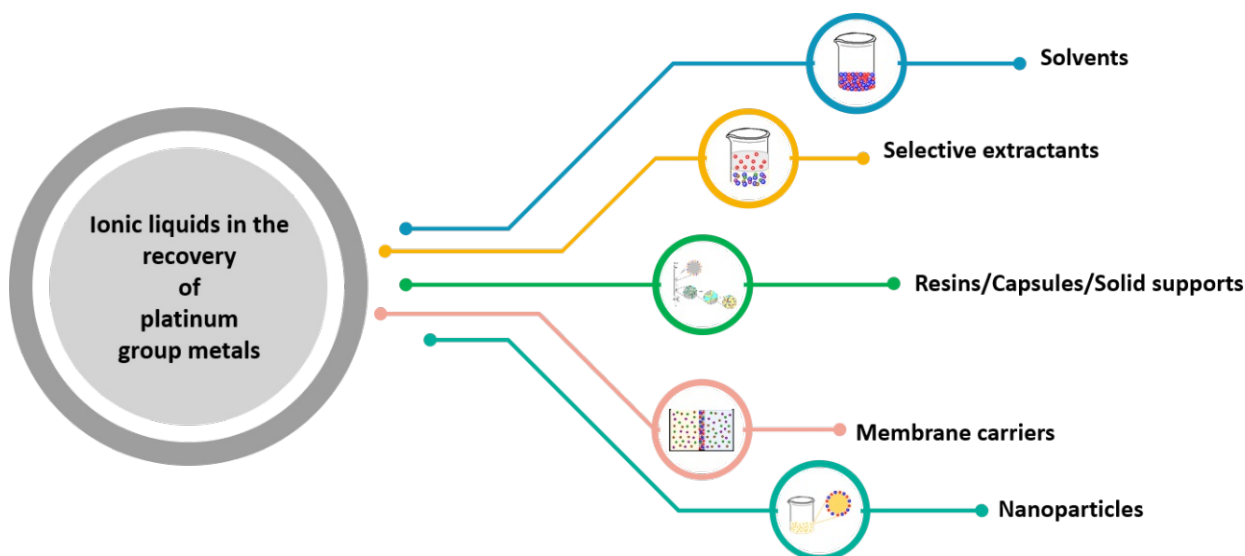


Figure 10. Application of ionic liquids in platinum group metal recovery.

### 3.1 Ionic liquids in liquid-liquid separations

In the liquid-based separations the following distinctions, as also noted by Gras et al.<sup>137</sup> and further expanded here, are made (Figure 11):

- selective extraction through the interaction of the IL anion (pure IL or diluted with organic solvent(s)) with the target metal (anion exchange or/and coordination) (Type A),
- ILs function as solvents in combination with conventional extracting agents (Type B),
- IL mixtures where one IL acts as a selective extractant and the other as solvent (Type C),
- task-specific ILs with a targeted functionality for complexation (Type D), and
- thermomorphic ILs with temperature-dependent phase behavior (Type E).

Due to the large number of ILs used as solvents for liquid-based separations (Type A and B), the conducted research is classified and presented according to the chemical structures of the employed ILs, i.e., ammonium, imidazolium, phosphonium, pyridinium and guanidinium-based ILs, while task-specific and thermomorphic ILs are addressed as separate categories. The PGM extraction conditions and results that will be discussed are summarized in tables that appear in each section. The type (A-E) of each IL is clearly stated in the respective table.

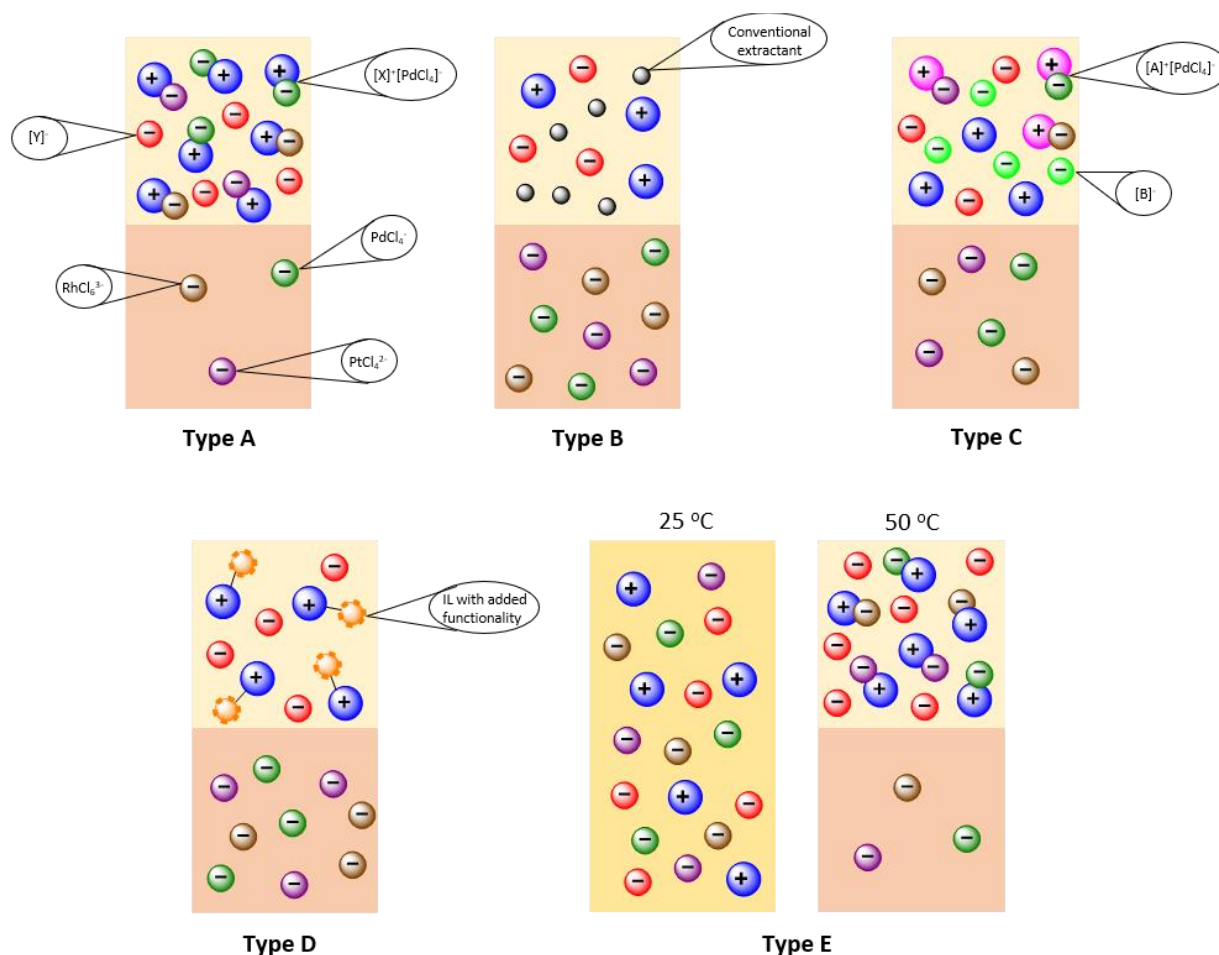


**Figure 11.** Categorization of ILs in liquid-based separations within the current chapter. Type A: selective extractants through IL anion, Type B: solvents combined with extracting agent, Type C: IL mixtures where one acts as extractant and the other as solvent, Type D: functionalized for a specific task and Type E: thermomorphic ILs (A, X = IL cation, B, Y = IL anion). Note: both aqueous and IL phases have the same net charge before and after separation. Due to space constraints and in order to avoid overloading of the figures, the charge-balancing ions have been omitted in the graphs. Electroneutrality is implied (detailed explanation is provided in the section where extraction mechanisms are discussed).

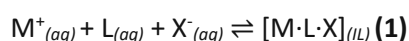
### 3.1.1 Extraction mechanisms of metals to ionic liquids

Before proceeding with the discussion of the work that has been performed on PGM extractions with ILs, it would be very important to address some mechanistic considerations. While in the majority of molecular solvents metals are extracted in the form of neutral hydrophobic metal-ligand complexes, the ionic character of ILs gives rise to different mechanistic processes. Unlike typical molecular solvents, ILs are capable of solvating ionic complexes; of course, the principle of electroneutrality cannot be violated, which implies concurrent transfer of the IL anion or cation components to the aqueous phase.

One might wonder where this unique capability of ILs could be attributed. Paradoxically, ILs are hydrophobic media despite their ionic character. It becomes, thus, immediately clear that conventional concepts used in molecular liquids, such as dipole moment, no longer apply. Ionic liquids mostly resemble molten salts, in the sense that charged solutes insert themselves in the molten salt structure, surrounding themselves with countercharges. Additionally, in their majority, ILs incorporate a cation with a charged head group and a long, neutral, usually aliphatic chain which is responsible for their inhomogeneity on a nanoscopic level. Their cationic charged head groups aggregate with anions forming strongly ionic clusters, while their aliphatic tails form a neutral aggregate, thereby, resulting in a medium that combines hydrophilic with hydrophobic domains. This inhomogeneous structure of ILs might as well explain the limited effect that water has on the polarity of ILs; water-saturated ILs retain their hydrophobic nature.<sup>138</sup>

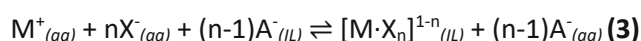
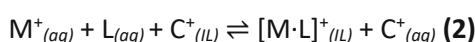
Electroneutrality, as already mentioned, is a principle that applies to IL mechanisms and when combined with the distinct possibility of solvation of charged complexes in the IL phase, it becomes apparent that multiple extraction mechanisms can occur in ILs. The mechanisms can be summarized as described below, where M denotes the metal, L represents a neutral ligand, C<sup>+</sup> and A<sup>-</sup> are the building ions of the IL and X signifies coordinating anions/cations that participate in the extraction process. Their location in the aqueous or IL phase, is denoted as “aq” and “IL”, respectively.

**Neutral extraction.** This mechanism resembles the typical extraction mechanism in molecular liquids; a neutral coordination complex is formed between the metal and the available ligand, which migrates to the IL phase. This can be represented by the following simplified way (equation 1):



The partitioning behavior of the formed complex is defined by its hydrophobic character and the hydrophobicity of the IL. Neutral extraction normally competes with ion exchange, however, when the cation of the IL has a pronounced hydrophobic character, the neutral extraction mechanism is the dominant one.<sup>138</sup>

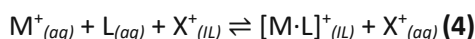
**Native ion exchange.** In this mechanism, the ion exchange entails component ions of the IL, thus, it is referred to as native. This mechanism can be represented by the following simplified equations, for cation exchange (equation 2) and anion exchange (equation 3), respectively:



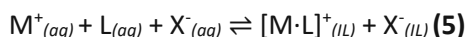
Quite interestingly, it has been experimentally demonstrated, that from a thermodynamic perspective, it is the solubility of the IL ion in the aqueous phase that propels the exchange rather than the coordination strength between the metal and the ligand. Of course, this leads to the highly undesirable effect of the degradation of the IL and the simultaneous contamination of the aqueous phase by IL ions (anions or cations).<sup>138,139</sup>

**Sacrificial ion exchange.** The issue of degradation of the IL and the contamination of the aqueous phase can be addressed with this approach. Specifically, a salt with ions more hydrophilic than the IL building

ions can be added to the IL phase. Since the ion exchange is thermodynamically controlled by the solubility of the ions in the aqueous phase, the salt ions will be “sacrificed” for the exchange and the IL will be spared degradation. This pathway can be described by the following simplified equation (equation 4):



**Neutral co-extraction.** A charged complex is formed, which migrates to the IL phase along with uncoordinated counterions, so that the electroneutrality principle is not violated. The mechanism can be described by the following simplified equation (equation 5):<sup>138</sup>



This mechanism has very important implications concerning the flexibility of neutral co-extraction as opposed to neutral extraction. While in neutral extraction the complex yield can be increased by increasing the concentration of the ligand or the  $X^-$ , its extraction is limited by its partition coefficient between the two phases (IL and aqueous). Additionally, the selected anion needs to be able to coordinate with the metal.

On the other hand, in neutral co-extraction, increasing the concentration of  $X^-$  can positively impact the extraction, since additional metal will be pushed to the IL phase. Furthermore, in this case, the anion does not coordinate to the formed complex, therefore, expanding the anion pool that can be employed in the extraction process.<sup>138</sup>

It should be noted here that, as Dietz and co-workers have proven experimentally,<sup>140</sup> the mechanistic pathway can be very much influenced by the hydrophobicity of the IL cation. Whether cation exchange or neutral extraction will take place, is something that can be controlled via cation hydrophobicity and, of course, a mixed extraction pathway is an additional distinct possibility. Cation exchange can be suppressed when highly hydrophobic cations are incorporated in the IL, shifting the mechanism toward neutral extraction.<sup>140</sup> The aqueous contamination associated with the cation exchange can, thus, be suppressed; however, high hydrophobic character of the cation comes with certain trade-offs. Long aliphatic chains, which are components of highly hydrophobic IL cations, are also toxic,<sup>139</sup> while an increase in hydrophobicity can lead to micelle formation through self-association of the IL.<sup>141</sup> The addition of ionizable ligands can further support the suppression of the ion-exchange mechanism when a hydrophobic IL cation is employed. It has been demonstrated that using dimer P-based ionizable ligands, promotes neutral extraction; the ionization of the extractants releases protons to the aqueous phase and produces neutral metal-ligand complexes that migrate to the IL phase.<sup>142</sup> Therefore, exploiting the hydrophilicity of the protons further favors neutral extraction. It should be pointed out, that both the pH of the aqueous phase as well as the identity of the acid employed in the process can impact the extraction pathway.<sup>143</sup>

The short discussion on the unique extraction mechanisms that are observed in IL media will allow a better insight into the conducted research that will be discussed in detail in this chapter. Additionally, it serves to highlight that a closer look and a deeper understanding of those mechanisms can provide researchers with a powerful toolbox that can be exploited in order to manipulate separation systems and affect their outcomes.

An excellent discussion on the topic of metal extraction to ILs is available in the literature by Janssen et al.<sup>138</sup> The experimental works of Dietz et al.,<sup>144,145</sup> Jensen et al.,<sup>146,147</sup> Visser et al.<sup>148,149</sup> and Janssen et al.<sup>150,151</sup> definitely deserve attention and can provide a profound insight into the mechanistic processes, while a thermodynamic perspective on the topic has been provided by Kobrak.<sup>152</sup>



### 3.1.2 Analyte partitioning in liquid-liquid separations

Liquid-liquid extraction can be described as an unequal distribution process of an analyte between two immiscible liquid phases originating from the different miscibility of the analyte in each liquid. This uneven distribution of the analyte can be expressed in a quantifiable manner with the aid of the distribution ratio (D).<sup>153</sup> According to the International Union of Pure and Applied Chemistry (IUPAC), the distribution ratio D is the ratio of the total analytical concentration of the target analyte in the organic phase ( $[A]_o$ , in all its chemical forms present) to its total analytical concentration in the aqueous phase ( $[A]_{aq}$ , in all its chemical forms present) measured at equilibrium (equation 6):<sup>154</sup>

$$D = [A]_o/[A]_{aq} \text{ (6)}$$

It is a measure of the efficiency of the extraction process, since it represents the analyte fraction in each phase; thus, the greater the value of D, the more analyte migrates to the organic phase.<sup>153</sup> D values that exceed 10 correspond to an extraction efficiency of the target analyte greater than 90.9%. On the other hand, when D is less than 1 the transfer of the target analyte to the organic phase is not favored. Distribution ratios as well as changes in their value can be determined accurately in the range 0.01-100.

Extraction efficiency (E) corresponds to the percentage of the analyte that migrates from the aqueous phase to the organic phase and it is the percentage ratio of the analyte that is extracted to the organic phase ( $[A]_o$ ) to the starting concentration of the analyte ( $[A]_s$ ) (equation 7):

$$\%E = ([A]_s - [A]_o)/[A]_s \times 100 \text{ (7)}$$

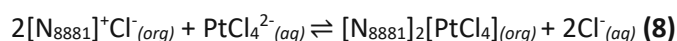
In the following detailed discussion of the available literature, the results will be reported in terms of %E and D, whenever both have been provided.

### 3.1.3 Liquid-liquid separations

#### 3.1.3.1 Ammonium-based ionic liquids

The PGM extraction conditions and results that will be discussed in the present section are summarized in Table 3.

Research on the potential of quaternary ammonium salt trioctylmethylammonium chloride (Aliquat 336) for Pt(II) extraction was already reported in 1985,<sup>155</sup> long before the tremendous increase in IL popularity. Mixing equal volumes of Aliquat in toluene with aqueous HCl model solutions of Pt, lead to its quantitative extraction in just 30 sec. The authors propose the anion-exchange mechanism for the extraction (equation 8):



Crucial factors are low HCl concentration (max. 0.1 M) and elevated temperature (60 °C) in order to maximize the loading of Pt in the IL. The authors mention that increasing HCl concentration negatively impacts the extraction; however, they, unfortunately, have not provided this data and they have not evaluated another  $Cl^-$  source, e.g., NaCl, to verify whether the  $Cl^-$  concentration is the decisive factor in the extraction efficiency, which is expected according to Le Chatelier's principle, if an anion-exchange mechanism is considered. The constructed extraction isotherm indicates that two stages are required for complete extraction of Pd, while the maximum loading of the IL is 9.8 M Pd. Recovery of Pt is feasible via stripping with  $Na_2HSO_3$  at 50 °C and, according to the respective isotherm, four stages yield complete stripping of Pd from the organic phase. The effect of heat on increasing both the extraction and the stripping capacity verifies the conclusions reached by the respective isotherms; both processes are endothermic.<sup>155</sup>

**Table 3.** Summary of PGM extraction conditions and results with ammonium-based ionic liquids.

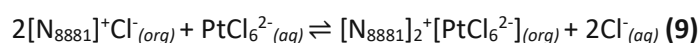
PGM Solution	Ionic Liquid (+ Diluent)	Ratio (O/A) <sup>a</sup>	Time (min) <sup>b</sup>	Extr. Efficiency (%) Distribution Ratio (D)	Type	Ref. No
6.5 mM Pt(II) in 0.1 M HCl	1% (v/v) Aliquat 336 in toluene <sup>c</sup>	1/1	0.5	99.5% Pt	A	155
10 mg/L Pt(IV) in 0.5 M NaCl, [H <sup>+</sup> ] = 0.02 M	4.0 mM Aliquat 336 in (dodecane + 4% dodecanol)	1/1	10	85% Pt	A	156
6.8 mg/L Pd(II), 13.1 mg/L Rh(III) in H <sub>2</sub> O (prepared from their chloride salts)	10% Aliquat 336 in benzene	1/1	5	100% Pd, 87.1% Rh	A	157
0.1 mM Pd(II) in 1.0 M HCl	5.0 mM Aliquat 336 + 10 mM LIX 65N in heptane/CHCl <sub>3</sub> (9:1)	1/1	240	95.6% Pd	B	158
100 mg/L Pd(II) in 1.0 M HCl	(2.0 mM Aliquat + 8.0 mM LIX 63) in 5% (v/v) 1-octanol in dodecane	1/1	30	100% Pd	B	159
0.16-1.2 μm/mL Pd(II) in 0.1 M sodium salicylate adjusted to pH 4.5-7	5% (w/v) Aliquat 336 in xylene	1/2.5	0.5	100% Pd	A	160
Pt(IV), Pd(II), Rh(III) in 1.0 M HCl	0.1 M Aliquat 336 in toluene	1/1	120	n.a.	A	161
Step 1 200 mg/L/metal: Au(III), Pt(IV), Pd(II) in 0.1 M HCl Step 2 Pt(IV), Pd(II) in 0.1 M HCl	Step 1 0.6 g/L Aliquat 336 in benzene Step 2 3 g/L Aliquat 336 in benzene	1/1	5	Step 1 99% Au, α <sub>Au/Pt</sub> =6800, α <sub>Au/Pd</sub> =3500, 3.5% Pt, 6.5% Pd Step 2 99% Pt, 100% Pd	A	162
1.0 mM Pd(II) in 1.0 M HCl	90% (v/v) 0.5 M Aliquat 336 in kerosene + 10% (v/v) 1-octanol	1/1	60	99.9% Pd, D <sub>Pd</sub> >1000	A	163
0.26 mM Pd(II) in 1.0 M HNO <sub>3</sub>	0.1 M [N <sub>8881</sub> ]Cl in CHCl <sub>3</sub> or 0.1 M [N <sub>8881</sub> ]NO <sub>3</sub> in CHCl <sub>3</sub> <sup>d</sup>	1/1	180	D <sub>[N<sub>8881</sub>]Cl</sub> > D <sub>[N<sub>8881</sub>]NO<sub>3</sub></sub>	A	164
0.5 mM/metal: Pt(IV), Rh(III) in 1.0 M HCl	0.01 M Aliquat 336 in kerosene	1/1	5	95% Pt, 3% Rh, α <sub>Pt/Rh</sub> >300	A	165
500 mg/LPt(IV), 28 mg/L Cr(III), 454 mg/L Mn(II), 950 mg/L Ni(II) in 3.0 M HCl	0.011 M Aliquat 336 in kerosene (x 2 contacts)	1/3	5	99.8% Pt, D <sub>Pt</sub> =100, β <sub>Pt</sub> =33000, 3% Ni, D <sub>Ni</sub> =0.1, 0% Cr, D <sub>Cr</sub> =0.01, 0% Mn, D <sub>Mn</sub> =0.01	A	166
349 mg/L Pt(IV), 59 mg/L Rh(III), 6701 mg/L Mg(II) in 1.0 M HCl	0.011 M Aliquat 336 in kerosene (x 2 contacts)	1/3.3	5	100% Pt, D <sub>Pt</sub> =3.4, 5.5% Rh, 0% Mg	A	167
5.0-7.0 g/L Pt(IV), Al(III), Fe(III) in aqua regia leach liquor	15% (v/v) Aliquat 336 in kerosene	1/1	15	99% Pt	A	168
4.0 mM/metal: Au(III), Pt(II), Pt(IV) in 0.1 M HCl	[N <sub>6666</sub> ][NTf <sub>2</sub> ] or [N <sub>8888</sub> ][NTf <sub>2</sub> ] <sup>c</sup>	1/4	i. 10 <sup>c</sup> ii. 1440 (24 h)	>95% Au, D <sub>Au</sub> >95, 0-2.5% Pt, D <sub>Pt</sub> <0.6	A	169
1.0-5.1 mM Pt(IV), 0.019-0.094 mM Pd(II), Na(I), Mg(II), K(I), Ca(II), Mn(II), Fe(III), Co(II), Ni(II), Cu(II), Zn(II), Ru(III), Rh(III), Cd(II) in 0.1 M HCl	10% (w/w) [N <sub>888</sub> ][NO <sub>3</sub> ] saturated with H <sub>2</sub> O in [N <sub>888</sub> ][NTf <sub>2</sub> ]	1/2	15	92.5% Pt, D <sub>Pt</sub> =24.7, 99.8% Pd, D <sub>Pd</sub> =803, 10.5% Cu, 4.9% Ru, 4.6% Rh, <2% each of the rest, D <sub>(Cu, Ru, Rh, rest)</sub> <0.25	C	170
0.074-0.054 mM Pt(IV), 0.1-0.73 mM Pd(II), 0.097 mM Rh(III), 0.11 mM Fe(III), 0.098 mM Cu(II), 0.1 mM Ni(II), 0.096 mM Zn(II), 0.01 mM Co(II), 0.11 mM Mn(II) in 0.1 M HCl	[N <sub>888</sub> ][NO <sub>3</sub> ] saturated with H <sub>2</sub> O	1/100	15	91% Pt, D <sub>Pt</sub> =960, >99% Pd, D <sub>Pd</sub> =24000, 50% Zn, D <sub>Zn</sub> =98, 11% Fe, D <sub>Fe</sub> =13, 13% Rh, D <sub>Rh</sub> =15, <10% each of the rest, D <sub>(Cu, Ni, Co, Mn)</sub> <10	A	171



0.02 M Rh(III) in 0.01 M HNO <sub>3</sub>	50% CMPO in [(CH <sub>3</sub> ) <sub>3</sub> NCH <sub>2</sub> CH <sub>2</sub> OMe][NTf <sub>2</sub> ]	1/1	60	94% Rh, D <sub>Rh</sub> =16.9	B	172
0.5 mM/metal: Pt(IV), Rh(III) in 0.1 M HCl	50 mg/mL [N <sub>8881</sub> ][HSO <sub>4</sub> ] in toluene or CH <sub>2</sub> Cl <sub>2</sub>	1/5	10	100% Pt, β <sub>Pt/Rh</sub> =267.5, 7% Rh	A	173
0.2-3.5g/L/metal: Pt(IV), Pd(II), Au(III), Rh(III) in 6.0 M HCl	1.75 M [N <sub>8881</sub> ]I water saturated	1/1	60	100% Pt, β <sub>Pt/Rh</sub> >1000, 100% Pd, β <sub>Pd/Rh</sub> >1000, 100% Au, β <sub>Au/Rh</sub> >1000, 12% Rh	A	174

<sup>a</sup> O= organic phase, A= aqueous phase. <sup>b</sup> All extractions were performed at RT. <sup>c</sup> Performed at 60 °C. <sup>d</sup> Performed at 30 °C.

Later on, another extraction and stripping procedure for Pt(IV) employing Aliquat 336 was developed by a different research group.<sup>156</sup> Aliquat 336 in dodecane modified with 4% dodecanol extracted >80% Pd from its aqueous model solution within 10 min. The H<sup>+</sup> concentration of the aqueous phase was kept low (0.02 M) while the ionic strength was adjusted to 0.5 M by addition of NaCl in the solution. Anion exchange is assumed (equation 9), while the independency of the distribution ratio from the concentration of Pt is experimentally verified (Figure 12).



To avoid the formation of IL aggregates in the organic solvent, the concentration of Aliquat was kept at low levels (<6.0 mM). A solution of NaClO<sub>4</sub> was established as an effective stripping agent for quantitative Pt removal. The developed system was implemented on a solid-supported liquid membrane which can transport Pt ions with the IL acting as the carrier. This application is discussed later in this chapter.<sup>156</sup>

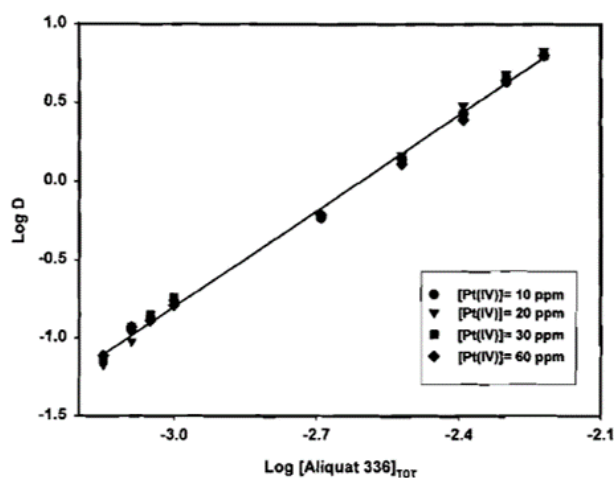


**Figure 12.** Experimental data of distribution ratio for Pt(IV) at different concentrations. Ionic strength 0.5 M, 0.02 M H<sup>+</sup>.<sup>156</sup>

Campbell<sup>157</sup> investigated the extraction of Pd and Rh with Aliquat 336 from the HNO<sub>3</sub> solution used in the treatment of spent nuclear waste, in which they are encountered in a complex nitrite form (presumably Na<sub>2</sub>[Pd(NO<sub>2</sub>)<sub>4</sub>], Na<sub>2</sub>[Pd(NO<sub>2</sub>)<sub>6</sub>], Na<sub>3</sub>[Rh(NO<sub>2</sub>)<sub>6</sub>]).<sup>157</sup> In the PUREX process, Pu and U are extracted with HNO<sub>3</sub> from the spent nuclear waste and the recovered waste solution is further treated. Fine-tuning of several extraction parameters is essential to maximize their recovery.<sup>175</sup> Simultaneous optimum extraction for both metals is feasible at pH 8, which is adjusted by addition of H<sub>2</sub>SO<sub>4</sub> or NH<sub>4</sub>OH. The amount of Aliquat used as well as the organic diluent additionally play a role in the extraction yield. The complete amount of Pd and 87.1% of Rh can be accessed by a 10% Aliquat in benzene solution. Temperatures below RT (9 °C) allow the quantitative extraction of Rh, however, in radiation-controlled atmospheres retention of low temperatures is hindered. Separation of Pd and Rh is attainable via a selective stripping process; removal of Rh with NH<sub>4</sub>NO<sub>3</sub> followed by stripping of Pd with a NH<sub>4</sub>SCN/NH<sub>4</sub>OH mixture.<sup>157</sup>

Significant acceleration in the extraction rate of Pd(II) from its model solutions is observed when Aliquat 336 is combined with LIX 65N. Simultaneous occurrence of two different reactions in the presence of Aliquat can explain the observed 9-fold increase in the rate;  $\text{PdCl}_4^{2-}$  reacts with LIX 65N in the aqueous phase and also forms an ion pair with the Aliquat cation into the organic phase where it reacts and forms Pd-LIX complexes, thus, releasing Aliquat which extracts again Pd-chlorocomplexes. The extraction yield is also significantly increased by addition of Aliquat, reaching almost quantitative level.<sup>158</sup>

The synergistic effect of Aliquat 336 with the anti-isomer of 5,8-diethyl-7-hydroxy-6-dodecanone oxime (LIX 63<sub>anti</sub>) was exploited in order to accelerate the extraction rate of Pd(II) from its aqueous model solutions. LIX 63 demonstrates capacity for quantitative extraction of Pd within a 2 h time frame, whereas Aliquat 336 does not seem to extract more than 50% of Pd. Nevertheless, the association of the two extractants leads to a dramatic acceleration of the extraction rate; 100% Pd in 10 min. LIX 63 functions as a solvating agent, while the extent of synergism is proportional to the concentration of Aliquat 336. The constructed distribution isotherms clearly indicate the impact of the synergistic effect, which becomes more significant at higher Aliquat concentrations (Figure 13).

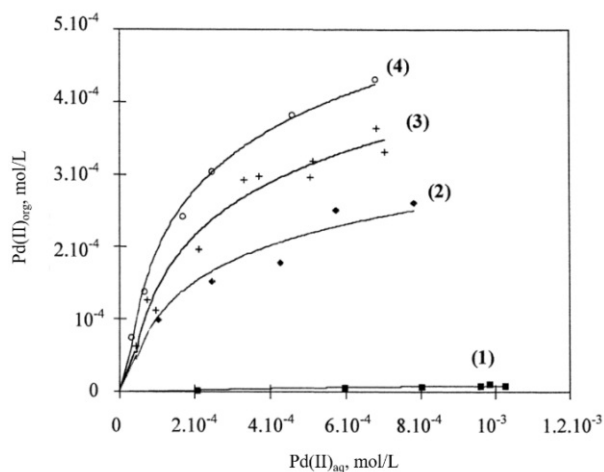
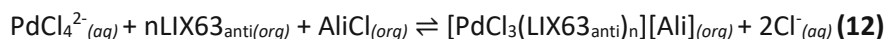


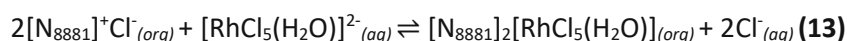
**Figure 13.** Distribution isotherms of Pd at 25 °C. Aqueous phase:  $10^{-4} \leq \text{Pd(II)} \leq 1.5 \cdot 10^{-3}$  mol/L, organic phase: (1)  $5 \cdot 10^{-4}$  mol/L Aliquat 336, (2)  $10^{-3}$  mol/L LIX 63<sub>anti</sub>, (3)  $2.5 \cdot 10^{-4}$  Aliquat 336 +  $10^{-3}$  mol/L LIX 63<sub>anti</sub> and (4)  $5.4 \cdot 10^{-4}$  Aliquat 336 +  $10^{-3}$  mol/L LIX 63<sub>anti</sub>.<sup>159</sup>

Relying on distribution isotherms and UV-Vis data, the authors demonstrated that, in addition to the formed  $[\text{PdCl}_4][\text{Ali}_2]$  and  $[\text{PdCl}_2][(\text{LIX63}_{\text{anti}})_2]$  complexes, it is the mixed species  $[\text{PdCl}_3(\text{LIX63}_{\text{anti}})_n][\text{Ali}]$  that largely contributes to the observed increase in the extraction rate (equations 10-12).<sup>159</sup>



Quantitative extraction of Pd(II) with the aid of Aliquat 336 (5% in xylene) from sodium salicylate model solutions has been reported.<sup>160</sup> The extraction is assumed to take place via an ion-pair formation between Aliquat and the palladium-salicylate complexes. Only 30 sec are required for complete Pd extraction and in order to maximize the extraction efficiency the pH of the solution should be maintained in the range 4.5-7.0. Separation of Pd from its binary synthetic mixtures with Ni, Co, Cu, Zn and Mn is possible by stripping the interfering metal ions with H<sub>2</sub>O. Quantitative Pd extraction from Pt ores and Pd catalysts, previously brought into solution via digestion, was successfully performed.<sup>160</sup>

The quantitative extraction of Pt and Pd from their respective aqueous model solutions with Aliquat 336 has been reported,<sup>161</sup> as well as its ability for partial Rh extraction. Mixing equal volumes of aqueous PGM solutions with Aliquat 336 in toluene is sufficient to yield these results in a time frame of 2 h, at RT. The difference in the extraction yields between Pt, Pd and Rh, can be interpreted if the extraction mechanism is taken into account which is anion exchange of the Cl<sup>-</sup> of the extractant and the anionic PGM-chlorocomplexes. While in the employed 1.0 M HCl solution Pt and Pd are present as pure chlorocomplexes, various complex species of Rh are found, based on the authors' calculations, and among them only the partially aquated and most labile, i.e., [RhCl<sub>5</sub>(H<sub>2</sub>O)]<sup>2-</sup>, is partially extracted to the organic phase, as UV-Vis measurements indicate. The authors proposed the following exchange equation for Rh (equation 13):



and they established the inverse relationship between Cl<sup>-</sup> concentration and distribution ratio of Rh (Figure 14).<sup>161</sup>

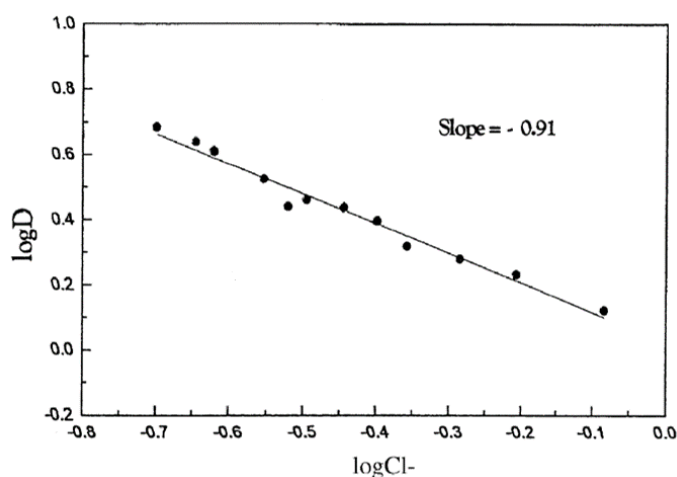
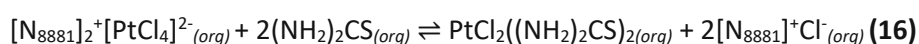
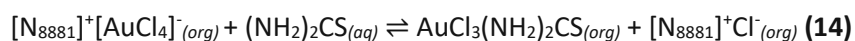


Figure 14. Experimental data of distribution ratio for Rh at different Cl<sup>-</sup> concentrations.<sup>161</sup>

Interestingly, the ability of Aliquat 336 to separate Au(III), Pt(IV) and Pd(II) from their model mixtures by simply tuning the extraction parameters has been proven. A combined metal solution adjusted at pH 1 and an organic phase consisting of 0.6 g/L Aliquat in benzene is the optimum for selective and quantitative extraction of Au, while negligible amounts of Pt and Pd are extracted. Presumably, the lower charge density of the AuCl<sub>4</sub><sup>-</sup> species, formed at this pH, makes this Au species more favorable to ion exchange than PdCl<sub>4</sub><sup>2-</sup> and PtCl<sub>6</sub><sup>2-</sup>. Complete recovery of Pt and Pd remaining in the aqueous solution is attained by simply increasing the concentration of Aliquat to 3 g/L, which serves as a further verification of the initial assumption that Au has binding priority with Aliquat; once more amount of Aliquat is added to the solution, more binding sites become available for the extraction of Pt and Pd. Selective stripping enables their consequent separation; 2 M NaOH removes 99% Pd, whereas 1.0 M thiourea in 2.0 M HCl removes Pt, yielding solutions with a purity of 99% and 95%, respectively. Concerning recovery of Au, 1.0 M HNO<sub>3</sub> scrubs traces of Pt and Pd from the organic phase, while 0.05 M thiourea in 0.1 M HCl affords a Au solution of 99% purity. During stripping, the IL is regenerated as follows (equations 14-16):



Recovery and reuse of the IL is feasible, for at least four cycles, without any loss in performance. A comprehensive flowsheet of the developed process has been constructed by the authors.<sup>162</sup>

A recovery process of Pd(II) from Aliquat 336 devoid of acidic media has been proposed as an industrial friendly approach that can minimize costly equipment corrosion. Quantitative extraction of Pd from HCl model solutions was performed with equal volumes of an Aliquat/kerosene/1-octanol mixture. As numerous authors have reported, adjusting the HCl concentration at a certain level (1.0 M in this particular system) is essential in order to maximize the extraction of the target metal. We should point out once more, that when an ion-exchange mechanism is involved in the extraction, then the observed changes in extraction capacity can be attributed to the changing concentration of Cl<sup>-</sup> and not H<sup>+</sup>. Stripping efficiency of >99% could be reached with 0.5 M thiourea in 0.5 M HCl. Replacing HCl with NH<sub>4</sub>Cl had no impact on the result, thus, indicating that stripping can be successfully performed in environments of neutral pH level.<sup>163</sup>

Difference in the extraction behavior of Pd(II) from HNO<sub>3</sub> model solutions by Aliquat 336 ([N<sub>8881</sub>][Cl]) and Aliquat 336N ([N<sub>8881</sub>][NO<sub>3</sub>]) have been noted. The distribution ratio of Pd in Aliquat 336 sharply decreases when the HNO<sub>3</sub> concentration exceeds 0.1 M, which is assumed to be a direct result of the strong complexing capacity of the Cl<sup>-</sup> anions present in Aliquat 336 that allows extraction at low HNO<sub>3</sub> concentrations. In the case of Aliquat 336N, a gradual increase, which peaks at 1.0 M, followed by a gradual decrease is observed (Figure 15). This could be attributed to extraction of the nitrate ions from HNO<sub>3</sub>. The authors assume the following extraction mechanism (equation 17):<sup>164</sup>

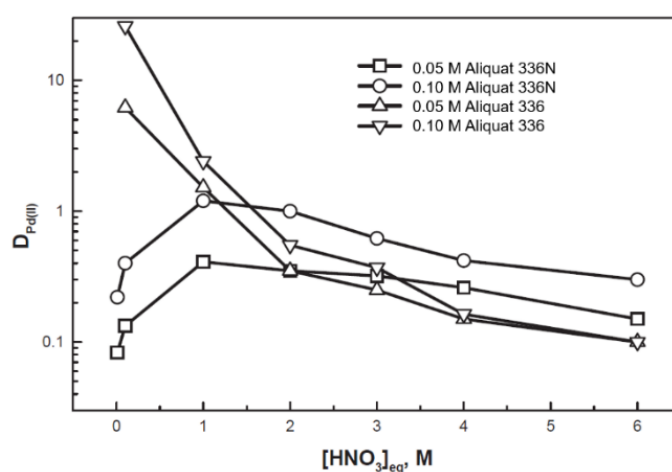
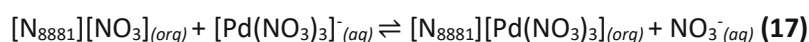


**Figure 15.** Experimental data of distribution ratio for Pd(II) at different HNO<sub>3</sub> concentrations. 0.26 mM Pd(II), T=30 °C, 3 h.<sup>164</sup>

The dependency of the distribution ratio of HNO<sub>3</sub>-based solutions of Pd on the employed solvent in its extraction with Aliquat 336N has been noted. For the experimentally studied system, the distribution ratio increases in the order decanol < decane + 10% decanol < butylbenzene < dichlorobenzene < diethylbenzene < *p*-xylene < benzene < toluene, while when hydrogenated pentapropylene, decane, dodecane or isooctane are used the formation of a third phase is observed.<sup>176</sup>

The extraction and separation of Pt(IV) and Rh(III) co-existing in acidic model solutions was investigated with the aid of Aliquat 336 mixed in kerosene. Various parameters were modified in order to evaluate their effect on the extraction behavior of Aliquat 336. Maximum extraction is obtained within a 5 min contact time and no increase is observed with additional contact time. There is a considerable increase in Pd yield to a nearly quantitative level when the acidity of the aqueous solution is increased, whereas

the opposite effect is observed on the extraction of Rh. Therefore, increasing acidity benefits the separation of the two metal ions. Even though the authors do not provide a plausible explanation and assume a combined solvation/ion-exchange mechanism, we should take into account the speciation; at higher acidities the more extractable species  $\text{PtCl}_6^{2-}$  and the less extractable  $\text{RhCl}_6^{3-}$  are formed, which could account for the observed behavior. The extraction for both Pt and Rh as well as their separation efficiency increases with increasing amount of Aliquat 336. Further, higher temperatures lead to the dehydration of the formed metal species which induces an increase on the extraction efficiency. Repeated contacts of the organic phase with an aqueous Pd solution verified the high loading capacity of Aliquat 336 (Figure 16). An acidified thiourea solution is efficient in stripping Pd completely from the organic phase, which can be reused for subsequent extractions. Ten successive extraction and stripping cycles were performed without any loss observed in the performance of the extractant mixture.<sup>165</sup>

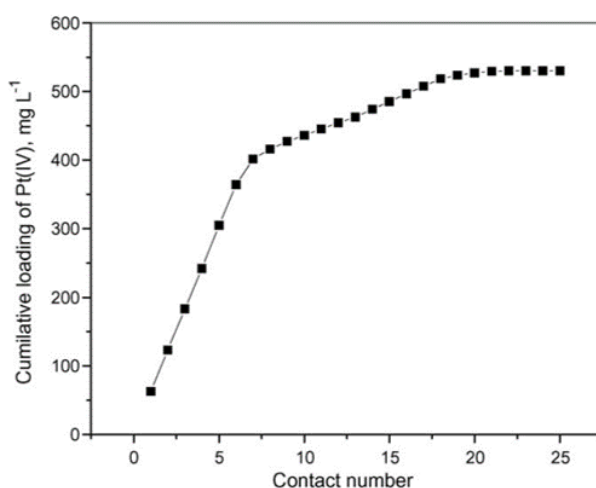


**Figure 16.** Loading capacity of Aliquat 336. 5.0 mM Pt(IV), 5.0 mM Aliquat 336, 1.0 M HCl.<sup>165</sup>

A complete scheme for the separation and recovery of Pt and Pd from a synthetic solution simulating a spent car catalyst leach liquor was developed (Figure 17). The acidic liquor contained Pd, Pt, Mn, Ni, Fe and Cr in 3.0 M HCl. Pd is quantitatively removed with tri-*n*-butyl phosphate ( $D_{\text{Pd}}=100$ ,  $D_{(\text{Pt},\text{Mn},\text{Ni},\text{Fe},\text{Cr})}\leq 1$ ,  $\beta_{\text{Pd}}=470000$ ) and Fe is precipitated with addition of an alkali solution. Contacting the Pd- and Fe-free synthetic feed solution with Aliquat 336 in kerosene, results in complete and selective removal of Pt leaving the other metals in the raffinate. Extraction isotherms, obtained by contacting the feed solution and the organic phase at different ratios, show that a two-stage extraction is required for quantitative Pt removal. Stripping of the extracted Pt is quantitatively performed with acidified thiourea and is attainable at two stages, as the isotherm indicates and experimental data prove.<sup>166</sup>

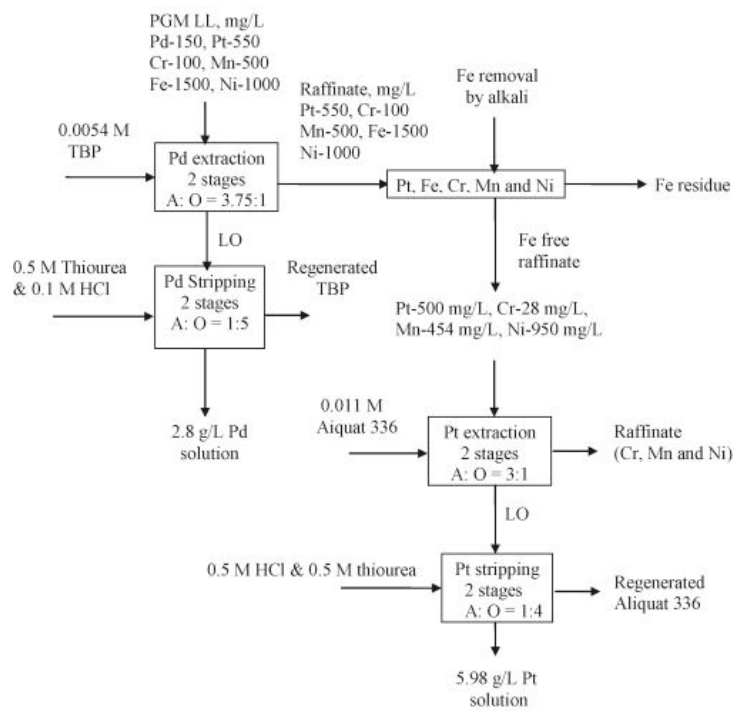


**Figure 17.** Flowsheet of the developed process for the separation and recovery of Pt and Pd from simulated spent car catalyst leach liquor.<sup>166</sup>

The authors developed an additional process to demonstrate the separation of Pt and Rh from a synthetic feed. The solution simulates the leachate obtained from the processing of LCD glass manufacturing scrap and contained Pt, Rh, Al, Mg and Fe in HCl < 1.0 M. Initially, addition of  $\text{Na}_3\text{PO}_4 \cdot 12\text{H}_2\text{O}$  quantitatively precipitated Al and Fe. Removal of metal impurities is followed by selective and quantitative extraction of Pt in Aliquat 336/kerosene from which it can be subsequently scrubbed with acidified thiourea. The authors constructed the McCabe-Thiele plot which demonstrates complete Pd extraction in two stages (Figure 18). A basification, heating, washing and drying process recovers pure Rh ( $\text{Rh}_2\text{S}_3$ ) from the remaining raffinate. A flowsheet detailing the separation process was constructed by the authors.<sup>167</sup>

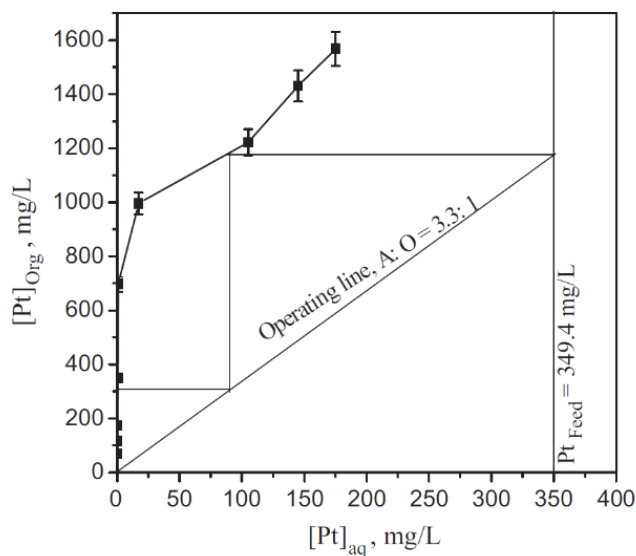
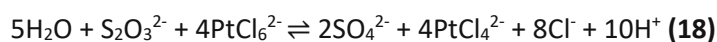


**Figure 18.** McCabe-Thiele plot for Pt extraction. Aqueous phase: 349 mg/L Pt, 59 mg/L Rh, 6701 mg/L Mg, pH 3.4, organic phase: 0.01 M Aliquat 336 in kerosene.<sup>167</sup>



The impact of different organic diluents on the extraction and separation capacity of trioctylammonium hydrogen sulfate ( $[N_{888}][HSO_4]$ ) toward Pt and Rh from their model mixtures has been investigated. Toluene and dichloromethane were the evaluated diluents for the synthesized  $[N_{888}][HSO_4]$ . Both diluents afforded 100% extraction of Pt within the first 10 min of contact of the organic and aqueous phase (1:5 mixing ratio), whereas extraction of Rh was 7% and dropped to 3% by extending the separation time to 20 min. It is concluded that the IL used is highly effective for the separation of Pt and Rh, regardless of the organic diluent employed.<sup>173</sup>

A selective extraction process relying on Aliquat 336 for the recovery of Pt(IV) from spent car catalyst leach liquor has been reported.<sup>168</sup> Only a small amount of Aliquat 336 mixed in kerosene (5% v/v) can fully extract Pt within 15 min from an equal volume of loaded *aqua regia* leach liquor (Pt, Al, Fe), exhibiting much higher loading capacity than commonly used extractants, also evaluated in the same study. While Pt is quantitatively removed from the liquor, no other metal is co-extracted under the employed conditions. Recovery of Pt from the organic phase is feasible via reduction of Pt(IV) to Pt(II) by addition of  $Na_2S_2O_3$  (equation 18).



Complete one-step removal of Pt is attained, when the stripping agent concentration exceeds 0.75 M. The pH has to be adjusted to 9.0 to avoid anion decomposition of the stripping agent and the concomitant release of the toxic  $SO_2$  gas. Additionally, five successive cycles of extraction and stripping indicate the excellent recyclability of Aliquat 336.<sup>168</sup>

Extensive tests based on tetrahexylammonium- and tetraoctylammonium-ILs with various building anions ( $Cl^-$ ,  $Br^-$ ,  $NTf_2^-$ ,  $DCA^-$ ,  $SCN^-$ ) lead to the development of two distinct strategies for the efficient separation of Au and Pt from their mixed synthetic solutions. The parameters established during single-element solution experiments were subsequently applied to mixed-element solutions. High extractability is observed for Au (>95%,  $D_{Au} > 1000$ ) with all employed ILs, a process which is driven by the formation of the highly hydrophobic ion pairs between the organic cations and the Au-chlorocomplexes. In contrast, Pt shows high affinity for ILs employing  $Br^-$ ,  $DCA^-$  and  $SCN^-$  cations (>90%,  $D_{Pt} > 1000$ ). Ion pairing and ion exchange are proposed for Au and Pt extraction, as UV-Vis data suggest. It should be noted though that the authors focused on the analysis of the organic phase only. The inability of Pt to be accessed by  $NTf_2^-$  anions is attributed to the higher charge density and standard Gibbs energy that divalent Pt cations possess compared to monovalent Au cations. This opportune difference was exploited to effectively separate the two elements from their mixtures. Selective removal of Au from the mixture is feasible by employing either  $NTf_2^-$ -based IL (tetrahexylammonium bis(trifluoromethylsulfonyl)imide ( $[N_{666}][NTf_2]$ ) or tetraoctylammonium bis(trifluoromethylsulfonyl)imide ( $[N_{888}][NTf_2]$ )). Alternatively, the selective back-extraction of Au from a loaded tetraoctylammonium dicyanamide ( $[N_{888}][DCA]$ ) phase with 0.2 M  $Na_2S_2O_3$  is an option, which despite being less efficient, nonetheless, it proves that separation of Au and Pt via selective Au recovery is feasible.<sup>169</sup>

Addition of ILs acting as anion exchangers to hydrophobic ILs offers the possibility to both increase and control their extraction capacity. Katsuta et al.<sup>170</sup> demonstrated that on the example of the water-saturated mixture of the hydrophobic trioctylammonium bis(trifluoromethylsulfonyl)imide ( $[N_{888}][NTf_2]$ ) with varying amounts of the trioctylammonium nitrate ( $[N_{888}][NO_3]$ ) which selectively and quantitatively extracted Pt(IV) and Pd(II) from diluted synthetic acidic mixtures containing Na, Mg, K, Ca, Mn, Fe, Co, Ni, Cu, Zn, Ru, Cd and Rh. Through investigation of different HCl concentrations and % (w/w) of the exchanger in the hydrophobic IL, the ideal conditions of 0.1 M HCl and 10% (w/w)  $[N_{888}][NO_3]$  were



established; at lower acidity, Fe, Zn and Cd, whose extractabilities reached approx. 70% by increasing HCl, could not be extracted, whereas Na, K, Ru, Cd and Rh were only slightly extracted regardless of the acidity. The distribution ratios for Pt and Pd are independent of their concentration when the mixture of 10% (w/w)  $[N_{888}][NO_3]$  in  $[N_{888}][NTf_2]$  is used. For the sake of comparison, the effect of the performance of pure ILs was also evaluated, namely  $[N_{888}][NTf_2]$ ,  $[N_{8881}][NTf_2]$  and  $[C_4mim][NTf_2]$ , as well as the effect exerted by addition of  $[N_{888}][NO_3]$ . It was indeed verified that the extractability significantly increases with increasing content of  $[N_{888}][NO_3]$ , as the significant increase in the distribution ratio of pure IL ( $D_{Pt}=6.32$ ,  $D_{Pd}=16.4$ ) and their mixture proves ( $D_{Pt}=24.7$ ,  $D_{Pd}=803$ ). The function of  $[N_{888}][NO_3]$  as an ion exchanger accounts for this observed increase in extractability. Although  $[N_{888}][Cl]$  increases the distribution ratios even further ( $D_{Pt}=187$ ,  $D_{Pd}=3520$ ) the IL comprising the  $NO_3^-$  anion was used to facilitate its regeneration during stripping with  $HNO_3$  ( $NO_3^-$  anions are supplied back to the IL via exchange with chlorocomplexes and  $Cl^-$ ). By contacting the metal-loaded IL phase with 8.0 M  $HNO_3$  twice, 91% Pt and 57% Pd can be stripped. Alternatively, selective one-step stripping of Pt (60%) is possible by adjusting the  $HNO_3$  concentration to 1.0 M. The IL is indeed regenerated during the back-extraction process and its extracting efficiency is retained in subsequent extractions.<sup>170</sup>

In consequent studies, the research group demonstrated the selectivity of the ammonium-based IL trioctylammonium hydrogen nitrate ( $[N_{888}][HNO_3]$ ) for the extraction of Pt(IV) and Pd(II), without the use of a second IL as a diluent but rather by exploiting the liquefaction of the IL at RT when it is saturated with  $H_2O$ . Its high selectivity for Pt and Pd, which are present in HCl model solutions along with the interfering ions Fe, Cu, Ni, Zn, Co and Mn, was established via comparison of its performance with other water-saturated ILs. Pt and Pd can be quantitatively extracted in as fast as 15 min over a wide range of HCl concentrations (0.1-2.0 M), however, it is essential to maintain the HCl concentration below 0.1 M in order to minimize the extraction of the accompanying elements to <10% (with the exception of Zn, 50% of which is extracted at 0.1 M HCl).

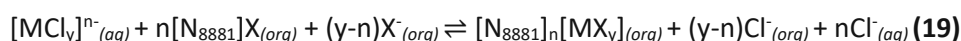
Complete stripping of Pd can be attained with an aqueous thiourea solution, whereas acidification of thiourea via  $HNO_3$  is necessary to benefit the back extraction of Pt (79-87%). By exploiting the different times required for the complexation of Pt and Pd with thiourea (120 min and 30 min, respectively), their partial separation during the stripping process can be accomplished. During extraction, the  $NO_3^-$  of the IL are exchanged by  $Cl^-$ , however,  $[N_{888}][NO_3]$  is successfully regenerated in the course of the stripping process, by exchange of  $Cl^-$  by  $NO_3^-$ , as indicated by the quantitative yield of Pt and Pd when the recycled IL is used for their extraction.<sup>171</sup>

The potential for quantitative extraction of Rh(III) from a  $HNO_3$  model solution was demonstrated by combining equal amounts of the IL (methoxyethyl)trimethylammonium bis(trifluoromethylsulfonyl)imide ( $[(CH_3)_3NCH_2CH_2OMe][NTf_2]$ ) with the extractant octyl-phenyl-*N,N*-diisobutylcarbamoyl methylphosphine oxide (CMPO). A wide acidity range and different extraction durations were evaluated; extractability reached its maximum at a concentration of 0.01 M  $HNO_3$  after 60 min.<sup>172</sup>

A split-anion exchange process has been recently introduced for the effective separation of Au(III), Pt(IV), Pd(II) and Rh(III) from their HCl (or other Cl-based) solutions, comprising water-saturated forms of Aliquat 336 ( $[N_{8881}][Cl]$ ,  $[N_{8881}][Br]$ ,  $[N_{8881}][I]$ ). The principle of split anion is the transportation of metals that form weak complexes (with anions such as  $SO_4^{2-}$  and  $Cl^-$ ) from the aqueous phase to the IL phase through formation of stronger complexes (with anions such as  $Br^-$ ,  $I^-$ ,  $SCN^-$ ). Incorporating different anions in the aqueous and IL phase keeps the contamination of the phases by foreign anions to a minimum, since foreign-anion exchange occurs only to maintain electroneutrality. The authors demonstrated that the extraction of Pt, Pd and Au is quantitative and independent of the HCl concentration (0.001-6.0 M);

however, they are most efficiently separated from Rh at higher HCl concentrations and when  $[N_{8881}]I$  is employed. Low Rh extraction at high HCl concentrations is generally observed due to formation of less extractable Rh species. Low Rh extraction with  $[N_{8881}]I$  specifically is observed for two reasons; the strongly hydrated  $Cl^-$  anions have higher affinity for the aqueous phase and tend to remain there and Rh(III) does not form halide complexes with  $I^-$  anions.

It is proposed that the extraction proceeds through two different simultaneously occurring reactions; first, the aqueous chlorocomplexes react with the IL anion ( $Br^-$  or  $I^-$ ) forming the respective bromo- or iodo-complexes, which are subsequently extracted to the IL phase (equation 19).



Upon contact with HCl,  $(y-n)X^-$  is exchanged for  $(y-n)Cl^-$ , thereby resulting in the formation of a  $[N_{8881}]Cl$  and  $[N_{8881}]I$  mixture during the extraction. The formation of  $[N_{8881}]Cl$  explains the observed, albeit low, co-extraction of Rh to the IL phase, although it does not complex with  $I^-$ ; Rh is transferred to the IL phase via an anion-exchange mechanism with the  $Cl^-$  of the IL. Although the ILs are used in their water-saturated form, experiments with the ILs diluted in *p*-cymene, indicate that increasing IL concentration results in an increase in the distribution ratio.

The authors note the salting-out effect, i.e., increase in the distribution ratio as salt concentration increases, as well as the opposite, salting-in effect, of some Cl-containing salts (Figure 19). Since increasing  $Cl^-$  concentration has no impact on the extraction of Pt, Pd and Au but it negatively affects Rh, especially when NaCl is the  $Cl^-$  source, this can be exploited in order to achieve, in this case, their partial separation from Rh.

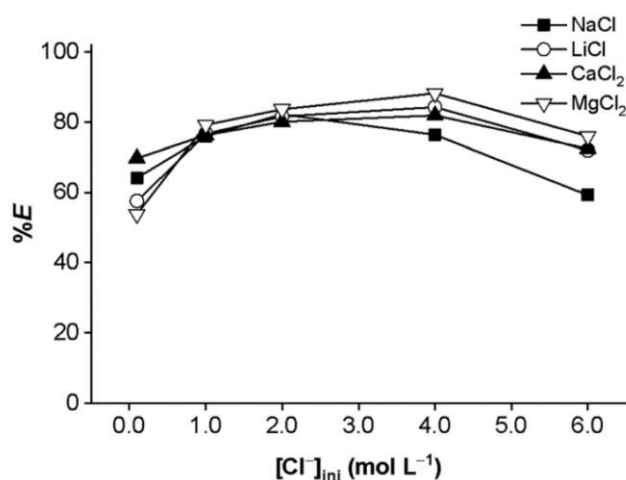
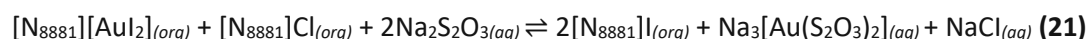
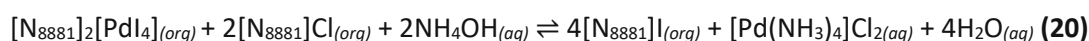


**Figure 19.** Salting-out effect on the extraction of Rh. Aqueous phase: 680 mg/L Pt(IV), 675 mg/L Pd(II), 128 mg/L Rh(III) and 28.3 mg/L Au(III) in 1 mM HCl, organic phase: water-saturated 1.75 M  $[N_{8881}]Br$ .<sup>174</sup>

Pt, Pd and Au can be efficiently separated through selective stripping steps; however, the order that the stripping agents are applied, as the authors prove, is critical to achieve the desired outcome. First, Pd is stripped with  $NH_4OH$ , then Au with  $Na_2S_2O_3$  and finally, Pt with acidified thiourea. The IL is regenerated during the stripping process (equations 20-22) and it can be reused without any loss in its extraction capacity.





The developed process was successfully applied to a solution simulating a car catalyst leachate from which metallic Pt, Pd and Rh were recovered with high purity (>99%). A comprehensive flowsheet of the developed process has been provided by the authors (Figure 20).<sup>174</sup>

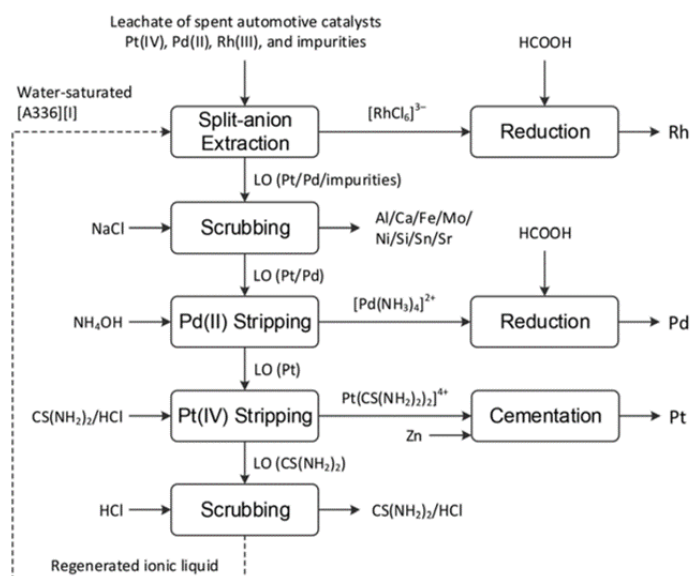
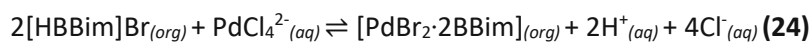
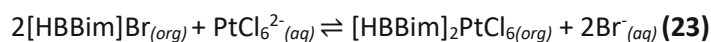


**Figure 20.** Proposed flowsheet for the separation of precious metals from the leachate of spent automotive catalyst by split-anion extraction, using water-saturated  $[\text{N}_{8881}]\text{I}$ .<sup>174</sup>

### 3.1.3.2 Imidazolium-based ionic liquids

The PGM extraction conditions and results that will be discussed in the present section are summarized in Table 4.

The successful one-step separation of Pd(II) and Pt(IV) from their aqueous HCl-based model mixture with the aid of the 1-butyl-3-benzimidazolium bromide ( $[\text{HBBim}]\text{Br}$ )/ $\text{CHCl}_3$  system was reported. The observed precipitation of Pt out of the solution is attributed to the anion exchange of the  $\text{Br}^-$  of the IL with the  $\text{Cl}^-$  of the Pt-chloro complex (equation 23), as verified via FT-IR,  $^1\text{H-NMR}$  and Job's method. The coordination of Pd with the IL (equation 24), a mechanism supported by single X-Ray diffraction (XRD) measurements, leads to its selective extraction into the organic phase.



The authors demonstrated that there is a direct relationship between the concentration of the IL and the respective extraction efficiencies. Additionally, the effect of the acidity of the aqueous solution on the extraction efficiencies was assessed; an increase in acidity yields a decrease in the precipitation efficiency of Pt and the extraction efficiency of Pd, induced by the excess of  $\text{H}^+$ . Addition of NaCl proves that, in the case of Pd, increasing  $\text{Cl}^-$  concentration has a detrimental effect on its extraction efficiency. Increasing ionic strength of the aqueous solution, demonstrated by use of  $\text{NaNO}_3$ , decreases the precipitation efficiency of Pt and the extraction efficiency of Pd. The quantitative back-extraction of both Pt and Pd from the organic to the aqueous phase was feasible, with hydrazine and acidified thiourea, respectively. Unfortunately, the authors have discussed neither the contamination of the aqueous phase by  $\text{Br}^-$ , as a result of the anion-exchange mechanism involved in the precipitation of Pt, nor the possibility of reusing the IL after the successful back-extraction process.<sup>177</sup>

The separation and two-step extraction of Pt(IV) and Au(III) from their acidic mixed model solution with the aid of two imidazolium ILs was investigated by Papaiconomou et al.<sup>178</sup> As demonstrated by the differences in the Au concentration of the acidic solution before and after mixing with 1,2-dimethyl-3-octylimidazolium bis(trifluoromethylsulfonyl)imide ([C<sub>8</sub>dmim][NTf<sub>2</sub>]), this imidazolium-based IL has the capacity for complete and selective Au extraction in the form of its chlorocomplexes, while at the same time it can only extract a negligible amount of the Pt-chlorocomplexes present in solution. This tendency is clearly reflected in the respective distribution ratios, D<sub>Au</sub>=410 and D<sub>Pt</sub>=0.37, at 5.0 M HCl. Subsequent to the separation of Au from Pt, the addition of KSCN induces the formation of Pt-thiocyanate complexes which can be quantitatively extracted by 1-octyl-3-methylimidazolium bis(trifluoromethylsulfonyl)imide ([C<sub>8</sub>mim][NTf<sub>2</sub>]) (D<sub>Pt</sub>>6000, at 0.1 M HCl), presumably due to the π-bonds as well as the soft and hard donor atoms present on the SCN<sup>-</sup> anion.<sup>178</sup>

Bearing these results in mind, the authors further investigated possible pathways for the separation of Au(III) and Pt(IV), additionally considering metal-bromocomplexes and a significantly broader range of HCl concentrations (0.1-11 M). Interestingly enough, the removal of Pt was proven to be quite versatile; Pt can be quantitatively removed either via precipitation or liquid-liquid extraction from a wide HCl concentration range, depending upon the complex species present in solution and the IL employed. Specifically, complexation of PtCl<sub>6</sub><sup>2-</sup> species (present at HCl<1.0 M) with the ILs 1-octyl-3-methylimidazolium chloride ([C<sub>8</sub>mim]Cl, equation 25) and 1,12-bis-(3-methylimidazolium-1-yl)dodecane bromide ([C<sub>12</sub>(mim)<sub>2</sub>][Br<sub>2</sub>], equation 26) almost quantitatively (91.2% and 98.2%, respectively) removes Pt from the solution via precipitation.

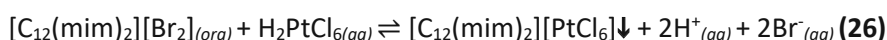
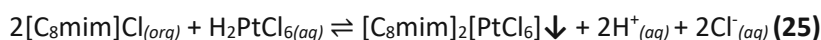


**Table 4.** Summary of PGM extraction conditions and results with imidazolium-based ionic liquids.

PGM Solution	Ionic Liquid (+ Diluent)	Ratio (O/A) <sup>a</sup>	Time (min) <sup>b</sup>	Extr. Efficiency (%) Distribution Ratio (D)	Type	Ref. No
156 mg/L Pt(IV), 84.8 mg/L Pd(II) in 7 mM HCl	30.33 mM [HBBim]Br in CHCl <sub>3</sub>	1/5	60	100% Pt, 100% Pd	A	177
0.8 mM Au(III), 0.4 mM Pt(IV) in i. 5.0 M HCl ii. HCl adjusted to 0.1 M	i. [C <sub>8</sub> dmim][NTf <sub>2</sub> ] pure ii. 5.0 M KSCN in [C <sub>8</sub> mim][NTf <sub>2</sub> ]	n.a.	n.a.	i. 98.99% Au, D <sub>Au</sub> =410 6% Pt, D <sub>Pt</sub> =0.37 ii. 99.99% Pt, D <sub>Pt</sub> >6000 <1% Au	A	178
A. L-L extraction 8.2 mM Pt(IV) in i. 0.1 M KSCN/1.0 M HCl ii. 1.0 M HBr B. Precipitation 8.2 mM Pt(IV) in i. 0.1 M HCl ii. 1.0 M HCl	A. L-L extraction i. [C <sub>8</sub> mim][NTf <sub>2</sub> ] ii. [C <sub>12</sub> (mim) <sub>2</sub> ][NTf <sub>2</sub> ] <sub>2</sub> B. Precipitation i. 16.4 mM [C <sub>8</sub> mim][Cl] in 0.1 M HCl ii. 8.2 mM [C <sub>12</sub> (mim) <sub>2</sub> ][Br <sub>2</sub> ] in 1.0 M HCl	A. 1/6 B. 1/1	n.a.	A. L-L extraction i. 99.9% Pt, D <sub>Pt</sub> =6150 ii. 98.2% Pt, D <sub>Pt</sub> =482 B. Precipitation i. 99.2% Pt ii. 98.2% Pt	A	179
200 mM Pt(IV), 465 mM Pd(II) in 1.0 M HCl	i. [C <sub>8</sub> mim][NTf <sub>2</sub> ] pure ii. P <sub>66614</sub> Br pure	1/1	720	i. 89% Pt, 4% Pd, D <sub>Pd</sub> <0.05 ii. >99.9% Pt, D <sub>Pt</sub> >5000 >99.9% Pd, D <sub>Pd</sub> =3400	A	180
10 mg/L Pd(II) in Britton-Robinson buffer (pH 4.1)	[C <sub>4</sub> mim][PF <sub>6</sub> ] pure	1.5 g/mL	3	>99% Pd	A	181

2.0 mM/metal: Pt(IV), Mn(II), Zn(II), Cu(II), Co(II), Ni(II), Fe(III), Al(III), Sn(IV) in 0.8 M HCl	0.3 M [C <sub>16</sub> mim]Cl in [C <sub>8</sub> mim][PF <sub>6</sub> ]	1/5	240	96.5% Pt, D <sub>Pt</sub> =138 <10% each of the rest, D<0.5	C	182
0.2 mM/PGM: Pt(IV), Pd(II), Rh(III), Ru(III) in 0.01 M HCl	i. 30 mM M [C <sub>6</sub> mim]Cl in [C <sub>6</sub> mim][NTf <sub>2</sub> ] ii. 8 mM [C <sub>6</sub> mim][DDTC] in [C <sub>6</sub> mim][NTf <sub>2</sub> ] iii. 50 mM [C <sub>6</sub> mim][DDTC] in [C <sub>6</sub> mim][NTf <sub>2</sub> ] iv. (NH <sub>4</sub> ) <sub>2</sub> S	1/10	30	i. 99% Pt, D <sub>Pt</sub> =1596 <10% each of the rest, D <sub>Pd</sub> =1.2, D <sub>Ru</sub> =1.1, D <sub>Rh</sub> =0.8 ii. >99% Pd, D <sub>Pd</sub> =2040, 9% Ru, D <sub>Ru</sub> =1.0, 6% Rh, D <sub>Rh</sub> =0.62 iii. >99% Pd, D <sub>Pd</sub> =1996 95% Ru, D <sub>Ru</sub> =227 iv. Rh precipitation	C	183
2 mM/metal: Pt(IV), Zn(II), Fe(III), Cu(II), Ni(II), Rh(III) in 0.1 M HCl	150 mM [C <sub>14</sub> Pim]Br in [C <sub>8</sub> mim][PF <sub>6</sub> ]	1/10	10	99.9% Pt, D <sub>Pt</sub> =8648, 4.6% Zn, 8.2% Fe, 5.6% Cu, 6.1% Ni, 11.7% Rh	C	184
1.0 mM/metal: Au(III), Pt(IV), Pd(II) in 0.01 M HCl	i. [C <sub>4</sub> mim][NTf <sub>2</sub> ] pure ii. [C <sub>4</sub> mim][PF <sub>6</sub> ] pure	1/2	1440	i. 97% Au, D <sub>Au</sub> =62 20% Pt, 8% Pd ii. 99% Au, 80% Pt, 10% Pd	A	185
1.0 mM/metal: Pt(IV), Pd(II), in 2.0 M HCl	[C <sub>8</sub> mim][NTf <sub>2</sub> ] pure	1/2	1440	85% Pt, D <sub>Pt</sub> =12.3 0% Pd, D <sub>Pd</sub> =0.04	A	186
200 mg/L Pt(IV), 100 mg/L Pd(II) in 1.0 M HCl	10% (w/w) P <sub>66614</sub> Cl in [C <sub>8</sub> mim][NTf <sub>2</sub> ]	1/2	180	>95% Pt, D <sub>Pt</sub> =37.2 <20% Pd, D <sub>Pd</sub> =0.27	C	187
0.1 mM Pd(II) in 0.1 M HCl	0.005 mM EEImT in [Emim][NTf <sub>2</sub> ]	1/10	3	98% Pd	B	188
0.2 mM Pd(II) in 0.8 mM HCl	0.01 M BMImSe in [C <sub>4</sub> mim][NTf <sub>2</sub> ]	1/10	5	100% Pd	B	189
0.5 M/metal: Pt(IV), Pd(II) in 1.0 M HCl	50% (v/v) [C <sub>8</sub> mim][PF <sub>6</sub> ] in CHCl <sub>3</sub>	1/1	4320	>85% Pt, <35% Pd	A	190
100 mg/L/metal: Pt(IV), Pd(II), Rh(III) in 3.0 M HCl	[C <sub>4</sub> mim][NTf <sub>2</sub> ] (C <sub>n</sub> , n=8 in amino moiety)	1/5	30	>98% Pt, >95% Pd, >70% Rh	A	191
100 mg/L/metal: Pt(IV), Pd(II), Rh(III) in 0.1 M HCl	triphasic system · [C <sub>4</sub> mim][PF <sub>6</sub> ] · 50% diisopentyl sulfide in nonane · aqueous HCl	1/6	10	IL phase: 72.3% Pt, 8.4% Rh Org. phase: 99.3% Pd, 0% Pt, Rh Aq. phase: 91.6% Rh, 27.7% Pt, 0% Pd	A	192

<sup>a</sup> O= organic phase, A= aqueous phase. <sup>b</sup> All extractions were performed at RT.

According to IR and NMR data collected from analysis of the yellow precipitate, it was concluded that both IL cations and Pt-chlorocomplexes are present in the precipitate, which has a crystalline structure, as XRD data revealed. Replacing the anion of the ILs with NTf<sub>2</sub><sup>-</sup> offers the possibility of Pt removal from a wide HBr concentration range (0.1-9 M). [C<sub>8</sub>mim][NTf<sub>2</sub>] efficiently extracts the PtBr<sub>6</sub><sup>2-</sup> species regardless of HBr concentration (0.1 M: 95.9%, D<sub>Pt</sub>=175, 1.0 M: 93%, D<sub>Pt</sub>=105, 9.0 M: 99.2%, D<sub>Pt</sub>=858), as well as the Pt(SCN)<sub>6</sub><sup>2-</sup> species (1.0 M HCl: 99.9%, D<sub>Pt</sub>=6150). The π-bond and negative charge on SCN<sup>-</sup> combined with the soft sulfur and hard nitrogen atoms is believed to have a favorable interaction with the imidazolium ring, thus exhibiting such extraction capacity. 1,12-bis-(3-methylimidazolium-1-yl)dodecane bis(trifluoromethylsulfonyl)imide ([C<sub>12</sub>(mim)<sub>2</sub>][NTf<sub>2</sub>]<sub>2</sub>) quantitatively extracts Pt (98.2%, D<sub>Pt</sub>=482) from 1.0 M HBr.

Extraction of the analogue  $\text{PtCl}_6^{2-}$  species with these two ILs is significantly lower and they exhibit distribution ratios lower than 10, due to the lower solvation energies that complexes comprising Cl-ligands exhibit compared to the ones with Br-ligands. Based on the observed behavior of Pt, the authors developed two processes for the separation of Au from Pt in water samples. In the first approach,  $[\text{C}_8\text{dmim}][\text{NTf}_2]$  selectively removes Au and after adjusting the pH to 1, Pt is quantitatively removed via anion exchange of the  $\text{Pt}(\text{SCN})_6^{2-}$  species with  $[\text{C}_8\text{mim}][\text{NTf}_2]$ . In the second process, Au removal via liquid-liquid extraction with  $[\text{MOPYRRO}][\text{NTf}_2]$  is followed by precipitation of  $\text{PtCl}_6^{2-}$  with  $[\text{C}_8\text{mim}]\text{Cl}$  (Figure 21). The formed precipitate can be dissolved in an acidic solution (11 M HCl) as well as in  $[\text{C}_8\text{mim}][\text{NTf}_2]$ .<sup>179</sup>

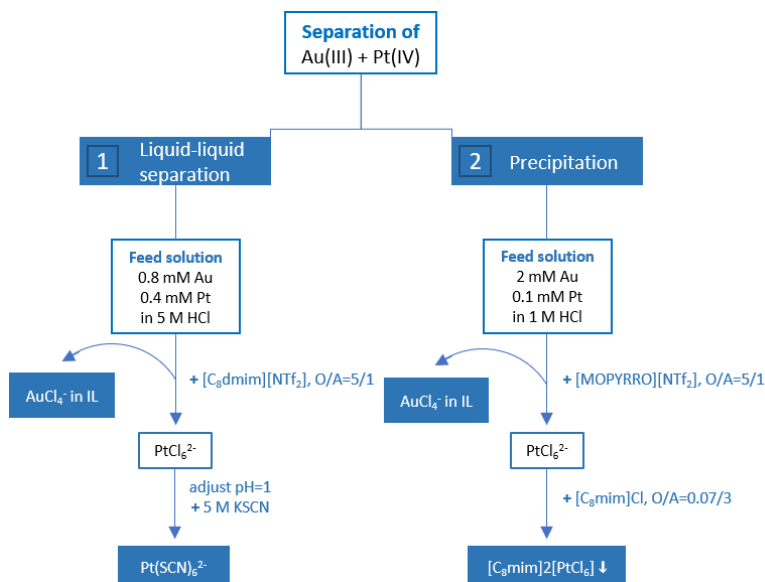


**Figure 21.** Simplified flowsheet of the two processes for Au(III) and Pt(IV) separation.<sup>179</sup>

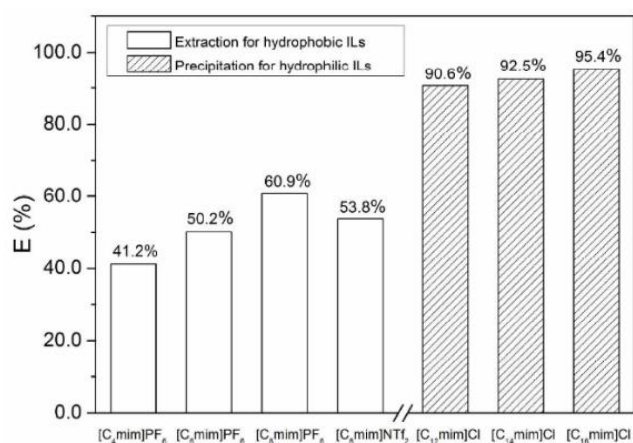
The selectivity of  $[\text{C}_8\text{mim}][\text{NTf}_2]$  toward Pt(IV) was further exploited for its separation from Pd(II). At 1.0 M HCl of their individual synthetic solutions, extraction of Pt was observed; however, due to its low distribution coefficient ( $D_{\text{Pt}}=11.2$  for 1 mM Pt,  $D_{\text{Pt}}=2.8$  for 8 mM Pt), it is foreseen that repeated extractions are necessary for quantitative Pt removal, whose required number increases as the Pt concentration in the solution increases. On the other hand, Pd remains in the aqueous phase, which is expected considering the low distribution ratio it exhibits ( $D_{\text{Pd}}<0.05$ ). Different solvation energies of the species  $\text{PtCl}_6^{2-}$  and  $\text{PdCl}_4^{2-}$  account for this difference in extraction behavior; the diameter of the Pt-species is larger, thus, exhibits a lower Gibbs solvation energy. Additionally, the extraction of Pd with the imidazolium IL was not possible under various HCl concentrations. In a different set of experiments, trihexyltetradecylphosphonium bromide (Cyphos 102) was evaluated, which demonstrated the ability to extract both metals quantitatively ( $D_{\text{Pt}}>5000$ ,  $D_{\text{Pd}}=3400$ , 1.0 M HCl). Based on these results, the authors proposed a separation process for Pt and Pd. In the first step, the imidazolium IL removes Pt from the mixture; however, quantitative extraction was not possible in practice and only 89% extraction was achieved, while 4% of Pd was co-extracted. Consecutive extractions did not lead to quantitative recovery either, presumably because after the 1<sup>st</sup> extraction cycle, which proceeds via ion exchange, the aqueous phase gets saturated with the ions released during the ion-exchange process ( $\text{C}_8\text{mim}^+$ ,  $\text{NTf}_2^-$ ), thus, association in the ensuing cycles might proceed between the Pt-species with the cations present in the aqueous phase. Evidently, when the distribution ratios are low, the ion-exchange mechanism does not allow efficient separation. In the second step,  $\text{P}_{66614}\text{Br}$  quantitatively removes Pd and the remaining amount of Pt. The proposed mechanism of Pd extraction is the following (equation 27).<sup>180</sup>





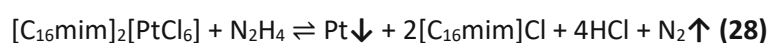
The selective extraction of Pd(II) from an acidic model solution with the aid of a pure IL has been reported. Both trace- and macro-amounts could be quantitatively extracted by the imidazolium-based IL 1-butyl-3-methylimidazolium hexafluorophosphate ( $[\text{C}_4\text{mim}][\text{PF}_6]$ ) in the presence of a number of interfering ions (K, Na, Ca, Zn, Mg, Ni, Cd, Fe). The adjustment of acidity at pH 4.1 was essential to maximize the extraction yield, which decreased notably below or above this pH value, while RT and a short equilibration time (3 min) were employed. The developed extraction process was successfully applied to the waste water of fuel cell catalyst.<sup>181</sup>

Mixtures of the amphiphilic IL 1-hexadecyl-3-methylimidazolium chloride ( $[\text{C}_{16}\text{mim}]\text{Cl}$ ) in the hydrophobic 1-octyl-3-methylimidazolium hexafluorophosphate ( $[\text{C}_8\text{mim}][\text{PF}_6]$ ) demonstrate significantly increased extractability for Pt(IV) compared to the respective performance of the individual ILs. With hydrophilic ILs ( $[\text{C}_n\text{mim}]\text{Cl}$ ,  $n = 12, 14, 16$ ) precipitation of Pt in the form of powder is observed, whereas with hydrophobic ILs ( $[\text{C}_n\text{mim}][\text{PF}_6]$ ,  $n = 4, 6, 8$ ) Pt is extracted to the IL. Nevertheless, the respective extracting behaviors of the ILs are enhanced with the increase of the alkyl side chain length (61% with  $[\text{C}_8\text{mim}][\text{PF}_6]$  and 95% with  $[\text{C}_{16}\text{mim}]\text{Cl}$ , Figure 22).



**Figure 22.** Extraction/precipitation efficiencies of Pt(IV) with hydrophobic/hydrophilic ILs with varying side-chain lengths.<sup>182</sup>

Based on these results, the effect of addition of varying amounts of  $[\text{C}_{16}\text{mim}]\text{Cl}$  in  $[\text{C}_8\text{mim}][\text{PF}_6]$  on the extraction efficiency was evaluated; increasing amount of hydrophilic IL in the hydrophobic IL indeed enhances the extraction performance by a maximum of 30% for 0.3 M hydrophilic IL in hydrophobic IL. Extraction efficiency is negatively affected by a rise in temperature given the exothermic nature of the reaction. As it has been reported various times in the literature cited in the present review, increasing HCl concentration favors the extraction up to a certain point (0.005-0.8 M) beyond which the extraction drops due to the competition between  $\text{Cl}^-$  and Pt-chloro complexes to associate with the IL cation. High selectivity and extractability for Pt (96.5%,  $D_{\text{Pt}}=138$ ) over other metals (Mn, Zn, Cu, Co, Ni, Fe, Al, Sn <1%,  $D < 0.5$ ) was observed. Stripping with hydrazine removes over 98% of Pt from the IL phase which can be regenerated (equation 28) and reused without any loss in extraction efficiency for at least five consecutive extraction cycles (Figure 23).<sup>182</sup>





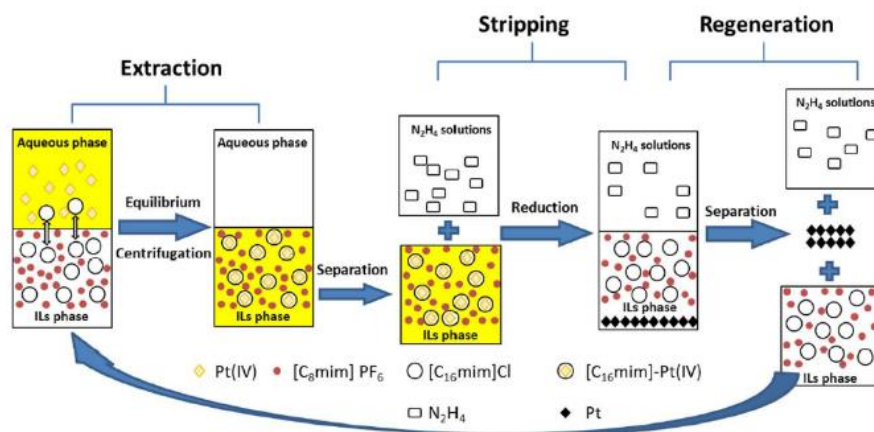
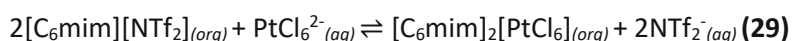
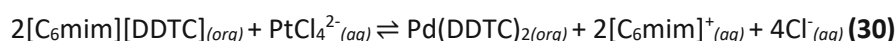


**Figure 23.** The extraction-stripping-regeneration process of Pt(IV) with the mixed hydrophobic/hydrophilic ILs.<sup>182</sup>

A model acidic solution comprising Pt(IV), Pd(II), Ru(III) and Rh(III) was used to effectively prove the ability of imidazolium-based IL mixtures to separate these elements from one another. Ion association between 1-hexyl-3-methylimidazolium bis(trifluoromethylsulfonyl)imide ([C<sub>6</sub>mim][NTf<sub>2</sub>]) and Pt is further enhanced by the addition of 1-hexyl-3-methylimidazolium chloride ([C<sub>6</sub>mim]Cl) to yield an extraction of 99% for Pt, while at the same time the extraction of the accompanying elements is below 10% regardless of the acidity of the solution. However, in order to maintain the extraction of Pt at high levels, concentrations of HCl below 0.3 M are required; at low concentration the distribution ratio is sufficiently high for effective extraction ( $D_{Pt} > 1500$ ), while as the HCl concentration increases a dramatic drop is observed ( $D_{Pt} = 63$ , at 1.5 M HCl). The extraction mechanism of Pt with the imidazolium IL is the following (equation 29):



A hydrophobic phase combining [C<sub>6</sub>mim][NTf<sub>2</sub>], serving as the diluent, and the functionalized IL 1-hexyl-3-methylimidazolium diethyldithiocarbamate ([C<sub>6</sub>mim][DDTC]) quantitatively extracts Pd leaving the majority of Ru and Rh in the aqueous phase. Specifically, any concentration of [C<sub>6</sub>mim][DDTC] over 8 mM yields sufficiently high distribution ratios ( $D_{Pd} > 2000$ ) to allow complete Pd recovery. Remarkably, the same IL mixture can extract Ru by simply increasing the concentration of [C<sub>6</sub>mim][DDTC] beyond a certain level. Nevertheless, the distribution ratios for Rh do not exceed 0.8, thereby rendering its extraction impossible. In any case, the concentration of Cl<sup>-</sup> anions in the aqueous solution should remain at low levels (below 0.2 M) in order to obtain maximum extraction efficiencies for both Pd and Ru. Association of the S atoms of DDTC with Pd and Ru is the mechanism to which UV-Vis, FT-IR and XRD data point (equation 30).



The amount of Rh remaining in solution can be effectively removed via precipitation with (NH<sub>4</sub>)<sub>2</sub>S. As demonstrated by the authors, the ions extracted in the hydrophobic-IL phase can be removed by back-extraction to the aqueous phase; Na<sub>2</sub>S<sub>2</sub>O<sub>3</sub> or acidified thiourea is effective for the removal of Pt while acidified thiourea removes Pd and Ru, thus, enabling the recovery and reuse of the hydrophobic-IL mixture (Figure 24). Unfortunately, the authors do not address the undesirable contamination of the aqueous phase by the C<sub>6</sub>mim<sup>+</sup> anions and the NTf<sub>2</sub><sup>-</sup> cations, which, as will be later discussed in this chapter, can be toxic to aquatic life and have ecotoxicological properties, respectively.<sup>183</sup>

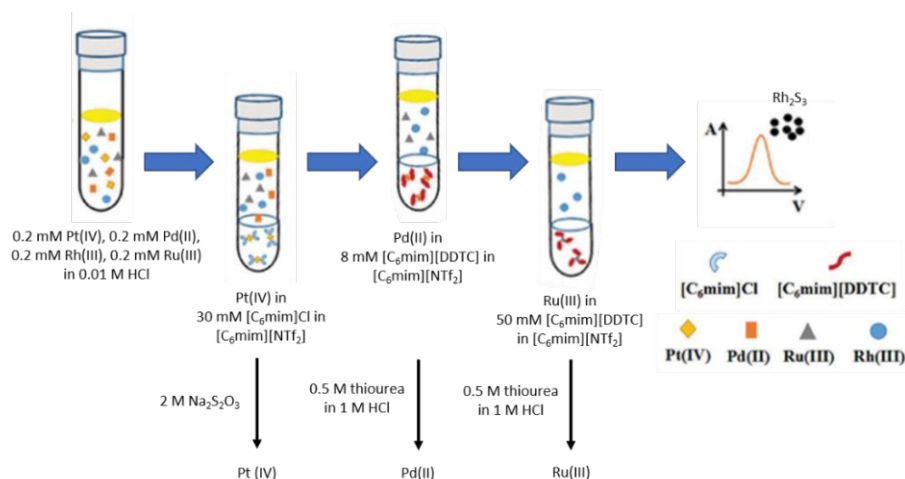


Figure 24. Separation process for Pt(IV), Pd(II), Ru(III) and Rh(III).<sup>183</sup>

Most recently, Chen et al.<sup>184</sup> proved the superiority, in terms of extraction efficiency and selectivity, of hydrophilic ILs mixed in hydrophobic ILs, as opposed to single-IL solutions. The research group synthesized and evaluated five imidazolium ILs; 1-dodecyl-3-propylimidazolium bromide ( $[\text{C}_{12}\text{Pim}]\text{Br}$ ), 1-tetradecyl-3-propylimidazolium bromide ( $[\text{C}_{14}\text{Pim}]\text{Br}$ ), 1-hexadecyl-3-propylimidazolium bromide ( $[\text{C}_{16}\text{Pim}]\text{Br}$ ), 1-tetradecyl-2-aminoethylimidazolium bromide ( $[\text{C}_{14}\text{NH}_2\text{Etim}]\text{Br}$ ) and 1-tetradecyl-3-butylimidazolium bromide ( $[\text{C}_{14}\text{Bim}]\text{Br}$ ).

Highly selective extraction of Pt(IV) (99.9%,  $D_{\text{Pt}}=8648$ ) from multi-metal solutions containing Zn(II), Fe(III), Cu(II), Ni(II) and Rh(III) was feasible with the  $[\text{C}_{14}\text{Pim}]\text{Br}/[\text{C}_8\text{mim}][\text{PF}_6]$  IL mixture (Figure 25), which, according to the calculated thermodynamic parameters, is a spontaneous exothermic process. FT-IR and  $^1\text{H-NMR}$  data indicate anion exchange between the  $\text{Br}^-$  of the IL and the  $\text{PtCl}_6^{2-}$  species. It is noteworthy that the extractable species,  $[\text{C}_{14}\text{Pim}]\text{-Pt(IV)}$ , exhibited excellent solubility in the IL mixture, which was not the case with the other tested ILs. Extraction efficiency benefits from an increase in the concentration of IL, however, increasing HCl concentration, i.e., increased  $\text{Cl}^-$  presence, leads to a modification of the hydrophobicity of the organic phase, thus, exerts a negative effect on the extraction efficiency. The authors noted the possibility to reuse the IL after electrodeposition of the extracted Pt; however, gradual decline in the extraction efficiency was observed most probably due to the dissolution of  $\text{C}_{14}\text{Pim}^+$  in the aqueous phase and the progressive mass loss of the organic phase during consecutive recycling steps.<sup>184</sup>

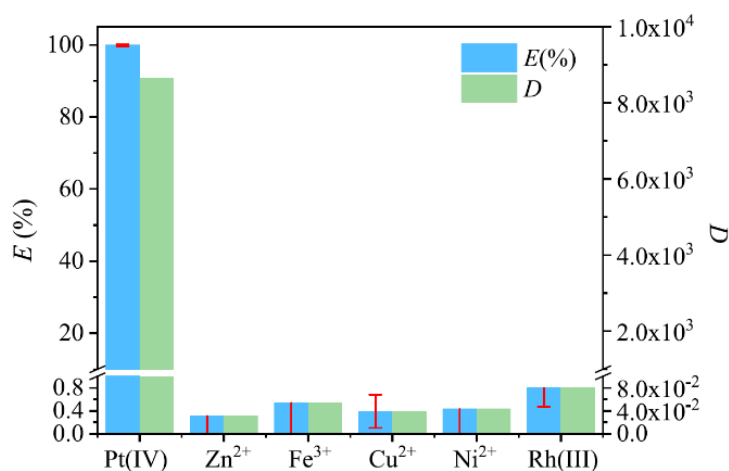


Figure 25. Selective extraction of Pt(IV) from multi-metal solutions obtained with  $[\text{C}_{14}\text{Pim}]\text{Br}$  in  $[\text{C}_8\text{mim}][\text{PF}_6]$ .<sup>184</sup>

The hydrophobicity of the IL building anion can significantly impact the extraction efficiency as was proven in a model HCl solution containing Au(III), Pt(IV) and Pd(II). Pure 1-butyl-3-methylimidazolium bis(trifluoromethylsulfonyl)imide ( $[\text{C}_4\text{mim}][\text{NTf}_2]$ ) is highly selective for Au, co-extracting only 20% Pt and 8% Pd at 0.01 M HCl. By replacing the  $\text{NTf}_2^-$  anion with its more hydrophobic  $\text{PF}_6^-$  analogue, a tremendous increase is observed in the extraction of Pt, which reaches 80%, whereas the effect on Au and Pd is negligible. It is suggested that the higher hydrophobicity of the  $\text{PF}_6^-$  facilitates the transfer of Pt to the IL phase via an anion-exchange mechanism. Proper selection of the building anion can, thus, impart the desired selectivity to the IL. Despite the quite interesting outcome of the reported experiments, the authors do not address the unfortunate fact that both the used anions and cations can have an ecotoxicological impact, as it is later discussed in detail.<sup>185</sup>

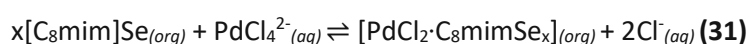
Aiming for a system that could effectively separate Pt(IV) from Pd(II), the authors evaluated the effect of ILs with varying alkyl chain length attached to the imidazolium moiety on their separation performance from a synthetic solution. By appending more methylene groups to the alkyl chain ( $\text{C}_n$ ,  $n = 4, 6, 8$ ), a dramatic increase in the extraction of Pt was obtained (23% to 85%), while the effect on Pd extraction was negligible (8% to 10%). This significant difference in extractability is also reflected in the respective distribution ratios,  $D_{\text{Pt}}=12.3$  and  $D_{\text{Pd}}=0.04$ . Nevertheless, it would have been interesting to investigate whether repeated extractions of the aqueous phase could yield quantitative extraction of Pt. The explanation for the difference in behavior lies in the species present in solution;  $\text{PtCl}_6^{2-}$  has a lower charge density and a smaller hydration shell than  $\text{PdCl}_4^{2-}$ , thus, favoring ion-pair formation with the cation of the IL. Additionally, the longer alkyl chain length of  $[\text{C}_8\text{mim}][\text{NTf}_2]$  has a stabilizing effect on the formed ion pair. Adjusting the HCl concentration of the metal containing solution, further promotes the separation between the two metals. Although gradual increase in HCl content has no effect on Pt, it completely forces Pd out of the IL phase, thereby leading to the selective extraction of Pt over Pd. Loading experiments of the organic phase do not show any saturation at Pt concentrations below 2 mM, suggesting capacity for high metal loading.<sup>186</sup>

The advantageous effect of mixing imidazolium-based ILs with other ILs has been reported.<sup>187</sup> The extraction capacity of the imidazolium-based IL  $[\text{C}_8\text{mim}][\text{NTf}_2]$  for Pt(IV) was further enhanced reaching a quantitative level in its mixture with 10% (w/w) trihexyltetradecylphosphonium chloride ( $\text{P}_{66614}\text{Cl}$ ). The respective increase in the distribution ratios of Pt and Pd from the single-IL system ( $D_{\text{Pt}}=4.07$ ,  $D_{\text{Pd}}=0.10$ ) to the mixed-IL system ( $D_{\text{Pt}}=37.2$ ,  $D_{\text{Pd}}=0.27$ ) are indicative of the positive impact that the addition of  $\text{P}_{66614}\text{Cl}$  has on the extraction efficiency of Pt. In the aqueous feed solution containing Pt(IV) and Pd(II), the addition of  $\text{P}_{66614}\text{Cl}$  releases the hydrophilic anion  $\text{Cl}^-$ , which is more hydrophilic than  $\text{NTf}_2^-$ , thus, the extraction of Pt which proceeds via an anion-exchange mechanism is further promoted. The extraction of Pd is only slightly increased, never exceeding 20%. The exchange mechanism is verified by the observed decreasing Pt extraction efficiency when the HCl concentration is increased, which implies that the Pt-chlorocomplexes and the additional  $\text{Cl}^-$  anions compete for extraction. Partial stripping of Pt and Pd from the IL phase was feasible with the aid of  $\text{HNO}_3$ , however, due to the large capacity of the IL, this did in no way hamper its reuse for further extraction cycles. Additionally, trihexyltetradecylphosphonium nitrate ( $\text{P}_{66614}\text{NO}_3$ ) formed during the stripping step is regenerated to  $\text{P}_{66614}\text{Cl}$  in the extraction step, presumably through anion exchange of  $\text{NO}_3^-$  with  $\text{PtCl}_4^-$ , thus, the extraction efficiency remains unaffected. However, lack of experimental verification of the assumed anion-exchange mechanism does not allow to assess the extent of the possible contamination of the aqueous phase by  $\text{NTf}_2^-$  anions.<sup>187</sup>

The extraction capacity of 1-ethyl-3-methylimidazolium bis(trifluoromethylsulfonyl)imide ( $[\text{C}_2\text{mim}][\text{NTf}_2]$ ) for Pd(II) from aqueous synthetic solutions as well as the extraction speed are dramatically increased by addition of the sulfur-ligand 1,3-diethyl-imidazole-2-thione (EElmT) (8% to 98%, 15 min to 3 min).

A 10-fold volume of aqueous phase compared to the organic one is needed. Introduction of additional Cl<sup>-</sup> via higher HCl concentration disrupts the coordination of Pd with the ligand, thus, lowering the extraction efficiency, unless the concentration of the ligand is carefully tuned (0.005 mM ligand/0.5 mL organic phase), in which case the dependency of the Pd extraction on the acidity of the solution becomes negligible. Pd can be quantitatively stripped with a thiourea/HCl or NH<sub>4</sub>SCN/NH<sub>4</sub>OH mixture. The developed extraction system additionally provides the possibility for the preparation of metal complex crystals. The extraction is attributed to a neutral coordination mechanism, as X-Ray single crystal diffraction and X-Ray powder diffraction of the extracted complex verify. This is the desirable scenario, since neutral extraction spares IL losses to the aqueous phase, normally observed in ion exchange, and prevents a reduction in the volume of the organic phase. A study of the structure of the formed complexes was performed with the aid of XRD; the Pd-EEImT complexes have a 1:1 and 1:2 stoichiometry, both of which are extracted in the organic phase in percentages correlated to the amount of the employed extractant. X-Ray crystallography data further verified the computational finding that the *cis* configuration of the extracted complexes is more energetically stable than the *trans*.<sup>188</sup>

The positive outcome of the thione extractant-based system further sparked the authors' interest in synthesizing and investigating its selone analogue. Organic phase comprising the novel extractant dissolved in imidazolium ILs ([C<sub>4</sub>mim][NTf<sub>2</sub>] or [C<sub>2</sub>mim][NTf<sub>2</sub>] or [C<sub>8</sub>mim][NTf<sub>2</sub>]) was mixed with 10-fold aqueous Pd(II) model solutions. Quantitative extraction of Pd was feasible regardless of the diluent employed, however, the shorter the chain attached to the IL the higher the amount of selone extractant required to attain maximum Pd extraction capacity. Employing higher amount of extractant in [C<sub>4</sub>mim][NTf<sub>2</sub>] is, nevertheless, a worthwhile trade-off considering that the robustness of the system to variations in acidity is greatly enhanced in this case. Ascending HCl concentration acidizes the BmimSe extractant, thus, inducing electronegativity to the Se atom, thereby it exhibits stronger interaction with Pd than its neutral version. Furthermore, based on <sup>1</sup>H-NMR data, it was concluded that at higher acidities selone dimerizes (Figure 26) and coordinates with Pd atoms as well. The proposed neutral extraction mechanism can be represented by the following equation (equation 31):



Changing the S donor atom from their previous work to Se, improves the extraction efficiency of Pd; however, the implications of using Se, which can get toxic beyond a certain concentration, have not been considered by the authors. Selone's high affinity for Pd is evident in multi-element synthetic solutions (Pd, Ni, Mn, Zn, Al, Mg, Sn, Cd), where Pd is quantitatively extracted, whereas there is negligible extraction of all other elements (<4%). A two-stage highly efficient stripping of Pd (98%) was performed with a mixture of NH<sub>4</sub>SCN/NH<sub>4</sub>OH. Despite their stripping efficiency, the environmental toxicity of these two compounds render them far from ideal from an environmental perspective.<sup>189</sup>

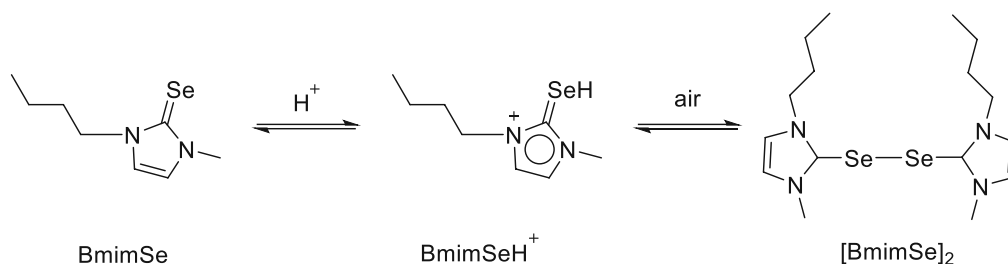


**Figure 26.** Acidization and dimerization of BmimSe.<sup>189</sup>

The extraction capacity of the IL [C<sub>8</sub>mim][PF<sub>6</sub>] for Pt(II), Pt(IV) and Pd(II) versus the commercially available quaternary ammonium metal extractant distearyldimethylammonium chloride (DSDMAC) was assessed. Metal salts were used for the preparation of Pt and Pd mixtures in HCl solutions, whereas the IL and the ammonium salt were dissolved in chloroform and mixed on a 1:1 volume ratio with the aqueous phase for the extraction. While the DSDMAC demonstrates a higher extraction efficiency for both metals, the IL yields a more efficient separation, which can be explained based on the proposed ion-pair formation mechanism; the ion-pair mechanism generally favors the extraction of Pt over Pd. This is reflected by the higher separation factor of Pt over Pd exhibited in the IL ( $\beta_{Pt/Pd}$ =4.1 and 27 for Pt(II) and Pt(IV), respectively) compared to the metal extractant DSDMAC ( $\beta_{Pt/Pd}$ =2.7 and 13 for Pt(II) and Pt(IV), respectively).<sup>190</sup>

The effect of the side-chain length and steric hindrance (of amino moieties) on the extraction efficiency of the imidazolium-based IL [C<sub>4</sub>mim][NTf<sub>2</sub>] was reported.<sup>191</sup> Amino moieties comprising varying chain lengths, as well as branched chains and cyclohexane units (Figure 27) were synthesized and subsequently evaluated for their PGM extraction capacity from their model solutions. As expected, hydrophobicity had a direct effect on the extraction efficiency; the ILs with attached C<sub>6</sub> and C<sub>8</sub> moieties exhibited the highest extraction yields for all three PGMs, namely >80% for Pt(IV) and Pd(II) over a wide HCl concentration range (0.3-4.0 M) and up to 70% for Rh at 3.0-4.0 M HCl. The dependency of Rh extraction on the HCl concentration is attributed to the variation of its complex species present at different concentrations; in the range 3.0-4.0 M HCl the dominating form is RhCl<sub>6</sub><sup>3-</sup> and it is the only species that can be extracted by the IL comprising the C<sub>8</sub> moiety. Ion pairing between the amino moiety and the metal-chloride ions is the extraction mechanism that FT-IR and <sup>1</sup>H-NMR data suggest. When moieties with steric hindrance were inserted in the IL, the extraction values for all three PGMs dropped dramatically. Approximately 80% of each metal can be back-extracted from the IL with the C<sub>6</sub> moiety with NH<sub>3</sub> (ranging from 0.5-12%), which can be further increased to 90% after a second back-extraction cycle, an effect stemming from the deprotonation of the protonated amino moiety by NH<sub>3</sub>, as <sup>1</sup>H-NMR data confirmed. Additionally, the IL can be reused without significant loss in the extraction efficiency of PGMs; however, the recovered IL needs to be redosed with fresh IL, since repeated extraction and back-extraction progressively deplete the IL. High selectivity toward PGMs was exhibited when the system was applied to a model car catalyst leach liquor solution containing Pt, Pd, Rh, Zn, Fe, Al, Cu, Ni and Mg.<sup>191</sup>

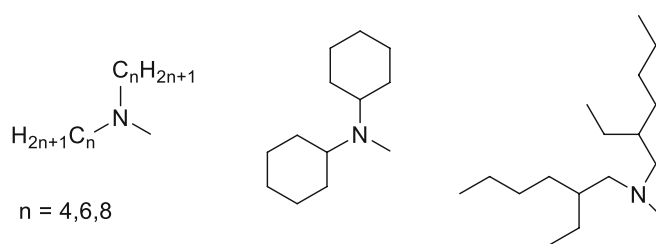
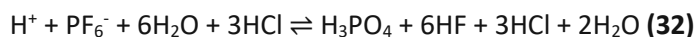


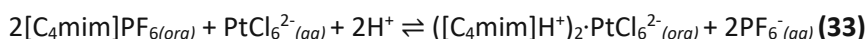
**Figure 27.** Structures of amino moieties attached to the IL to enhance the extraction efficiency of [C<sub>4</sub>mim][NTf<sub>2</sub>].<sup>191</sup>

Zhang et. al<sup>192</sup> contributed a novel approach to the separation of Pt(IV), Pd(II) and Rh(III) relying on their selective partitioning in a three-liquid-phase system comprising the hydrophobic IL [C<sub>4</sub>mim][PF<sub>6</sub>]. Simple adjustment of the HCl concentration in the aqueous model solution comprising the three elements to values below 1.0 M promotes the migration of Pt to the IL phase (72.3%), Pd to the organic nonane containing the Pt-selective extractant diisopentyl sulfide phase (99.3%), while Rh remains in the aqueous solution (91.6%). Increasing acidity has no effect on Pd and negligible effect on the partition of Rh, however, it dramatically decreases the partition of Pt into the IL phase. This phenomenon can be attributed to the degrading effect that high acidities exert on the IL (equation 32), as IR data verified.





Similarity in the sizes of  $\text{PtCl}_6^{2-}$  and  $\text{PF}_6^-$  facilitates the exchange mechanism between them and the selective extraction of Pt in the IL phase. On the contrary, the difference in size of  $\text{PdCl}_4^{2-}$  and  $\text{RhCl}_6^{3-}$  to  $\text{PF}_6^-$  prevents their co-extraction with Pt. The effect of NaCl concentration on the partition behavior of the three PGMs was investigated (Figure 28). The presence of excess  $\text{Cl}^-$  leads to the complexation of Pt, Pd and Rh, thereby inhibiting their hydration, which results in their increased partitioning in the IL phase. Addition of salts (KCl, LiCl,  $\text{Na}_2\text{SO}_4$ ,  $\text{K}_2\text{SO}_4$ ,  $\text{Li}_2\text{SO}_4$ ,  $\text{NaNO}_3$ ) to the aqueous phase generates a surge in the amount of Pt forced in the IL phase proportional to their salting-out capacity. Back-extraction of 90% Pd is feasible by contacting twice equal volumes of the organic phase with 1.0 M  $\text{NH}_3$ , while  $\text{HNO}_3$  or HCl can strip increasing amounts of Pt with increasing acidity. Nevertheless, this approach is far from ideal considering that high acidities lead to the decomposition of the expensive IL. Additionally, the proposed extraction mechanism (equation 33)



implies contamination of the aqueous phase with  $\text{PF}_6^-$  anions, which, as later discussed, can hydrolyze and produce HF.<sup>192</sup>

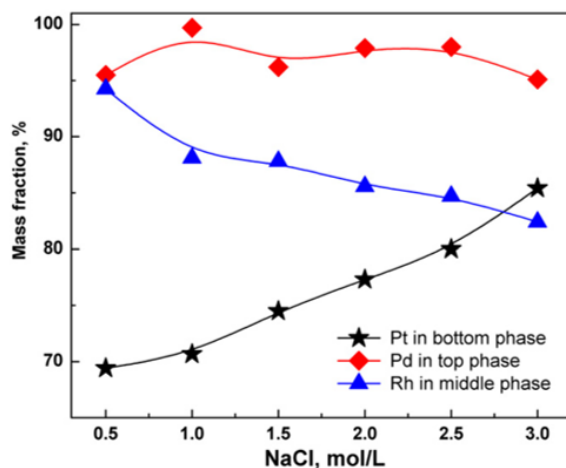


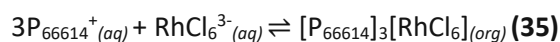
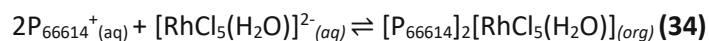
**Figure 28.** Effect of  $\text{Cl}^-$  concentration in initial aqueous solutions on partition of Pt(IV), Pd(II) and Rh(III) in two-phase system  $[\text{C}_4\text{mim}][\text{PF}_6]/\text{H}_2\text{O}$  1:6, 1.0 M HCl.<sup>192</sup>

### 3.1.3.3 Phosphonium-based ionic liquids

The PGM extraction conditions and results that will be discussed in the present section are summarized in Table 5.

Ionic liquids comprising the  $\text{P}_{66614}^+$  cation proved very effective in the extraction and separation of Pd(II) and Rh(III). Acidic solutions of the metals were prepared and mixed with pure hydrophobic ILs with different building anions ( $\text{Cl}^-$ ,  $\text{Br}^-$ ,  $\text{DCA}^-$ ) on a 4:1 (w/w) ratio. Between the halogen-anion analogues, higher extraction efficiencies for both metals were observed with the ones containing the  $\text{Br}^-$  anion due to the fact that the PGM-Br complexes are larger with lower solvation energies as opposed to their PGM-Cl equivalents. Kinetics of Rh extraction in trihexyltetradecylphosphonium dicyanamide ( $\text{P}_{66614}\text{DCA}$ ) is extremely slow (in the order of days), which can be exploited for its separation from Pd that can be extracted within minutes only. Separation of the two metals is quite easy by simple adjustment of the HCl concentration in the aqueous phase when the halogen-containing ILs are employed; concentrations over 2 M have a dramatic impact on the extraction of Rh, whereas quantitative extraction of Pd with HCl up to 6 M is feasible. As previously noted by other authors, the formation of the  $\text{RhCl}_6^{3-}$  complex, formed

at higher HCl concentrations, has a more negative charge, thus, a higher solvation energy than the  $[\text{RhCl}_5(\text{H}_2\text{O})]^{2-}$  species present at lower concentrations, therefore, it is not as easily extracted. This tendency of Rh extractability to decrease with increasing acidity is also reflected by the gradual decrease of its distribution ratio (Figure 29). The authors assume the following equations for the extraction mechanism (equations 34 and 35):



with (34) taking place at  $[\text{HCl}] \leq 3 \text{ M}$  and (35) at  $[\text{HCl}] \geq 6 \text{ M}$ . The authors quite sensibly argue that the observed decrease in Rh extractability could also be attributed to the increasing competition between  $\text{Cl}^-$  and the Rh-chloro complexes for ion exchange. Therefore, the mechanism described by (34) and the exchange with  $\text{Cl}^-$  anions are expected to occur simultaneously. According to a previous work of the authors,<sup>193</sup> experimental data fitting proved these two seemingly different mechanisms to be in fact equivalent. Nevertheless, the authors do not conclusively suggest a predominant mechanism for the extraction of Rh.<sup>194</sup>

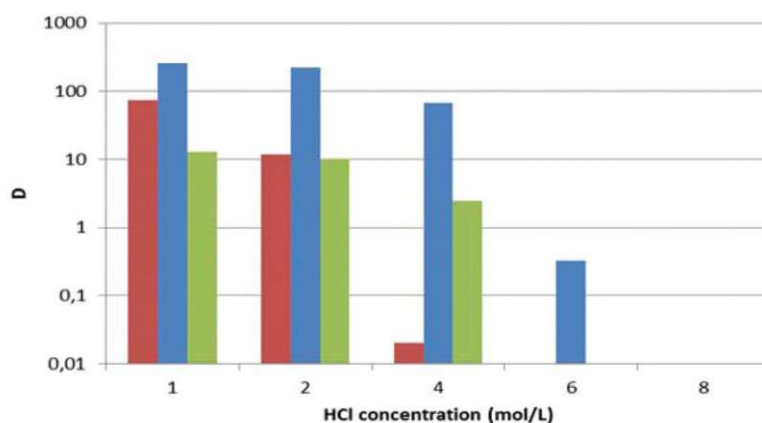


**Figure 29.** Distribution ratio for Rh(III) as a function of HCl concentration. 250 mg/L Rh(III), red is  $\text{P}_{66614}\text{Cl}$ , blue is  $\text{P}_{66614}\text{Br}$  and green is  $\text{P}_{66614}\text{DCA}$ .<sup>194</sup>

The research group used the extraction of Rh(III) with  $\text{P}_{66614}\text{Cl}$  to decipher the extraction mechanism as well as the extracted species of Rh.<sup>195</sup> Key assumption was that the ligand to metallic-ion ratio ( $R = [\text{Cl}^-]/[\text{Rh(III)}]$ ) and the Rh species are intrinsically connected. A Rh speciation diagram was constructed by modelling with principal component analysis and multivariate curve resolution of UV-Vis spectra collected at various  $R$  values (Figure 30). The authors used the classical extended Debye-Hückel expression for the activity coefficient to calculate the successive thermodynamic complexation constants. They used the following simplified expression for the activity coefficient (equation 36):

$$\log \gamma = \frac{AZ^2\sqrt{I}}{1+B\sqrt{I}} + CI \quad (36)$$



**Table 5.** Summary of PGM extraction conditions and results with phosphonium-based ionic liquids.

PGM Solution	Ionic Liquid (+ Diluent)	Ratio (O/A) <sup>a</sup>	Time (min) <sup>b</sup>	Extr. Efficiency (%) Distribution Ratio (D)	Type	Ref. No
i. 250 mg/L/metal: Pd(II), Rh(III) in 6.0 M HCl ii. 250 mg/L Pd(II), 50 mg/L Rh(III) in 8.0 M HCl	i. P <sub>66614</sub> Cl pure ii. P <sub>66614</sub> Br pure	1/4	1140	i. >99% Pd, D <sub>Pd</sub> =570 <6% Rh, D <sub>Rh</sub> =0.19 ii. >99% Pd, D <sub>Pd</sub> =740 <6% Rh, D <sub>Rh</sub> =1.38	A	194
428 mg/L Pt(IV), 142 mg/L Rh(III), 169 mg/L Ru(III) in 0.1 M HCl	5.0 mM P <sub>66614</sub> Br in toluene	1/1	20	Fresh >90% Pd, 50% Rh, 60% Ru Aged >90% Pd, 44% Rh, 10% Ru	A	196
2.5 mM/metal: Rh(III), Ru(III), Pt(IV) or Pd(II) in 0.1 M HCl	0.005 M P <sub>66614</sub> Cl in toluene 0.005 M P <sub>66614</sub> DOP in toluene	1/1	20	Fresh 50% Rh, D <sub>Rh</sub> =1.25, 60% Ru, D <sub>Ru</sub> =1.5, 95% Pt, 100% Pd Aged 40% Rh, 3% Ru, 95% Pt, 100% Pd	A	197
5.0 mM Pd(II) in 0.1 M HCl	5.0 mM P <sub>66614</sub> Cl in toluene	1/1	2	97% Pd	A	198
5.0 mM Pd(II) in 0.1 M HCl	5.0 mM P <sub>66614</sub> Cl in toluene	1/1	5	97% Pd, D <sub>Pd</sub> =31.62	A	199
2.5 mM/metal: Pd(II), Pt(IV), Rh(III), Ru(III), Cu(II), Ni(II), Fe(III), Pb(II) in 0.1 M HCl	2.5-5.0 mM i. P <sub>66614</sub> Cl in toluene or ii. P <sub>66614</sub> DOP in toluene	1/1	2	i, ii. 66% Pd, 20% Pt, <3% each of the rest	A	200
2.5 mM Pd(II) in 0.1 M HCl	5.0 mM P <sub>66614</sub> Br in toluene	1/1	1	100% Pd	A	201
5.0 mM Pd(II) in 0.1 M HCl	5.0 mM P <sub>66614</sub> DOP in toluene	1/1	5	96% Pd, D <sub>Pd</sub> >80	A	202
2.5 mM/metal: Ru(III), Rh(III) in 0.1 M HCl	5.0 mM i. P <sub>66614</sub> Cl ii. P <sub>66614</sub> Br iii. P <sub>66614</sub> DOP iv. P <sub>66614</sub> NTf <sub>2</sub> <sup>-</sup> in toluene	1/1	5	i-iii. 60-65% Ru i-iii. 45-55% Rh iv. 5% Ru, 0% Rh	A	203
0,5 mM/metal: Pt(IV), Rh(III) in 0.1 M HCl	0.1 M P <sub>66614</sub> Cl in toluene	1/5	10	100% Pt, 2.5% Rh, β>267	A	173
1.1 mM Pt(IV), 0.8 mM Pd(II), 0.6 mM Ru(III), 0.4 mM Rh(III) in 0.8 M HCl	20.0 mM P <sub>66614</sub> Cl in toluene	1/1	20	>95% Pt, >95% Pd, 55% Ru, 15% Rh β <sub>Pd/Pt</sub> =0.41, β <sub>Pd/Ru</sub> =1700, β <sub>Pd/Rh</sub> =210000	A	204
100 mg/L Pt(IV), 55 mg/L Pd(II), 25 mg/L Rh(III) in 0.1 M HCl	2.0 M P <sub>66614</sub> Cl in xylene	1/1	10	98.1% Pt, D <sub>Pt</sub> =15.85, 99.9% Pd, D <sub>Pd</sub> =18.79, <2% Rh	A	205
200mg/L/metal: Pt(IV), Pd(II), Rh (III) in 0.5 M HCl	P <sub>88812</sub> Cl pure	1/2	80	100% Pt, D <sub>Pt</sub> =2.24, 100% Pd, D <sub>Pd</sub> =2.14, 85% Rh, D <sub>Rh</sub> =1.12	A	206

<p>Step 1 367.6 mg/L Pd, 32.5 mg/L Rh, 77.7 mg/L Pt, 32.2 mg/L Fe, 52.9 mg/L Zr, 3898 mg/L Al, 107.9 mg/L Ce, 39.3 mg/L La, 379.2 mg/L Ba, 555.4 mg/L Mg in 5.0 M HCl</p> <p>Step 2 Pd, Rh, Pt, Fe, Zr, Al, Ce, La, Ba, Mg in 1.0 M HCl</p>	P <sub>88812</sub> Cl pure	1/2	<p>Step 1 10</p> <p>Step 2 300</p>	<p>Step 1 100% Pd, 85% Fe, 55% Zr, &lt;10% each of the rest</p> <p>Step 2 84% Rh, 62% Fe, &lt;10% each of the rest</p>	A	207
<p>Step 1 78.7 mg/L Pt, 156 mg/L Pd, 26.8 mg/L Rh, 50.2 mg/L Fe, 21.6 mg/L Zn, 3792 mg/L Al, 399 mg/L Ce, 523 mg/L La, 1016 mg/L Mg, 8.2 mg/L Cu in 5.0 M HCl leachate</p> <p>Step 2 Rh, Zn, Cu in 2.0 M HCl raffinate</p>	P <sub>88812</sub> Cl pure	1/2	10	<p>Step 1 100% Pt, 99% Pd, 80% Rh, 97% Cu, 95% Zn</p> <p>Step 2 80% Rh</p>	A	208
100 mg/L/metal: Au(III), Pd(II), Pt(IV) in 1.0 M HCl/2.0 M NaCl	1.9 mM P <sub>66614</sub> Cl/10 g/L TX-100/H <sub>2</sub> O <sup>c</sup>	n.a.	60	94.7% Au, 68.4% Pd, 89.1% Pt	A <sup>d</sup>	209

<sup>a</sup> O= organic phase, A= aqueous phase. <sup>b</sup> All extractions were performed at RT. <sup>c</sup> Performed at 60 °C. <sup>d</sup> An IL-in-water microemulsion was used.

Investigating HCl concentrations in the range 0.75-12.0 M, they concluded that three species of Rh are encountered in acidic solutions;  $[\text{RhCl}_4(\text{H}_2\text{O})_2]^-$ ,  $[\text{RhCl}_5(\text{H}_2\text{O})]^{2-}$  and  $\text{RhCl}_6^{3-}$ . The distribution ratio for Rh dramatically decreased by increasing R value and increasing  $\text{Cl}^-$  concentration ( $D_{\text{Rh}}=61.83$  at 0.75 M HCl,  $D_{\text{Rh}}=0.81$  at 8.00 M HCl), which is in line with a decrease in the amount of  $\text{RhCl}_4^-$ , thus, it can be deduced that  $\text{RhCl}_4^-$  is the mainly extractable species, whereas the other two species have no significant contribution to the extraction mechanism. Although the Rh extraction mechanism could be explained either by ion-exchange or ion-pair formation, the solubility of P<sub>66614</sub>Cl in H<sub>2</sub>O, mainly accounts for the equivalency of these two mechanisms in hydrophobic ILs.<sup>195</sup>

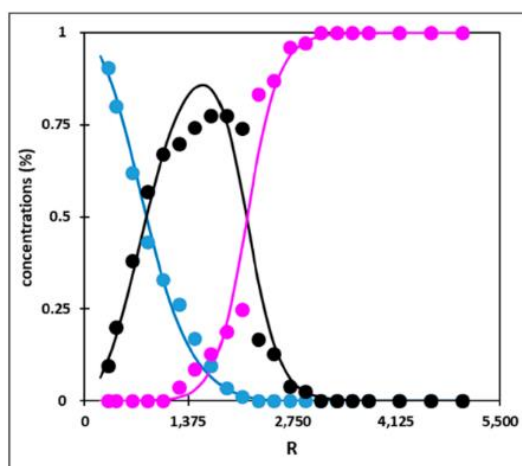


**Figure 30.** Speciation diagram of Rh constructed by Svecova et al. Concentration profile of  $[\text{RhCl}_4(\text{H}_2\text{O})_2]^-$  (blue dots),  $[\text{RhCl}_5(\text{H}_2\text{O})]^{2-}$  (black dots) and  $\text{RhCl}_6^{3-}$  (pink dots). The data has been fitted using the extended Debye-Hückel expression (lines).<sup>195</sup>

The impact of solution ageing on the capacity of Pt(IV) and Rh(III) to be extracted by P<sub>66614</sub>Br from their synthetic mixtures was assessed. A 5.0 mM solution of the IL in toluene is brought in contact with an equal volume of a 0.1 M HCl solution that contains the metals of interest, upon which instant extraction of Pt (>90%, 1 min) and fast extraction of Rh (<50%, 5 min) was observed. Ageing of the solutions (2 weeks) had no effect on Pt extraction, however, the extraction of Rh was decreased by approx. 15%. Addition of NaCl decreases the extraction for both metals in fresh solutions, however, in aged solutions it has no significant effect on the already decreased extraction of Rh (Figure 31). Regardless of the age of the solution, the extraction of Pt remains constant in the region 0.1-5.0 M HCl, whereas the approx. 10% decrease for Rh over time can be eliminated by employing a 5.0 M HCl solution. Partial stripping of Pt (54%) and Rh (38%) from fresh solutions, was performed with 0.5 M NH<sub>4</sub>OH and 5.0 M HCl, respectively. Further studies are required to elucidate the extraction mechanism and clarify the difference observed in selectivity over time. The authors assume anion exchange is taking place; however, they have not addressed the inevitable contamination of the aqueous phase by Br<sup>-</sup> and how this might affect the performance of the IL in case it is reused. We should not neglect to mention that toluene is a possible carcinogenic, while NH<sub>4</sub>OH poses a danger to the aquatic environment.<sup>196</sup>

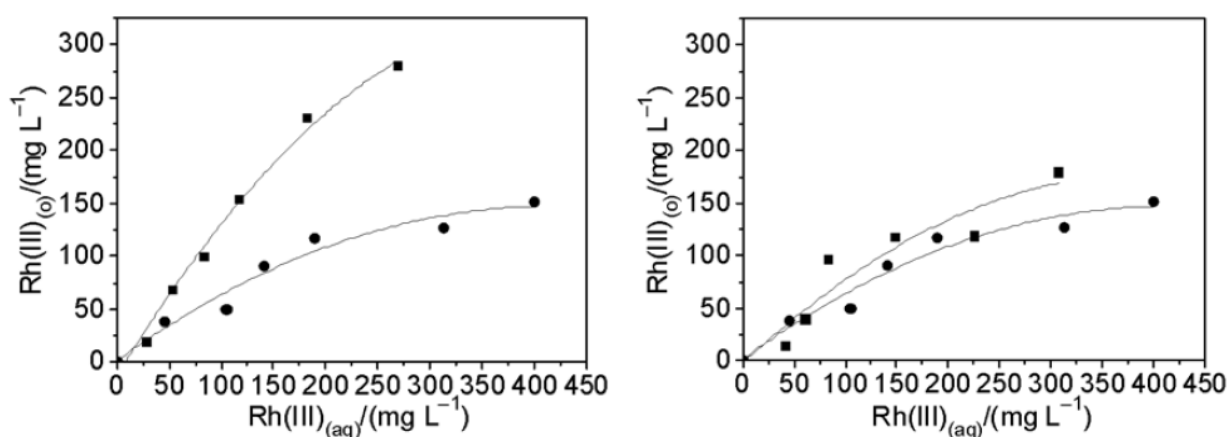


**Figure 31.** Extraction isotherms for Rh from fresh solutions (left) and aged solutions (right), with NaCl (■) and without NaCl (●).<sup>196</sup>

The authors further expanded the research on the effect of solution ageing on the extracting capabilities of P<sub>66614</sub>Cl and trihexyltetradecylphosphonium bis-(2,4,4-trimethylpentyl)phosphinate (P<sub>66614</sub>DOP). Synthetic acidic solutions containing Rh(III), Ru(III) and Pt(IV) or Pd(II) were employed in these studies. Overall, P<sub>66614</sub>Cl demonstrates slightly better performance in terms of extraction compared to its DOP counterpart, thus, ageing effects were assessed in the former. In fresh solutions, Rh extraction is dramatically impacted by HCl concentrations exceeding 0.1 M, which is completely reversed for Ru. Ageing (14 days) has a significant effect on the extraction of Rh and Ru, but only below 1.0 M HCl. The implication that arises from this observation is that over time the initially formed Rh- and Ru-chlorocomplexes transform to less extractable species, as verified by UV-Vis data, whereas increased HCl concentrations have a stabilization effect on the initially formed complexes. On the contrary, Pt and Pd are quantitatively extracted regardless of the solution age. A very interesting observation of the authors is that an increase of the concentration of HCl or NaCl in the solution, has a negative impact on the distribution ratios of Rh (Figure 32).<sup>197</sup> The same observation was made in many of the studies cited in this review and it is a quite important one; it points to the fact that, when an ion-exchange mechanism is involved, reduced extractability at increasing HCl concentration can be possibly assigned to the impact of increasing Cl<sup>-</sup> concentration rather than increasing acidity of the solution, according to Le Chatelier's principle.

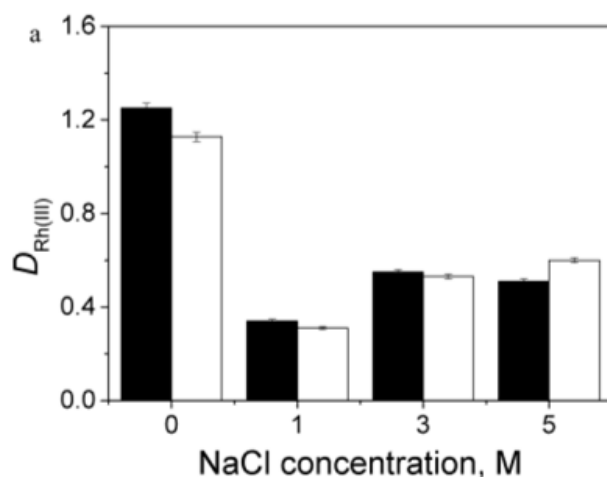


**Figure 32.** Effect of NaCl concentration on the distribution ratio of Rh, in P<sub>66614</sub>Cl (black) and P<sub>66614</sub>DOP (white).<sup>197</sup>

The extraction of Pd(II) from HCl model solutions with the hydrophobic IL P<sub>66614</sub>Cl in toluene was investigated. A negative effect, in terms of extraction efficiency, with increasing HCl concentration and NaCl addition was established. The Pd extraction isotherms were provided by the authors (Figure 33). The proposed mechanism, which leads to the virtually quantitative extraction of Pd (97%), is anion exchange.<sup>198</sup>

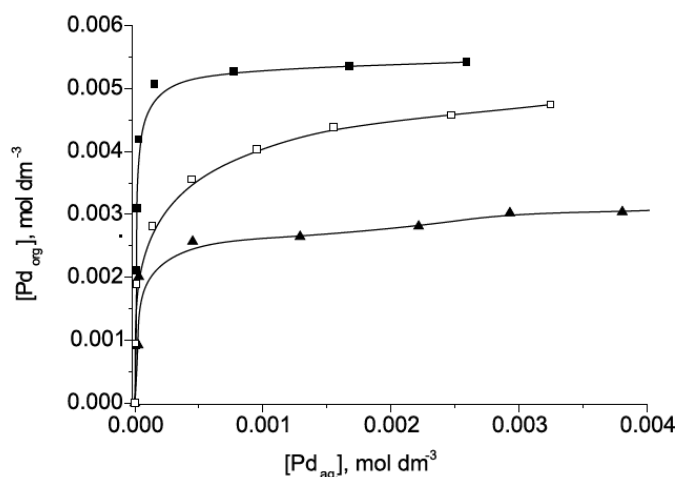


**Figure 33.** Isotherms of Pd(II) extraction from 0.1 M HCl (■), 3.0 M HCl (▲) and 0.1 M HCl/0.5 M NaCl (□). Aqueous phase: 1-5 mM Pd, organic phase: 5 mM P<sub>66614</sub>Cl in toluene.<sup>198</sup>

The authors further built on their initial investigation, proving that the phosphonium-based IL P<sub>66614</sub>Cl is highly efficient in the fast and quantitative extraction of Pd(II) from HCl model solutions. To facilitate the handling of the highly viscous IL, its mixture with toluene was used as an organic phase. A contact time of 5 min with the aqueous phase was adequate to achieve complete extraction of Pd. Interestingly enough, upon contact of the two phases (without shaking) there is an instantly spontaneous transfer of Pd to the organic phase, suggesting that the migration of Pd is controlled by diffusion. The acidity of the aqueous solution plays a critical role in the extraction efficiency, with increasing HCl concentrations exerting a negative influence. An anion-exchange mechanism is proposed and it was proven in a previous publication of the same authors<sup>198</sup> that the extraction is negatively affected both by increasing concentration of HCl and NaCl; however, they seem to associate the dependency of Pd extraction on the acidity of the solution rather than the Cl<sup>-</sup> concentration. This assumption is probably not true, or not entirely true, since increasing Cl<sup>-</sup> concentration, whether introduced via HCl or NaCl, simply means higher competition between the Cl<sup>-</sup> and the Pd-chlorocomplexes for exchange with the IL anion. To achieve

quantitative extraction, the ratio of the IL to Pd should exceed 1 and the HCl concentration should not exceed 0.1 M. Construction of the Pd extraction isotherm with the IL at two different HCl concentrations indicates that the loading capacity of the IL is almost double at lower HCl concentrations (5.4 mM at 0.1 M HCl, 2.8 mM at 3 M HCl). The economic aspect of the process is demonstrated via the recycling possibility of the IL. The strong ionic bond between Pd and the IL is broken by addition of  $\text{NH}_4\text{OH}$ , as demonstrated by the fast and complete stripping of Pd. The recovered IL can be reused without any significant drop in its extraction capacity.<sup>199</sup>

In subsequent investigations, the authors proved the high selectivity of  $\text{P}_{66614}\text{Cl}$  and  $\text{P}_{66614}\text{DOP}$  for the extraction of Pd(II) over a number of other metals (Cu, Ni, Pd, Fe, Rh, Ru, Pt) from HCl model solutions. Selectivity toward the extraction of Pd from aqueous multi-metal solutions to the (equal volume) organic phase containing the IL diluted in toluene is decidedly affected by the concentration of HCl in the aqueous phase. Since the authors assume an anion-exchange mechanism, it is most probably the increasing Cl<sup>-</sup> concentration when HCl increases and not the increasing acidity that negatively impacts the extraction. Selective extraction of Pd (66%) with  $\text{P}_{66614}\text{Cl}$  from a 0.1 M HCl solution is feasible with accompanying elements extracted by less than 10% and 20% Pt extracted along with Pd. Increasing HCl concentrations lead to significant deterioration in selectivity toward Pd. The most probable explanation for this behavior is the competition of  $\text{PtCl}_6^{2-}$ , which forms at higher acidity, with  $\text{PdCl}_4^{2-}$ . The extraction tendency of PGMs is known to follow the order  $[\text{MCl}_6^{2-}] > [\text{MCl}_4^{2-}] \geq [\text{MCl}_6^{3-}]$ , which is consistent with this experimental observation. Subsequent stripping of the organic phase with 0.5 M  $\text{NH}_3$  allows further and almost complete separation of Pd from Pt.<sup>200</sup>

The authors further assessed the extractability of  $\text{P}_{66614}\text{Br}$  (Cyphos 102) toward Pd(II) from its aqueous solutions. Mixing of Cyphos 102 in toluene with Pd in HCl yielded quantitative extraction within a few minutes. Low HCl content (0.1 M) favors the extraction, which can be reduced by 10-15% by increasing HCl up to 5.0 M. In contrast, increasing ionic strength, which was evaluated via NaCl addition in the aqueous feed in varying concentrations, had only a minor impact on the extraction efficiency; however, the loading capacity of the organic phase is different depending on whether NaCl is present or not (Figure 34). Stripping was equally fast (10 min) and efficient (90%) with a  $\text{NH}_4\text{OH}$  solution, thus, allowing the reuse of the organic phase for further extractions. Based on these results, the authors were further inspired to apply the IL on a polymer membrane where it functions as a carrier for the transport of Pd ions across the membrane. This application will be discussed in detail later in the present chapter.<sup>201</sup>

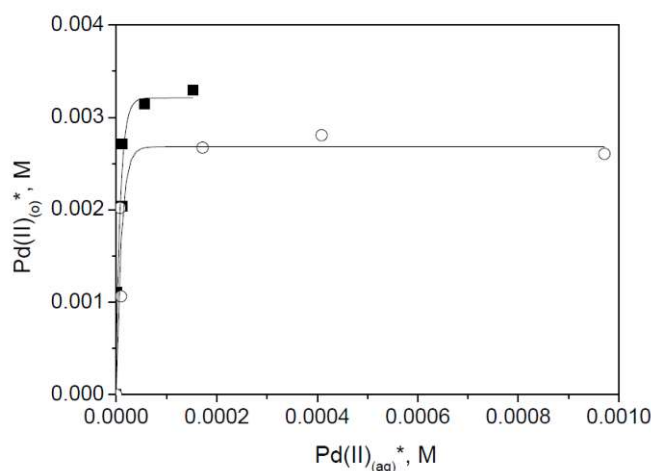


**Figure 34.** Isotherms of Pd(II) extraction, with NaCl (○) and without NaCl (■). Aqueous phase:  $10^{-3}$ - $5 \cdot 10^{-3}$  M Pd in 0.1 M HCl, organic phase:  $5 \cdot 10^{-3}$  M Cyphos 102.<sup>201</sup>

Cyphos® IL 104 (P<sub>66614</sub>DOP) mixed with toluene can be effectively used for the fast (5 min) and quantitative extraction of Pd(II) from HCl model solutions. Addition of toluene facilitates the handling of the highly viscous IL. There is a correlation between the HCl concentration and the loading capacity of the IL phase in Pd, which decreases to almost half when the HCl concentration is increased from 0.1 M to 3.0 M (96% and 52%, respectively). The extraction proceeds via an anion-exchange mechanism, as <sup>31</sup>P-NMR indicates the ion pairing of the P<sub>66614</sub><sup>+</sup> with Pd. According to calculated thermodynamic parameters, the reaction is exothermic, thus, raising the temperature up to 70 °C has a negligible effect on the extraction efficiency. Formation of stable Pd complexes with ammonia renders NH<sub>4</sub>OH a highly effective stripping agent for the removal of Pd from the organic phase in a single step. The authors constructed the isotherm for Pd extraction with the IL at two different HCl concentrations and concluded that the loading capacity of the IL is almost double at lower HCl concentrations (5 mM at 0.1 M HCl, 2.6 mM at 0.1 M HCl). The developed process is environmentally and financially beneficial, since the IL has been proven to retain its extractive capability after five extraction/stripping cycles. Unfortunately, the authors did not mention possible contamination of the aqueous phase by the phosphinate anion or associated reduction of the organic phase volume.<sup>202</sup>

The effect of the building anion of P<sub>66614</sub>-based ILs on their extraction capacity for Rh(III) was additionally investigated by the authors. Acidic metal model solutions were mixed with equal volumes of phosphonium ILs dissolved in toluene (5.0 mM), comprising the anions Cl<sup>-</sup>, Br<sup>-</sup>, DOP<sup>-</sup> and NTf<sub>2</sub><sup>-</sup>. Although all ILs, with the exception of Cyphos 109 trihexyltetradecylphosphonium bis(trifluoromethylsulfonyl)imide (P<sub>66614</sub>NTf<sub>2</sub>), could extract over 40% of Rh, P<sub>66614</sub>Cl was the most efficient one yielding 55%. Maintaining the HCl to 0.1 M is essential in order to maximize the Rh extraction, which drops significantly with increasing HCl concentration. The substantially higher hydrophobicity of the NTf<sub>2</sub><sup>-</sup> anion, in comparison with the other anions employed, justifies the inability of the hydrophilic and hydrated Rh-chlorocomplexes to undergo an anion-exchange mechanism in the presence of Cyphos 109. Correlation between the nature of the loaded IL and stripping efficiency was also established; 20% Rh could be removed from P<sub>66614</sub>Cl with 0.5 M HNO<sub>3</sub>, whereas the same agent could strip 40% Rh from P<sub>66614</sub>DOP.<sup>203</sup>

A comparative study of the extraction and separation efficiency of P<sub>66614</sub>Cl toward Pt and Rh, from their mixed model solution, when it is diluted with different solvents was performed. P<sub>66614</sub>Cl diluted in CH<sub>2</sub>Cl<sub>2</sub> (0.1 M) and mixed with the acidic metal solution (1:5) extracted 95% Pt within the first 10 min, however, 20 additional minutes were required to yield complete extraction. On the other hand, only 7% Rh could be extracted. Switching to toluene increased the Pt to 100% within the first 10 min, whereas only 2.5% of Rh was extracted ( $\beta_{Pt/Rh} > 267$ ). Therefore, using toluene as the IL diluent increased the separation efficiency and shortened the separation time.<sup>173</sup>

A detailed and effective process for the separation of Pt(IV), Pd(II) and Rh(III) from their acidic model solutions has been proposed. Quantitative extraction of Pt and Pd from HCl solutions (0.8 M) proved successful by contacting the aqueous phase with an equal volume of organic phase containing 5 mM P<sub>66614</sub>Cl in toluene. Simultaneously, their separation from Rh was attained since the bulky octahedral Rh complexes comprising large hydration layers can only be extracted to a negligible extent. In the ensuing stripping with 0.1 M thiourea in 0.5 M HCl, Pd is quantitatively removed from the organic layer leaving Pt behind, the majority of which is subsequently recovered with the aid of 1 M HNO<sub>3</sub>. As FT-IR data prove, regeneration of the IL is feasible with addition of H<sub>2</sub>O and HCl which scrub the nitrates formed in the organic phase after the 2<sup>nd</sup> stripping step (Figure 35). Additionally, it seems that, after stripping, H<sub>2</sub>O molecules enter the organic phase, as the O-H stretch in the IR spectrum of the IL after stripping with H<sub>2</sub>O indicates. The regenerated IL exhibits lower extraction capacity than the fresh one,



i.e., 2-fold decrease for Pt and 4-fold decrease for Pd; however, by contacting the aqueous phase twice with the regenerated IL more than 90% of each metal is extracted. It is quite interesting that the extraction capacity of the regenerated IL is compromised, considering that FT-IR data did not indicate any change in the IL structure, despite the introduction of H<sub>2</sub>O molecules in the organic phase after stripping. This change in behavior is quite interesting and would be worth investigating further.<sup>204</sup>

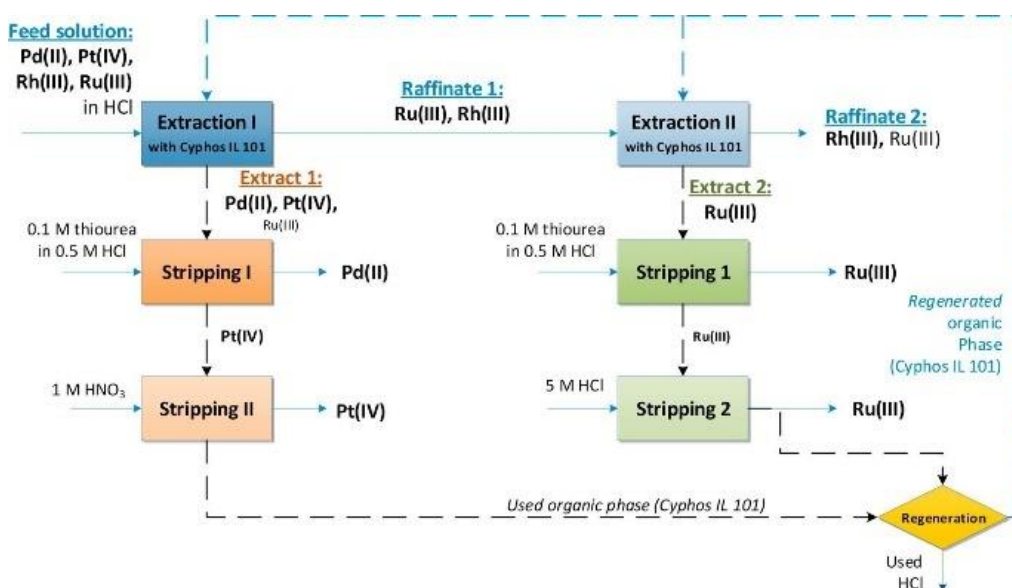


**Figure 35.** Separation flowsheet of Pt(IV), Pd(II), Rh(III) and Ru(III) from their mixture with Cyphos 101.<sup>204</sup>

Successful recovery and separation of Pt(IV) and Pd(II) from Rh(III) present in HCl mixed model solutions has been reported.<sup>205</sup> Comprehensive stripping studies additionally provided an approach for separation of Pt and Pd with purities >99%. Evidently, there is a direct correlation between the amount of the IL used and the yields recovered in the organic phase, which reach their maximum value (Pt 98.1%, Pd 99.9%) and plateau at P<sub>66614</sub>Cl 2.0 M in xylene. In the case of Rh, there was no extraction achieved at any concentration level. Highest extraction efficiency for Pd is attainable at Cl<sup>-</sup> 0.1 M and it steadily drops when the concentration is increased up to 4.0 M, which is also reflected in the 5-fold decrease of its distribution ratio (from D<sub>Pd</sub>=2.68 to 0.56). The same tendency is not observed for Pt which only exhibits a slight decrease. This observation is in line with what other authors previously noted; increase in acidity gives rise to PtCl<sub>6</sub><sup>2-</sup> species which are preferably extracted over PdCl<sub>4</sub><sup>2-</sup>.<sup>200</sup> The authors hypothesize that this decrease can be attributed to competition of Cl<sup>-</sup> with PGM-chlorocomplexes, which is an immediate result of the nature of the anion-exchange mechanism. Again, Rh is not affected and remains in the aqueous phase. Steric effects arising from the geometry of its octahedral complexes hinder their extraction to the organic phase. An ion-exchange mechanism is involved in the extraction of Pt and Pd and the stoichiometric ratios of the formed complexes were elucidated using the continuous variation method; Pt:P<sub>66614</sub>Cl ratio 1:1 independent of the HCl concentration and Pd:P<sub>66614</sub>Cl ratios 1:1 and 1:3 at 0.1 and 4.0 M HCl, respectively. Data provided by <sup>1</sup>H-NMR and <sup>31</sup>P-NMR spectroscopy, verify the extracted species expected according to an anion-exchange mechanism. Calculated thermodynamic parameters indicate the exothermic nature of the extraction. Two-stage extraction is predicted by McCabe-Thiele plots for quantitative removal of Pt and Pd. Selective and quantitative stripping of Pt is feasible with 0.1 M NaSCN contacted three times with the solution, as McCabe-Thiele plots indicate, and subsequent one-step complete removal of Pd is performed with 0.01 M thiourea in 5% HCl. Consecutive extraction/stripping cycles demonstrate that the recycling of the IL does not alter its capacity for Pt and Pd extraction.<sup>205</sup>

The favorable properties of the novel-synthesized IL trioctyl-dodecylphosphonium chloride ( $P_{88812}Cl$ ) for PGM extraction compared to its widely used commercial phosphonium analogue  $P_{66614}Cl$  were demonstrated. Properties with advantageous effects for the extraction, such as low viscosity, low density, low  $H_2O$  content and low P release were quantified. Aqueous PGM synthetic solutions prepared in HCl were used and the aqueous phase was mixed with the IL phase on a 2:1 ratio. Shorter equilibration times were observed for the novel IL compared to its tested analogue (Pt(IV), Pd(II): 30 min vs 60 min, Rh(III): 80 min vs 150 min), a behavior which is a direct reflection of the different viscosities of the two ILs; lower viscosity implies higher metal ion-transfer rates.

In terms of extraction dependency on HCl concentration, both ILs demonstrated the same trend; Pt and Pd are quantitatively extracted in the entire tested HCl concentration range (0.5-5.0 M) with a negligible decline at concentrations over 0.5 M. This observation is in stark contrast with what has been previously observed with  $P_{66614}Cl$ , i.e., Pd extraction significantly decreasing and Pt extraction slightly affected, with increasing HCl concentration; it can be hypothesized that the higher hydrophobicity of  $P_{88812}Cl$  might be the parameter responsible for this. Concerning Rh, its extraction efficiency reaches its maximum at 0.5 M HCl and dramatically declines with any further increase in concentration. The transformation of the  $RhCl_5^{2-}$  species to the lower charge density species  $RhCl_6^{3-}$  at higher HCl concentrations is presumed to be the reason for its declining extraction (the extraction efficiency is proportional to the metal ion charge density).

The suggested extraction mechanism is ion exchange and this is supported by slope analysis. Additional studies on the extraction mechanism, indicate that in the case of  $RhCl_3^{6-}$  complexation of the metal ion requires three IL molecules, which is a sterically hindered configuration. Elevated temperatures (up to 60 °C) negatively affect the extraction efficiency for both ILs, which is corroborated by the calculated values of thermodynamic parameters. Thermodynamic data also suggest that  $P_{88812}Cl$  is more ordered than  $P_{66614}Cl$ , which is directly associated with the effect that the  $H_2O$  molecules present in the IL exert on the enthalpy of the extraction system. This observation is in line with the experimentally verified favorable behavior of  $P_{88812}Cl$  for the extraction of Pt, Pd and Rh. Efficient (70-90%) although not selective stripping (except for Rh) was feasible with  $HNO_3$ , thiourea and HCl, for Pt, Pd and Rh, respectively. Regenerated  $P_{88812}Cl$  only had an insignificant decline in its efficiency over three extraction cycles, whereas the decrease was slightly more significant for  $P_{66614}Cl$ , presumably due to the faster release of the anion of the latter IL into the aqueous phase. An interesting observation of the authors is the lower leachability of P from the  $P_{88814}^+$  cation compared to the  $P_{66614}^+$  cation, which was assessed after repeated contact of the IL phase with fresh aqueous phase (Figure 36). The lower P leachability of  $P_{88812}Cl$  probably accounts for the lower loss in extraction capability of the regenerated IL as opposed to its evaluated counterpart.<sup>206</sup>

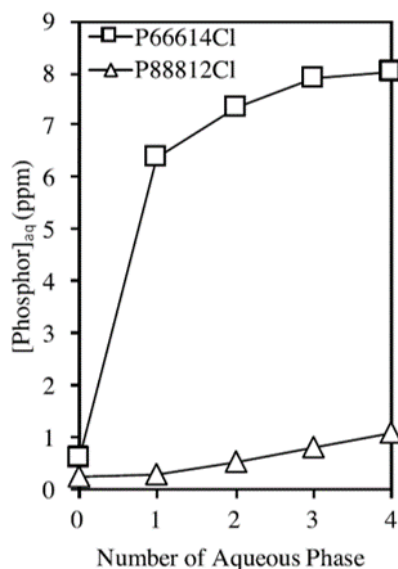


**Figure 36.** Ionic liquid cation release to the aqueous phase after repeated contact with an aqueous phase.<sup>206</sup>

In later studies, the authors demonstrated, with the aid of the same IL, an effective approach for the separation and recovery of PGMs from spent car catalyst leach liquor. The authors used the undiluted P<sub>88812</sub>Cl as a solvent for the extraction of Pd(II) and Rh(III) and investigated the effect of several parameters on their extraction behavior from a model leach liquor solution, the composition of which was determined based on the elemental quantification of an actual leach liquor, obtained from addition of concentrated HCl (5.0 M) on a grinded car catalyst material. Apart from Pd and Rh, also Pt, Fe, Zr, Ce, La, Ba, Al and Mg were present in the model liquor.

By varying the HCl concentration of the liquor, the dependency of the extraction efficiency on the acidity was demonstrated; Pd(II) was quantitatively extracted regardless of the HCl concentration, whereas 80% of Rh(III) could be accessed up until 1 M HCl with increasing acidity having a detrimental effect on its extraction. Concentrations beyond 1 M HCl yield an 80% Fe extraction and Zr extraction gradually increases reaching up to 60% at 7 M HCl. Less than 10% of the interfering elements was extracted to the IL phase under any circumstances. By employing a 5 M HCl concentration, Pd is selectively extracted over Rh, and due to its fast extraction rate, it can be simultaneously partially separated from Fe and Zr (Figure 37). Complexes with square planar geometry, such as PdCl<sub>4</sub><sup>2-</sup>, exhibit higher reactivity than tetrahedral ones, such as FeCl<sub>4</sub><sup>-</sup>. Scrubbing up to 88% Fe from the IL phase is feasible with the aid of Na<sub>2</sub>SO<sub>3</sub> at RT, which allows the subsequent selective stripping of 90% Pd, with thiourea, with high purity (97%). A second contact of the IL with the liquor adjusted to 1 M HCl extracts approx. 85% of Rh, 80% of which is effectively stripped with 5 M HCl.

Application of the developed process to the actual leach liquor is equally effective and allows recovery of both Pd and Rh with high purity (99% and 95%, respectively). Nevertheless, an additional Fe scrubbing step is required after the extraction of Rh, since a considerable amount of Fe that was not removed in the first scrubbing step is co-extracted with Rh in the IL phase. Regeneration of the IL is feasible by contact with highly concentrated HCl and only insignificant loss in extraction efficiency is observed in subsequent cycles.<sup>207</sup>

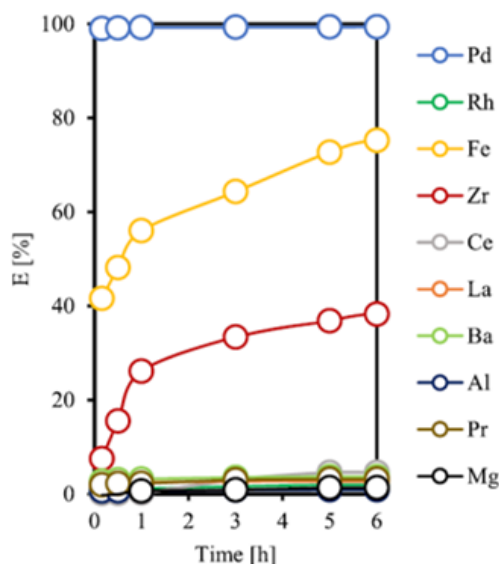


**Figure 37.** Effect of contact time on the extraction of metals from a model leach liquor.<sup>207</sup>

The authors updated the scheme for the separation and recovery of PGMs from spent automotive catalyst leach liquor to further include Pt(IV) (Figure 38). Quantitative leaching of PGMs from the spent catalyst is performed with HCl 5.0 M, at 60 °C, for 48 h. Additionally, Zn, Fe, La, Ce, Al, Mg and Cu are leached, however only Zn, Fe and Cu partition to the IL phase. As demonstrated in previous studies,  $P_{8,8,8,12}Cl$  selectively extracts Pt and Pd at 5.0 M HCl, leaving Rh in the raffinate. Selective stripping affords recovery of Pt (90%) and Pd (94%) with high purities (>98%);  $Na_2SO_3$  scrubs Fe, and subsequent addition of acidified thiourea and  $HNO_3$  strips Pd and Pt, respectively. The IL phase can be recovered after removal of Cu and Zn with  $H_2SO_4$ . Mixing of the Rh-containing raffinate, acidified to 2.0 M HCl, with fresh IL leads to 80% extraction of Rh, 80% of which can be subsequently recovered by  $Na_2SO_3$  leading to a 99% pure Rh solution. Overall, 94% Pt, 90% Pd and 64% Rh in the acidic leachate are accessed.<sup>208</sup>

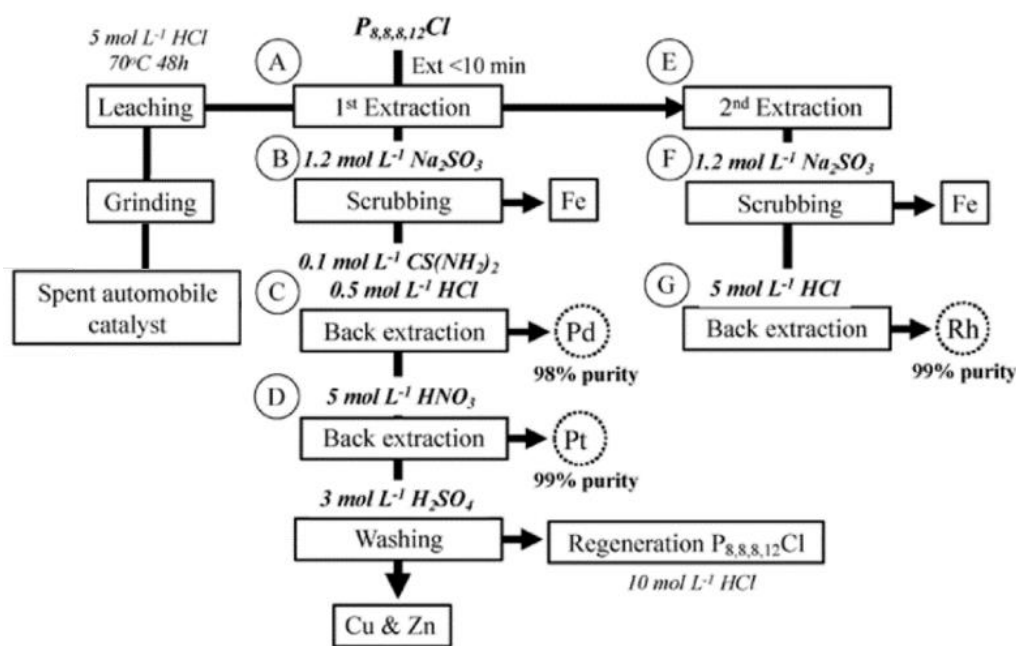
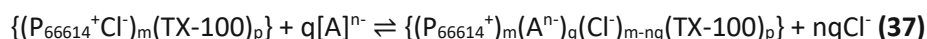


**Figure 38.** Flow chart summarizing the separation and recovery process of PGMs from an automotive catalyst leachate.<sup>208</sup>

An IL-based microemulsion process for extraction of Au(III), Pd(II) and Pt(IV) from their model mixed solution and their subsequent recovery in highly pure metallic form (>99%) has been developed by Ngyen et al.<sup>209</sup> The P<sub>66614</sub>Cl/triton X-100 (TX-100)/H<sub>2</sub>O microemulsion (IL-in-water microemulsion) is an environmentally benign system that encompasses all the positive aspects that ILs have to offer, while at the same time its low viscosity, high selectivity and recyclability without loss of performance render it an ideal candidate for industrial applications. Prior to extraction experiments, the phase behavior and the structure of the microemulsion was fully determined. According to <sup>31</sup>P-NMR data, the following mechanism is proposed (equation 37):



where A<sup>n-</sup> refers to the anionic metal species to be extracted, p is the average aggregation number of the TX-100 micelles, m the average number of P<sub>66614</sub><sup>+</sup>Cl<sup>-</sup> molecules in each (TX-100)<sub>p</sub> micelle and q denotes the average number of A<sup>n-</sup> species extracted per micelle. The extraction behavior is dependent on the employed temperature, the concentrations of the IL, surfactant, and Cl<sup>-</sup> anions, whereas acidity did not have a significant impact. At RT the microemulsion and the aqueous metal containing solution constitute a homogeneous mixture which can be thermally split into two phases. The optimal conditions (1.0 M HCl, 2.0 M NaCl, 1.9 mM P<sub>66614</sub>Cl, 10 g/L TX-100, 60 °C, 60 min) afforded efficiencies of 94.7%, 68.4% and 89.1% for Au, Pd and Pt, respectively. According to <sup>31</sup>P-NMR data, the anion-exchange mechanism is supported (Figure 39). Selective and quantitative stripping of Au is performed with Na<sub>2</sub>S<sub>2</sub>O<sub>3</sub>, while Pd and Pt are separated and selectively recovered (86% and 56%, respectively) by simply varying the concentration of thiourea in 5% HCl.<sup>209</sup>

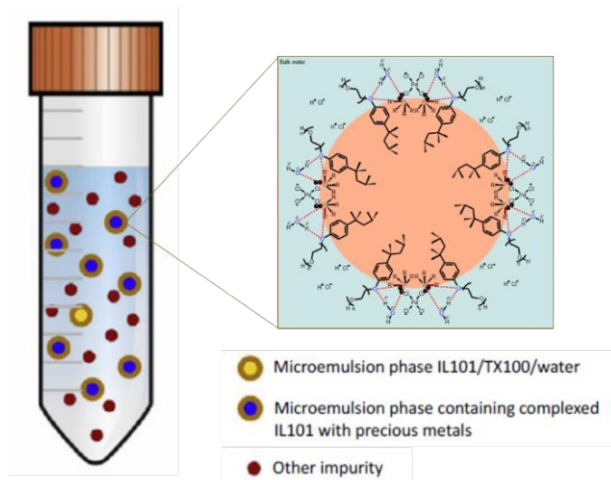


**Figure 39.** Experimental schematic for the extraction of precious metals using the microemulsion P<sub>66614</sub>Cl/TX-100/H<sub>2</sub>O along with the simplified chemical structure of the extracted Pd species.<sup>209</sup>

### 3.1.3.4 Pyridinium-based ionic liquids

The PGM extraction conditions and results that will be discussed in the present section are summarized in Table 6.

The highly selective extraction of Pd(II) from its HCl-based model solution with the aid of the system hexadecylpyridinium chloride ([Hpy]Cl)/CHCl<sub>3</sub> in the presence of base ions has been reported.<sup>210</sup> The fast and selective extraction of Pd can be largely attributed to the amphiphilic structure of the employed IL which speeds up the reaction by lowering the interfacial tension between the organic and aqueous phase, as well as the strong interaction of Pd with the nitrogen atom of Hpy. The extraction proceeds via an anion-exchange mechanism, as verified by UV-Vis, <sup>1</sup>H-NMR, IR spectra and the continuous variations approach (Job's method). Within the first 5 min of contact, the majority of Pd (98.8%) is extracted and



only an additional 5 min are required to reach a 100% value. The basic prerequisite to maximize the extraction yield is to maintain the ratio of the IL to Pd higher than 4. Increasing amount of Cl<sup>-</sup> ions dramatically decreases the extraction yield, which can be attributed to the competition of Pd-chlorocomplexes and Cl<sup>-</sup> ions to attach to Hpy (anion-exchange mechanism). This assumption is further verified by observing similar decrease in the yield when NaCl is added as a Cl<sup>-</sup> ion source. Based on thermodynamic calculations, the negative effect of increasing temperature on the extraction efficiency is established.

Comparison of the extractability of Pd with [C<sub>16</sub>mim]Cl proves the superior performance of [Hpy]Cl just as the higher extraction yields and distribution ratios imply (20 vs >500). Additionally, the high selectivity of [Hpy]Cl is established in the presence of added cations Cu(II), Co(II), Ni(II), Fe(III), Al(III), Sn(IV) at the same concentration level as Pd; all added cations have extraction yields below 8%. Stripping of Pd in the form of a precipitate is feasible by addition of oxalic acid, thus, consequent recovery of the IL in chloroform is achieved. Subsequent extraction attempts with the recovered IL, demonstrate both the retention of its extraction capacity and its high recycling rate (95%).<sup>210</sup>

### 3.1.3.5 Guanidinium-based ionic liquids

The PGM extraction conditions and results that will be discussed in the present section are summarized in Table 6.

The guanidinium-based IL 2,2-diheptyl-1,1,3,3-tetramethyl-guanidinium bromide ([diHTMG]Br) proved to be a selective extracting agent for Pt(IV) from a mixed-metal solution containing Mn(II), Al(III), Cu(II), Co(II), Fe(III) and Mg(II) (Figure 40).

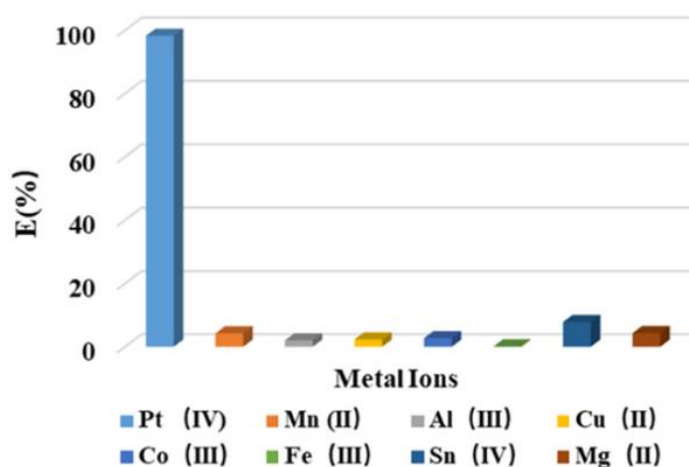
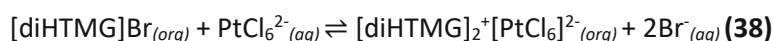


**Figure 40.** Selective extraction of Pt(IV) with the guanidinium-based IL [diHTMG]Br. 10g/L IL in CHCl<sub>3</sub>, 1 mM/metal in 0.5 M HCl, 10 min, O:A 1:5.<sup>211</sup>

Single-element experiments demonstrated that the extraction efficiency of Pt is favored by increasing concentration of IL in CHCl<sub>3</sub>, whereas increasing Cl<sup>-</sup> concentration beyond a certain point, either by HCl or NaCl addition, has a negative impact on its extraction. This effect can be attributed to the limited distribution ratio of Br<sup>-</sup> to the aqueous phase when Cl<sup>-</sup> is present at elevated concentration. FT-IR characterization data and UV-Vis data of the extractant and the extracted species supports the anion-exchange mechanism (equation 38).





Calculated thermodynamic parameters indicate the spontaneous and exothermic nature of the reaction. Extraction isotherms indicate that the organic phase can quantitatively extract Pt, in two stages, according to McCabe-Thiele plots, before reaching saturation. Acidified thiourea can strip Pt effectively from the loaded organic phase. This results in the reduction of Pt(IV) to the Pt(II) species, which leads to dissociation of Cl<sup>-</sup> anions from the PtCl<sub>6</sub><sup>2-</sup> complex and their subsequent combination with the IL anion, thus, generating [diHTMG]Cl; nevertheless, it was demonstrated that this IL modification has no impact on its extraction capacity in the following extraction cycles. Both extraction and stripping processes require two counter-current extraction steps for complete Pt removal.<sup>211</sup>

### 3.1.3.6 Task-specific ionic liquids

The PGM extraction conditions and results that will be discussed in the present section are summarized in Table 6.

Piperidinium and pyrrolidinium task-specific ionic liquids (TSILs) with appended nitrile functional groups and NTF<sub>2</sub><sup>-</sup> building anions are simultaneously selective and efficient extractants for Pd. A stable complex between the TSILs and Pd is formed which results in the complete removal of Pd from its aqueous solutions at neutral pH. Attaching nitrile groups to the IL cations significantly increases their extraction efficiency toward Pd indicating that the cation has an important impact on the extraction capacity of the TSIL.<sup>212</sup>

High extraction efficiencies for Pd from its aqueous solutions (prepared from PdCl<sub>2</sub>) have been reported<sup>213</sup> with functionalized piperidinium, pyrrolidinium and pyridinium ILs comprising the NTF<sub>2</sub><sup>-</sup> anion, specifically, 1-methyl-1-[4,5-bis(methylsulfide)]pentylpiperidinium bis(trifluoromethylsulfonyl)imide ([MPS<sub>2</sub>PIP][NTf<sub>2</sub>]) (IL1), 1-methyl-1-pentenepyrrolidinium bis(trifluoromethylsulfonyl)imide ([MPTPYRRO][NTf<sub>2</sub>]) (IL2), 1-methyl-1-pentenepiperidinium bis(trifluoromethylsulfonyl)imide ([MPTPIP][NTf<sub>2</sub>]) (IL3), 1-butyronitrile-1-methylpiperidinium bis(trifluoromethylsulfonyl)imide ([MBCNPIP][NTf<sub>2</sub>]) (IL4), 1-butyronitrile-4-methylpyridinium bis(trifluoromethylsulfonyl)imide ([4MBCNPYR][NTf<sub>2</sub>]) (IL5). Extraction efficiencies of >99.5% are exhibited with ILs 1-3, 96.7% with IL4 and 91% with IL5 when the pH is set to 2.8. The distribution ratio for Pd when the IL comprising a functional group is employed is significantly higher than the others, which indicates a strong interaction of the S in the functional group with Pd (Figure 41). The metal concentration in solution was in the range of 100-200 mg/kg and the mixing ratio of the IL to the aqueous phase was 1:5.<sup>213</sup>

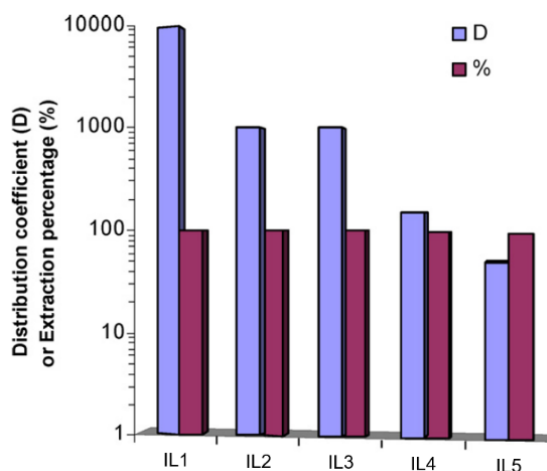


Figure 41. Distribution ratios and extraction percentages of Pd from aqueous solution, pH 2.8.<sup>213</sup>

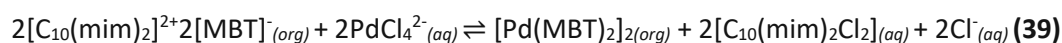
**Table 6.** Summary of PGM extraction conditions and results with pyridinium-, guanidinium-based and task-specific ionic liquids.

PGM Solution	Ionic Liquid (+ Diluent)	Ratio (O/A) <sup>a</sup>	Time (min) <sup>b</sup>	Extr. Efficiency (%) Distribution Ratio (D)	Type	Ref. No
10 mg/L/metal: Pd(II), Cu(II), Co(II), Ni(II), Fe(III), Al(III), Sn(IV) in 0.1 M HCl	1.88 mM [Hpy]Cl in CHCl <sub>3</sub>	1/5	10	98.8% Pd, D <sub>Pd</sub> >500, <8% each of the rest	A	210
1.0 mM/metal: Pt(IV), Mn(II), Al(III), Sn(IV), Fe(III), Co(III), Mg(II), Cu(II) in 0.5 M HCl	10 g/L [diHTMG]Br in CHCl <sub>3</sub>	1/5	10	98.2% Pt, D <sub>Pt</sub> >100, 4.2% Mn, 2.0% Al, 7.8% Sn, <1% Fe, 4.7% Co, 4.3% Mg, 2.3% Cu	A	211
200 mg/L PdCl <sub>2</sub> , pH 7	[4MPYRCN][NTf <sub>2</sub> ] or [MPIPNCN][NTf <sub>2</sub> ]	1% (w/w) in 20 g stock solution	4320	100% Pd, D <sub>Pd</sub> >1000, D <sub>(rest)</sub> <1.0	A, D	212
100-200 mg/L Pd, pH 2.8	[MPSZPIP][NTf <sub>2</sub> ], [MPTPYRRO][NTf <sub>2</sub> ] or [MPTPIP][NTf <sub>2</sub> ]	1/5	20	>99.5% Pd, D <sub>Pd</sub> ≥1000	A, D	213
0.5 mM/metal: Pt(II), Pd(II), Ag(I), Cu(I), Mn(II), Co(II), Ni(II), Zn(II), Sn(II), Li(I), Mg(II), Ca(II), Sr(II) in 200 mM acetate buffer	[3-TPPy][NTf <sub>2</sub> ]	1/2	n.a.	>99% Pt, >99% Pd at pH 5, >99% Ag, >99% Cu at pH 5.5, 0% of the rest	A, D	214
0.2 mM/metal: Pd(II), Ni(II), Al(III), Co(II), Pt(IV), Ru(III), Rh(III) in 0.1 M HCl	2.1 mM [C <sub>10</sub> (mim) <sub>2</sub> ] <sup>2+</sup> 2[MBT] <sup>-</sup> in [C <sub>8</sub> mim][NTf <sub>2</sub> ]	10/1	15	99.4% Pd, D <sub>Pd</sub> >1500 <10% each of the rest, D <sub>(rest)</sub> <1	C, D	215
i. 10mg/L/metal: Pd(II), Pt(IV) in 4.0 M HCl/0.50 M NaCl ii. 100mg/L/metal: Pd(II), Pt(IV) in 4.0 M HCl/0.50 M NaCl	i. 1.0 mM IL1 in [Bmim][NTf <sub>2</sub> ] ii. 10 mM IL1 in [Bmim][NTf <sub>2</sub> ]	1/4	30	i. 100% Pd, 1.4% Pt ii. 99.3% Pd, 6.4% Pt α <sub>Pd/Pt</sub> =72	C, D	216

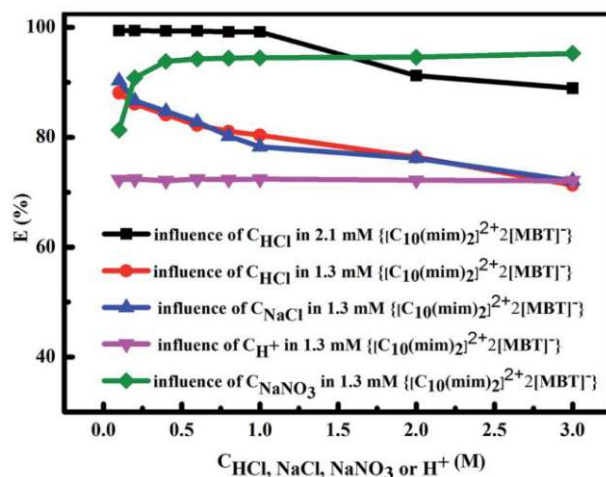
<sup>a</sup> O= organic phase, A= aqueous phase. <sup>b</sup> All extractions were performed at RT.

Functionalization of a pyridinium-based IL (3-thiapentylpyridinium bis(trifluoromethylsulfonyl)imide, [3-TPPy][NTf<sub>2</sub>]) with sulfide affords complete extraction of Pt(II) and Pd(II) from their respective aqueous synthetic solutions, whereas no extraction is possible in the absence of the functional group. Strong coordination of the S-donor atom with the metal ions is attributed to its strong affinity (soft base) to precious metal ions (soft acids). The authors showed the dependency of the distribution ratios of Cu and Ag to the IL concentration and demonstrated the recyclability of the IL which extracted comparable amounts of Cu and Ag in repeated extraction cycles; unfortunately, they did not provide the respective data for Pt and Pd.<sup>214</sup>

The selectivity of the functionalized hydrophobic IL 2-mercaptobenzothiazolate ([C<sub>10</sub>(mim)<sub>2</sub>]<sup>2+</sup>2[MBT]<sup>-</sup>) toward Pd(II) from an acidic medium containing Pt(IV), Rh(III), Ni(II), Al(III), Co(II) and Ru(III) was demonstrated. Increasing concentration of the IL in the employed diluent, i.e. [C<sub>8</sub>mim][NTf<sub>2</sub>], as well as ionic strength, promote the migration of Pd to the hydrophobic-IL phase, whereas increasing HCl concentration of the aqueous solution has the opposite effect. The authors proved, by replacing HCl with NaCl, that it is the excess of the Cl<sup>-</sup> anions rather than H<sup>+</sup> cations that has this impact on the extraction. On the other hand, addition of various NaNO<sub>3</sub> concentrations indicated that ionic strength promotes the extraction of Pd (Figure 42). The deciphering of the extraction mechanism, with the aid of FT-IR, <sup>1</sup>H-NMR and UV-Vis data, revealed that Pd(II) is simultaneously coordinated with nitrogen and sulfur atoms of the MBT<sup>-</sup> anion, which was additionally verified by XRD data. The following extraction mechanism is proposed (equation 39):

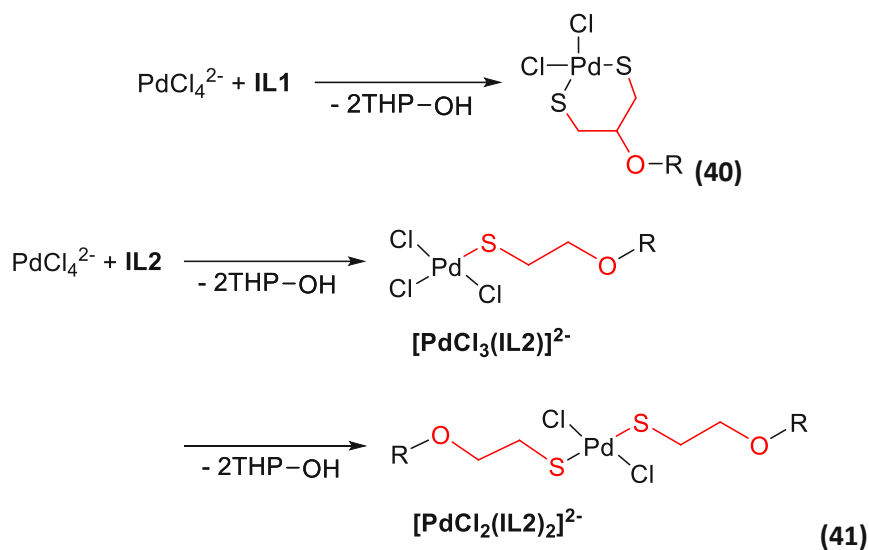


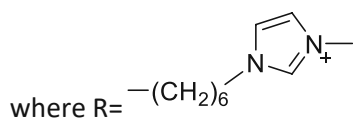
Extraction efficiency of almost 100% is achieved for Pd while, at the same time, less than 10% of the other metals is co-extracted to the IL phase. Acidified thiourea has the capability of stripping Pd out of the hydrophobic IL and back to the aqueous phase. The results are undoubtedly quite interesting; however, the contamination of the aqueous phase by  $[C_{10}(\text{mim})_2\text{Cl}_2]$  should be pointed out, which, as will be later discussed, has potential ecotoxicological effects and does not degrade easily.<sup>215</sup>



**Figure 42.** Extraction of Pd(II) as a function of HCl, NaCl, NaNO<sub>3</sub> and H<sup>+</sup> concentration under different  $[C_{10}(\text{mim})_2]^{2+}2[\text{MBT}]^-$  concentrations. Aqueous phase: 0.2 mM Pd(II), organic phase: 1.3 mM and 2.1 mM  $[C_{10}(\text{mim})_2]^{2+}2[\text{MBT}]^-$  in  $[C_8\text{mim}][\text{NTf}_2]$ .<sup>215</sup>

A set of novel imidazolium-based TSILs for the selective extraction of Pd(II) from its aqueous mixed model solutions with Pt(IV) was designed. The organic phase comprised the tetrahydropyran-2*H*-yl (THP)-protected groups dissolved in  $[C_4\text{mim}][\text{NTf}_2]$  mixed with a 4-fold amount of the aqueous phase. Both evaluated TSILs exhibited high selectivity for Pd over Pt, however, IL1 could afford 100% yield, unlike the Pd selective extractant di-*n*-hexyl sulfide (DHS) dissolved in  $[C_4\text{mim}][\text{NTf}_2]$  or the pure  $[C_4\text{mim}][\text{NTf}_2]$ . In contrast to the general trend that has been thus far observed by the majority of authors with all employed ILs, there was a notable difference in the extraction behavior of Pd with IL1 by increasing HCl concentration (Figure 43). Interestingly enough, increasing the HCl concentration induced a spike to the extraction efficiency, which implied the influence of a mechanism other than ion exchange. The authors propose the following mechanism (equations 40, 41):





As the HCl concentration increases, there is a decrease in the  $[\text{PdCl}_3(\text{H}_2\text{O})]^-$  species and a simultaneous increase in  $\text{PdCl}_4^{2-}$  while an orange colored precipitate is observed, which is soluble in  $[\text{C}_4\text{mim}][\text{NTf}_2]$ . Interpretation of  $^1\text{H-NMR}$  data suggests that precipitation is brought about the selective deprotection of the THP-thiol groups in the presence of Pd(II) salts and the ensuing formation of  $[\text{C}_4\text{mim}][\text{NTf}_2]$ -soluble Pd(II)-IL1 complexes with Pd-S bonding. Selective and quantitative Pd extraction was observed over a wide range of Pd and Pt concentrations (10-100 mg/L), whereas the amount of Pt extracted was in any case negligible.<sup>216</sup>

It should be noted here that comparison of the synthesized ILs and DHS in terms of Pd extraction efficiency from HCl-based solutions is rather misleading. First, efficient recovery of Pd with DHS as well as sulfides, sulfoxides and phosphine sulfides has been reported from  $\text{HNO}_3$ -based solutions.<sup>217,218</sup> Specifically, 10% DHS in dodecane affords distribution ratios for Pd(II), after 30 min (the contact time also used in this DHS vs IL experiment), of 1000-5000, at 0.1-6 M  $\text{HNO}_3$ .<sup>219</sup> Second, extraction of Pd from HCl solutions has proven to be a very slow process, which can take hours to reach equilibrium. The extraction from HCl solutions can be significantly accelerated in the presence of a sulfur atom-containing diamide tridentate ligand, such as *N,N'*-dimethyl-*N,N'*-di-*n*-octyl-thiodiglycolamide<sup>220</sup> or in the presence of alkylammonium salts that function as phase-transfer catalysts.<sup>219</sup> Alternatively, the extraction rate can be notably increased if DHS is replaced either by a monoamide compound, such as *N*-methyl-*N*-*n*-octyl-4-diapentanamide,<sup>221</sup> or a fluorinated asymmetric sulfide,<sup>219</sup> as extracting agents.

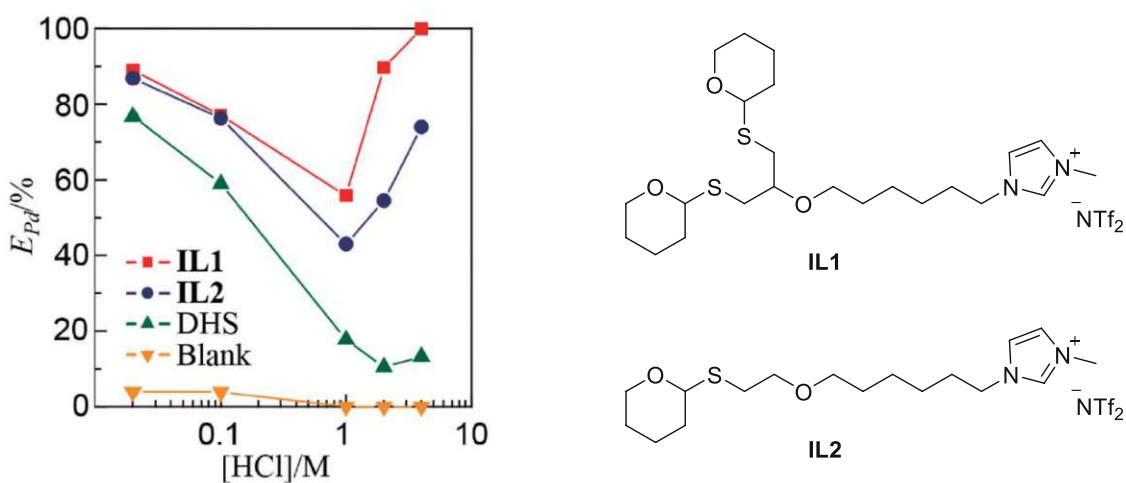


Figure 43. Extraction behavior of Pd with IL1 and varying HCl concentration (left) and structures of IL1 and IL2 (right).<sup>216</sup>

### 3.1.3.7 Thermomorphic ionic liquids

The PGM extraction conditions and results that will be discussed in the present section are summarized in Table 7.

The protonated betaine bis(trifluoromethylsulfonyl)imide ( $[\text{Hbet}][\text{NTf}_2]$ ) has a demonstrated ability toward extraction of rare earth metal oxides, including PdO. It is a TSIL; the cation is essentially a protonated betaine where a hydroxyl group has been replaced by a carboxylic acid group. In conjunction with the  $\text{NTf}_2^-$  anion, it forms an IL with low melting point (57 °C) and additionally, it exhibits thermomorphic behavior; upon mixing with an aqueous solution, a homogeneous mixture is formed at temperatures above the melting point, which separates into two distinct phases when the mixture is

cooled down (Figure 44). Furthermore, the phase separation is pH dependent; basification leads to the formation of a homogeneous system that can be converted to a biphasic system by acidification.

Metal oxides are characterized by hydrophilic surfaces, whereas the IL is hydrophobic, thus, the metal oxides are mixed with the IL in the presence of added H<sub>2</sub>O to promote their dissolution in the IL. Stoichiometric compounds can be formed between the metal and the IL and after evaporation of the H<sub>2</sub>O, metal-betaine complexes are obtained. Simple addition of an acidified aqueous solution to the formed metal complex, leads to regeneration of the IL and migration of the metal to the aqueous phase.<sup>222</sup>

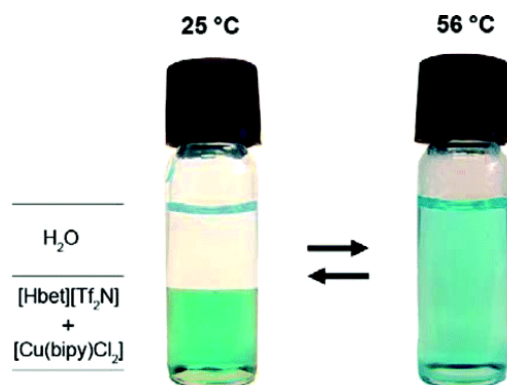


**Figure 44.** Temperature-dependent behavior of a binary [Hbet][NTf<sub>2</sub>]/H<sub>2</sub>O mixture. The blue [Cu(bipy)Cl<sub>2</sub>] complex was dissolved in the IL to accentuate the phase boundaries.<sup>222</sup>

**Table 7.** Summary of PGM extraction conditions and results with thermomorphic ionic liquids.

PGM Solution	Ionic Liquid (+ Diluent)	Ratio (O/A) <sup>a</sup>	Time (min)	T (°C)	Extr. Efficiency (%) Distribution Ratio (D)	Type	Ref. No
20 mM/metal: Pd(II), Rh(II), Ru(III) in 0.3 M HNO <sub>3</sub>	[Hbet][NTf <sub>2</sub> ] equilibrated with HNO <sub>3</sub>	1/1	10	25	100% Pd, D <sub>Pd</sub> >3000, α <sub>Pd/Rh</sub> >1000, α <sub>Pd/Ru</sub> >1000, 70% Rh, D <sub>Rh</sub> >2, 40% Ru, D <sub>Ru</sub> <1	A, E	223
10 mM Pd(II), 20 mM Rh(II), 20 mM Ru(III) in 0.3 M HNO <sub>3</sub>	[Hbet][NTf <sub>2</sub> ] equilibrated with HNO <sub>3</sub>	1/1	40 sec	MW-200W	>90% Pd, D <sub>Pd</sub> >10, 68% Rh, D <sub>Rh</sub> >10, 35% Ru, D <sub>Ru</sub> >10	A, E	224
5 mM Pd(II), 3 mM Rh(II), 7 mM Ru(III) in 0.3 M HNO <sub>3</sub>	[Hbet][NTf <sub>2</sub> ] equilibrated with HNO <sub>3</sub>	1/1	180	80	>80% Pd, D <sub>Pd</sub> >2, 96.5% Rh, D <sub>Rh</sub> >40, 99.2% Ru, D <sub>Ru</sub> >100	A, E	225
Pt(IV), Ni(II), Fe(III), Co(II)	P <sub>44414</sub> Cl + H <sub>2</sub> O + HCl	n.a.	n.a.	25-50	>95% Pt, >95% Fe, >90% Co, <20% Ni	A, E	137

<sup>a</sup> O=organic phase, A=aqueous phase.

The IL comprising a betainium cation (Hbet<sup>+</sup>) and an NTf<sub>2</sub><sup>-</sup> anion, has been proven effective for the extraction of Pd(II), Rh(III) and Ru(III) from mixed model HNO<sub>3</sub> solutions; quantitative extraction of Pd is observed, whereas approx. 70% of Rh and approx. 40% of Ru are extracted.

There is a clear dependency of the extraction yield on the HNO<sub>3</sub> concentration, which is more significant for Rh and Ru; low concentrations of HNO<sub>3</sub> favor the extraction, as well as the separation between the respective metals. Additionally, the pH of the aqueous phase should be maintained below 0.5, to prevent the hydrolysis and consequent precipitation of Pd and Rh. The proposed extraction mechanism is coordination of the metal with the functional group of betainium, followed by a cation exchange between the H<sup>+</sup> of the betainium cation of the formed complex (Equation 42).



As the authors conclude, it would be premature to propose a detailed extraction mechanism since more experimental evidence is needed.<sup>223</sup>

The thermomorphic properties of the betainium IL were further exploited by the authors in subsequent investigations, in order to accelerate the extraction of Rh(III) and Ru(III). Individual aqueous synthetic HNO<sub>3</sub> solutions (0.3 M), each containing one of the elements Pd(II), Rh(III) or Ru(III) were prepared and mixed with IL in equal volumes. While heating up the mixture over 55 °C (upper critical solution temperature) results in the formation of a homogeneous phase of the two components, which are normally immiscible at RT, supplying microwave irradiation at 200 W for 40 sec to the system was necessary in order to increase the low extraction efficiencies of Rh and Ru to almost quantitative levels. Unlike Rh and Ru, Pd is rather labile so its extractability was almost quantitative (>90%) at RT, at a thermostated water bath (60 °C) and with the irradiation approach. Despite the slow ligand-substitution kinetics, simple heating (water bath at 60 °C) does not significantly promote the extraction kinetics for Rh and Ru, which implies that the irradiation has a non-thermal effect on the kinetic acceleration of the extraction. Additionally, microwave irradiation enhances the extraction of all three metals in the studied HNO<sub>3</sub> concentration range (0.3-2.0 M); however, as previously observed, it decreases with increasing HNO<sub>3</sub> concentration (Figure 45). Although separation of these three metals from their mixture was not possible, partial separation of Pd and Rh from Ru is feasible by simple tuning of the irradiation time.<sup>224</sup>

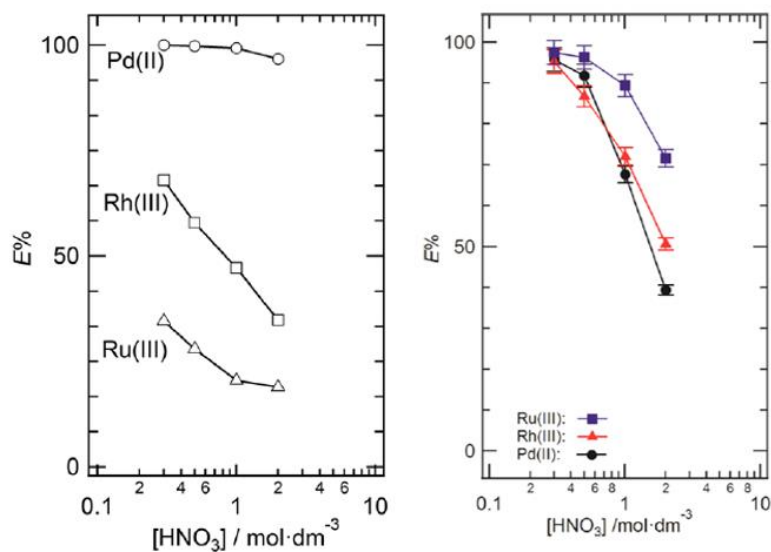


**Figure 45.** Extraction efficiency (%) for Pd, Rh and Ru with [Hbet][NTf<sub>2</sub>] at various HNO<sub>3</sub> concentrations, at RT (left) and under microwave irradiation (right).<sup>223,224</sup>

The objective of clarification of the driving force behind the PGM extraction to the betainium-based IL lead to further studies of the developed extraction system. Following deprotonation of the -COOH group, the zwitterionic betaine coordinates with the metal. In order to form an extractable species, the hydrated H<sub>2</sub>O molecules bound to the metal have to be substituted by betaine. Fast and slow extraction rates for Pd(II) and Rh(III), respectively, were no surprise given the fact that the life time of the H<sub>2</sub>O molecule in the 1<sup>st</sup> coordination sphere of Pt<sup>2+</sup> and Rh<sup>3+</sup> is in the order of 10<sup>-3</sup> sec and a few years, respectively (the lifetime of the H<sub>2</sub>O molecule is a measure of the lability of the metal ion). Additionally, the phase transfer rate of the extractable complex between the aqueous and organic phase has an impact on the extraction kinetics. Heating of the system offers two advantages; the reaction rate is increased and there is formation of a homogeneous system due to the thermomorphic nature of the IL. Fast extraction of Pd



is independent of the temperature, however, in the case of Rh the possibility for its quantitative extraction is decreased from 113 days, at RT, to just 3 h, at 80 °C. As stated in previous work, HNO<sub>3</sub> concentration exceeding 0.3 M dramatically decreases the extraction efficiencies. Observation of the ligand substitution process over time, with the aid of UV-Vis spectroscopy, revealed that the rate-determining step of the extraction is the formation of the extractable species. The authors have concluded that the complexation of the PGMs with the betainium moiety leads to the deprotonation of Hbet<sup>+</sup> and subsequent release of a H<sup>+</sup> to the aqueous phase. Furthermore, the extraction is accelerated via heating whether that is via convection or a microwave source.<sup>225</sup>

Gras et al.<sup>137</sup> presented a novel acidic aqueous biphasic system (AcABS) which relies on its thermomorphic behavior for simultaneous extraction and separation of metals (Pt(IV), Ni(II), Fe(III), Co(II)), essentially creating a “one-pot” approach. The hydrophilic tributyltetradecyl phosphonium chloride (P<sub>44414</sub>Cl), H<sub>2</sub>O and HCl are the building components in variable concentrations. Freedom to manipulate the formation of the biphasic system by simply adjusting its composition and the working temperature allows the separation of the leaching acid from the IL into which the metals partition. Additionally, the degree of phase separation is temperature controlled (Figure 46). Experimental data, employing a mixture of selected metals in synthetic HCl solutions, show that Pt is nearly quantitatively extracted to the IL phase and can be efficiently separated from Ni, which for the major part remains in the acidic phase.<sup>137</sup>

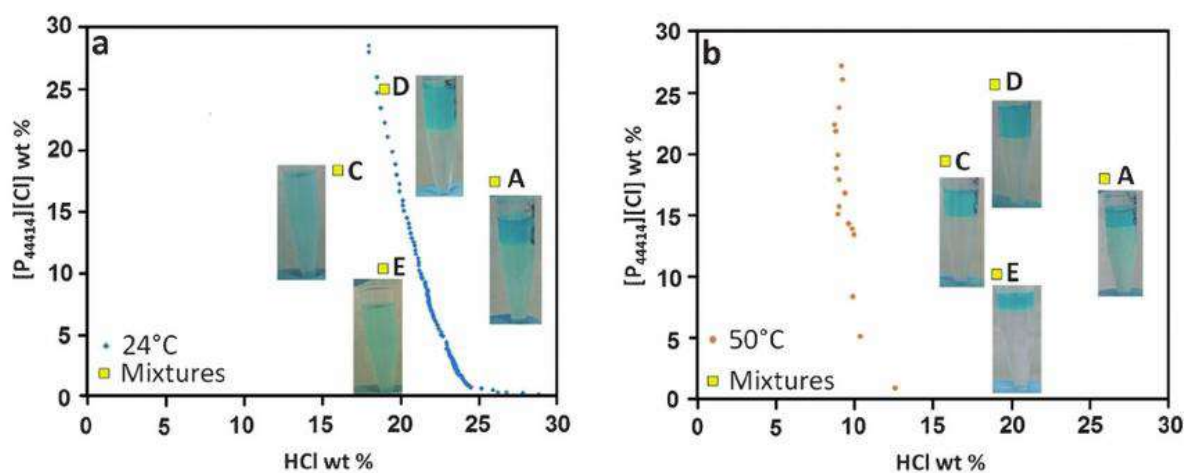


**Figure 46.** Phase diagrams at 24 (left) and 50 °C (right) and related snapshots taken after extraction of Co(II) using P<sub>44414</sub>Cl/HCl/H<sub>2</sub>O. The blue and orange points correspond to binodal curves obtained at 24 and 50 °C, respectively.<sup>137</sup>

### 3.2 Ionic liquids in solid-liquid separations

While the overwhelming majority of published research addresses the use of ILs in liquid-based separations, their use in solid-based separations involving IL-based materials provides an attractive alternative. This emerging concept for the use of ILs relies on their immobilization on solid-support materials, such as membranes and resins. Several drawbacks encountered in liquid-liquid separations employing ILs can be overcome with this approach. Mass-transport limitations and use of excessive amounts of ILs are effectively avoided, while ILs remain intact on the solid support when high temperatures are applied due to their thermal stability. Additionally, the inner surface of the porous solid offers large specific area for interaction, limitations arising from high IL viscosity are lifted and the transport rate is accelerated since the diffusion distance becomes shorter.<sup>226,227</sup>

Immobilization of ILs on solid materials is an emerging trend also applied for the separation of PGMs, as an alternative approach that can minimize mass-transfer limitations associated with liquid-liquid separations, while at the same time allowing a more economic use of ILs without losing any of their advantageous properties. In this section, resins, capsules, membranes, and nanoparticles as support materials are discussed (Figure 47).

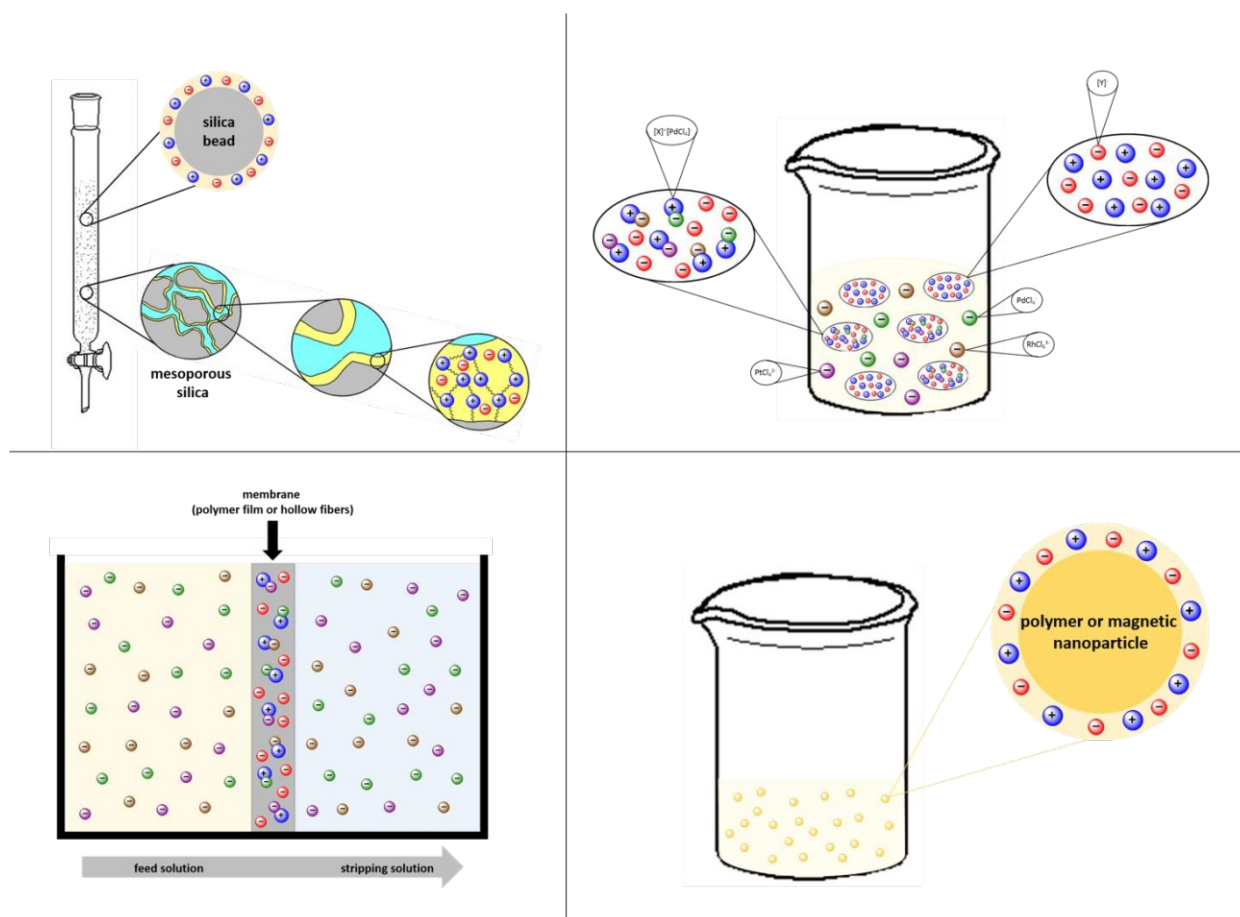


**Figure 47.** Ionic liquids in solid-based separations are implemented in (clockwise from upper left to bottom right): resins, capsules, membranes and nanoparticles (X = IL cation, Y = IL anion).

The PGM extraction conditions and results that will be discussed in the present section are summarized in Table 8.

For solid-liquid separation purposes, ILs can be attached on the solid surface either via physisorption (impregnation, sol-gel method, encapsulation) or via chemical binding (covalent bond between the solid material and the anion or cation of the IL). The solid support materials used for immobilization can be activated carbon, silica gel, aluminum oxide ( $\text{Al}_2\text{O}_3$ ), polystyrene resins or polymer membranes.<sup>227</sup>

There are three approaches for the preparation of supported ionic liquid materials; via direct immersion of the solid material in the IL which allows the impregnation of the solid material with the IL, application of pressure that forces the IL into the pores of the solid material or application of vacuum to displace the air located in the pores of the solid material by the IL. Homogeneous distribution of the IL in the pores of the solid material is accomplished by employing either of the three methods.<sup>228</sup>

Traditionally, PGMs are separated with the aid of ion-exchange resins (IXRs). Interaction with the metals is possible through different mechanisms; either ion association, chelation or their combination.<sup>229</sup> In the first case, the ion exchanger can be either cationic or anionic. Cationic exchangers are acidic in nature and can be bound with  $-\text{SO}_3\text{H}$ ,  $-\text{COOH}$ ,  $-\text{OH}$ , while anion exchangers are bases, such as ammonium groups (primary, secondary, tertiary, quaternary), quaternary phosphates and tertiary sulfones.<sup>230</sup> Chelating resins have functional groups with donor atoms ( $-\text{N}$ ,  $-\text{S}$ ,  $-\text{P}$ ) attached on their surface, thereby achieving separation via complex formation with the metals.

Due to the lack of selectivity toward PGMs, IXRs that involve the ion-association mechanism are ideally suited for simultaneous separation of PGMs from other base metals. Selective adsorption of Pt over Pd is favored at high  $\text{Cl}^-$  concentrations, where Pd extraction is suppressed, which means higher reagent consumption and consequent reduction in the loading capacity of the resin.<sup>229</sup> Despite the ability of cation exchangers to selectively remove Pt from mixed metal solutions, its subsequent elution can be difficult and insufficient. Although high recoveries of PGMs on anion exchangers are attainable from mixed basic metal solutions, the presence of  $\text{Zn(II)}$  and  $\text{Al(III)}$  significantly decrease selectivity toward Pd.<sup>230</sup>

On the other hand, chelating IXRs with functional groups containing  $-\text{N}$  or  $-\text{S}$  are characterized by high selectivity toward Pd. Selective elution of Pd with  $\text{NH}_3$  is possible, however, removal of Pt requires high concentration of  $\text{NH}_3$  and elevated temperatures, which can lead to thermal deterioration of the resin. For the same reason, the typically slow sorption kinetics cannot be accelerated with the aid of increased temperatures. Additionally, PGMs cannot be separated from their mixed solution in the presence of  $\text{Au(III)}$  and  $\text{Ag(I)}$ .<sup>229</sup>

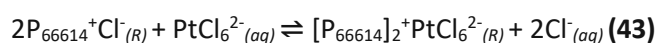
In any case, depending on the acidity of the PGM-containing solution and its  $\text{Cl}^-$  concentration, different PGM-chlorocomplexes are present; since different complexes exhibit different extractability, the adsorption behavior of the IXR is very much dependent on the pH and  $\text{Cl}^-$  concentration of the PGM solution. Particularly for Rh, aged solutions give rise to Rh chlorocomplexes that are kinetically inert, therefore, resulting in lower Rh recovery.<sup>231</sup>

Chelating resins have a polymeric support and they can be functionalized either by modification of the supporting polymer or impregnation of the resin with an organic solvent.<sup>229</sup> In the available literature that is discussed below, commercially available resins are impregnated with ILs comprising ammonium, phosphonium and imidazolium functional groups. It is worth mentioning though, that commercial resins with ammonium (e.g., Dowex,<sup>232,233</sup> Amberlite<sup>234,235</sup>) functionalities have been known for quite a long time for their capacity for PGM separation. A detailed review on the use of IXRs for PGM separation has been

provided by Hubicki et al.<sup>230</sup> and Lee et al.,<sup>229</sup> while for a review with a specific focus on synthetically modified IXRs, the work of Cyganowski is worth a read.<sup>236</sup>

### 3.2.1 Solid-supported ionic liquids as novel resins

Amberlite XAD-7 impregnated with P<sub>66614</sub>Cl has been reported for the extraction of Pt(IV) from its concentrated HCl solutions. Amberlite XAD-7 is a mesoporous nonionic polyacrylic acid ester type resin ((CH<sub>2</sub>-CH(COOR)<sub>n</sub>) characterized by a hydrophilic character. The sorption behavior of the impregnated resin is contingent upon the acidity and metal concentration of the solution, as well as the IL loading on the resin. Anion exchange between the Cl<sup>-</sup> of the IL and the anionic Pt-chloro complexes enables the retention of the metal ions on the resin, according to the following proposed mechanism (equation 43):



At low IL loadings, competition between the Cl<sup>-</sup> of the HCl and the Pt-chloro complexes limits the retention of Pt, because the IL preferentially extracts Cl<sup>-</sup> and consequently, limited binding spots are available for the binding of the Pt-chloro complexes. Retention is proportional to the loading and reaches quantitative levels at low HCl concentration (0.01 M) with the highest IL loading tested (586 mg IL/g resin). Additionally, increasing loading equals a decrease in the specific surface area which has a negative impact on the sorption rate; there is an increased absorption rate within the first 5-6 h regardless of the loading, however, the quantitative uptake is prolonged from 1 day to 4 as the IL loading increases. The authors do not address possible leakage of the IL from the sorbent; however, they support that the dry impregnation method they employ promotes stabilization of the IL on the resin. Highly efficient desorption of Pt (>95%) is achieved with HNO<sub>3</sub> (Figure 48).<sup>237</sup>

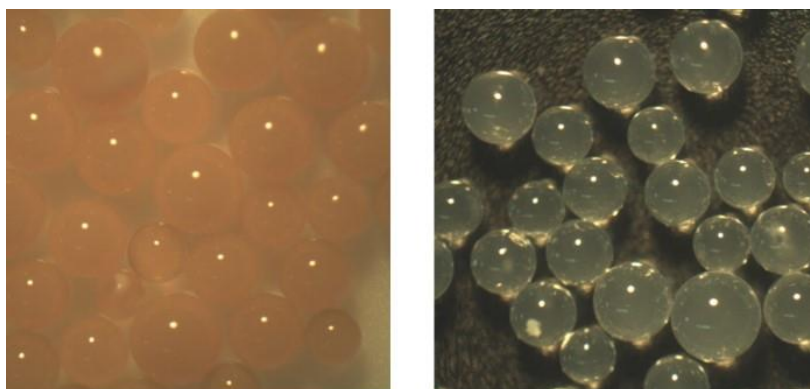


**Figure 48.** Microphotograph of Amberlite XAD-7/Cyphos 101, after Pt sorption (left) and Pt desorption (right).<sup>237</sup>

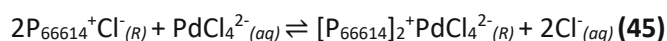
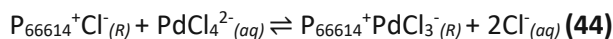
The group additionally investigated the extraction behavior of the impregnated resin toward Pd(II) containing model solutions. Similarly to Pt, the acidity, the metal concentration of the solution and the IL loading on the resin affect its sorption capacity toward Pd. Previous experimental data<sup>238</sup> indicated that exceeding a loading of 600 mg/L leads to partial leakage of the IL out of the solid support. No leakage was observed in the present experiments. Nevertheless, the retention mechanism is dependent on the HCl concentration range. At concentrations over 0.5 M, sorption proceeds via ion exchange, whereas at lower concentrations additional binding of the Pd-complexes on the resin contributes to its sorption. Increased HCl concentrations prevent sorption of Pd on the solid support, because the increasing amount of Cl<sup>-</sup> reverses the binding reaction, considering an anion-exchange mechanism is involved. Elevated temperature (40 °C) shortens the time needed to reach equilibrium (30 vs 96 h), presumably due to a decrease in viscosity of the IL and consequent improvement in mass transfer. Acidified thiourea

completely eliminates Pd from the resin, which can be reused for at least five more extractions without any loss in its retention capacity. However, on the downside, thorough washing with HCl is required after desorption for the removal of residual thiourea otherwise leaching of thiourea during the sorption step will prevent the metal from binding to the IL.<sup>239</sup>

**Table 8.** Summary of PGM extraction conditions and results with ionic liquid-impregnated resins and capsules.

PGM Solution	Ionic Liquid on Resin	Ratio (resin/solution)	Time (min)	T (°C)	Max. Sorption Capacity/g of Resin	Ref. No
80-600 mg/L Pt(IV) in 0.01 M HCl	291 mg P <sub>66614</sub> Cl/g of Amberlite XAD-7	2 g/L	2880	20	75 mg Pt	237
30-400 mg/L Pd(II) in 0.01 M HCl	401 mg P <sub>66614</sub> Cl/g of Amberlite XAD-7	2 g/L	2880	20	71 mg Pd, D <sub>Pd</sub> >10000	239
0.3 mM/metal: Pt(IV), Pd(II), Au(III) in 0.01 M HCl	391 mg P <sub>66614</sub> Cl/g of Amberlite XAD-1180	2 g/L	1 week	20	56 mg Pt, 32 mg Pd, 59 mg Au	240
50 mg/L/metal: Pt(II), Pt(IV), Pd(II) in 0.1 M HCl	Polymerized TSIL CP-AMIN (82% grafting rate)	15 g/L	300	60	293 mg Pt(II), 283 Pt(IV), 285 mg Pd(II)	241
150 µg/mL Pt, 293 µg/mL Pd, 343 µg/mL Rh in 1 M HCl	20% polymer on SILP	200g/L	1	RT	6888 µg Pt, 20608 µg Pd, 81 µg Rh	242
20-250 mg/L Pt in 0.1-2 M HCl/1 M NaCl	654 mg P <sub>66614</sub> Cl/g of biopolymer capsule	0.7 g/L	2880	RT	177 mg Pt, D <sub>Pt</sub> >10	243
20-250 mg Pd in 0.1-1 M HCl/0.05 M NaCl	654 mg P <sub>66614</sub> Cl/g of biopolymer capsule	0.7 g/L	4320	RT	145 mg Pd, D <sub>Pd</sub> >10	244

An efficient approach for the separation of Au, Pt and Pd from their mixed synthetic solutions using Amberlite XAD-1180 impregnated with Cyphos 101, in combination with selective stripping steps, was presented by the same research group.<sup>240</sup> XAD resins are characterized by high pore volumes and large pore sizes that favor retention kinetics. Increasing IL loading enhances the sorption capacity; however, it markedly affects the kinetics. An uptake of 50-90% occurs within the first 5 h of contact of the Amberlite beads with the metal containing solutions and a gradual decrease in the uptake rate enables the complete recovery of the metals over a period of several weeks. A decrease in the mass-transfer rate is imparted by the saturation of the resin with IL. Quantitative retention of Au(III) and partial retention of Pt(IV) (40-50%) is feasible independent of the HCl concentration. On the contrary, Pd(II) exhibits sensitivity to changes in the HCl content of the solution and its sorption is inversely proportional to the HCl concentration. This is a result of the competition between the Cl<sup>-</sup> of the HCl and the metal-chloro complexes, as it was discussed earlier. Specifically for Pd, the decrease is more pronounced due to the different binding mode of Pd to the IL depending on the HCl concentration; the IL:metal 1:1 stoichiometry observed at low HCl concentrations changes to 2:1 at higher acidity (equation 44 at HCl=0.1 M, equation 45 at HCl=3 M).



Desorption of Pd (83%) and Pt (23%) is performed with highly concentrated HCl followed by stripping of the remaining Pd and Pt by either HNO<sub>3</sub> or HClO<sub>4</sub>, therefore, mixed solutions of pure Pt and Pd are recovered. Subsequently, Au is desorbed with acidified thiourea. The affinity of the impregnated resin toward base elements (Co, Cu, Ni, Fe, Zn, Cd) is limited with reported extraction efficiencies <8.5% (with the exception of Cd, 18.7%). The recyclability of the sorbent was demonstrated for five sorption and



desorption cycles, for Au only, while rinsing in between desorption cycles was necessary to remove residual thiourea (used for Au stripping in this case). The authors employ the dry impregnation method, just like before, however, they do not address possible leakage of the IL.<sup>240</sup>

An imidazolium-based TSIL attached to polystyrene beads proved to be an efficient and selective extraction medium for Pt(II), Pt(IV) and Pd(II) in synthetic solutions, of environmentally friendly and industrially relevant character. FT-IR data of the beads verify the presence of the IL, which is not modified after heating of the solid material up to 60 °C, thus, implying the thermal stability of the synthesized imidazolium-based TSIL on chloromethylated polystyrene beads (CP-AMIN). Attachment of the IL on the beads enhances the surface area according to SEM images. Various parameters, namely temperature, Cl<sup>-</sup> concentration, HCl concentration, extraction time and IL loading affect the retention behavior of the CP-AMIN. Increasing temperature favors the extraction, which reaches a maximum at 60 °C. On the other hand, higher Cl<sup>-</sup> and HCl concentrations have a negative impact on the extraction, which can be attributed to the competition of the excess of Cl<sup>-</sup> ions with the Pt- and Pd-chlorocomplexes for anion exchange. A more dramatic decrease in extraction is observed in the case of increasing HCl concentration due to the additional hydrolysis of the CP-AMIN induced by the excessive H<sup>+</sup> concentration. In any case, higher loadings yield higher extraction efficiencies, reaching 97% and 98% after 5 h, for Pt and Pd, respectively. Extraction of Pt and Pd from a mixed metal solution (Ni, Mn, Cd, Cr, Cu, Co) in 20-fold concentrations (1000 mg/L), simulating a complex hydrometallurgical system, is highly selective with the extraction of the majority of the accompanying elements remaining below 20% ( $D_{Pt(II)/rest} > 9$ ,  $D_{Pt(IV)/rest} > 17$ ,  $D_{Pd(II)/rest} > 43$ ). Almost complete desorption of Pt and Pd is feasible with thiourea solutions (Figure 49). The recyclability potential of the CP-AMIN was demonstrated with seven absorption/desorption cycles in which no decline in its sorption capacity was observed. Unfortunately, the authors have not addressed possible leakage of the IL from the polystyrene beads.<sup>241</sup>

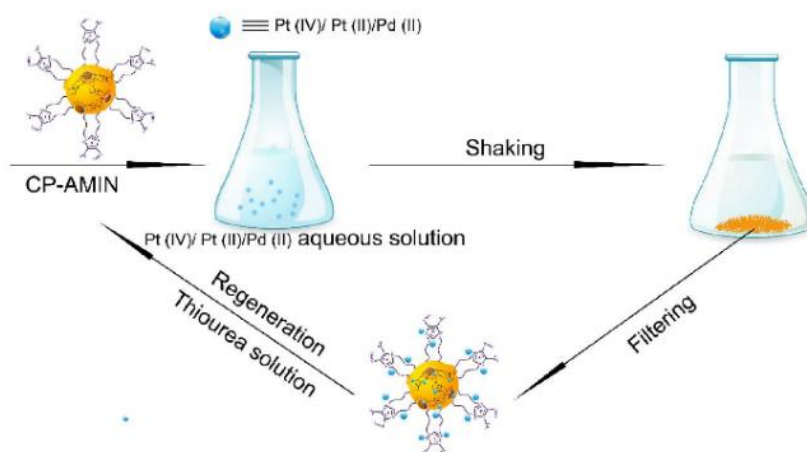


**Figure 49.** Adsorption and desorption of PGMs from aqueous solution in CP-AMIN.<sup>241</sup>

In this thesis, a novel and efficient scheme for the separation of Pt and Pd from Rh and accompanying elements leached from a spent car catalyst with the aid of a phosphonium-based polymerized IL covalently bound on a silica surface will be presented. Initial experiments on PGM model solutions indicated that parameters such as dilution level, acidity of solution and IL loading on silica have no effect on the retention of Pt and Pd on the sorbent material, which is quantitative. On the other hand, higher dilution levels (1:7 w/w) and intermediate sorbent loadings (20% w/w) favor the retention of Rh. By employing the conditions that favor Rh retention on the real leachate experiments and with the application of selective stripping, pure Pt and Pd could be recovered in solution, with respective recoveries of 86% and 96%. Additionally, the comparison between polymerized IL covalently bound on



silica (polySILP) and ILs physisorbed on silica (SILPs), proved the merit of the former over the latter; more efficient separation of the PGMs is achieved with the polySILP and significantly less amount of IL is leaching out of the solid support during the metal loading and stripping of the sorbent material.<sup>242</sup>

### 3.2.2 Capsules

The PGM extraction conditions and results that will be discussed in the present section are summarized in Table 8.

Cyphos 101 encapsulated in biopolymer beads by an ionotropic gelation process was evaluated as a potential sorbent for Pt from its aqueous model solutions (Figure 50). Sorption is attributed to an ion-exchange mechanism between the encapsulated IL and the Pt-chlorocomplexes. Although increasing IL loading favors the sorption capacity, the reaction rate is significantly decreased and the diffusion is hampered by reduced accessibility of Pt to the reactive groups in the presence of excessive amount of IL, thus, the loading should be optimized according to the target application. Variation in the  $H^+$  concentration does not markedly affect the maximum Pt uptake, which is in line with the independency of protonation of the phosphonium groups from the acidity of the solution, implying acidity has no effect on the ion-exchange mechanism. On the other hand, at  $Cl^-$  1.0 M sorption capacity reaches its maximum. Drying of the resin beads prior to mixing with the Pt solutions causes an irreversible collapse of its structure upon rehydration and leads to a reduction of the active groups that are accessible to Pt, thereof dried resins exhibit lower sorption capacities than wet ones. Additionally, the uptake rate of the dried resins is dramatically decreased; 2 to 3 days to reach equilibrium as opposed to 12-24 h required by wet resins. Metals that form only neutral or cationic species, such as Ni and Cu, have a negligible effect on the sorption capacity for Pt, whereas metals that form anionic chlorocomplexes, such as Zn, have a substantial impact prompted by the competition with Pt-chlorocomplexes for an ion-exchange interaction. Acidified thiourea and  $HNO_3$  can desorb Pt quantitatively. Leaching of 10-15% of the IL from the capsules was observed after three sorption/desorption cycles, possibly originating from sequential acidic treatments and mechanical breakage of the polymeric beads.<sup>243</sup>

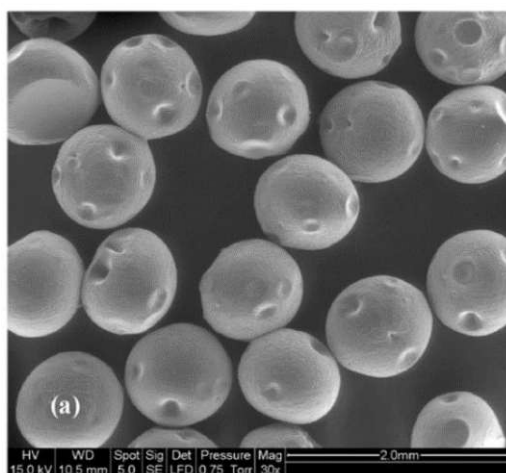


**Figure 50.** SEM image of dry polymeric beads containing immobilized Cyphos 101.<sup>243</sup>

The authors further tested the performance of the biopolymer capsules in the extraction of Pd from synthetic solutions.<sup>244</sup> The sorption capacity is markedly dependent on the  $Cl^-$  concentration, whether the  $Cl^-$  source is HCl or NaCl, exhibiting a dramatic decrease in sorption as  $Cl^-$  concentration increases, which is more pronounced in the case of HCl. This is due to the competition for binding to the resin, as previously mentioned, since an anion-exchange mechanism is assumed. Additionally, degradation of the capsules,

beyond a certain HCl concentration, accounts for this behavior. Similar observations as in the case of Pt were made for the sorption of Pd in connection with the IL loading, the presence of Ni, Cu and Zn ions and the use of wet versus dry resins. The drying process reduces the bead diameter to half and induces several structural changes to the biopolymer; the external polymer network is restricted, thus, the accessibility to internal sites is affected and that is demonstrated in the difference in kinetics between the two forms of the resin. Additionally, volume particle reduction causes a steric hindrance that hampers the access to the internal porous network. Accessibility to certain sites is further restricted by the changes imposed upon the dispersion and geometrical arrangement of the IL in the polymer network by drying. Interestingly, freeze-drying of the resin markedly enhances the sorption kinetics; the brittleness of the material introduced during the freeze-drying process exposes internal reactive groups. Nevertheless, this occurs at the detriment of the resin lifetime. In Pt and Pd mixtures, even though at low HCl concentrations (1.0-2.0 M) there is a sorption preference for Pt over Pd, the difference is not significant enough to allow efficient separation of the two metals. Quantitative Pd sorption is possible with acidified thiourea or HNO<sub>3</sub>, however, as observed in the case of Pt, the loading capacity degrades after three sorption/desorption cycles. Leaching of approx. 15% of the IL from the capsules was observed after three sorption/desorption cycles, possibly due to degradation of the loaded capsules subjected to sequential acidic treatments.<sup>244</sup>

### 3.2.3 Membranes

The PGM extraction conditions and results that will be discussed in the present section are summarized in Table 9.

The capacity of Aliquat 336/PVC membranes for rapid extraction of Pd(II) from its synthetic acidic solutions has been theoretically and experimentally reported. Aliquat 336 has a dual function of plasticizer and extractant. Immersion of the membrane into an acidic Pd solution leads to the extraction of the metal via complexation of Aliquat 336 with PdCl<sub>4</sub><sup>2-</sup> (present at 1.0 M HCl) on the membrane interface and subsequent diffusion of the formed complex into the bulk of the membrane. Increasing Aliquat loading on the membrane enhances the diffusivity of the formed complex. Based on extraction data for Pd, Au, Cu and Cd, it is concluded that the membrane preferentially extracts Pd. Membrane saturation is observed at 100 mg/L of Pd where the membrane gets turbid, while exceeding 300 mg/L leads to a precipitate formation on the membrane surface. The authors have provided mathematical models that describe the diffusion of Aliquat as well as the kinetics of the interfacial complexation reaction. Potential application of these membranes for quantitative Pd determination and industrial recovery from waste solutions is envisioned.<sup>245</sup>

Different kinetic behavior of Pt(IV), Pd(II) and Rh(III) across supported-liquid membranes, where Aliquat 336 acts as a carrier, can be exploited for their separation, as demonstrated in mixed synthetic PGM solutions. A polydifluoroethylene film was the selected microporous support for the liquid membrane. Aquated chlorocomplexes of Rh are highly hydrophilic, thus, their extraction into organic solvents is limited. Addition of NaSCN to aqueous Rh solutions and subsequent heating at 90 °C, for 2 h, induces the formation of the non-aquated and much less hydrophilic Rh(SCN)<sub>6</sub><sup>3-</sup> species, which can be effectively extracted by anion exchange in the presence of Aliquat. The membrane permeability is favored by dissolving Aliquat in an organic solvent, namely dodecane, and it can be further enhanced by modification of the membrane with 1-dodecanol (6% required to maximize permeability). Transfer of Pd across the membrane is independent of prior heating of the solution due to the labile character of its chlorocomplexes, thereby allowing the easy formation of the Pd(SCN)<sub>4</sub><sup>2-</sup> species. Under these conditions, transport of Pd is much faster than that of Pt, while Rh cannot be transported since in the absence of

heating the  $\text{Rh}(\text{SCN})_6^{3-}$  complexes have not been formed, thus, complete separation of Pt and Pd from Rh and partial separation from each other is achieved (Figure 51). Application of heat leads to formation of Rh complexes which can be effectively stripped with 1.0 M  $\text{NaHSO}_3$ .<sup>246</sup>

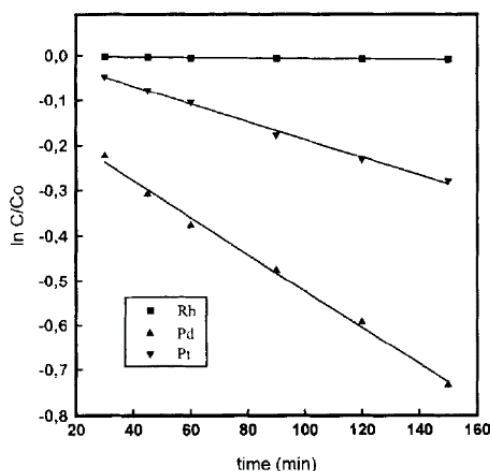


**Figure 51.** Transport of Rh(III), Pt(IV) and Pd(II) through the liquid membrane. 10 mg/L metal, 10 mM  $\text{SCN}^-$ , 0.15 M Aliquat 336 in dodecane + 4% 1-dodecanol.<sup>246</sup>

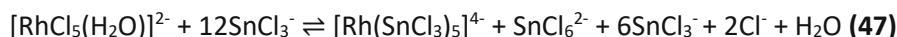
The group further investigated the transport of Pt(IV) ions across the developed solid-supported liquid membrane system. As previously discussed, permeability is dependent on the concentration of 1-dodecanol and it reaches its maximum at 6%, however, due to the increase in hydrophilicity and subsequent loss of organic solutions 1-dodecanol is reduced to 4%. A significant decrease in the permeability of the membrane is observed if Pt exceeds 40 mg/L. Stripping of Pt is feasible with 0.5 M  $\text{NaClO}_4$  via an anion-exchange mechanism.<sup>156</sup>

Focusing on the transport of Rh(III), the group additionally developed a supported-liquid membrane system comprising polypropylene hollow fibers, which can extend the lifetime of the liquid-membrane system and allow their easy regeneration. Aliquat 336 in dodecane containing 4% dodecanol was used for the impregnation of the fibers, while the feed solution was supplied at a continuous mode with the aid of a peristaltic pump. While increasing the concentration of the IL has a detrimental effect on the membrane permeability introduced by the increase in viscosity, higher flow rates favor the permeability by decreasing the thickness of the boundary diffusion layer. The fibers retain their initial permeability level for fifteen cycles of 24 h each, between which the fibers are washed and re-impregnated with fresh membrane solution. Additionally, a 6-day non-stop operation of the system is feasible.<sup>247</sup>

In subsequent experiments, the group developed a process for the separation of Pt, Pd and Rh from leach liquor of car catalysts, relying on the combination of two hollow fiber supported-liquid membranes, where triisobutylphosphine sulfide (Cyanex 471) and Aliquat 336 function as carriers. An acidified synthetic solution containing the three PGMs is passed first through the hollow fiber which has been impregnated with Cyanex 471, which is highly selective for Pd. The circulation of the solution through the second, Aliquat 336-impregnated fiber, retains Pt, thus, leaving Rh in solution. Addition of  $\text{SCN}^-$  is necessary in order to improve the permeability of Pt.<sup>248</sup>

Liquid-surfactant membranes comprising the IL  $[\text{C}_8\text{mim}][\text{PF}_6]$  were synthesized and evaluated for the extraction of Rh(III) from its aqueous model solutions. A water-in-oil microemulsion was generated by mixing the IL and the surfactant polyoxyethylene 80 sorbitan monooleate (Span 80) in  $\text{CHCl}_3$  with the Rh-containing aqueous phase. Modification of the hydrophilic Rh complexes, such as  $\text{RhCl}_6^{3-}$  and

$[\text{RhCl}_5(\text{H}_2\text{O})]^{2-}$ , is necessary to facilitate extraction of Rh into the hydrophobic extractant. Reduction of Rh to  $[\text{Rh}(\text{SnCl}_3)_5]^{4-}$ , with the aid of  $\text{SnCl}_2$ , favors its extraction (equations 46, 47).



Selective recovery of Rh over Sn is accomplished with the IL-containing liquid-surfactant membrane (LSM). Additionally, rapid (5 min), quantitative (95%) and selective stripping of Rh is reported with the aid of Tris.<sup>249</sup>

**Table 9.** Summary of PGM extraction conditions and results with ionic liquid-based membranes.

PGM Solution	Ionic Liquid on Membrane	T (°C)	Max. Permeability	Ref. No
<100 mg/L Pd(II) in 1.0 M HCl	50% Aliquat 336 in PVC	n.a.	n.a.	245
10 mg/L Rh(III) in 3 mM HCl/1 M NaCl/1 mM NaSCN, pH 2.5	0.15 M Aliquat 336 in dodecane and 4% 1-dodecanol on polydifluoroethylene film	RT	0.015 cm/min	246
10 mg/L Pt(IV) in 0.02 M HCl/0.5 M NaCl	4 mM Aliquat 336 in dodecane and 4% 1-dodecanol on liquid membrane	RT	0.30 cm/min, $D_{\text{Pt}} > 2$	156
8.56 mg/L Rh(III) in HCl/1.0 mM NaSCN/1.0 M NaCl, pH 5	0.15 M Aliquat 336 in dodecane and 4% 1-dodecanol on polypropylene hollow fibers	n.a.	0.015 cm/min, Rh pre-concentration by a factor of 24	247
10 mg/L/metal: Pt, Pd, Rh in HCl/0.1 M NaCl/0.1 M NaSCN	Module 1: 40 mM Cyanex 471 in decaline and 20% cumene Module 2: 0.15 M Aliquat 336 in dodecane and 4% 1-dodecanol on polypropylene hollow fibers	n.a.	n.a.	248
4 mg/L Rh(III) in 1 M HCl	0.05 M $[\text{C}_8\text{mim}][\text{PF}_6]$ on liquid membrane	25	n.a.	249

### 3.2.4 Nanoparticles

Magnetic task-specific polymeric IL-based nanoparticles (Figure 52) have been synthesized and applied to the preconcentration of Pt(IV) and Pd(II). The  $\text{Fe}_3\text{O}_4$  core imparts the magnetic properties, while silanization of the  $\text{SiO}_2$  coating provides binding sites for the polymerization of the TSIL. Due to its high affinity toward soft metals, such as noble metals, the sulfur atom was selected for the functionalization of the polymeric IL. The thiol group located on the IL anion is an additional driving force toward the recovery of noble metals. In order to suppress the competition between the cation moiety and the  $\text{H}^+$  for anion exchange and to ensure that the nanoparticle structure remains intact, the pH value in solution should not be below 3.0, while, at the same time, it should not be exceeded to prevent hydrolysis of the metals. Quantitative extraction of both Pt and Pd is achieved within 15 min, while the presence of foreign cations, up to 4000-fold level, does not have any impact on the extraction efficiencies of Pt and Pd. Thiourea can be applied for the desorption of Pt and Pd.<sup>250</sup>

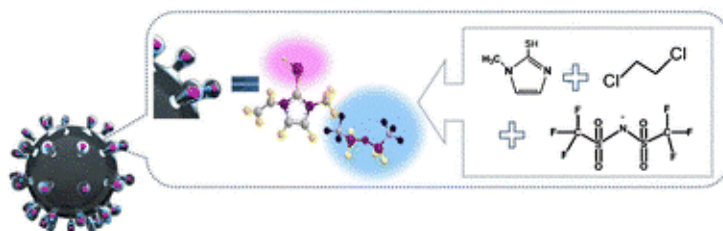


**Figure 52.** Nanoparticle with attached magnetic task-specific polymeric IL.<sup>250</sup>

A solid sorbent material comprising magnetic nanoparticles of  $\text{Fe}_3\text{O}_4$  coated with an IL-functionalized polymer (polyethyleneglycol) was reported as an effective approach for fast (30 min) and quantitative recovery of Pt(IV) (98%) and Pd(II) (99%) from model chloride solutions (Figure 53). Among the evaluated imidazolium and phosphonium ILs, only Cyphos 101 demonstrated capacity for quantitative extraction, presumably due to its lower hydrophobicity compared to the other candidates. Nevertheless, there is an optimum IL concentration above which sorption capacity is reduced due to the progressive coverage of the functional groups by the excess of the IL load. Additionally, the HCl concentration of the solution should ideally not exceed 1.0 M to avoid hydrolysis of PGMs and dissolution of the synthesized nanoparticles. The extraction efficiency of Pt and Pd is not interfered by the presence of 4-fold concentrations of Cu(II), Ni(II) and traces of Rh(III). Au(III) is quantitatively extracted along with Pt and Pd, however, they can be selectively desorbed from the particles with the aid of a  $\text{HNO}_3$  solution.<sup>251</sup>

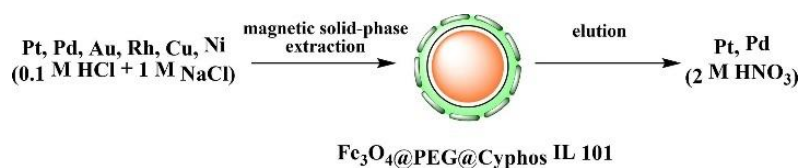


**Figure 53.** Recovery of Pt and Pd with  $\text{Fe}_3\text{O}_4$  magnetic nanoparticles coated with an IL-functionalized polymer.<sup>251</sup>

### 3.3 Experimental gaps and omissions in the literature

A great deal of work on the extraction of PGMs with ILs has already been performed. However, in this mutual scientific road to discovery, it is ideal to have a common frame of reference so expectations can be effectively managed and results fairly and sensibly evaluated.

As it was discussed in the introductory part of this thesis and throughout this entire chapter, the mechanistic route of the extraction process is a fairly important aspect that is, in some cases, overlooked. The necessity of this information is 2-fold; first, familiarity with the extraction mechanism can assist in the evaluation of its response to parameter changes, which is invaluable information that can be used for the development of targeted processes and tailoring to specific goals. Second, with the aim of limiting the environmental impact and the financial demands of the process, the knowledge of the mechanism allows the detection of possible degradation of the IL as well as aqueous phase contamination from the IL components, which, as is evident from the discussed literature, happens in many cases. And this is of particular significance when highly toxic and/or highly expensive ILs are used.

It is clear in many cases that, when the anion-exchange mechanism takes place, there is a decisive impact of the HCl concentration on the extraction efficiency of the target metal. However, this could be an effect of increasing amount of Cl<sup>-</sup> anions competing for exchange with PGM-chlorocomplexes. It could also be an effect of the change in complex speciation toward less extractable species as the acidity increases. In any case, data with both HCl, and Cl salts should be provided, as several authors have done, in order to clarify the decisive impact on the observed behavior. We should also consider that the concentration of a component is not the same thing as its activity. So, when the ionic strength of the solution is adjusted with the aid of a salt, e.g., NaCl, it does not mean that adjustment with another Cl compound, e.g., HCl, will generate identical results. Activity and concentration are equal only in ideal solutions, where no electrostatic interaction between the ions is assumed. In reality, we should consider that the behavior of a solution with different ions of different charges and sizes will deviate from the ideal behavior, even more as the concentration increases. In this sense, it is advisable to investigate the effect of Cl<sup>-</sup> both at different concentrations and with various counter cations.

Different salts act differently according to their nature and their respective concentration. This can be attributed to the two different effects that different salts can exert; (i) bind H<sub>2</sub>O molecules in the aqueous phase so less free H<sub>2</sub>O is available for the dissolution of the extractable species and (ii) break down the hydrogen bond structure of H<sub>2</sub>O, thereby facilitating the dissolution of the extractable species in the aqueous phase. These two effects are demonstrated in Figure 54, where effect (i) dominates in the case of NH<sub>4</sub>Cl and effect (ii) in the case of NaClO<sub>4</sub>.<sup>252</sup> The same salting-out effect, i.e., increase in the distribution ratio as salt concentration increases, as well as the opposite, salting-in effect, have also been observed in IL-based separations, as it was noted in this chapter. Unfortunately, the examination of this potentially exploitable phenomenon for separation is scarce among the herein reported literature.

The same behavior is evident on the extraction capacity of PGMs with anion-exchange resins. As reported by Wołowicz et al.,<sup>253</sup> varying the ionic strength of a Pd-feed solution (NaCl at fixed concentrations mixed with varying concentrations of HCl) is a decisive factor in the extraction behavior of the anion-exchange resin, which is manifested as a shift in the distribution ratios as well as the constructed breakthrough curves of the resins. This particular experimental approach can serve as a useful example for IL-based separations, all the more because the resins used in this work are strong anion-exchange resins of type 1,<sup>253</sup> quaternary ammonium groups where tri-methyl groups are attached on the N atom,<sup>254</sup> thereby resembling a solid version of Aliquat 336.



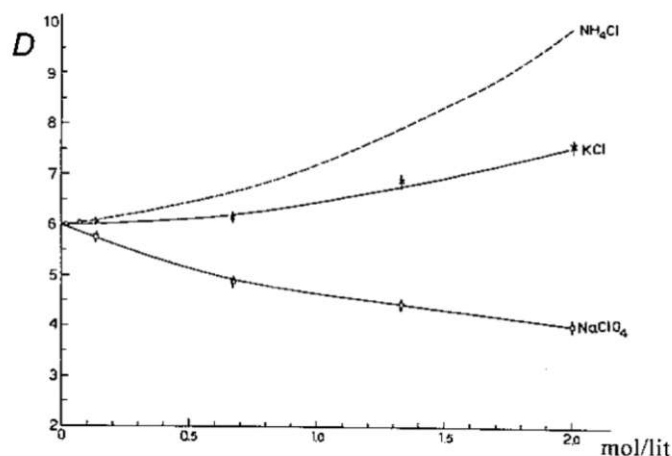


**Figure 54.** Distribution ratio of undissociated acetylacetonate between benzene and aqueous phase containing different inorganic salts.<sup>252</sup>

This naturally raises the question whether the adjustment of ionic strength, which can be used as a tool to shift the forward extraction of target compounds and increase the separation between metals, can also be used for back-extraction. In the cases where anion exchange is the predominant extraction mechanism, e.g., when Aliquat 336 is used, the  $\text{Cl}^-$  anions of Aliquat are exchanged with the PGM-chlorocomplexes, thereby forming a complex and releasing  $\text{Cl}^-$  in the aqueous phase. If Le Chatelier's principle is taken into consideration, it would be a rational assumption that a highly concentrated  $\text{Cl}^-$  solution could shift the thermodynamic equilibrium from the products (complex and  $\text{Cl}^-$ ) back to the reactants (Aliquat and PGM-chlorocomplex). If a shift in the chemical equilibrium rather than stripping of the target metal is considered, there are two clear advantages; the use of toxic stripping reagents, e.g., thiourea, is minimized or eliminated and Aliquat is restored to its original state.

With regard to PGM speciation, specifically Rh, there still seem to be many unanswered questions as to which Rh species are the extractable ones. The majority of authors support that the  $\text{RhCl}_6^{3-}$  species is the hardest to extract due to its higher charge density and the bulky octahedral structure of the complex. Others suggest that both  $[\text{RhCl}_5(\text{H}_2\text{O})]^{2-}$  and  $\text{RhCl}_6^{3-}$  are quite difficult to extract, while  $\text{RhCl}_6^{3-}$  has also been reported to be the extracted species. It is thus obvious that there is still no consensus on this fundamental topic. Without a doubt, the chemistry of Rh is extremely complex and challenging to decipher; however, to avoid perpetuation of possible errors, experimental data that point to the extractable species should be provided rather than literature-based assumptions.

Most authors have provided distribution ratios along with extraction efficiencies, which is necessary, since the distribution ratio actually indicates how efficient the separation will be. However, even more valuable than the  $D$  of the system under certain experimental conditions is the entire slope analysis in order to estimate the system's response/sensitivity to parameter changes. Only a complete slope analysis will provide the necessary information for the full evaluation of the efficiency of the develop process.

Another topic that has been sparingly addressed, in the literature that is reported herein, is the loading capacity of the ILs in liquid-based separations. While it seems to be common, maybe even intuitive, to address the loading capacity of IL-impregnated resins, as is evident by all relevant publications presented here, this is not the case when ILs are employed in liquid-based separations. A number of authors have constructed extraction isotherms for their processes; however, it is imperative that this is regularly practiced, especially if industrial application of the experimental findings is envisioned.

In several cases, the contamination of the aqueous phase by IL ions is entirely neglected or simply mentioned without any discussion of possible implications. Additionally, in extraction with solid sorbents impregnated with ILs, data on the possible leakage of ILs out of the solid is notably absent. These topics are quite important, as mentioned earlier, due to both environmental and financial implications.

On a more fundamental topic, it is quite unfortunate that several results (distribution ratios, extraction efficiencies, concentrations) have been reported without any error values. While experimental findings are quite important, when errors values are omitted, these findings can easily become questionable.

As it will be presented in detail in the next section, the environmental fate of ILs is quite important, considering the toxic nature of some of them. Unfortunately, any discussion on toxicity of ILs and organic solvents employed in conjunction with ILs has been left out of the reported research. It is definitely interesting to discover new systems and alternative ways to reach desired extraction goals, but with full awareness of their implications and willingness to judge their usefulness and viability, in terms of environmental and financial impact, if the desired sustainability goals are to be met.

### 3.4 Environmental considerations

Ionic liquids are often, perhaps too optimistically, labelled as “green” alternatives to commonly employed organic solvents, a characterization attributed to them primarily due to the absence of vapor pressure. However, this is only one aspect to be considered when one makes “greenness” claims; the ease and the extent of the recovery of the employed IL is a factor that can significantly affect its industrial viability. Additionally, the attractive feature of non-volatility does not come without a trade-off; product isolation and purification become considerably complex and problematic. Not to mention that the task of selecting an IL candidate which is appropriate for the task at hand can be a really daunting task, considering the seemingly endless options (approx.  $10^6$ ) and the little added value if the selected candidate cannot increase process performance to a worthwhile degree.<sup>255</sup> Many times, the “greenness” of ILs, perhaps out of excitement for their novelty, has been exaggerated to the point that they have been presented as the cornerstone of low environmental-impact processes. However, as the excitement subsides and new data emerge, it appears that not all is as it may have initially seemed.

Data on the environmental fate of the most extensively studied imidazolium-based ILs was gathered and presented by Stepnowski.<sup>256</sup> In his studies, he demonstrated the strong and irreversible binding of ILs to soils, sediments and minerals, which increases with increasing alkyl chain of the IL. This can potentially reduce their bioavailability in marine ecosystems, however, the effect of parameters, such as pH and temperature, on the sorption and desorption behavior of ILs need to be addressed.<sup>256</sup> Not to mention that even the most hydrophobic of ILs still appear to be soluble in water, to a certain degree, meaning that their dispersion into aquatic systems is inevitable.<sup>257</sup> Since industrial effluents will eventually contain certain IL amounts, their degradation potential was also evaluated; even though it proved to be possible with advanced photodegradation techniques, it appears to be in line with the alkyl chain of the IL, i.e., longer chain equals less resistance to photodegradation, while symmetry in the cation increases the IL’s stability to degradation. Regarding ecotoxicity, they have shown the potential to disrupt biological barriers, even more so as the length of their alkyl chain, i.e., lipophilicity, increases.<sup>256</sup> It is clear by the research work that has been thus far conducted with imidazolium-based ILs and presented in this review, that imidazolium ILs with long octyl carbon chains are commonly employed for PGM recovery, either as the sole extracting agent<sup>178,186,187,190</sup> or in combination with other imidazolium ILs comprising dodecyl,<sup>179</sup> tetradecyl<sup>184</sup> or even hexadecyl<sup>182</sup> carbon chains. On the other hand, asymmetrical cations are employed, while symmetry in the cation has only been reported once.<sup>179</sup>

The toxicity of ILs comprising the most commonly used cations has been evaluated with the aid of the human cervical carcinoma cells HeLa.<sup>258,259</sup> These cells are representative of prototypical human epithelial cells which are generally the site of the first contact of an organism with toxic compounds.<sup>259</sup> The relative toxicity of certain ILs and some single cations is presented in Figure 55.

Evidently,  $\text{NTf}_2^-$  is more toxic than its halide counterparts. Nevertheless, as the  $\text{EC}_{50}$  values reflect, increasing the alkyl chain length of the IL cation has a more pronounced negative effect on toxicity. The  $\text{EC}_{50}$  value for  $[\text{C}_2\text{mim}][\text{BF}_4]$  is 9.9 mM and for the corresponding  $\text{Br}^-$  and  $\text{NTf}_2^-$  analogues, 8.4 mM and 1.8 mM, respectively. At the same time, they are still less toxic than  $[\text{C}_8\text{mim}]\text{Br}$  with 0.3 mM.<sup>258</sup>

Stepnowski et al.<sup>259</sup> proved that IL hydrophobicity is probably only a secondary toxicity factor in ILs comprising chains with up to 6 carbon atoms. Among compared ILs comprising the  $\text{C}_4\text{mim}^+$  cation and the  $\text{Cl}^-$ ,  $\text{PF}_6^-$  and  $\text{BF}_4^-$  anions, the lowest  $\text{EC}_{50}$ , for 24 h of incubation, is exhibited by  $[\text{C}_4\text{mim}][\text{BF}_4]$  (0.6 mM), while the other two exhibit relatively high  $\text{EC}_{50}$  values ( $>12$  mM).  $[\text{C}_6\text{mim}][\text{BF}_4]$  is significantly less toxic (11.5 mM) than its  $\text{C}_4$  analogue; however, elongation of the cation alkyl chain to  $\text{C}_{10}$ , i.e.  $[\text{C}_{10}\text{mim}][\text{BF}_4]$ , induces a dramatic increase in toxicity (0.07 mM). Additionally, replacing the methyl chain attached to

the imidazolium cation with an ethyl chain decreases the toxicity, as demonstrated with the aid of [C<sub>4</sub>eim][BF<sub>4</sub>] (3.4 mM), which is rather surprising considering its higher hydrophobicity compared to [C<sub>4</sub>mim][BF<sub>4</sub>].<sup>259</sup>

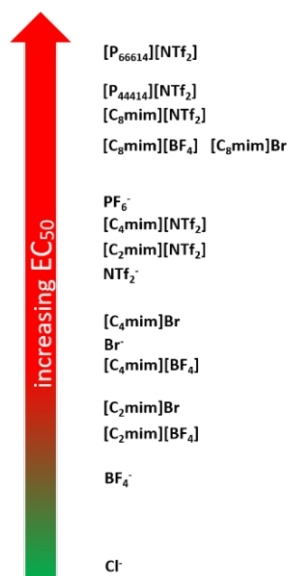


**Figure 55.** Relative toxicity of some commonly employed ILs expressed in EC<sub>50</sub> values.

In any case, these ILs exhibit higher toxicity than some commonly employed solvents, such as acetone, ethanol, dichloromethane and phenol (Table 10).<sup>258,259</sup>

**Table 10.** Toxicity of some common solvents and salts toward HeLa cells.<sup>258,259</sup>

Compound	EC <sub>50</sub> (mM)
Acetone <sup>a</sup>	449 ± 69
Acetonitrile <sup>a</sup>	>2900
Ethanol <sup>a</sup>	866 ± 37
Dichloromethane <sup>b</sup>	71 ± 21
Phenol <sup>b</sup>	43 ± 3
Xylene <sup>b</sup>	52 ± 29
Sodium dodecylbenzenesulfonate <sup>b</sup>	0.18 ± 0.01
Sodium chloride <sup>b</sup>	101 ± 32
Lithium chloride <sup>b</sup>	41 ± 2

<sup>a</sup> Determined after 48 h. <sup>b</sup> Determined after 3 h.

The high toxicity of Aliquat acesulfame and Aliquat saccharine on the colon carcinoma cell lines HT-29 and CaCo-2 has been demonstrated. At concentrations of 0.1 mM, only 20% of the exposed cells were viable.<sup>260</sup>

Mehrkes and Karunanithi<sup>261</sup> employed a correlation model provided by the Environmental Protection Agency to convert *in vitro* toxicity data to *in vivo*, which they subsequently used to predict human toxicity of some imidazolium ILs. For the C<sub>4</sub>mim<sup>+</sup> ILs comprising the anions PF<sub>6</sub><sup>-</sup>, BF<sub>4</sub><sup>-</sup> and Br<sup>-</sup>, they reported LD<sub>50</sub> values of 3.0 mmol/kg, 2.7 mmol/kg and 2.5 mmol/kg, respectively.<sup>261</sup>

Certain studies have also provided LC<sub>50</sub> values of ILs on animals (freshwater snail *Physa Acuta*)<sup>262</sup> and fish (zebrafish *Danio Rerio*).<sup>263</sup> With regard to the freshwater snail, imidazolium ILs [C<sub>n</sub>mim]Br, with n = 4, 6, 8, exhibit LC<sub>50</sub> (96 h) of 229 mg/L, 56 mg/L and 8 mg/L, respectively, following the increasing toxicity trend with increasing alkyl chain length. For the sake of comparison, some common solvents employed on manufacturing and disinfection facilities, e.g., ammonia and phenol, have respective LC<sub>50</sub> values of

1.40 mg/L and 260 mg/L.<sup>262</sup> Imidazolium ILs based on the C<sub>4</sub>mim<sup>+</sup> cation with several anions, i.e., BF<sub>4</sub><sup>-</sup>, PF<sub>6</sub><sup>-</sup> and NTf<sub>2</sub><sup>-</sup>, all exhibit LC<sub>50</sub> (96 h) over 100 mg/L.<sup>263</sup>

A comprehensive review of the available toxicity data of ILs has been provided by Pham et al.<sup>264</sup> A discussion on the potential toxicity of ILs accompanied by an extensive list of performed toxicity studies has been provided in the review by Flieger et al.<sup>265</sup>

Apart from the potential toxicity of ILs, the environmental implications associated with their preparation should not be overlooked. The synthetic routes for some ILs require excess use of reagents, e.g., production of 3 g of [C<sub>n</sub>mim]X, where X=halide, produces 100 g of waste (toluene, acetonitrile, ethyl acetate), which is far from ideal from an environmental perspective. Additionally, the formation of halide salt in stoichiometric amounts as waste in the metathesis step is far from ideal in light of sustainability. Raw materials used in their synthesis, such as imidazole and haloalkanes, come from the non-sustainable petroleum resources, while certain salts employed in the process are highly toxic, e.g., LiN(CF<sub>3</sub>SO<sub>3</sub>)<sub>2</sub> in the synthesis of [C<sub>4</sub>mim]NTf<sub>2</sub>. Lifecycle analysis on [C<sub>4</sub>mim]Cl proved the major impact of 1-methylimidazole on the categories of global warming, aquatic toxicity and human toxicity. An additional downside, is the high demand in terms of energy and financial expenses, especially during the quaternization step of the synthetic process.<sup>266</sup>

It is evident that most researchers are aware of the importance of addressing aspects pertaining to the sustainability of their proposed methods. Recycling of the IL is definitely a step that could help minimize environmental impact and the work of most researchers referenced in this thesis has addressed this quite important issue <sup>162,165,168,170,171,174,182,183,187,199,201,202,204,205,206,207,210,211,239,240,241,243,244</sup> On the other hand, some authors report the effective use of ILs employing fluorinated anions, namely PF<sub>6</sub><sup>-</sup>,<sup>181,182,184,185,190,192,249</sup> however, there is no mention of the possible toxicity that can result from using these particular anions. Specifically, even though ILs comprising the PF<sub>6</sub><sup>-</sup> anion are only slightly soluble in water, when they are employed in liquid-based separations from acidic phases, the anion can hydrolyze generating toxic HF.<sup>267</sup> However, it should be pointed out here, that while with PF<sub>6</sub><sup>-</sup>-containing ILs small amounts of HF are released in solution, in the state-of-the art PGM-recovery processes mineral acids are used in pure undiluted form or in mixtures. i.e., *aqua regia*. It is well known that *aqua regia* generates toxic gases,<sup>45</sup> while high temperatures are used which also promote the evaporation of the dangerous and corrosive mineral acids.<sup>60</sup> Additionally, the use of excessive amounts of acids implies generation of waste water with high acid content.<sup>58</sup> In the case of ILs, high concentration of HNO<sub>3</sub> (8 M) accelerates the conversion of PF<sub>6</sub><sup>-</sup> anions to PO<sub>4</sub><sup>3-</sup> (H<sup>+</sup> + PF<sub>6</sub><sup>-</sup> + 6H<sub>2</sub>O + 3HNO<sub>3</sub> → H<sub>3</sub>PO<sub>4</sub> + 6HF + 3HNO<sub>3</sub> + 2H<sub>2</sub>O).<sup>268</sup> While phosphate is not *per se* toxic, release of excessive amounts into aquatic environments can promote algal growth and lead to eutrophication.<sup>269</sup> Regarding NTf<sub>2</sub><sup>-</sup>, which has been reported by many researchers referenced in this thesis,<sup>169,170,172,178,179,180,183,185,186,187,188,189,191, 212,213,214,215,216,223,224,225</sup> its ecotoxicological potential has been established.<sup>270</sup>

The overwhelming majority of publications presented herein, reports the use of some organic solvent as a diluent for the IL. Unfortunately, in certain cases, the use of toxic solvents, i.e., CHCl<sub>3</sub><sup>164,177,190,210,211</sup> and benzene,<sup>157,162</sup> has been reported. Benzene additionally poses an environmental hazard, just as NH<sub>4</sub>SCN,<sup>189</sup> NH<sub>4</sub>OH<sup>189</sup> and (NH<sub>4</sub>)<sub>2</sub>S.<sup>183</sup> The two latter are also corrosive agents. Moreover, in a number of publications, solvents with potentially negative impacts on human health appear, namely, toluene,<sup>155,161,173,196,197,198,199,202,203,204</sup> nonane,<sup>192</sup> CH<sub>2</sub>Cl<sub>2</sub><sup>173</sup> and dodecane.<sup>156,159</sup>

Regarding the recovery of the PGMs that are extracted in the liquid or solid-based IL phase, either mineral acids, e.g., HNO<sub>3</sub>, toxic organic compounds, e.g., thiourea, or their combinations, e.g., thiourea in HCl are

commonly employed. The use of the highly toxic hydrazine hydrate as a stripping agent has also been reported (Table 11).

**Table 11.** Stripping conditions used for the recovery of PGMs from ionic liquid phases.

Stripping solution	Ratio (O/S) <sup>a</sup>	Time (min)	T (°C)	Stripping efficiency (%) Distribution Ratio (D)	Ref. No
2.0 M NaHSO <sub>3</sub> (x 4 contacts)	1/2	20	50	97.6% Pt (from 0.5% (v/v) Aliquat 336 in toluene), D <sub>Pt</sub> =0.055	155
0.5 M NaClO <sub>4</sub>	1/1	15	n.a.	100% Pt	156
i. 5.0 M NH <sub>4</sub> NO <sub>3</sub> ii. 4.0 M NH <sub>4</sub> SCN/1.5 M NH <sub>4</sub> OH	1/1	n.a.	RT	i. 98.4% Rh, 9.2% Pd ii. 93.7% Pd, 98.4% Rh	157
Step 1 i. 1.0 M HNO <sub>3</sub> ii. 0.05 M thiourea/0.1 M HCl Step 2 i. 2.0 M NaOH ii. 1.0 M thiourea/2.0 M HCl	1/1	5	n.a.	Step 1 i. 100% Pd, 85% Pt ii. 100% Au Step 2 i. 100% Pd, 0.7% Pt ii. 100% Pd	162
0.5 M thiourea/0.5 M HCl or 0.5 M thiourea/0.5 M NH <sub>4</sub> Cl	1/2	720	n.a.	>99% Pd	163
0.75 M thiourea/5.0 M HCl (x 2 contacts)	n.a.	n.a.	n.a.	100% Pt (single-element solution)	165
0.5 M thiourea/0.5 M HCl (x 2 contacts)	4/1	n.a.	n.a.	99.9% Pt	166
0.5 M thiourea/0.5 M HCl (x 2 contacts)	6/1	n.a.	n.a.	99.9% Pt, D <sub>Pt</sub> =0.17	167
0.75 M Na <sub>2</sub> S <sub>2</sub> O <sub>3</sub>	1/1	5	n.a.	100% Pt	168
8.0 M HNO <sub>3</sub> (x 2 contacts) or 1.0 M HNO <sub>3</sub>	1/2	60	n.a.	91% Pt, 57% Pd or 60% Pt, 3.1% Pd	170
0.1 M thiourea/1.0 M HNO <sub>3</sub>	1/10	30	n.a.	91% Pd, 34% Pt	171
i. 1.0 M NH <sub>4</sub> OH ii. 1.0 M Na <sub>2</sub> S <sub>2</sub> O <sub>3</sub> iii. 1.0 M thiourea/1.0 M HCl	3/1	20	RT	i. 89.8% Pd, 4.25% Rh, 0.98% Pt, 0.04% Au ii. 98.4% Au, 2.16% Pt, 1.63% Rh, 0.09% Pd iii. 62.6% Pd, 25.4% Pt, 6.85% Rh, 2.91% Au	174
i. 0.5 M thiourea/1.0 M HCl ii. N <sub>2</sub> H <sub>4</sub>	n.a.	n.a.	n.a.	i. 100% Pd ii. 100% Pt	177
0.5 M N <sub>2</sub> H <sub>4</sub> ·H <sub>2</sub> O	n.a.	2	60	98.2% Pt	182
i. 2.0 M N <sub>2</sub> S <sub>2</sub> O <sub>3</sub> ii. 0.5 M thiourea/1.0 M HCl (x 3 contacts) iii. 0.5 M thiourea/1.0 M HCl (x 3 contacts)	n.a.	n.a.	n.a.	i. 100% Pt ii. >98% Pd iii. >98% Ru	183
5.0 M HNO <sub>3</sub>	1/4	n.a.	n.a.	>98% Pt, 100% Pd	187
0.5 M thiourea/1.0 M HCl or 4.0 M NH <sub>4</sub> SCN/1.5 M NH <sub>4</sub> OH	1/4	n.a.	n.a.	>96% Pd	188
4.0 M NH <sub>4</sub> SCN/1.5 M NH <sub>4</sub> OH (x 2 contacts)	n.a.	n.a.	n.a.	98% Pd	189
1% (w/w) NH <sub>3</sub> (x 2 contacts)	n.a.	n.a.	n.a.	>90% Pt, >90% Pd, >90% Rh	191
i. 1.0 M NH <sub>3</sub> ·H <sub>2</sub> O (x 2 contacts) ii. 1.0 M HNO <sub>3</sub> or 6.0 M HCl	1/1	i. 30 ii. 10	n.a.	> 90% Pd, 56% Pt	192
i. 0.5 M NH <sub>4</sub> OH ii. 0.5 M NH <sub>4</sub> OH iii. 5.0 M HCl	1/1	15	n.a.	i. 54% Pt ii. 38% Rh iii. 39% Ru	196
0.5 M NH <sub>4</sub> OH	n.a.	10	n.a.	97.1% Pd	199



0.5 M NH <sub>3</sub>	1/1	n.a.	n.a.	73% Pd, 7% Pt (model mixture)	200
0.5 M NH <sub>4</sub> OH	1/1	10	n.a.	90% Pt	201
0.5 M NH <sub>4</sub> OH	n.a.	n.a.	n.a.	90% Pd	202
0.5 M HNO <sub>3</sub>	n.a.	n.a.	n.a.	20% Rh (from P <sub>66614</sub> Cl) 40% Rh (from P <sub>66614</sub> DOP)	203
i. 0.1 M thiourea/0.5 M HCl ii. 1.0 M HNO <sub>3</sub>	1/1	20	n.a.	i. 95.3% Pd, 2.4% Pt, 7.5% Ru ii. 69.1% Pt, 0% Pd, 0% Ru	204
i. 0.1 M NaSCN (x 3 contacts) ii. 0.01 M thiourea/5% HCl	1/1	10	n.a.	i. >90% Pt, 0% Pd ii. 99% Pd, <2% Pt	205
i. HNO <sub>3</sub> ii. CS(NH <sub>2</sub> ) <sub>2</sub> iii. HCl	1/1	n.a.	n.a.	i. 74.9% Pt, 13.6% Pd, 31.8% Rh ii. 91.2% Pd, 21.2% Pt, 3.71% Ru iii. 73.7% Rh, 0.30% Pt, 0.07% Pd	206
Step 1 i. 1.2 M Na <sub>2</sub> SO <sub>3</sub> ii. 1.0 M thiourea Step 2 i. 1.2 M Na <sub>2</sub> SO <sub>3</sub> ii. 5.0 M HCl	1/2	i. 30	Step 1 i. 50 Step 2 i. 50	Step 1 i. 88% Fe ii. 97% Pd Step 2 i. 90% Fe ii. 78% Rh	207
Step 1 i. 1.2 M Na <sub>2</sub> SO <sub>3</sub> ii. 0.1 M thiourea/0.5 M HCl iii. 5.0 M HNO <sub>3</sub> Step 2 5.0 M HCl	1/2	30	i. 30	Step 1 i. 98% Fe ii. 90% Pd, 2.7% Pt iii. 85% Pt Step 2 82% Rh	208
i. Na <sub>2</sub> S <sub>2</sub> O <sub>3</sub> ii. 0.01 M thiourea/5% HCl	n.a.	60	90	i. 83.3% Au ii. 85.5% Pd, 56.2% Pt	209
1.0 M oxalic acid	1/1	240	65	complete Pd precipitation	210
0.5 M thiourea/0.5 M HCl	1/1	60	25	> 99%	211
0.5 M thiourea/1.0 M HCl	10/1	n.a.	n.a.	99% Pd	215
5 M HNO <sub>3</sub> or 1 M HClO <sub>4</sub>	2 g/L	1440	20	>95% Pt	237
1 M thiourea/0.5 M HCl (x 2 times)	2 g/L	1440	20	100% Pd	239
5 M HNO <sub>3</sub>	2 g/L	1440	20	100% Pd, 85% Pt, 4.8% Au	240
1 M thiourea	7.5 g/L	1440	30	95% Pt(II), 98% Pt(IV), 99% Pd(II)	241
Step 1 0.01 M thiourea/0.01 M HCl Step 2 1.0 M thiourea/1.0 M HCl	Step 1 33 g/L Step 2 8 g/L	n.a.	RT	Step 1 99.9% interfering elements Step 2 100% Pt, 100% Pd, 0% Rh	242
0.1 M thiourea/0.1 M HCl	2.4 g/L	1440	n.a.	99% Pt	243
0.1 M thiourea/0.1 M HCl	2.4 g/L	1440	n.a.	96% Pd	244
1.0 M NaHSO <sub>3</sub>	100/100 mL	0	n.a.	100% Rh	246
0.2 M NaHSO <sub>3</sub> /0.8 M NaSCN, pH 5	500/3 mL	n.a.	n.a.	208.3 mg/L <sup>b</sup>	247

<sup>a</sup> O= organic phase, S= stripping agent. <sup>b</sup> Metal recovered.

It should be explicitly pointed out though, that addressing or not addressing an important environmental aspect of a process does not automatically serve as a declaration of the process as “green” or not. Aside from the fact that all steps need to be evaluated, it should be clearly stated that the term “green” is only relative. A “green” assessment can be made only in a comparative sense, i.e., “greener” than something else.<sup>271</sup> A recently published critical review, by Maciel et al.,<sup>272</sup> on the topic of available life-cycle

assessment (LCA) studies on processes employing ILs has shed a light on the progress that has been made thus far. Lamentably, it is quite clear that LCA has not yet caught up with the fast-moving pace that the IL research is unravelling.

The limited number of relevant studies has mainly focused on imidazolium-based ILs, with the vast majority addressing ILs comprising the  $C_4mim^+$  cation. Quite notably, the life cycle of processes has only partially been evaluated (cradle-to-gate vs cradle-to-grave approach), while not all impact categories have been assessed. Out of the 23 impact categories only 5 are encountered in the majority of published reports; eutrophication, acidification, ozone depletion, global warming and human toxicity.<sup>272</sup>

One of the factors that significantly hampers the completeness of LCA is the limited life-cycle inventory (LCI) data both on ILs and their precursor compounds. Additionally, different researchers use different approaches and data sources to construct their LCIs, which calls into question the quality of said data. Despite ISO protocols stating that data quality evaluation is a compulsory step of LCA, quite unfortunately no researcher has addressed this parameter, which casts doubts on the accuracy of the LCA interpretation.<sup>272</sup>

In all reported studies in this thesis, there seems to be an absence of any environmental impact data of developed processes; this could stem either from fear of a process being unfairly judged as harmful based on a single component or lack of available data or both. However, no single process or chemical is inherently “good” or “bad” for the environment but it is rather the entire process, the quantities of chemicals and their overall handling that defines the final environmental impact. Critical assessment of all the steps of a developed process is absolutely necessary to get a full understanding of its impact and to advance the understanding of ILs and their environmentally responsible use. In the end, there is not a one-fits-all approach; while ILs can offer several advantages in some processes, in some other processes they simply have no effect, thus do not need to be considered as potential substitutes.

### 3.5 Financial considerations

Environmental considerations are undoubtedly an important aspect of any developed process, especially when it is intended for industrial-scale operations. Nevertheless, the financial aspect is an additional and largely significant factor that needs to be taken into account when designing an industrial-scale process.

However, in order to get an idea of what using an IL means in terms of cost, ILs typically have a price that is 2-100 times the price of organic solvents. Such a broad price range should not be surprising considering the variety of building anions. Ionic liquids that contain precious metals, e.g. Au, are expected to be expensive, while even some more commonly used ILs, such as [C<sub>n</sub>mim]-based ILs can get pricey, especially in combination with the NTf<sub>2</sub><sup>-</sup> anion.<sup>273</sup> For example, as a quick search of the Sigma-Aldrich online catalogue reveals, [C<sub>6</sub>mim]Cl (171058-17-6, >97%, HPLC) retails at 43.70€ for 5 g, [C<sub>2</sub>mim][BF<sub>4</sub>] (143314-16-3, >99%, <1000 ppm H<sub>2</sub>O) at 401.00€ for 25 g and [C<sub>4</sub>mim][PF<sub>6</sub>] (174501-64-5, for catalysis, >98.5%) at 63.90€ for 5 g. Additionally, P<sub>66614</sub>Cl (258864-54-9, >95% (NMR)) costs 17.00€ for 5 g, and Aliquat 336 (5137-55-3, >97% (AT)) costs 76.20€ for 10 g. Pyridinium is by far the cheapest IL, among the ones discussed in this review, with [Hpy]Cl (6004-24-6) retailing at 121.00€ for 100 g. Regarding in-house synthesized ILs, the cost of the starting materials should be clearly considered, while an estimate of the energy consumed during synthesis can give a more accurate estimate of the real cost of the IL. For the sake of comparison, we should mention that 2.5 L of toluene (108-88-3, ACS, >95%) cost 75.20€, while 2.5 L of CHCl<sub>3</sub> (67-66-3, >98% (HPLC)) cost 115.00€.

A comprehensive discussion on the financial aspect of ILs used as extraction solvents has already been provided in the literature by Passos et al.<sup>274</sup>

### 3.6 Concluding remarks on ionic liquid-based separations

The research that has been conducted thus far clearly demonstrates that ILs introduce improvements in terms of extraction yields and speed, while the possibility for quantitative extraction at low temperatures is a feature that can massively reduce the amount and cost of process energy, both of which can become significant considerations on industrial scale separations. Tunability is a very useful feature, especially when selectivity toward a certain metal in mixed-metal solutions can be adjusted to the desired degree. In many cases, ILs are or seem to be more environmentally benign compared to traditionally used solvents, thus, they introduce a new path to reach the goal of a sustainable future. The properties of an IL in this regard have to be carefully evaluated of course prior to setting up an industrial-scale separation process.

Nevertheless, all these advantages do not come without any drawbacks. Even though the extraction efficiencies are higher than in conventional solvents, liquid-liquid separations in many cases are accompanied by leaching of the ILs to the extracted phase due to the ion-exchange mechanism, which eventually reduces their lifetime, thus, their economical use and increases their environmental impact. As great a property as tunability may be, in many cases it requires high synthetic effort and/or increased costs. Not to mention that actual separation is a rather difficult and complex process.

Despite their, in some cases, more benign nature and their ability to reduce waste and be recycled for a number of times without significant performance loss, both of which are definitely in line with a more sustainable goal, there is no long-term or large-scale data at this point to reliably assess this “greenness” claim. Furthermore, in many occasions, their high viscosity still requires the use of traditional organic solvents in conjunction with the IL to allow its handling. Clearly, in that case, the claim of a “greener” approach is not easy to sustain. Alternatively, an increase in temperature can decrease viscosity, but the trade-off is that handling at high temperatures becomes harder and the process is no longer energy efficient.

No process so far has been presented that involves solely ILs in every single step. Apart from the IL-based process steps, which many times include traditional solvents anyway, many other steps still entirely require the use of existing processes. For example, toxic reagents, such as thiourea, or reagents that generate toxic gases, such as  $\text{Cl}_2$ , are used for the stripping of PGMs from the IL phases. Additionally, the pre-treatment steps of EOL materials still rely on existing processes, which employ dangerous and corrosive solvents and elevated temperatures.

The research findings have definitely proven the merit of ILs, while novel and surprising new discoveries are shedding more light on the immense possibilities ILs seem to be able to offer in the field of metal separations. Nevertheless, the application of said findings on real samples is notably scarce in the literature. Undoubtedly, the study of model solutions is essential to enable a deeper understanding of the complex behavior of ILs, but at the same time it is necessary to take the next step and investigate how they perform in “real” samples derived from EOL materials, in order to effectively exploit the advantages they have to offer. Additionally, as it is evident from the few such samples that have been investigated, recovery of a PGM in pure form is not easy as it is always accompanied by the presence of other metal ion traces. That begs the question; how significant do these traces become when the developed process is implemented on an industrial scale? Furthermore, when a developed process is upscaled, parameters such as price, efficiency and safety need to be evaluated, however, lab-scale data is not sufficient to reliably quantify these parameters on an industrially-relevant level.

## 4 The Platirus Project

The presented thesis was performed within the frame of the EU project Platirus and received funding from the European Union’s Horizon 2020 Research and Innovation program under Grant Agreement No 730224.

The aim of the project was the development of methods for the recycling of PGMs that would have potential to contribute to a more sustainable approach as opposed to the state-of-the-art methods. Key focus of the project was the development of novel extraction and separation technologies with potential for industrial upscaling, aiming for a final process with high metal recovery and minimized environmental impact. Thereby, it additionally sought to achieve independency of Europe’s PGM demand from the global market.

The consortium of the project comprised 12 international, recognized and experienced partners representing industry, research organizations and academic institutions; Tecnalia (Spain), Monolithos (Greece), KU Leuven (Belgium), TU Wien (Austria), VITO (Belgium), SINTEF (Norway), CRF (Italy), FORD OTOSAN (Turkey), BOLIDEN (Finland), Johnson Matthey (UK), PNO (Belgium), ENV AQUA (UK).

The project was separated into 9 work packages, planned out for a duration of 4 years. Research and development, life cycle analysis and financial assessment, project dissemination and industrial exploitation of the developed innovative processes as well as lab validation and industrial upscaling of selected processes were all addressed within the project. The present thesis was embedded in work packages 3 and 4, which addressed the leaching of PGMs with the aid of ILs and DESs and their subsequent separation employing ILs, in liquid form or immobilized on a solid material, respectively (Figure 56).

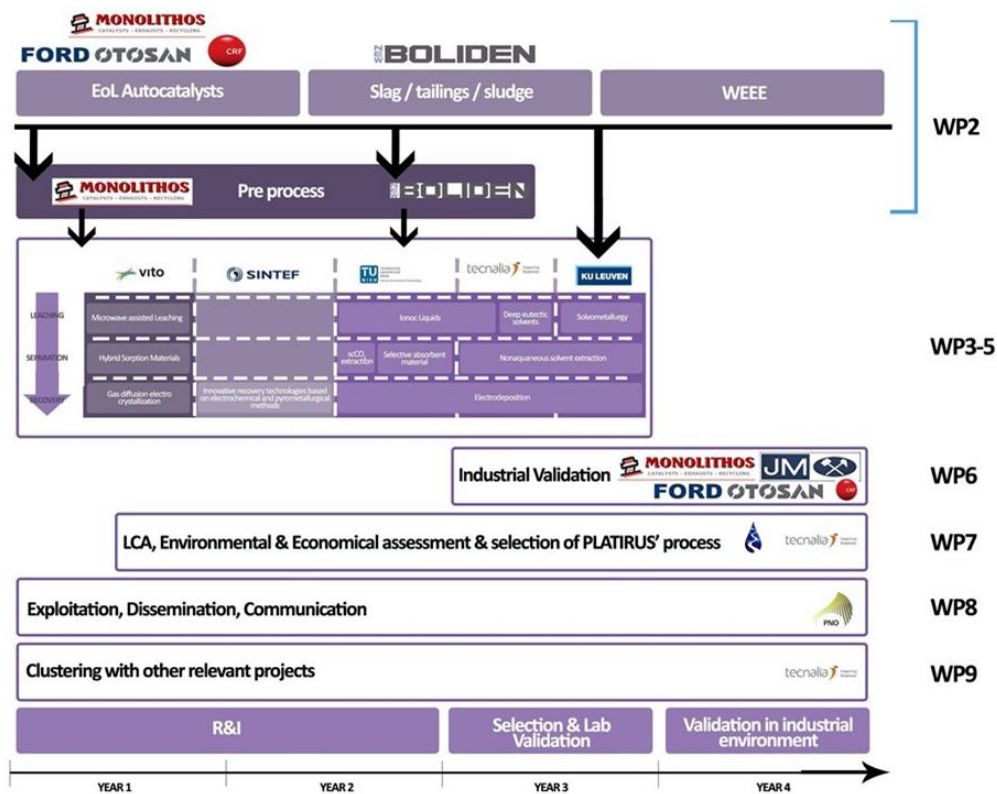


Figure 56. Overview of the Platirus project.

## 5 Research Goal

In line with the Platirus project objectives, the main goal of the work was to develop IL-based technologies for the recovery of PGMs from spent car catalysts, taking into account the key criteria of potential for industrial upscaling, minimized environmental impact and overall sustainability. Considering both the scarcity and high value of the target metals (Pt, Pd, Rh), the effort to maximize their recovery was among the core goals of all developed processes.

The first step in the recovery process was the leaching of the target metals out of the car catalyst material. To that end, several ILs and DESs were synthesized and evaluated in conjunction with different oxidizing agents and under varying process conditions of temperature, mixing ratios and time. The desirable outcome was the complete leaching of the target metals with minimal co-extraction of interfering elements present in the car catalyst matrix.

Since the leaching of other impurities alongside the target metals is inevitable, the subsequent task was to design and evaluate strategies that would allow the recovery of the target metals in a purer form. Separation processes also relying on ILs were employed, with ILs either in liquid form or immobilized on solid supports. In the liquid-liquid separation approach, an IL that would allow the formation of a biphasic system was employed, so that the target metals could partition between the two phases, thereby getting separated. In the solid-liquid separation approach, an IL that has the ability to complex with PGMs was immobilized on a solid support aiming for selective retention of the target metals on the solid support.

The recovery of PGMs in their pure metallic form was beyond the scope of the present work; however, this task was addressed within the Platirus project and the goal was to use the metal-containing leachate as input for other processes, developed within the project, which specifically targeted the recovery of the metals in their metallic form.



## 6 Results and Discussion

### 6.1 Development of analytical approaches

#### 6.1.1 Validation of selected method for PGM quantification in car catalyst sample

Reliable and accurate quantification of the PGMs present in the input car catalyst material was the cornerstone of the research project, since it would serve as a reference for subsequent determination of PGM extraction efficiencies. Additionally, full characterization of the car catalyst was performed to allow assessment of PGM separation from other metals in subsequent experiments.

Prior to any quantification attempts, the car catalyst needed to be digested in order to convert the solid sample into a solution suitable for ICP-MS analysis. A mixture of mineral acids (3 mL HNO<sub>3</sub>, 4 mL HCl, 2 mL HF) was used for the car catalyst digestion (100 mg) which was performed in a microwave oven (Figure 57). With the use of elevated temperature (max. 240 °C) and pressure (max. 40 bar), complete mineralization of the powdered catalyst material was possible, resulting in clear sample solutions without any remaining solid residues.



**Figure 57.** Microwave oven (left) and digestion unit (right) where car catalyst digestion was performed.

Prior to quantification by ICP-MS, the fitness for purpose of the analytical measurement method was verified with the aid of the certified reference material ERM-EB504. The recovered digest was mixed with a solution of 5% HCl and diluted to a concentration level appropriate for ICP-MS measurement. Analysis was conducted with a quadrupole ICP-MS (iCAP Qc, Thermo Fisher Scientific) using the standard settings recommended by the manufacturer. The good agreement of the measured values with the ones provided in the reference material certificate (Figure 58) confirmed the applicability of the developed digestion procedure for the analysis of PGMs in the car catalyst material.

Reliable analytical procedures for PGM quantification were a vital part in the leaching experiments and liquid-liquid separation experiments, given the fact that they provide the tools for quantification of the PGM extraction efficiencies in DESs and separation efficiencies in ILs.

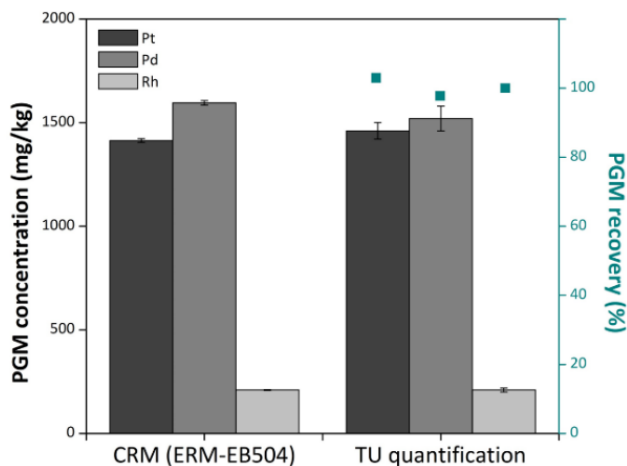


**Figure 58.** PGM concentrations provided by certificate versus PGM concentrations determined by ICP-MS.

### 6.1.2 Analytical challenges associated with deep eutectic solvents

Deep eutectic solvents have certain properties which render them challenging for conventional analytical approaches, namely ICP-MS and ICP-OES. Their high carbon content introduces carbon related interferences; specifically, the presence of carbon in the DES samples increases the ionization efficiencies of the target analytes. Moreover, the viscosity and surface tension of the sample directly affects the efficiency of the sample introduction system. Particularly in the case of ICP-MS, carbon-based compounds can accumulate on the interface cones over time, thus, shortening the maintenance time of the instrument and the lifetime of the cones. Aspiration of high C content directly to the plasma can extinguish it.<sup>275</sup> An aspiration tube and ICP-OES chamber are presented in Figure 59.

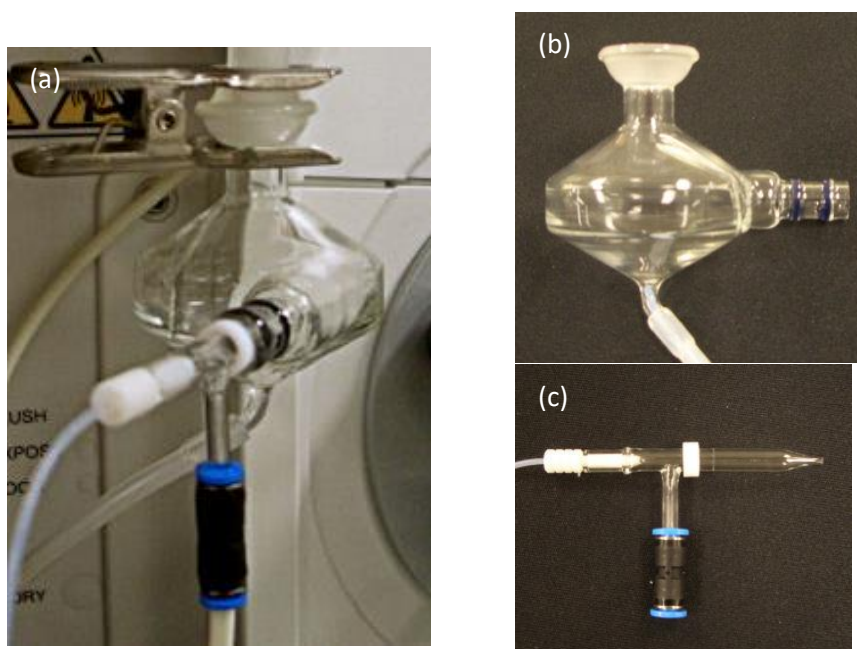


**Figure 59.** (a) Liquid sample introduction system consisting of (b) a spray chamber and (c) a nebulizer.

Furthermore, ICP-MS is subject to isobaric (different elements whose isotopes share a common mass) and polyatomic (combination of two or more isotopes from different elements) interferences,<sup>276</sup> whereas ICP-OES suffers from spectral interferences.<sup>277</sup> Taking into account the fact that the spent car catalyst is a multi-element complex matrix and the complications introduced to the measurement by the high C content of DESs and ILs, it becomes immediately apparent that optimization steps were required in order to obtain reliable measurements.

### 6.1.3 Development of analytics for quantification in deep eutectic solvents

The measurement method of choice for DESs and hydrophilic ILs was ICP-MS and ICP-OES. Since choline-based DESs are hydrophilic, an aqueous solvent was used for their dilution. Addition of water serves an additional purpose; it decreases the viscosity of the input sample therefore eliminating the negative effect it has on sample introduction efficiency.<sup>278</sup> Nevertheless, the solvent had to be adjusted so that (i) it could accommodate for the interference caused by the C present in the ILs and (ii) would keep the PGM complexes stable in solution and (iii) would allow reproducible and stable measurements without causing nebulizer clogging or instrumental drifts.

The C interference was adjusted by the process of “matrix matching”. An organic solvent was added to the calibration standards (aqueous solution of 1% EtOH in 5% HCl) of the PGMs in order to increase the ionization efficiency (caused by the presence of C) of the target analytes, therefore rendering the signals between the standards and the samples comparable. In order to keep the PGMs stable in solution, HCl was added because it forms stable anionic complexes with PGMs.

Concerning polyatomic interferences, they can be significantly attenuated by employing the KED mode in the collision/reaction cell of the ICP-MS (Figure 60). The analyte ions as well as the polyatomic interferences collide with He atoms in the cell resulting in the loss of kinetic energy in the process. At the exit of the cell, a barrier is set for kinetic energy values and if polyatomic species formed in the plasma have a lower kinetic energy than the set barrier, they are ejected from the cell to the waste and they do not reach the quadrupole, therefore they do not interfere in the  $m/z$  separation step. Thus, polyatomic interferences which are heavier and lose more kinetic energy during collision, can be effectively suppressed.<sup>278</sup>



**Figure 60.** Simplified drawing of ICP-MS system with Universal cell technology.

On the other hand, ICP-OES is more robust toward organic loads; even though the PGM quantification in the preliminary extraction and separation experiments was performed with ICP-MS, further measurements during the development steps were performed with ICP-OES, since the sensitivity provided by this technique was sufficient. The concentrations of the quantified metals are not low enough to mandate the use of a high-sensitivity instrument, such as ICP-MS, while the accumulation of C on

ICP-MS cones and the contamination of the system with metals is far from ideal, especially for subsequent users whose applications require high sensitivity. Therefore, with these downsides in mind, ICP-OES was employed for the bulk of measurements during this work.

#### 6.1.4 Quality evaluation of the analytical results

As mentioned before, the concept of external calibration with matrix-matched standards was applied for the quantitative assessment of the prevailing PGM levels. However, in order to verify the correctness of the results, standard addition as well as spike-recovery experiments were performed.

##### 6.1.4.1 Standard addition experiments

Standard addition experiments were conducted in order to evaluate whether the DES/IL matrix after PGM leaching/separation interferes ICP-OES analysis, causing a bias in the obtained analytical result (elemental quantification) and needs to be compensated for that effect.

Two series of calibration standards were prepared; one with PGM calibration standards prepared from commercially available PGM stock solutions and one with the same calibration standards spiked with the sample. Specifically, the standard for each calibration point was spiked with aliquots of fixed amounts of the unknown sample (1 g) and the mixed solution was diluted with the solvent to a certain final mass (10 g) (Figure 61).

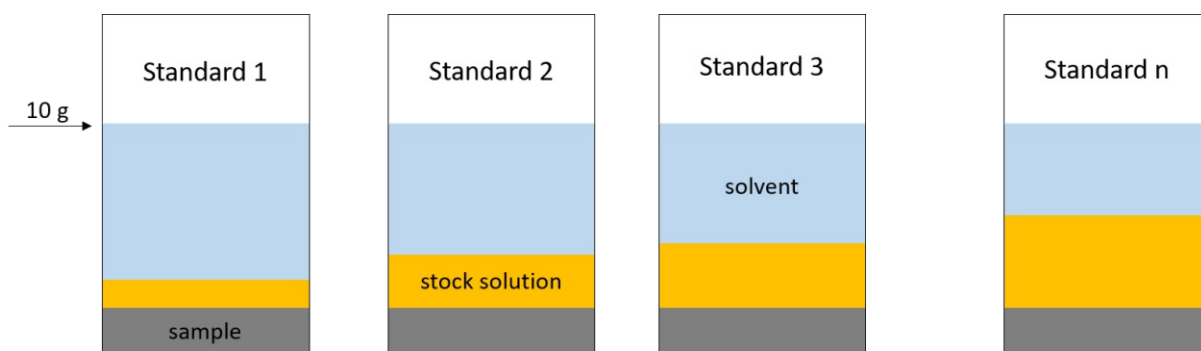


Figure 61. Standard addition process graphic for the evaluation of interference with the quantification results.

The response of both calibration curves, spiked and non-spiked, were plotted and their slopes were calculated and compared. Normally, if a statistically significant difference is detected between the two slopes, it indicates a severe influence of the sample matrix on the measurement process. That means that the matrix impacts the analytical result and this can be simply corrected by extending the spiked calibration curve until it meets the X axis of the Cartesian plane. The magnitude of the negative value along the X axis is the analyte concentration that corresponds to the response of the non-spiked solution in the calibration curve and based on this the new calibration curve values can be extrapolated. However, in the experiments herein reported, there was an overlap of both calibration curves, spiked and non-spiked, which leads to the conclusion that the sample matrix has no impact on the analyte signal. Thus, an external non-spiked calibration is sufficient and reliable for the quantification of the target elements.

#### 6.1.4.2 Spike-recovery experiments

For complete elimination of matrix related effects, a high dilution of the samples is necessary, which is always accompanied with a loss in sensitivity. Thus, usually measurements were performed with slightly diluted samples only to ensure sufficient detection limits, which might be problematic for samples with high matrix load. In order to assess whether the selected diluent and also dilution level for a sample is suitable spike-recovery experiments are performed. These types of experiments are used to determine whether the accuracy in the target analyte quantification is affected by differences between the diluent used to prepare the sample and the sample matrix.

A certain amount of the unknown sample was spiked with different levels of the target analytes and the selected diluent was spiked with the same concentration levels. The analytical signal of these two types of samples was compared based on values calculated from a standard calibration curve.

The agreement of the analytical responses was adjusted by modifying the concentration of EtOH that was used as part of the diluent (1% EtOH-5% HCl). Due to the high C load of ILs and DESs, the need for optimization of the solvent composition was expected.

In order to calculate the recovery, the following equation is used:

$$\%R = \frac{C \text{ measured in spiked sample} - C \text{ measured in non - spiked sample}}{C \text{ of added spike}} * 100$$

The ideal recovery value is, of course, 100%, however different criteria regarding the accepted recovery range are applicable depending on the analytical task at hand.

## 6.2 Characterization of the car catalyst sample

Reliable and accurate quantification of the PGMs present in the input car catalyst sample was the cornerstone of the research project, since it would serve as a reference for subsequent determination of PGM extraction efficiencies. Additionally, full characterization of the car catalyst was performed to allow assessment of PGM separation from other metals in subsequent experiments.

### 6.2.1 Quantification of the car catalyst elemental matrix

The spent car catalyst used in this study was fully characterized prior to the leaching and separation experiments (Figure 62). It was digested with the aid of a mixture of mineral acids in a microwave oven, prior to measurement, for the dissolution of the ceramic material, which primarily comprises the car catalyst. The following digestion programme was employed; 8 min at 500 W, hold 8 min, 15 min at 900 W, hold 35 min. The quantification was performed by ICP-OES with appropriate sample dilution. The microwave extract was diluted up to 40 mL and was centrifuged for 5 min at 17000 rpm, to remove possible residual ceramic that was not completely digested. After centrifugation, 0.1 g supernatant were mixed with In as internal standard (final concentration of 1 ppb) and diluted with 1 % HNO<sub>3</sub> to a total mass of 10 g.

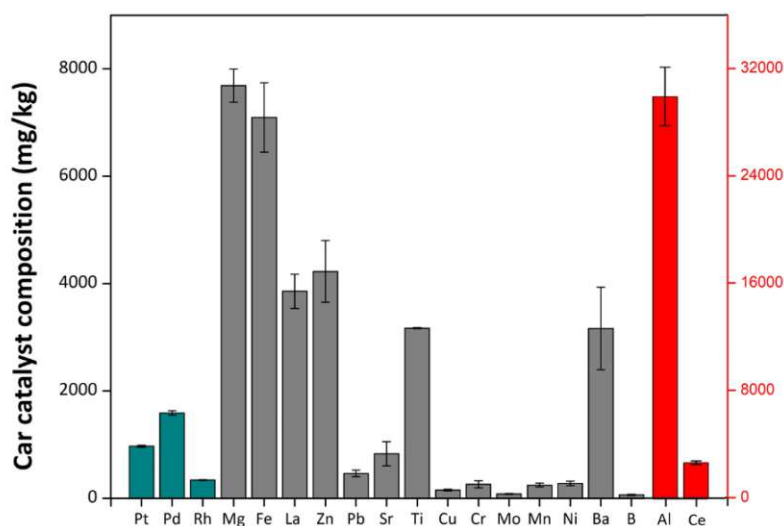


Figure 62. Concentration of elements present in the car catalyst material.



## 6.2.2 XRD analysis of the car catalyst sample

The recorded X-Ray diffractogram of the spent car catalyst material (Figure 63) indicates that the car catalyst comprises a cordierite support. Hydroxides present in the catalyst were also detected.

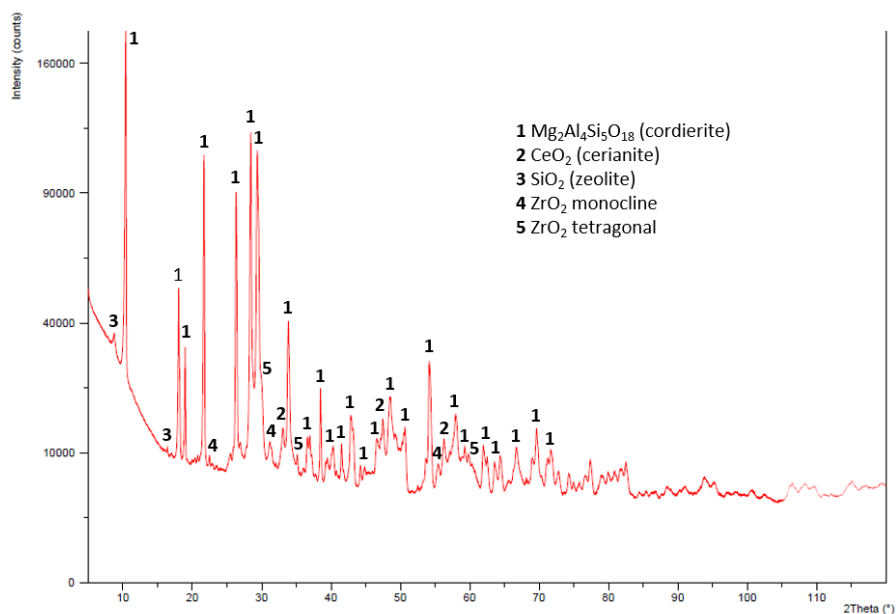


Figure 63. X-Ray diffractogram of car catalyst material used in the present study.

## 6.3 Leaching of platinum group metals from spent car catalyst

### 6.3.1 Goals and objectives

The main objective of the studies was to develop a leaching system that yields quantitative extraction efficiencies for all target PGMs, at mild conditions and reduced process times. In addition, the developed system should be relatively easy to upscale to industrially-compatible levels while at the same time it should allow for fast, reliable and easy analytical approaches available or simple to implement on-site. A secondary but equally important goal was the evaluation of the stability of the ILs and DESs in the leaching process and their potential for recovery and reuse in consequent leaching cycles. For this purpose, the stability of the ILs and DESs was monitored on a qualitative and quantitative basis.

### 6.3.2 Classification of selected ionic liquids and deep eutectic solvents for leaching studies

In order to allow a better overview and facilitate the experimental planning of leaching, the ILs used in PGM extractions were classified in four different categories according to their chemical properties/behavior: choline based ILs (also referred to as DESs), Brønsted acidic ILs, protic ILs and hydrophobic ILs (Figure 64). All selected ILs can be optionally combined with additional acids and/or oxidizing agents in the leaching process.

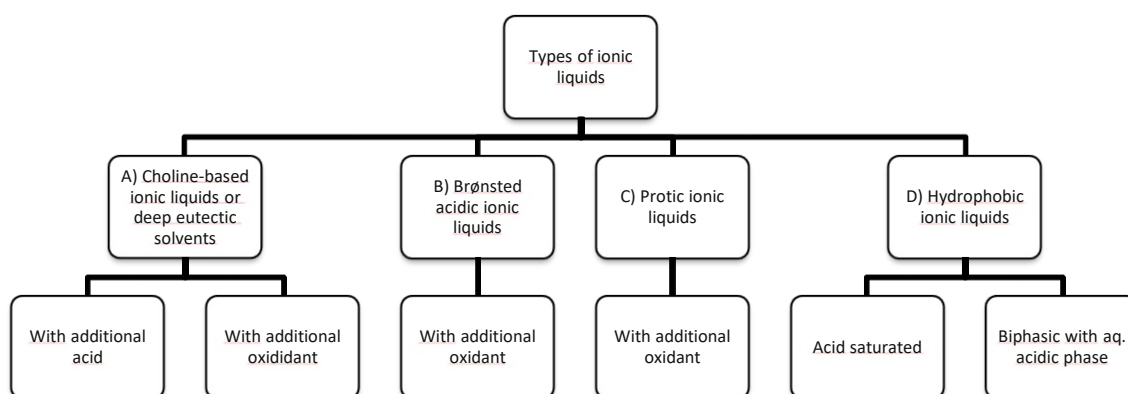


Figure 64. Classification of ILs and DESs evaluated in PGM leaching studies.

The ILs were selected based on specific features, such as their chemical properties, financial viability, potential for PGM extraction and expected low environmental impact. So far, a considerable number of ILs has been used in metal extraction,<sup>279,280</sup> for example in the extraction of rare earth elements<sup>281,282,283</sup> as well as separation<sup>192</sup> and extraction<sup>200</sup> of PGMs.

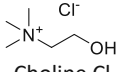
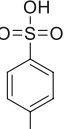
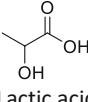
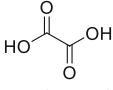
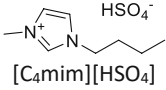
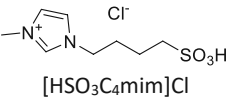
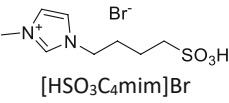
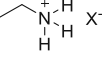
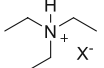
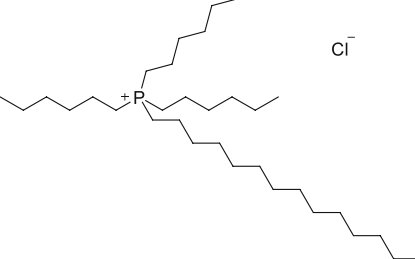
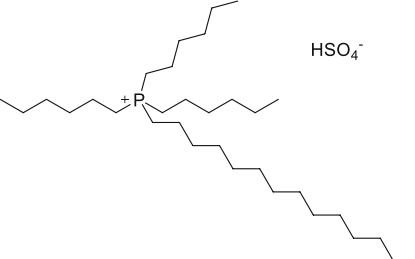
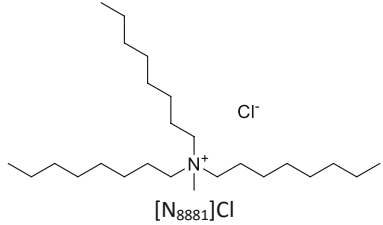
- Choline-based ILs (Type A) are based on the bio-derived choline cation and are optionally used in the presence of various hydrogen bond donors. These have significantly lower melting points than their individual components. In general, choline chloride (choline Cl) is a cheap and accessible chemical of low cost and environmentally friendly nature. By modifying the hydrogen bond donor, the solvating properties of the DES can be adjusted to fit the requirements of specific processes. Choline-based ILs with hydrogen bond donors, such as ethylene glycol, have been employed in the dissolution and recovery of precious metals, for example in the separation of Au and pyrite.<sup>284</sup>
- Brønsted acidic ILs (Type B) are a subset of ILs, which have been functionalized in a way that an acidic proton is available in the cation or in the anion.<sup>285</sup> It has already been shown in previous

studies that Brønsted acidic ILs are able to dissolve and extract precious metals, e.g., Ag or Au from gold bearing ores.<sup>280</sup>

- Protic ILs (Type C) are formed through a proton transfer from a Brønsted acid to a Brønsted base, which leads to availability of one proton for hydrogen bonding on the cation of the IL. Even though the proton transfer may not be complete, the inherent acidity, in combination with their relatively simple preparation renders protic ILs ideally suited for the task at hand.<sup>285</sup>
- Hydrophobic ILs (Type D) based on phosphonium cations are thermally stable and therefore suitable for applications in a wide temperature range. Furthermore, their hydrophobic nature allows direct stripping of the PGMs from the IL phase.<sup>286</sup> Hydrophobic phosphonium-based or ammonium-based ILs have already been applied in a number of extraction processes for metals from aqueous solutions, for example in the recovery of metals and metal compounds, such as Pt, Ag, Cu and Ni, from communal waters.<sup>287</sup>

An overview of typical candidates from all categories used in this project is given in Table 12.

**Table 12.** Representative ionic liquids of all categories used in the leaching studies.

Hydrophilic Ionic Liquids			Hydrophobic Ionic Liquids	
Type A	Type B	Type C	Type D	
 <p>Choline Cl</p>	<p><b>acids/H-donors</b></p>  <p><i>p</i>-TsOH</p>  <p>Lactic acid</p>  <p>Oxalic acid</p>	 <p>[C<sub>4</sub>mim][HSO<sub>4</sub>]</p>  <p>[HSO<sub>3</sub>C<sub>4</sub>mim]Cl</p>  <p>[HSO<sub>3</sub>C<sub>4</sub>mim]Br</p>	 <p>X = NO<sub>3</sub><sup>-</sup>, Cl<sup>-</sup>, HSO<sub>4</sub><sup>-</sup></p>  <p>X = NO<sub>3</sub><sup>-</sup>, Cl<sup>-</sup>, HSO<sub>4</sub><sup>-</sup></p>	 <p>P<sub>66614</sub>Cl</p>  <p>P<sub>66614</sub>·HSO<sub>4</sub></p>  <p>[N<sub>8881</sub>]Cl</p>

### 6.3.3 Preliminary leaching experiments with selected ionic liquids and deep eutectic solvents

#### 6.3.3.1 Leaching process

The efficiency of the systems tested for the extraction of PGMs was evaluated as follows; first the leaching of the PGMs in the ILs/DESs was performed and consequently the recovered PGM-rich leachate was appropriately diluted and measured by the appropriate analytical technique.

In a typical leaching experiment, 100 mg of spent car catalyst powder (MONOLITHOS, batch #2, particle size <math><0.16\text{ mm}</math>) were mixed with 500 mg IL/DES and optionally 100 mg of oxidizing agent were added. The mixture was stirred in a sealed glass vial for 4 h, at 80 °C, at a stirring speed of 300 rpm. Upon completion of mixing, the mixture was placed in an Eppendorf tube and consequently centrifuged (13.500 rpm, 30 min) for the separation of the PGM-rich leachate from the solid catalyst sample (Figure 65). After the centrifugation, the IL/DES was recovered and appropriately diluted for measurement.

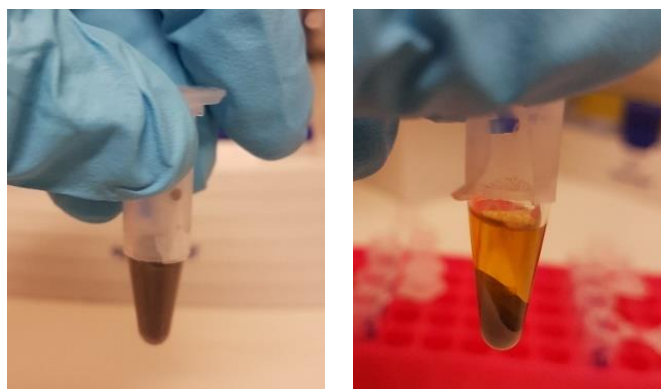


Figure 65. Leachate before centrifugation (left) and after centrifugation (right).

#### 6.3.3.2 Evaluation of platinum group metal leaching with various ionic liquids and deep eutectic solvents

Representative candidates of each of the four categories were evaluated for their performance on PGM leaching on small scale. The standard conditions of 80 °C at a fixed solid:liquid ratio of 1:5 were preselected and applied in all experiments with optional addition of an oxidizing agent ( $\text{HNO}_3$ ,  $\text{H}_2\text{O}_2$ ,  $\text{I}_2$ ,  $\text{KI}$ ,  $\text{KBr}$ ,  $\text{KHSO}_5$ /thiourea,  $\text{Fe}_2(\text{SO}_4)_3$ ). Quantitative leaching for Pd has been achieved with several ILs (Type A, B, C and D). Additionally, quantitative extraction for Pt could be observed with both Type A and B ILs. Concerning Rh, up to 45% could be extracted with Type A ILs. Type C and D ILs are interesting in the sense that no extra acid/oxidizing agent is required, since this is incorporated in the IL structure. Eventually, type D ILs seem to have high selectivity toward Pd, while lower values were obtained for Pt and Rh (Table 13).

#### 6.3.3.3 Pre-selection of leaching system

The final selection of the system for further optimization was based on different parameters, such as the extraction efficiency for all three target PGMs, the difficulty of preparation and cost of IL/DES and the properties that make it an easy-handling and environmentally friendly system. The system comprising choline Cl/*para*-toluenesulfonic acid (*p*-TsOH)/ $\text{HNO}_3$  was selected since it ideally satisfies all the prerequisites mentioned above.

Specifically, DESs comprising the quaternary ammonium salt choline Cl and a hydrogen bond donor (DES type III),<sup>115</sup> have been employed in a wide range of applications due to their versatile nature. The simplicity of their preparation, low reactivity with  $\text{H}_2\text{O}$ , biodegradability and low cost along with their wide solvation range and tunability of their properties, which is largely attributed to the large number of

available hydrogen bond donors, renders these DESs particularly interesting.<sup>115</sup> With respect to metal extraction, choline-based DES applications have, among others, been reported in the extraction of rare earth elements from magnets,<sup>123</sup> the selective extraction of transition metals from mixed metal oxide matrixes<sup>124</sup> and the extraction of metal traces from barley.<sup>125</sup>

**Table 13.** Platinum group metal extraction efficiencies with selected leaching systems.

Ionic Liquids	Oxidizing Agent	% Recovery from Catalyst <sup>a,b</sup>		
		Pt	Pd	Rh
<b>Type A Ionic Liquids</b>				
Choline Cl/ <i>p</i> -TsOH	-	33 ± 4	91 ± 6	30 ± 2
Choline Cl/ <i>p</i> -TsOH	0.1 g HNO <sub>3</sub> /H <sub>2</sub> O	61 ± 4	83 ± 2	24 ± 5
Choline Cl/ <i>p</i> -TsOH	0.5 g HNO <sub>3</sub>	78 ± 4	0	15 ± 26
Choline Cl/ <i>p</i> -TsOH	0.1 g HNO <sub>3</sub>	116 ± 4	106 ± 6	58 ± 2
Choline Cl/ <i>p</i> -TsOH	0.1 g H <sub>2</sub> O <sub>2</sub>	110 ± 7	95 ± 6	60 ± 2
Choline Cl/ <i>p</i> -TsOH	0.1 g I <sub>2</sub>	111 ± 0	90 ± 1	60 ± 1
Choline Cl/ <i>p</i> -TsOH	KHSO <sub>5</sub> /thiourea	108 ± 9	10 ± 1	23 ± 2
Choline Cl/Oxalic acid	0.1 g HNO <sub>3</sub>	98 ± 34	115 ± 2	60 ± 2
Choline Cl/Oxalic acid	0.1 g H <sub>2</sub> O <sub>2</sub>	120 ± 3	76 ± 2	48 ± 1
Choline Cl/Oxalic acid	0.1 g I <sub>2</sub>	92 ± 8	74 ± 7	60 ± 1
Choline Cl/Oxalic acid	KHSO <sub>5</sub> /thiourea	102 ± 1	13 ± 6	18 ± 7
Choline Cl/Lactic acid	0.1 g HNO <sub>3</sub>	113 ± 3	84 ± 2	39 ± 1
Choline Cl/Lactic acid	0.1 g H <sub>2</sub> O <sub>2</sub>	108 ± 2	19 ± 1	25
Choline Cl/Lactic acid	0.1 g I <sub>2</sub>	30	30 ± 15	34 ± 5
Choline Cl/Lactic acid	KHSO <sub>5</sub> /thiourea	89 ± 3	7	13 ± 4
<b>Type B Ionic Liquids</b>				
[HSO <sub>3</sub> C <sub>4</sub> mim]Cl	0.1 g HNO <sub>3</sub>	89 ± 2	95 ± 2	36 ± 3
[HSO <sub>3</sub> C <sub>4</sub> mim]Cl	0.1 g I <sub>2</sub>	84 ± 8	95 ± 4	43 ± 8
[HSO <sub>3</sub> C <sub>4</sub> mim]Cl	-	28 ± 8	74 ± 20	18 ± 4
[HSO <sub>3</sub> C <sub>4</sub> mim]Br	0.1 g HNO <sub>3</sub>	18 ± 3	32 ± 3	8 ± 2
[HSO <sub>3</sub> C <sub>4</sub> mim]Br	0.1 g I <sub>2</sub>	4 ± 11	25 ± 3	5 ± 7
[HSO <sub>3</sub> C <sub>4</sub> mim]Br	-	0	10	1
[C <sub>4</sub> mim][HSO <sub>4</sub> ]	0.1 g HNO <sub>3</sub>	75 ± 3	3 ± 1	15 ± 1
[C <sub>4</sub> mim][HSO <sub>4</sub> ]	0.1 g H <sub>2</sub> O <sub>2</sub>	2 ± 1	1 ± 1	7 ± 1
[C <sub>4</sub> mim][HSO <sub>4</sub> ]	0.1 g I <sub>2</sub>	1	0	22 ± 1
[C <sub>4</sub> mim][HSO <sub>4</sub> ]	KHSO <sub>5</sub> /thiourea	49 ± 1	3	33 ± 1
<b>Type C Ionic Liquids</b>				
[EtNH <sub>3</sub> ]NO <sub>3</sub>	0.1 g HNO <sub>3</sub>	2 ± 19	68 ± 6	7 ± 6
[EtNH <sub>3</sub> ]NO <sub>3</sub>	-	0	23 ± 12	1 ± 20
[EtNH <sub>3</sub> ]Cl	-	2 ± 11	71 ± 8	6 ± 8
[EtNH <sub>3</sub> ][NO-Cl]	-	59 ± 9	72 ± 10	25 ± 9
[HNEt <sub>3</sub> ][HSO <sub>4</sub> ]	0.1 g HNO <sub>3</sub>	65 ± 6	5 ± 1	14 ± 1
[HNEt <sub>3</sub> ][HSO <sub>4</sub> ]	0.1 g H <sub>2</sub> O <sub>2</sub>	2 ± 1	3 ± 1	7 ± 1
[HNEt <sub>3</sub> ][HSO <sub>4</sub> ]	0.1 g I <sub>2</sub>	20 ± 8	24 ± 2	17 ± 3
[HNEt <sub>3</sub> ][HSO <sub>4</sub> ]	KHSO <sub>5</sub> /thiourea	61 ± 3	5 ± 0	9 ± 1
<b>Type D Ionic Liquids</b>				
[N <sub>8881</sub> ]Cl·HCl	-	0	19 ± 3	0
[N <sub>8881</sub> ]Cl·HNO <sub>3</sub>	-	0	21 ± 6	0
[N <sub>8881</sub> ]Cl·HCl:HNO <sub>3</sub>	-	0	20 ± 4	0
P <sub>66614</sub> Cl	-	2 ± 18	9 ± 9	2 ± 11
P <sub>66614</sub> Cl·HCl	-	2 ± 54	26 ± 16	6 ± 11
P <sub>66614</sub> Cl·HNO <sub>3</sub>	-	36 ± 4	101 ± 2	17 ± 9
P <sub>66614</sub> Cl·HCl:HNO <sub>3</sub>	-	37 ± 10	97 ± 7	11 ± 43

<sup>a</sup> Conditions: solid:liquid 1:5, 80 °C, 4h. <sup>b</sup> For each sample 4 replicas were prepared.

### 6.3.4 Optimization of selected leaching system

The PGM leaching capacity of the selected DESs was assessed at variable conditions. Specifically, parameters such as the solid:liquid ratio, the leaching temperature, the leaching duration, the amount and nature of the added oxidizing agent, the presence or absence of additives and the dilution of the leaching medium with H<sub>2</sub>O, were evaluated for their effect on the PGM leaching behavior of the system. The effect of these parameters is presented in the following sections on the example of the DES system relying on choline Cl/*p*-TsoH due to its simple preparation and promising performance in pre-studies. This particular DES is simple and easy to prepare, and during initial assessment of various DES-based leaching systems it demonstrated a very promising performance in terms of extraction efficiency for all three target PGMs.

The dissolution of PGMs in various acidic media is easier when they are encountered in their elemental form.<sup>14</sup> Even though they are originally deposited on the catalyst support as metallic particles, in the EOL catalysts they have been partly converted to their respective oxides.<sup>57</sup>

Platinum group metals form stable complexes with soft ligands, such as Cl<sup>-</sup>, and are soluble as chlorocomplexes in acidic and oxidizing environments. According to thermodynamic data, Pd has the highest solubility in its chloride form, followed by Pt and Rh.<sup>70</sup> Rhodium, particularly, is quite inert and not soluble or only slightly soluble in acids.<sup>56</sup> This is also the case for Rh<sub>2</sub>O<sub>3</sub>, which is less readily chlorinated than metallic Rh and stable over a wide range of temperature and pressure.<sup>71</sup>

#### 6.3.4.1 Amount and nature of oxidizing agent

The effect of different oxidizing agents as well as their respective amount on the PGM extraction efficiency of the DES system (solid:liquid 1:5, 80 °C, 4 h) was assessed. The addition of HNO<sub>3</sub> yields quantitative extraction of Pt, whereas the leaching efficiency of Pd appears to be almost independent of the oxidizing agent used, reaching quantitative levels even in the absence of oxidizing agent. Additionally, an increase in the extraction of Rh is observed in the presence of HNO<sub>3</sub> in contrast to its extraction behavior when other oxidizing agents are employed (Figure 66). Various amounts of the evaluated oxidizing agents ranging from 0.05-0.5 g were tested, however quantities less than 0.1 g were insufficient to obtain maximum leaching efficiencies, while amounts higher than 0.1 g hampered PGM extraction.

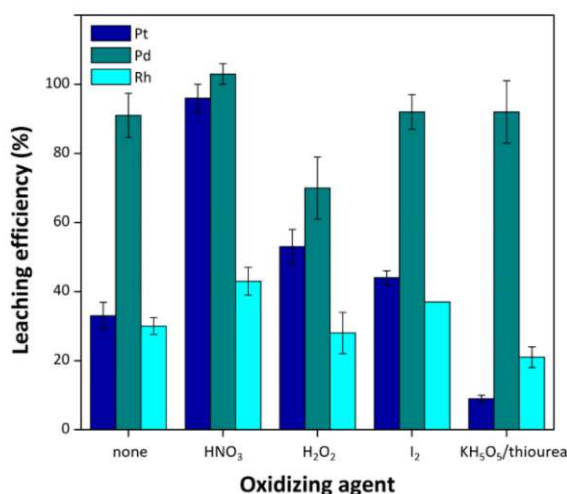


Figure 66. PGM leaching efficiency (%) with different oxidizing agents, at 80 °C, 4 h, solid:liquid 1:5.



### 6.3.4.2 Effect of solid:liquid ratio

Multiple ratios of car catalyst:DES were tested with the choline Cl/*p*-TsOH system with HNO<sub>3</sub> as the oxidizing agent, employing a temperature of 80 °C, for 4 h. The extraction efficiency is almost quantitative in all cases for Pd, indicating that it is easily accessible to the Cl<sup>-</sup> anions for complexation, while, at the same time, its dissolution is particularly assisted by the presence of HNO<sub>3</sub>.<sup>2</sup> On the other hand, quantitative extraction for Pt is obtained only at the car catalyst:DES ratio of 1:5, whereas any ratio above or below that does not yield comparably high extraction efficiencies for any of the three PGMs. Due to its inert nature, Rh can only be leached partly, with the highest efficiency reached at a car catalyst:DES 1:5 ratio. The latter ratio is the optimum in order to obtain maximum leaching efficiencies for all three target PGMs (Figure 67).

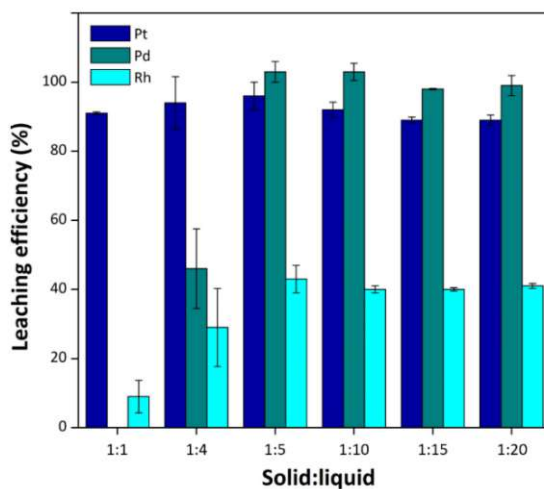
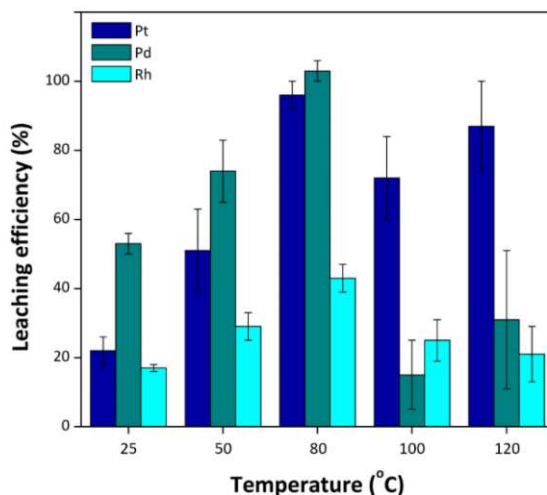


Figure 67. PGM leaching efficiency (%) at different solid:liquid ratios, at 80 °C, 4 h.

The possibility of reducing the solid:liquid ratio in the selected system was investigated as an alternative to decrease the amount of employed DES and to lower the viscosity of the mixture. To this end, the leaching was performed with solid:liquid:H<sub>2</sub>O:HNO<sub>3</sub> ratio of 1:4:1:1 yielding similar results with the solid:liquid ratio 1:5. The addition of H<sub>2</sub>O in the 1:4 system is deemed necessary to reduce the viscosity, while the excellent extraction performance could be maintained.

### 6.3.4.3 Effect of leaching temperature

It is quite evident that the selected DES system has a considerable extraction capacity for Pd at temperatures close to RT (Figure 68). Additionally, it is evident that the leaching of the PGMs is dependent on the process temperature, with the highest extraction yield for all three PGMs obtained at 80 °C. Employing the solid:liquid ratio of 1:5, quantitative recovery of Pt and Pd is achieved with temperatures as low as 80 °C, whereas the partial extraction of Rh is not affected by any further increase in temperature. Additionally, temperatures above or below 80 °C appear to hamper the extraction capacity of the DES, indicating that the temperature needs to be carefully selected and monitored in order to fully exploit the advantageous effect of the DES in the extraction process. Additionally, what was mentioned earlier should be pointed out here; working with choline-based DESs at temperatures exceeding 80 °C is not recommended since it has been reported that over this temperature the progressive degradation of the DES takes place.



**Figure 68.** PGM leaching efficiency (%) at different temperatures, solid:liquid 1:5, 4 h.

The kinetic and thermodynamic behavior of PGM-chloro complexes is contingent upon the oxidation state in which the metal is encountered in solution. Additionally, certain properties, such as solubility, are directly affected by the charge and size of the formed complex species. Varying amounts of DES imply various concentrations of  $H^+$  and  $Cl^-$  in solution, therefore, variable composition in terms of formed PGM-chloro complexes.<sup>68</sup> The formation of various complexes of different kinetic and thermodynamic properties and solubilities could be a plausible explanation as to why Pd does not yield constant extraction efficiency with the modification of the temperature, while this effect does not seem to be that pronounced in the case of Pt. Additionally, the possibility of Pd precipitation out of solution cannot be excluded and might be a reason for the decreasing yield.

#### 6.3.4.4 Effect of leaching duration

The leaching efficiency of the system (solid:liquid 1:5, 80 °C) was evaluated over a period of 12 h at regular intervals. The equilibrium was reached after 4 h; lower leaching duration was not enough for quantitative extraction of Pt and Pd, while durations over the 4 h mark had no added advantage on the extraction efficiency of Rh and no effect on Pt and Pd (Figure 69).

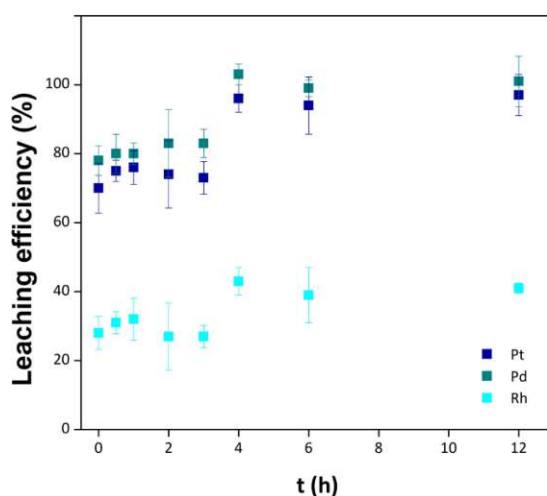


**Figure 69.** PGM leaching efficiency (%) at different leaching times, at 80 °C, solid:liquid 1:5.

### 6.3.5 Preconcentration of platinum group metals in the leachate

The possibility to reuse the DES in subsequent leaching cycles, thus, the preconcentration of PGMs in cumulative steps, was investigated with the objective of preserving DES while at the same time maximizing the leached PGM amount in a constant amount of DES. The PGM-rich leachate obtained from a leaching cycle was recovered and used for subsequent leaching cycles with new catalyst material, redosing DES as necessary and adding new amount of oxidizing agent (Figure 70). The PGMs extracted after every leaching cycle were quantified by ICP-OES.

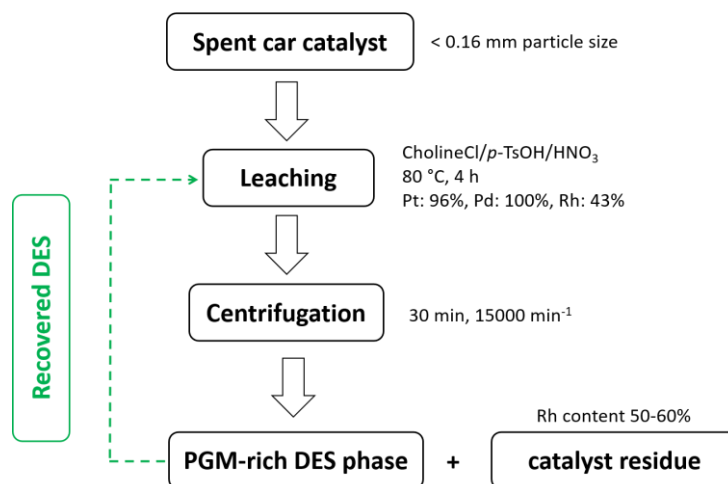


Figure 70. DES reuse in the process flowsheet of PGM recovery.

The number of PGM preconcentration cycles as well as the cumulative PGM leaching (ppm) and DES recovery (%) per leaching cycle are presented in Table 14. The experiments were performed on a 1 g car catalyst scale. The reported results refer to solid:liquid 1:4 system with addition of H<sub>2</sub>O, since the cumulative recovery of the PGMs was slightly higher in that case (as opposed to solid:liquid 1:5).

Table 14. Cumulative PGM leaching (ppm) and DES recovery (%) per leaching cycle.

Cycle No		1	2	3	4
% DES Recovery		90	86	77	80
Cumulative Concentration of Leached PGMs (ppm)	Pt	911 ± 19	1445 ± 29	1940 ± 35	2037 ± 30
	Pd	1590 ± 11	2798 ± 116	2878 ± 45	3116 ± 211
	Rh	127 ± 3	172 ± 25	144 ± 13	137 ± 31

The DES medium allows the preconcentration of Pt in subsequent leaching steps, however, there is a considerable drop in the leached amount after the 3<sup>rd</sup> leaching cycle. The preconcentration of Pd was also successful, however it reached a plateau after the 2<sup>nd</sup> leaching cycle. In contrast, no additional Rh could be extracted beyond the 1<sup>st</sup> leaching step.

### 6.3.6 Pre-treatment of the car catalyst material

A challenging aspect of PGM leaching was the significantly lower extraction efficiency of Rh compared to the other target PGMs, Pt and Pd, a behavior which was not entirely unexpected given its inert nature.<sup>288</sup> This can be possibly attributed to the fact that in the high temperature that car catalysts operate,  $\text{Rh}_2\text{O}_3$  is formed which does not readily convert to its metallic form and is poorly soluble even in *aqua regia*.

The possibility of increasing the extraction efficiency of Rh was investigated. To this end, different pre-treatment pathways, chemical<sup>14,57,289</sup> and thermal,<sup>14,57,290</sup> of the grinded car catalyst material were evaluated for their effect on the extraction efficiency of Rh. In addition to the Ar-based pre-treatment,  $\text{N}_2$  was also evaluated as an alternative and more viable option, from a financial perspective, to Ar, for industrial-scale applications. An overview of the pre-treatment conditions is presented in Table 15.

**Table 15.** Conditions of chemical and physical pre-treatment of the car catalyst material.

	Conditions	T (°C)	t (h)	Treatment Scale (g)	Mass Loss (%)
Chemical Pre-treatment	$\text{H}_2$	300	3	10	1.1
	i. Air, ii. $\text{H}_2$	i. 500, ii. 300	i. 3, ii. 3	10	2.4
	15% $\text{HCOOH}$	60	1	10	11.4
	25% $\text{HCOOH}$	60	1	10	12.5
Thermal Pre-treatment	Ar	1200	2	10	3
	Ar	1200	2	100	3
	Ar	1200	1	10	2.9
	$\text{N}_2$	1200	2	10	2.8
	$\text{N}_2$	1200	0.5	10	2.9

In all pre-treatment processes, loss in the mass of the treated car catalyst material was observed; we presume that this could be attributed to the loss of humidity and the evaporation of volatile compounds present in the car catalyst matrix, which occur when the sample is subjected to high temperatures during the pre-treatment process. In the case of pre-treatment with  $\text{HCOOH}$ , a significant mass loss was observed, unlike in the other cases, which could be attributed to the loss of certain elements been washed off the catalyst matrix. Specifically, significant Al amount contributes predominantly to the loss, followed by considerable amounts of Zn and Fe, as well as traces of La, Mn, Ni and Cr. Measurements on the recovered  $\text{HCOOH}$  via ICP-OES after the completion of the pre-treatment, verified that no PGMs are washed off.

Car catalyst samples which were pre-treated with the methods summarized in Table 15 were subsequently leached with the optimized system (choline  $\text{Cl}/p\text{-TsOH}/\text{HNO}_3$ , solid:liquid 1:5, 80 °C, 4 h).

The chemical pre-treatment of the samples had no effect on the PGM extraction efficiencies yielding comparable efficiencies to the untreated car catalyst. On the contrary, all the physical pre-treatment strategies were effective in increasing the extraction efficiency of Rh by approximately 25% (Figure 71). Surprisingly, the extraction efficiencies for both Pt and Pd in the physically pre-treated sample dropped by 20%. In temperatures exceeding 300 °C, the metal particles undergo sintering (growth into larger particles) and their specific surface area, thus their active sites, decreases leading to a loss in their extractability.<sup>291</sup> Repeated experiments with pre-treated catalyst yielded the same extraction efficiencies.

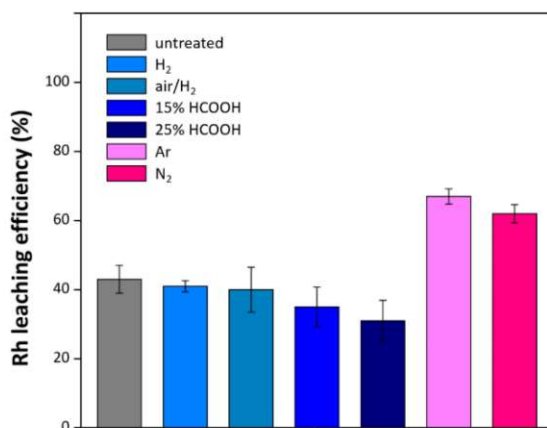


**Figure 71.** Effect of catalyst pre-treatment (chemical and thermal) on the extraction efficiency of Rh.

### 6.3.7 Upscaling of selected and optimized leaching system

#### 6.3.7.1 Upscaling with untreated car catalyst sample

Based on the previously optimized leaching system relying on choline Cl/*p*-TsOH/HNO<sub>3</sub>, additional experiments were performed to study the leaching behavior of PGMs in an upscaled version. The upscaled experiments were performed both on a solid:liquid 1:5 and 1:4 ratio, on a 35 g catalyst scale and a 100 g catalyst scale, respectively. The upscaled leaching set-up consisted of a three-neck round bottom flask with a mechanical stirrer and a reflux condenser (Figure 72). To avoid a violent and exothermic reaction, the oxidizing agent (HNO<sub>3</sub>) was added dropwise before heating the mixture to 80 °C.



**Figure 72.** Upscaled leaching set-up on a 100 g catalyst scale.

The PGM extraction behavior was monitored over a 24 h period (Figure 73). The following conclusions can be reached for the upscaled leaching process:

(i) the equilibrium was reached within 4-6 h

(ii) the extraction efficiency of all PGMs in the equilibrium point was comparable to the leaching efficiencies obtained in the small-scale leaching experiments (100 mg car catalyst) with the selected and optimized leaching system; Pt 970 ppm, Pd 1590 ppm, Rh 145 ppm, corresponding to 100%, 100%, 42% recoveries, respectively.

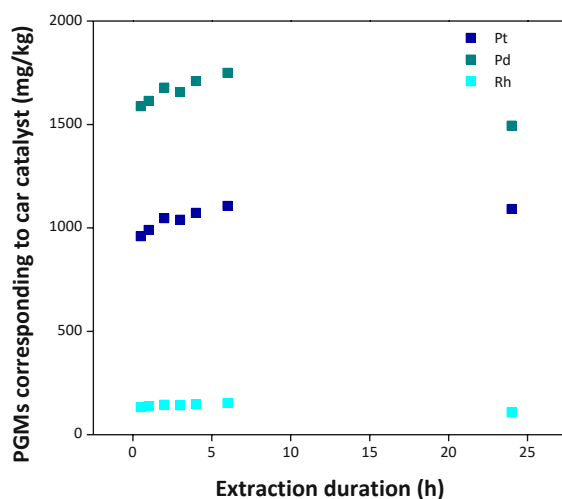


Figure 73. PGM extraction monitoring over a 24 h time frame.

### 6.3.7.2 Upscaling with pre-treated car catalyst sample

Upscaled leaching experiments were additionally performed with pre-treated car catalyst (Ar, 1200 °C, 2 h) and the extraction behavior of the system was also monitored over a 24 h period. The upscaled experiments were performed employing a solid:liquid ratio 1:5, on a 50 g catalyst scale ((50 ± 1) g car catalyst + (250 ± 5) g choline Cl/*p*-TsOH + (50 ± 1) g HNO<sub>3</sub>).

Although the behavior of the upscaled system over time was comparable to that of the untreated catalyst sample, the extraction efficiencies were different:

- Upscaled leaching without pre-treatment:  
Pt 970 ppm, Pd 1590 ppm, Rh 137 ppm, corresponding to 100%, 100%, 40% recoveries, respectively
- Upscaled leaching with pre-treatment:  
Pt 737 ppm, Pd 1177 ppm, Rh 226 ppm, corresponding to 76%, 74%, 66% recoveries, respectively (calculated based on untreated catalyst characterization data).



## 6.4 Quality control of the deep eutectic solvent employed in leaching experiments

The DES used in the leaching process was evaluated for its stability. It is foreseen that the DES can be reused for additional leaching cycles, thereby, minimizing the operational cost and the generated waste.

### 6.4.1 Qualitative control via $^1\text{H-NMR}$

The DES used in the selected leaching system was qualitatively evaluated after the completion of a leaching cycle via NMR spectroscopy. The comparison of the  $^1\text{H-NMR}$  spectra before and after leaching, clearly demonstrates that the DES did not degrade during the leaching process (Figure 74).

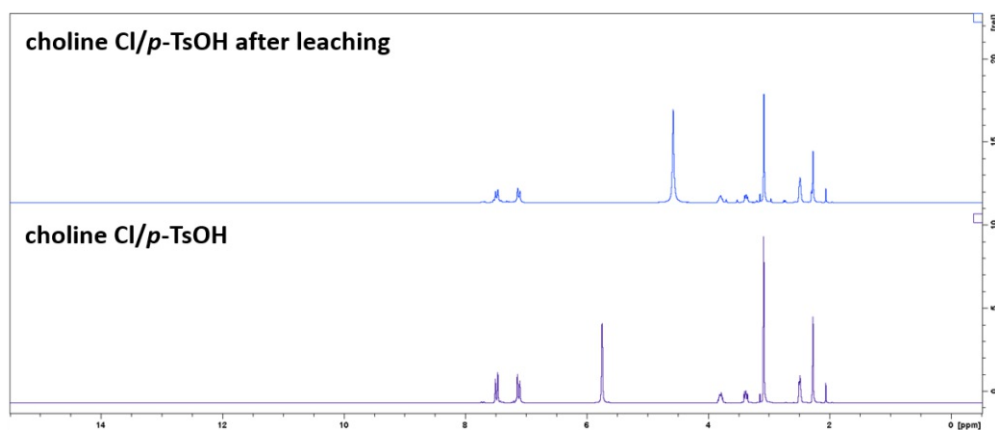


Figure 74.  $^1\text{H-NMR}$  spectra of choline Cl/*p*-TsOH recorded before (pure DES) and after leaching.

### 6.4.2 Quantitative control via UHPLC

#### 6.4.2.1 UHPLC-MS with ELS detector for the quality control of the deep eutectic solvent

A typical UHPLC chromatogram of the DES and the peaks corresponding to its two individual components is presented (Figure 75). After optimization of conditions, parameters were found that allowed base-line separation of the two components in less than 2 minutes.

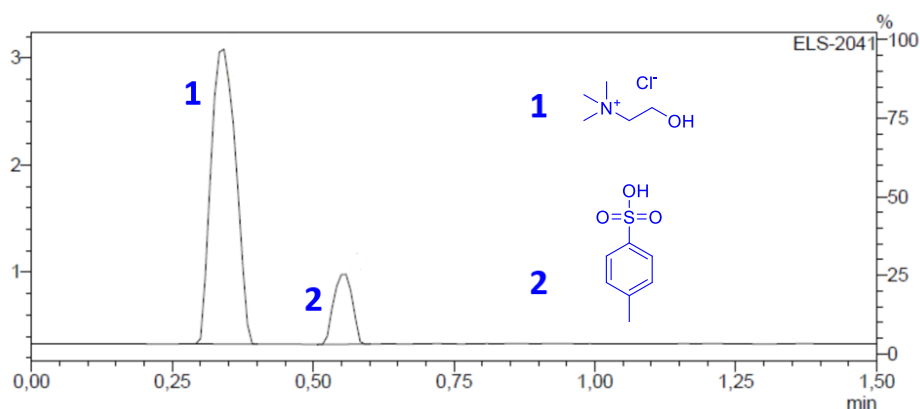


Figure 75. Chromatogram of choline Cl/*p*-TsOH recorded on a C4 column with an ELS detector.

The assignment of the DES component peaks was further verified via mass spectroscopic detection (Figure 76).

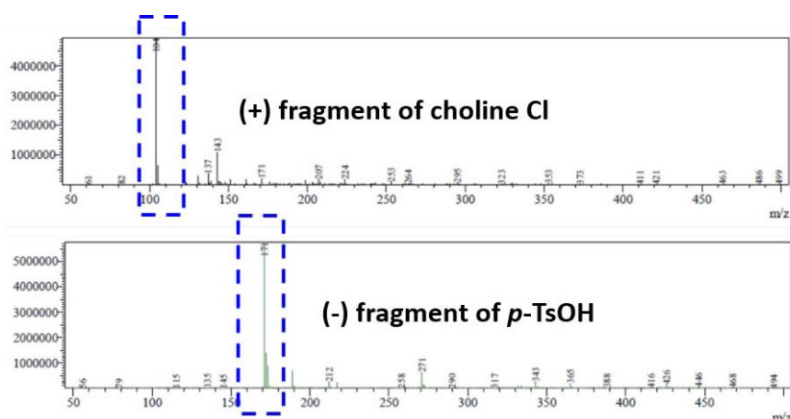


Figure 76. Mass spectroscopic assignment of choline Cl/*p*-TsOH components in ESI +/- mode.

#### 6.4.2.2 Application of UHPLC-MS with ELS detector method to authentic catalyst leachate samples

Based on the previously developed UHPLC-ELS method, linear calibration curves ( $r^2 > 0.99$ ) for choline Cl and *p*-TsOH were obtained (Figure 77), allowing for rapid and efficient process analytics.

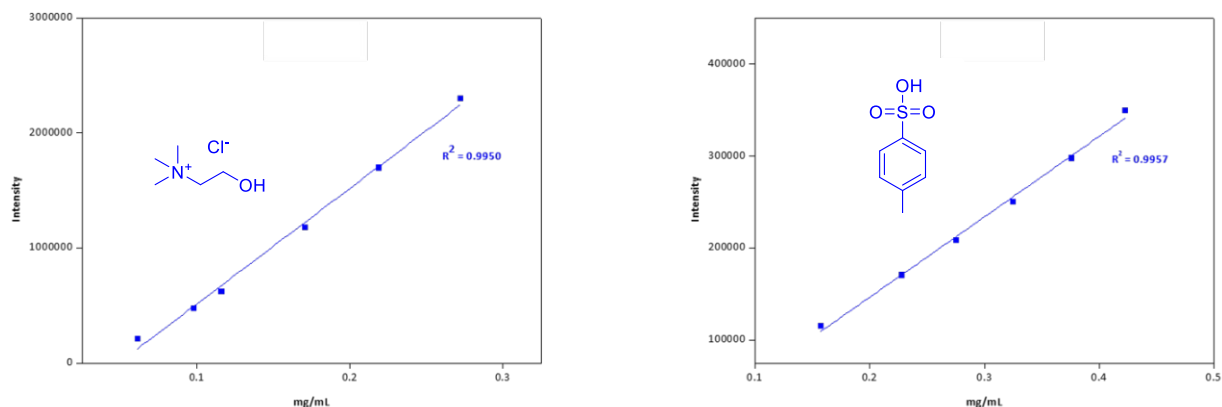


Figure 77. Calibration curves obtained for choline Cl and *p*-TsOH.

Based on the calibration curves obtained for choline Cl and *p*-TsOH, the individual components of the pure DES and DES which had been employed in the PGM leaching from spent car catalyst, were quantified. The quantification data are presented in Table 16.

Table 16. Quantification of DES components in DES before leaching and after leaching.

Measured	Choline Cl in Leachate (mg/mL)	<i>p</i> -TsOH in Leachate (mg/mL)
before leaching	256.6	583.6
after leaching	255.6	533.1

Based on the UHPLC-ELS quantification results, it is concluded that there was no significant degradation of the choline Cl component of the DES during the leaching process. However, the same behavior is not observed for *p*-TsOH for which there is approx. an 8% loss after the leaching. As it was already mentioned, DESs tend to degrade at temperatures over 80 °C. Choline Cl decomposes at 302 °C, however, in the DES its decomposition temperature is significantly depressed. Thus, it could be assumed that a potential explanation for the loss of *p*-TsOH is that its degradation already starts at the employed temperature, which results in the drop of its concentration in the DES.

## 6.5 Liquid-liquid separation of platinum group metals leached in deep eutectic solvent

### 6.5.1 Goals and objectives

The leaching of the PGMs from the automotive catalyst sample with the aid of DES is the first step in the PGM recovery process. In subsequent steps, the PGMs need to be selectively separated from other co-extracted metal ions, which are present in the digested catalyst matrix, as well as from each other. To this end, a liquid-liquid (L-L) separation process incorporating ILs as selective extractants was developed. The role of the ILs in the L-L separation step of the PGM recovery process is briefly presented in Figure 78.

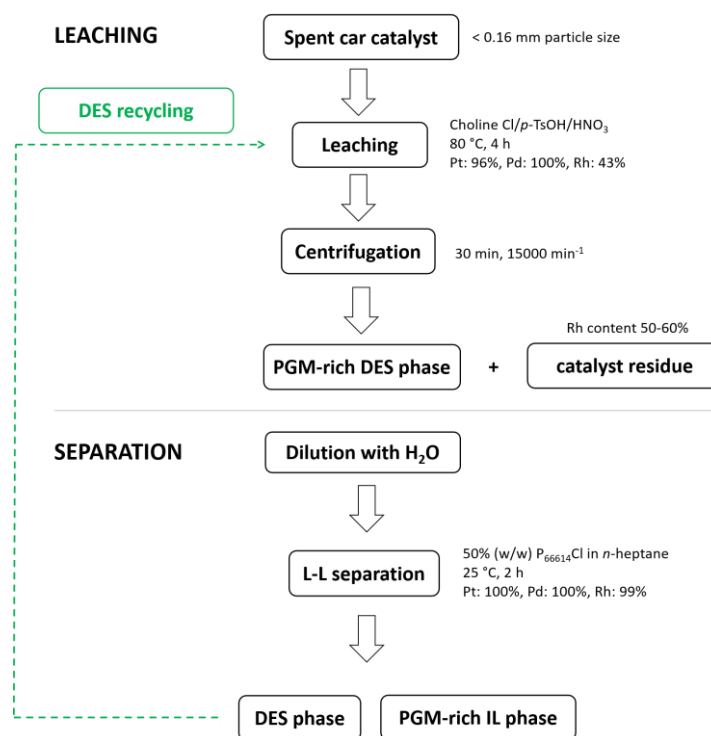
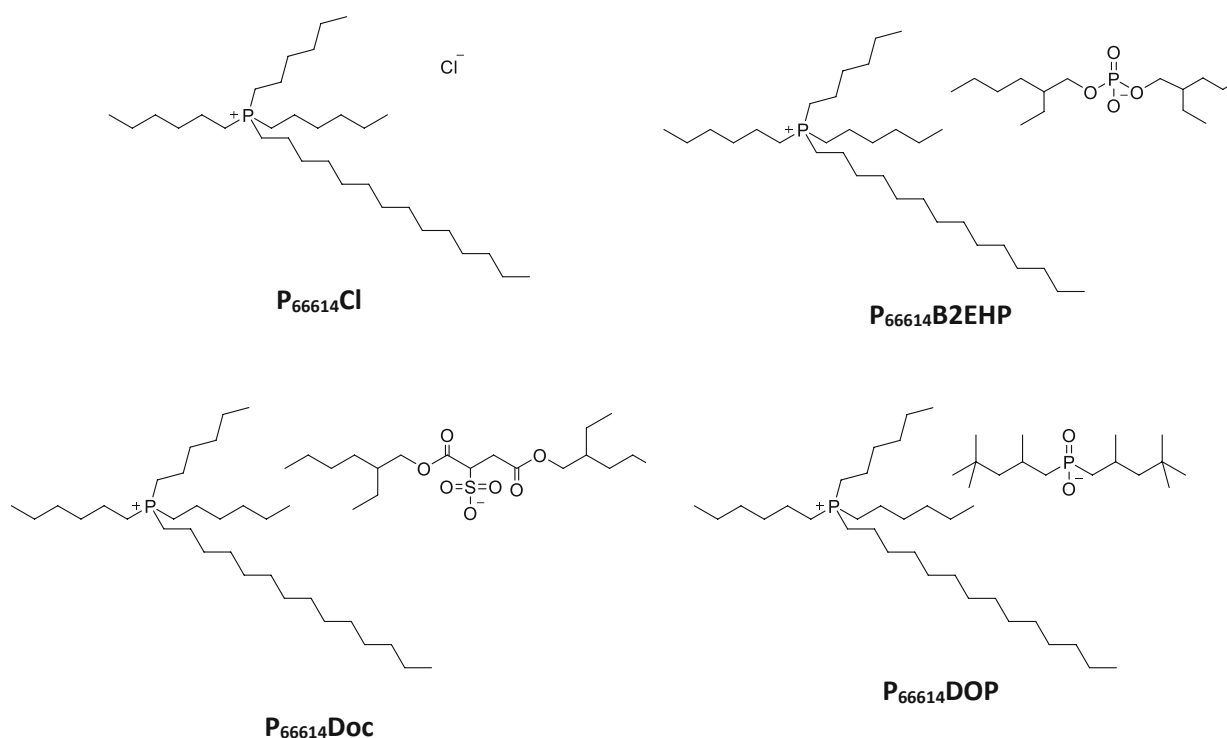


Figure 78. Position of liquid-liquid separation in the process flowsheet of PGM recovery.

### 6.5.2 Selection of hydrophobic ionic liquids for liquid-liquid separation studies

The presented ILs (Figure 79) were selected with certain key criteria in mind. First, hydrophobic nature was a required characteristic, in order to achieve formation of a biphasic liquid system and subsequent separation of PGMs from accompanying elements by partitioning between the two liquid phases. High PGM selectivity was also an indispensable characteristic that would ensure the success of the separation process. The evaluated ILs are based on the phosphonium cation with a long alkyl chain, which is responsible for their hydrophobic nature. Specifically, hydrophobic ILs based on phosphonium cations are thermally stable and therefore suitable for applications in a wide temperature range. Furthermore, their hydrophobic nature allows direct stripping of the PGMs from the phosphonium-IL phase.<sup>281</sup> Phosphonium-based ILs have already been applied in PGM recovery and separation from model solutions<sup>201,194,173</sup> and car catalyst acidic liquor.<sup>208</sup> The ILs P<sub>66614</sub>Cl and P<sub>66614</sub>Doc were purchased and the rest were synthesized in house. The detailed synthetic procedures are provided in the experimental section of the thesis.



**Figure 79.** Hydrophobic ionic liquids evaluated for PGM separation.

### 6.5.3 Preliminary liquid-liquid separation experiments

#### 6.5.3.1 Liquid-liquid separation process

The model PGM solutions used in the preliminary experiments contained 48 ppm of each individual metal (Pt, Pd, Rh) in 1.0 M HCl, which was mixed with choline Cl/*p*-TsoH (1:1.8 eq) and 65% HNO<sub>3</sub>. The solutions were freshly prepared on the day that the experiments were conducted. The spent car catalyst leachate contains 162 ppm Pt, 265 ppm Pd and 23 ppm Rh. The extraction efficiency of the evaluated hydrophobic ILs was calculated as follows; first the PGMs in the model solution or leachate were quantified by ICP-OES. Subsequently, 400 mg of PGM acidic model solution was mixed with 400 mg of 50% (w/w) hydrophobic IL in *n*-heptane (the addition of *n*-heptane facilitates the handling and mixing of the formed biphasic system by lowering the viscosity of the hydrophobic IL). The mixture was stirred in a sealed glass vial for 2 h, at RT, at a stirring speed of 300 rpm. Upon completion of the stirring time, the mixture was placed in an Eppendorf tube and subsequently centrifuged (13.500 rpm, 30 min) for fast and efficient separation of the two phases. After the centrifugation, the aqueous acidic phase was recovered and appropriately diluted for PGM quantification by ICP-OES. Specifically, 500 mg of the leachate, before and after separation, were mixed with In as internal standard (final concentration in solution 1 ppm) and diluted to a final mass of 5 g with 1%EtOH-5% HCl. The extraction efficiency of the PGMs to the hydrophobic IL was calculated by subtracting the measured PGM concentrations before and after separation.

#### 6.5.3.2 Evaluation of separation with selected hydrophobic ionic liquids

The performance of the selected phosphonium ILs was evaluated with the aid of a PGM model solution based on the DES used in the developed leaching process; 1 part aqueous mixed PGM solution:5 parts DES:1 part HNO<sub>3</sub> were all mixed together with the aim of creating a model PGM solution that would most closely resemble the DES leachate. The reference to PGM model solution in this section will imply this solution.

Due to the high viscosity of the involved ILs, it was decided to work with diluted ILs and solutions of phosphonium ILs in *n*-heptane on a 1:1 (w/w) ratio were chosen, to initially investigate the effect of different ILs. As standard conditions, RT and DES to 50% (w/w) phosphonium IL in *n*-heptane 1:1 ratio, were preselected and applied in all experiments. Quantitative extraction for Pt and Pd was obtained with P<sub>66614</sub>Cl, whereas lower yet still high extraction yields were obtained with P<sub>66614</sub>B2EHP followed by P<sub>66614</sub>Doc. In all cases, the extraction of Rh to the hydrophobic-IL phase was significantly lower compared to Pt and Pd. The results of the systems tested for L-L separation are presented in Figure 80.

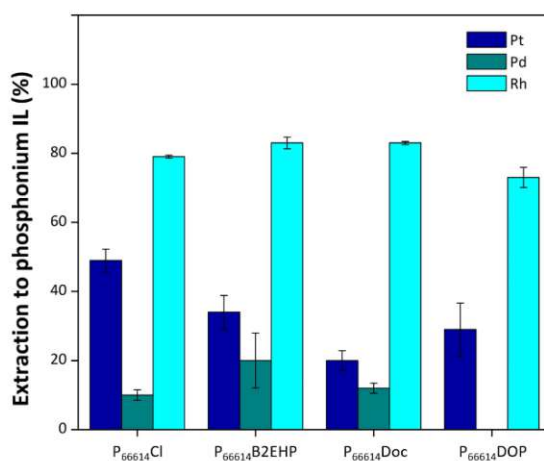


**Figure 80.** Extraction efficiencies (%) of PGMs from model solution with different phosphonium-based ILs.

All further optimization steps were performed with the model DES-based PGM solution.

## 6.5.4 Optimization of liquid-liquid separation parameters

### 6.5.4.1 Effect of dilution of the hydrophilic DES phase

Along with the model PGM solution in DES, a 1:1 and 1:5 dilution with H<sub>2</sub>O were also evaluated. Additionally, the effect of a 1:1 dilution with NaCl 1 M was tested, since it has been previously reported in the literature that it can enhance PGM extraction.<sup>192,292</sup> The respective extraction efficiencies to the hydrophobic phosphonium-IL phase are presented in Figure 81.

The dilution of the PGM-rich hydrophilic DES phase had a significant impact on the extraction efficiencies of all three PGMs to the phosphonium ILs. Evidently, dilution of the hydrophilic phase is necessary in order to achieve maximum extraction of the PGMs to the phosphonium IL. This cannot be attributed to lowering of the concentration brought about through dilution but rather to the decrease in viscosity or/and formation of PGM species that are easier to extract. Application of the same experimental conditions to the real leachate, which has a 4-fold concentration of Pt and 6-fold concentration of Pd compared to the model solution, proves that addition of H<sub>2</sub>O indeed enhances extraction which arises from an effect other than the lowering of the concentration, thus, at least 1:1 dilution with H<sub>2</sub>O is necessary to achieve quantitative yield. Additionally, the dilution level does not seem to play a role in the extraction yield, except in the case of P<sub>66614</sub>Doc, where higher dilution with H<sub>2</sub>O clearly favors the extraction of both Pt and Pd. Contrary to reported data, addition of NaCl does not seem to further improve the extraction efficiencies, therefore, it was not used in subsequent optimization steps.

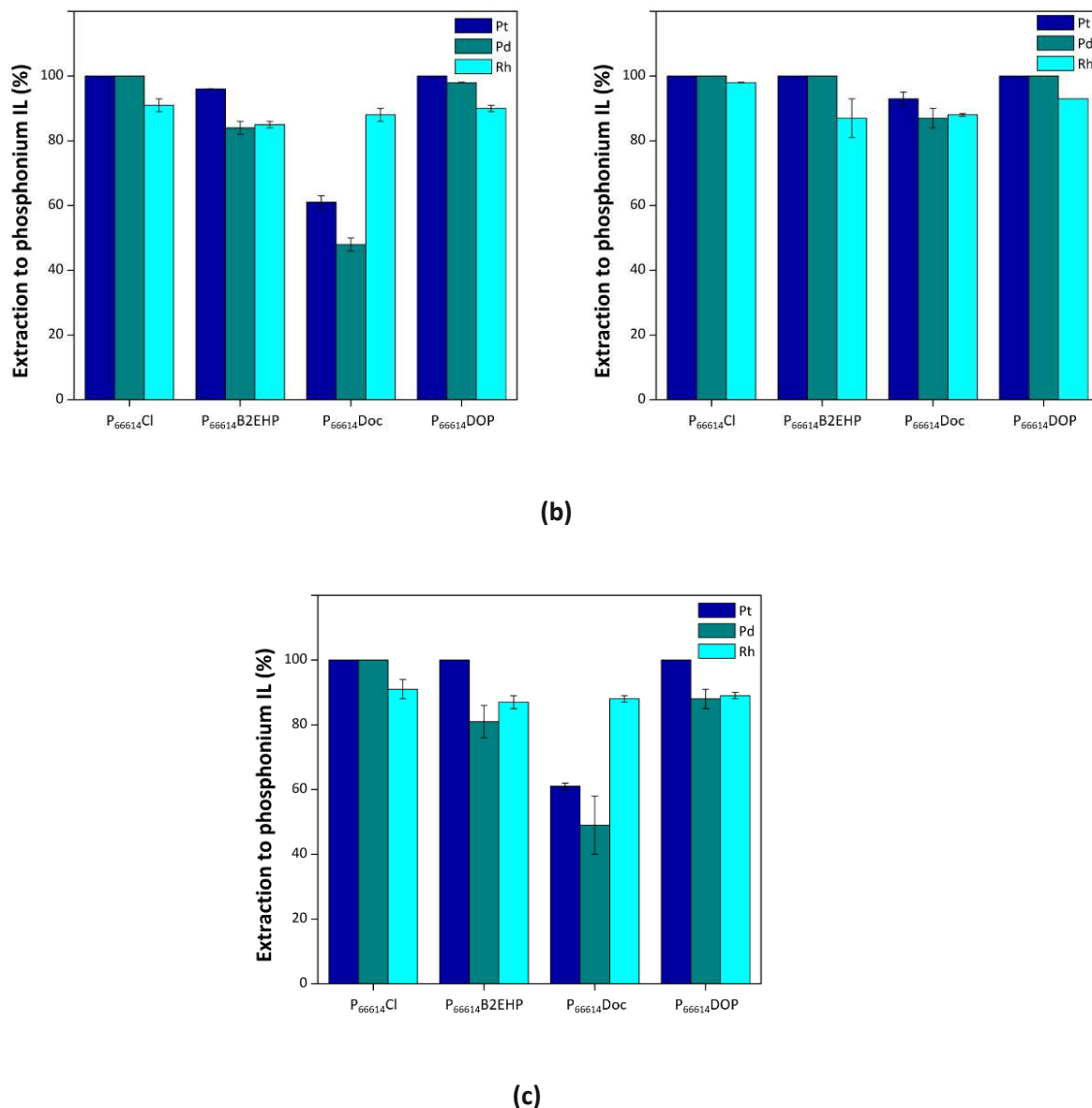


**Figure 81.** Extraction efficiencies (%) of PGMs from PGM model solution to phosphonium ILs with DES phase (a) diluted 1:1 with H<sub>2</sub>O, (b) diluted 1:5 with H<sub>2</sub>O, (c) diluted 1:5 with NaCl.

#### 6.5.4.2 Effect of dilution of the hydrophobic phosphonium-IL phase

The separation experiments were performed with 50% (w/w) phosphonium ILs in *n*-heptane in order to facilitate their handling and mixing in the formed biphasic liquid system. Nevertheless, the impact of the pure phosphonium ILs on the extraction efficiency was also considered.

Since the optimization parameters presented previously demonstrated that the dilution of the hydrophilic phase was essential in order to obtain the maximum extraction efficiencies, all the subsequent optimization steps were performed with a 1:1 dilution with H<sub>2</sub>O of the PGM model system prior to separation. Therefore, from here on, whenever PGM model system is discussed in the separation experiments, the 50% diluted version is implied.

In the experiments presented below, the PGM model system was mixed on a 1:1 ratio with the pure phosphonium ILs. The obtained extraction efficiencies are presented in Figure 82.



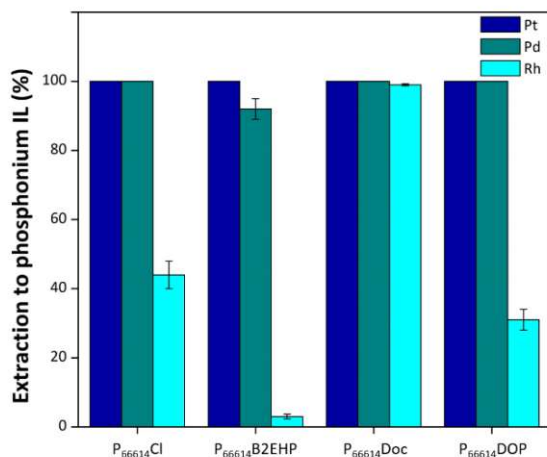


**Figure 82.** Extraction efficiencies (%) of PGMs to pure (undiluted) phosphonium ILs.

It is evident that employing pure phosphonium ILs in the separation step does not allow complete extraction of Rh, with the exception of P<sub>66614</sub>Doc. Therefore, in the subsequent optimization steps 50% (w/w) phosphonium ILs in *n*-heptane were employed, since dilution of the phosphonium IL is a more economical approach than employing it in its pure form.

#### 6.5.4.3 Effect of acidity of hydrophilic-IL phase

It has been reported in literature that modification of PGM solution acidity by HCl addition allows effective separation of Pt and Pd from Rh.<sup>205,293,294</sup> This dependency of the extraction of Rh on the HCl concentration can be attributed to the presence of different Rh-chloro complexes at different HCl concentrations and their different extractability.<sup>72</sup> This approach was evaluated as a possible strategy for the separation of Rh from Pt and Pd. The concentration of HCl in the model PGM solution was adjusted to 3.7 M and 9.7 M. The extraction efficiencies in the respective acidities are presented in Figure 83. An increase in the HCl concentration from the original 1.0 M to 3.7 M and 9.7 M in the hydrophilic-IL phase resulted in complete separation of Rh from Pt and Pd, with all three different phosphonium ILs.

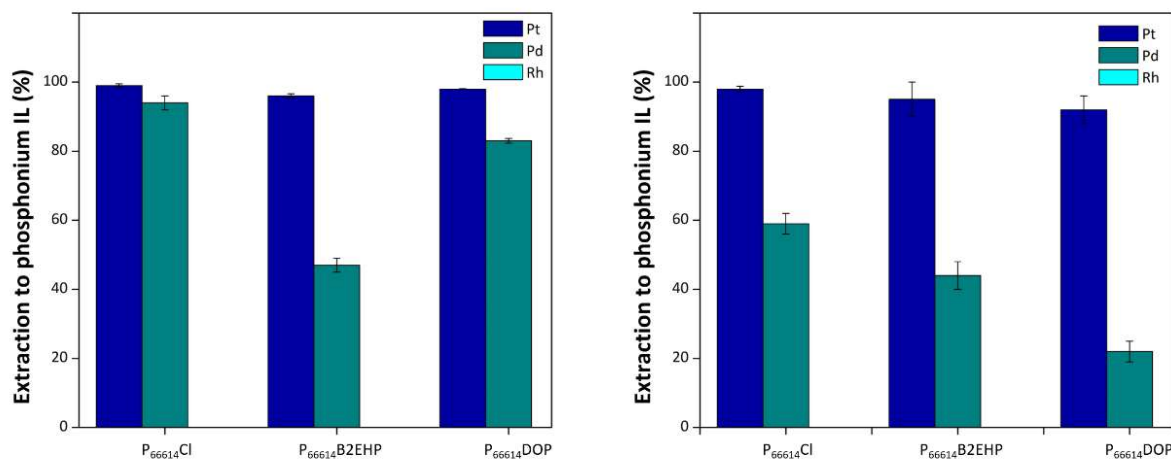


**Figure 83.** Extraction efficiencies (%) of PGMs to phosphonium ILs from PGM model solution, at 3.7 M HCl (left) and at 9.7 M HCl (right).

### 6.5.5 Application of optimized liquid-liquid separation system to authentic car catalyst leachate

Based on the optimization experiments performed with the model PGM solution, the optimum conditions that allow for maximum extraction of the PGMs to the phosphonium IL are the following; mixing ratio of DES phase with phosphonium IL 1:1 (w/w), DES phase (without HCl addition) diluted 50% (w/w) with H<sub>2</sub>O, phosphonium-IL phase diluted 50% (w/w) with *n*-heptane, mixing time 2 h, at RT. Additionally, P<sub>66614</sub>Cl was further evaluated because it has higher extraction efficiencies for all three PGMs while it is commercially available and P<sub>66614</sub>B2EHP, because it demonstrated the capability to separate Pt and Pd from Rh in the model solution. These conditions and these two ILs were employed to the real car catalyst leachate.

Interestingly enough, contrary to the observations in the model solutions, when real leachate was employed quantitative extraction of all three PGMs to both P<sub>66614</sub>Cl and P<sub>66614</sub>B2EHP was obtained. Additionally, unlike in the case of the model PGM solution, where Pt and Pd partitioned to the phosphonium IL and Rh remained in the DES phase, adjustment of the HCl concentration to higher levels, namely 3.7 M and 9.7 M, had no effect on the separation of Rh from Pt and Pd with both evaluated phosphonium ILs, affording quantitative extraction for all three PGMs. On the contrary, regardless of the HCl concentration, quantitative extraction of Rh to both phosphonium ILs along with Pt and Pd is observed when the DES-based leachate is diluted with H<sub>2</sub>O prior to L-L separation (Figure 84). Since both phosphonium ILs demonstrated similar PGM extraction from the real leachate, P<sub>66614</sub>Cl was employed in further experiments, since it is commercially available.

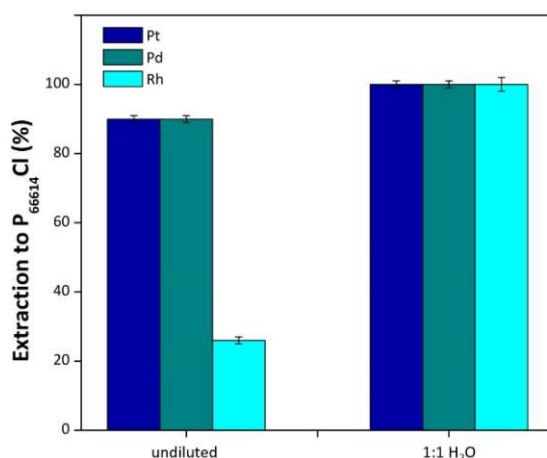


**Figure 84.** Extraction efficiency (%) of PGMs to P<sub>66614</sub>Cl from car catalyst DES-based leachate.

Subsequently, the performance of P<sub>66614</sub>Cl in the separation of PGMs from co-extracted interfering elements was evaluated. The quantification was based on multi-element analysis of the DES leachate before and after the separation step and the results are presented in Figure 85.

It is apparent that along with the PGMs numerous other elements are extracted with Al, Fe and Zn dominating as the major co-extracted elements in the phosphonium IL. In terms of extraction efficiency to the hydrophobic-IL phase, the following correspond to each element (%): Pt 100, Pd 100, Rh 100, Al 20, Fe 100, Zn 98, Pb 91, Cu 56, Sr 80 and Ni 52. The validity of the results presented was verified by standard addition experiments.

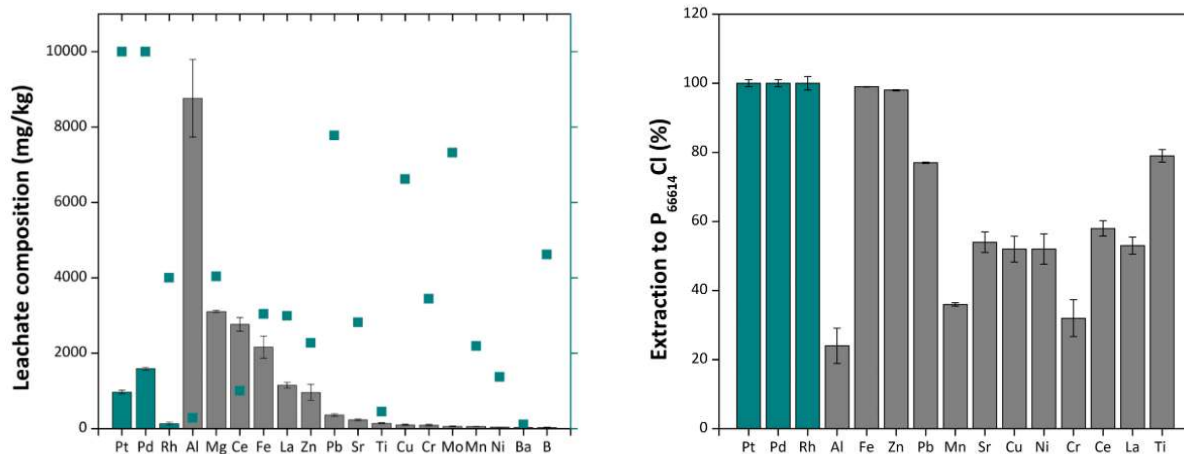


**Figure 85.** Concentration (mg/kg) of elements in car catalyst with their respective extraction efficiencies to the DES phase (left) and their respective extraction efficiencies to the phosphonium-IL phase (right).

### 6.5.6 Recycling of hydrophilic deep eutectic solvent after liquid-liquid separation

The possibility of recycling and reusing the DES for new leaching cycles after separation was investigated. The PGM-rich leachate obtained from a leaching cycle was subsequently subjected to separation during which all PGMs were extracted to the phosphonium IL, thus, leaving the DES free from PGMs. The PGM-free DES was recovered and reused for subsequent leaching cycles. The goal of these experiments was to evaluate the capacity of the recycled DES to effectively leach PGMs and its stability throughout this process.

#### 6.5.6.1 Leaching efficiency and DES recovery after L-L separation

The recycling experiments were performed in four consecutive cycles and repeated for verification of the results. The number of leaching and separation cycles as well as the respective PGM extractions are presented in Figure 86. The recovery of the DES in each cycle was in the range of 50-60% of the input; the DES loss can be attributed partly to its viscosity and to handling losses during the experimental process which are more severe in the small scale that these experiments were performed.

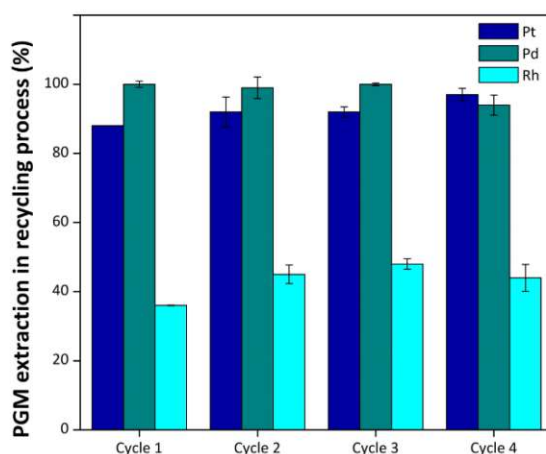


**Figure 86.** Extraction efficiency (%) of PGMs to P<sub>66614</sub>Cl with recycled DES.

No loss is observed in the leaching efficiency of the DES in the consecutive cycles performed, however, there is a considerable loss of the DES itself.

This can be attributed to physical losses related to high viscosity after the leachate centrifugation, but also to the migration of *p*-TsOH from the DES to P<sub>66614</sub>Cl in the L-L separation step, which is reflected on the modification in the appearance of the DES after L-L separation, namely the color changes from dark pink to yellow (Figure 87). This is also verified via <sup>1</sup>H-NMR spectroscopic data (Figure 88).

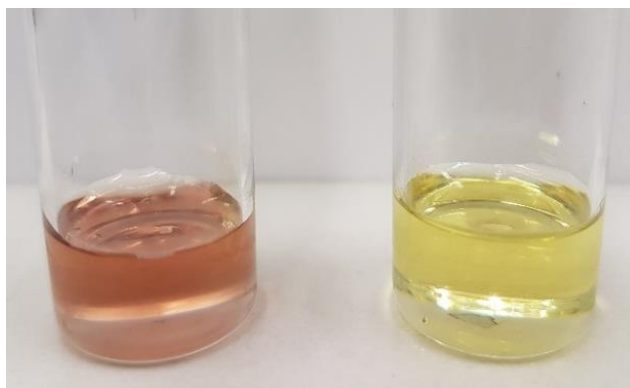


**Figure 87.** Hydrophilic DES appearance before leaching (left) and after leaching/L-L separation (right).

#### 6.5.6.2 Quality control of hydrophobic IL and hydrophilic DES stability in recycling

The IL and DES stability was qualitatively evaluated via <sup>1</sup>H-NMR spectroscopy. It can be deduced from the recorded spectra that the hydrophobic IL remained stable throughout the entire four consecutive recycling steps, whereas in the case of the hydrophilic DES it was verified that indeed *p*-TsOH migrated from the hydrophilic to the hydrophobic phase during L-L separation (Figure 88).

The migration of the *p*-TsOH to the hydrophobic phase did not have a detrimental effect on subsequent leaching cycles. The missing amount of the hydrophilic DES was simply redosed and the subsequent leaching cycle yielded the same extraction efficiencies that a freshly prepared DES would have yielded.

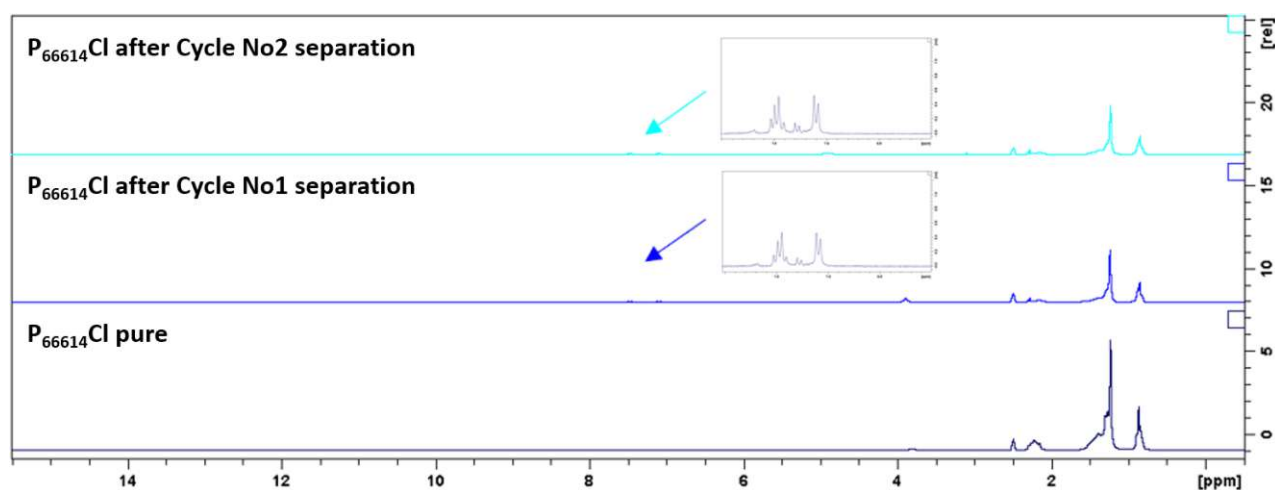


**Figure 88.** <sup>1</sup>H-NMR spectra of P<sub>66614</sub>Cl before and after L-L separation.

### 6.5.7 Upscaling of liquid-liquid separation system

Based on the previously optimized L-L separation system, additional experiments were performed to study the extraction behavior of PGMs in an upscaled version. The upscaled experiments were performed on a 100 g PGM leachate diluted with H<sub>2</sub>O 1:1 (w/w). The upscaled L-L separation set-up consisted of a round-bottom flask with a mechanical stirrer. The two phases were mixed at RT, for 2 h. The following conclusions can be reached for the up-scaled L-L separation process; (i) the equilibrium was reached within 2 h and (ii) the extraction efficiency for all PGMs in the hydrophobic phase was comparable to the efficiency obtained in the small-scale L-L separation experiments (Pt 100%, Pd 100%, Rh 100%).

## 6.6 Solid-liquid separation of platinum group metals from acidic leachate

A new concept that emerged along with the expanding interest in ILs was their immobilization on solid-support materials which entails the deposition of a thin IL layer on a solid surface. Supported-ionic liquid phases (SILPs) are an attractive alternative approach to exploiting the advantages that ILs have to offer while at the same time circumventing accompanying problems of liquid-based processes, such as mass-transport limitations and use of excess amount of ILs.<sup>226</sup> The field that have predominantly benefited from the novelty introduced by the SILP concept is catalysis,<sup>295,296,297</sup> whereas metal separations have received less attention. Rare earth element separation with phosphonium, imidazolium and quaternary ammonium salt-based SILPs has been reported in the literature.<sup>298,299</sup> Supported phases impregnated with phosphonium- and quaternary ammonium-based ILs have been employed for the selective recovery of post-transition metals from transition metal-containing solutions.<sup>237,300</sup>

### 6.6.1 Goals and objectives

Although SILP technology has been used for the separation of various elements, there is no literature available on its application for PGM separation. Additionally, polymerized SILPs (polySILPs) have only been reported so far in catalysis applications, but have never been applied to metal separations. The aim was to develop a rapid and efficient PGM recovery process with high separation from accompanying elements leached from the car catalyst material. The role of the ILs in the S-L separation step of the PGM recovery process is briefly presented in Figure 89.

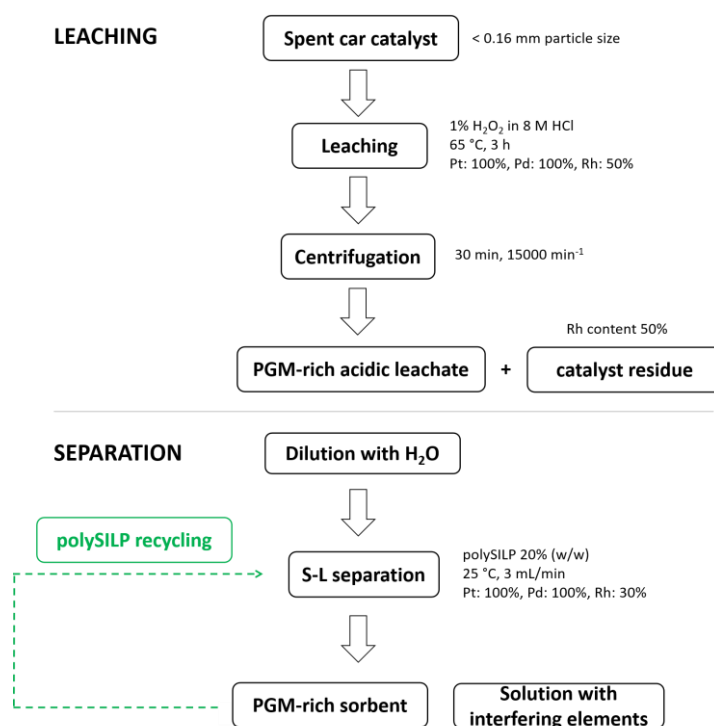


Figure 89. Position of solid-liquid separation in the process flowsheet of PGM recovery.

### 6.6.2 Classification of solid sorbent materials for solid-liquid separation studies

Two different types of solid sorbent materials comprising ILs were synthesized and evaluated (Figure 90). The physisorption of the IL layer on the silica support in the case of SILP materials is based entirely on *van der Waals* forces which are weaker compared to chemical interactions, therefore there is the possibility of the physisorbed IL to leach out of the solid support. While this problem is rarely faced in



well-established catalytic processes in gas phase, losses of IL from SILP materials is a considerable problem for catalysis in liquid phase, particularly in the case of continuous processing.<sup>301</sup> In order to overcome this foreseeable problem, the concept of the polySILPs, which are based on the chemisorption of the IL on the silica support, was introduced.

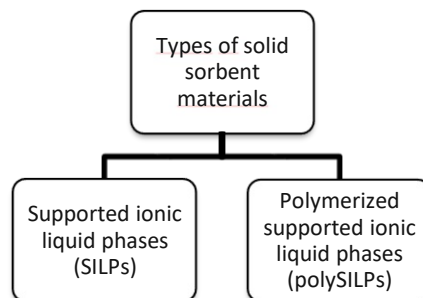


**Figure 90.** Classification of ionic liquid-based solid sorbent materials evaluated in PGM solid-liquid separation experiments.

Based on the L-L extraction results for PGM recovery from acidic media, the hydrophobic IL  $P_{66614}Cl$  was selected for the preparation of SILP materials on silica support (Figure 91). Phosphonium-based ILs have already been applied to PGM recovery and separation from model solutions<sup>194,201,173</sup> and car catalyst acidic liquor.<sup>208</sup> In general, hydrophobic ILs with strongly coordinating anions, such as the  $Cl^-$  anion, demonstrate high affinity toward the chelation of metal anions.<sup>302,281</sup> Moreover, phosphonium-based IL cations typically exhibit higher thermal and electrochemical stabilities compared to the widely investigated nitrogen- and imidazolium-based ILs and are, as in the case of the employed  $P_{66614}Cl$ , already often liquid at RT.<sup>303,304</sup>

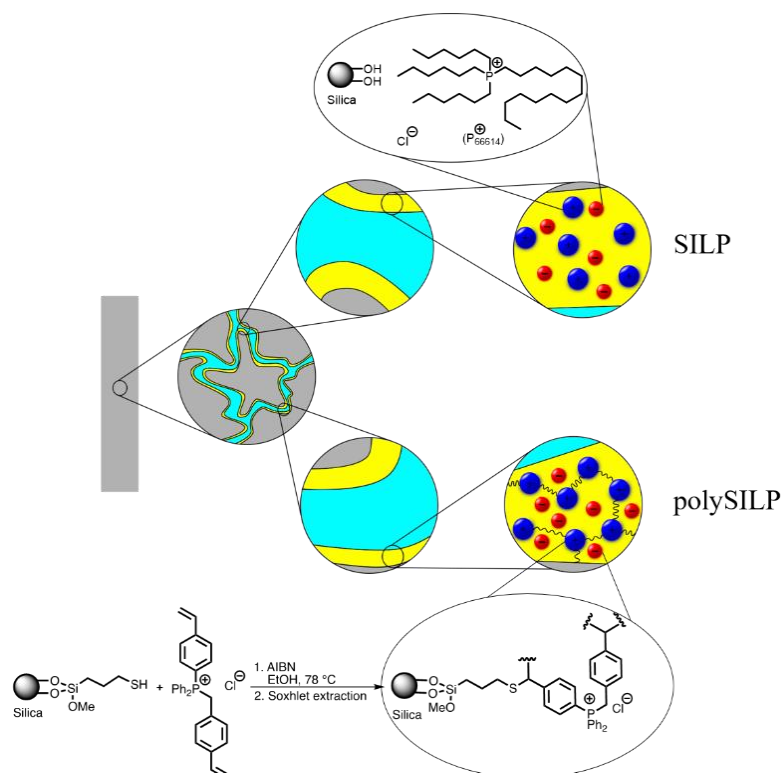


**Figure 91.** Concept and structure of SILP and polySILP materials as solid sorbents for PGM recovery.

The preparation of polySILPs was performed in a “grafting-from-surface” approach, relying on surface modification of silica with reactive thiol groups, followed by deposition of a thin IL layer and subsequent radical polymerization (Figure 91). It was envisioned that this type of silica-polymer hybrid materials would improve stability toward leaching of the IL compared to conventional SILPs. Due to the commercial availability of precursor molecules, the tetraalkylphosphonium cations used in the SILP materials were switched to aryl-functionalized species in the case of polySILPs, since the corresponding monomer, diphenyl(4-vinylbenzyl)(4-vinylphenyl)phosphonium chloride, provides an easily accessible precursor for the preparation of a cross-linked polymer layer on the mesoporous support of the polySILP. The synthetic process of the polySILP materials was adapted from literature procedures.<sup>305,306</sup>

### 6.6.3 Characterization of synthesized solid sorbent materials

SILP materials with physisorbed P<sub>66614</sub>Cl and polySILP materials relying on the diphenyl(4-vinylbenzyl)(4-vinylphenyl)phosphonium chloride monomer with different loadings (10-50% (w/w)) were prepared. The amount of IL monomer corresponding to the polySILP target loading was initially physisorbed on the S-grafted silica and subsequently polymerized by addition of a radical initiator (AIBN). Nevertheless, lower than the target loadings were afforded, which can be attributed to the inevitable deceleration of the polymerization process. For the polySILP target loadings of 10, 20 and 50%, actual loadings of 7, 14 and 39% were obtained, respectively. Apart from the gravimetric data, a number of characterization techniques, such as thermogravimetric analysis (TGA), diffuse reflectance infrared Fourier transform-infrared spectroscopy (DRIFT-IR), scanning electron microscopy (SEM) and Brunauer-Emmett-Teller (BET) analysis were conducted for the systematic characterization of these materials. Prior to each analysis, the samples were dried overnight to a residual pressure of 0.1 mbar in order to eliminate interferences due to the absorbed H<sub>2</sub>O molecules.

#### 6.6.3.1 Thermogravimetric analysis

The thermal decomposition temperatures of these materials were found to be higher than 350 °C (Figure 92). Moreover, in the case of the polySILPs, the weight loss allowed calculation of the actual loading after radical polymerization and removal of residual monomers via Soxhlet extraction.

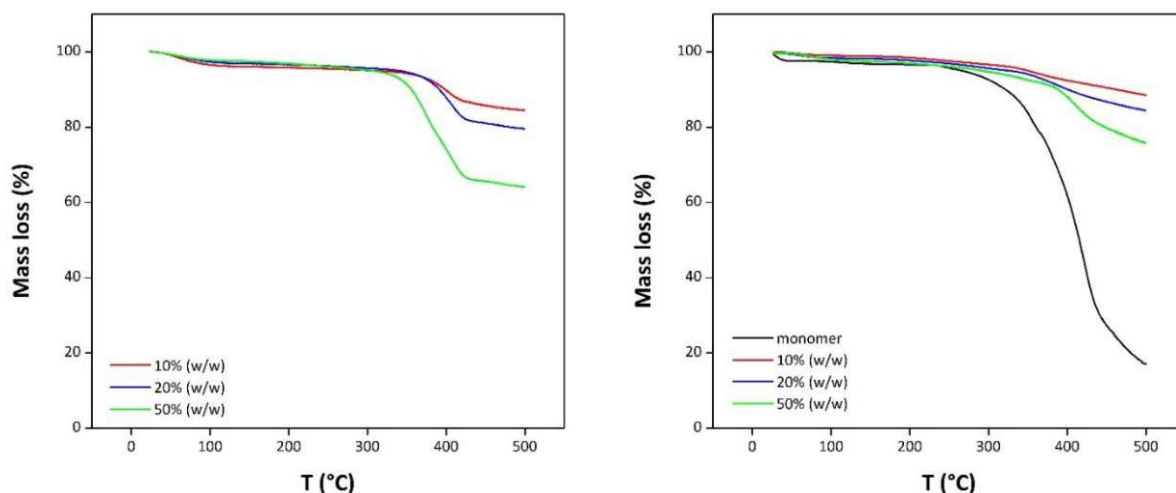


**Figure 92.** TGA curves of SILP (left) and polySILP (right) with loadings of 10, 20 and 50% (w/w).

### 6.6.3.2 DRIFT-IR and ATR-IR spectroscopy

Successful loading of the polymer on the silica is evident from the IR spectra (Figure 93, right), where peaks in the region 2500-3500  $\text{cm}^{-1}$  and in the region 1400-2000  $\text{cm}^{-1}$  suggest the presence of polymerized IL on the surface. The symmetric and asymmetric stretches of the double bonds (C=C) are exhibited as peaks in the 1400-2000  $\text{cm}^{-1}$  region, while the presence of =CH bonds is evident by the visible peaks in the 2500-3500  $\text{cm}^{-1}$  region. The absence of the characteristic thiol group (S-H) peak at 2550  $\text{cm}^{-1}$ , which is present in the S-grafted silica (Figure 93, left), further indicates the successful attachment and polymerization of the IL monomer on the S-grafted silica surface.

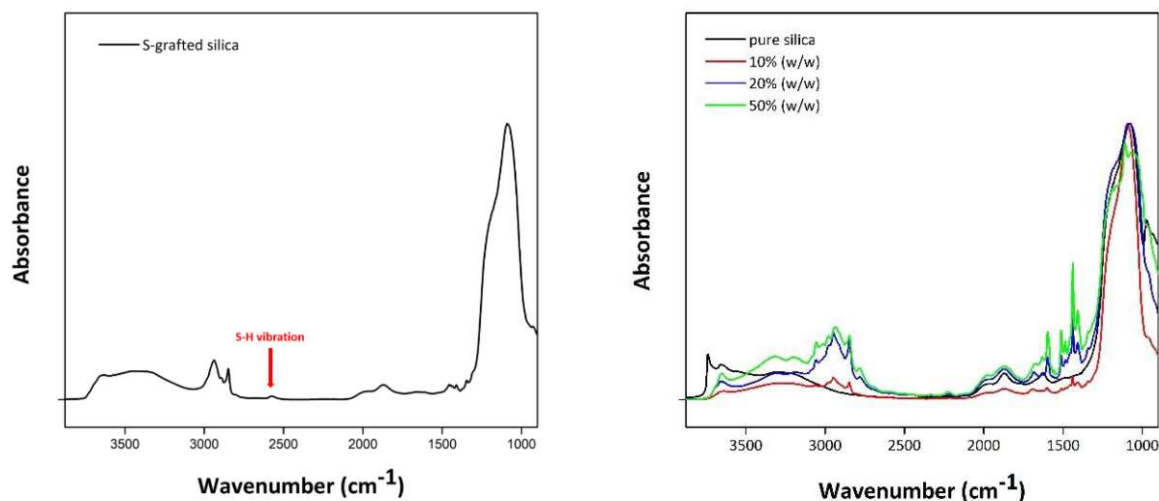


**Figure 93.** DRIFT-IR spectra of S-grafted silica (left) and pure silica and polySILP loadings of 10, 20 and 50% (w/w) (right).

Additionally, the comparison of the attenuated total reflection-infrared spectroscopy (ATR-IR) spectrum of the polySILP 20% and the PGM-loaded polySILP 20% (Figure 94) indicates that the S atom does not coordinate with any of the PGMs. The C–S stretching vibration appears at 692  $\text{cm}^{-1}$  in both spectra, meaning that a coordination extraction mechanism is very unlikely.

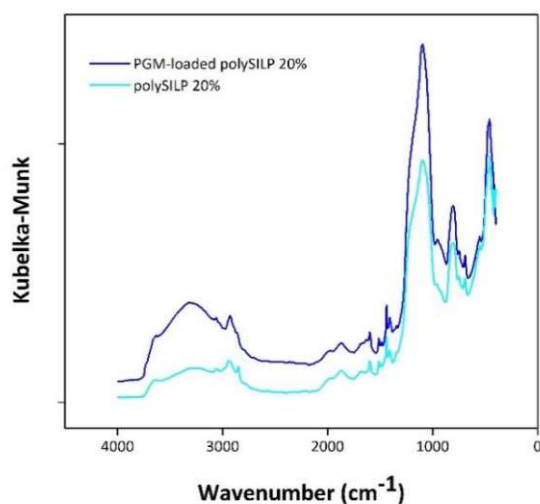


**Figure 94.** ATR-IR spectra of polySILP 20% (w/w) and PGM-loaded polySILP 20% (w/w).

### 6.6.3.3 Scanning electron microscopy

The SEM data recorded for the polySILP 20%, both pure and after every process step (Figure 95) do not reveal any modification on the physical appearance of the sorbent material surface. Unfortunately, the detection limit of the SEM measurements did not allow the quantification of the elements absorbed on the polySILP, since it is approximately 100 times higher than the concentration of the absorbed elements.

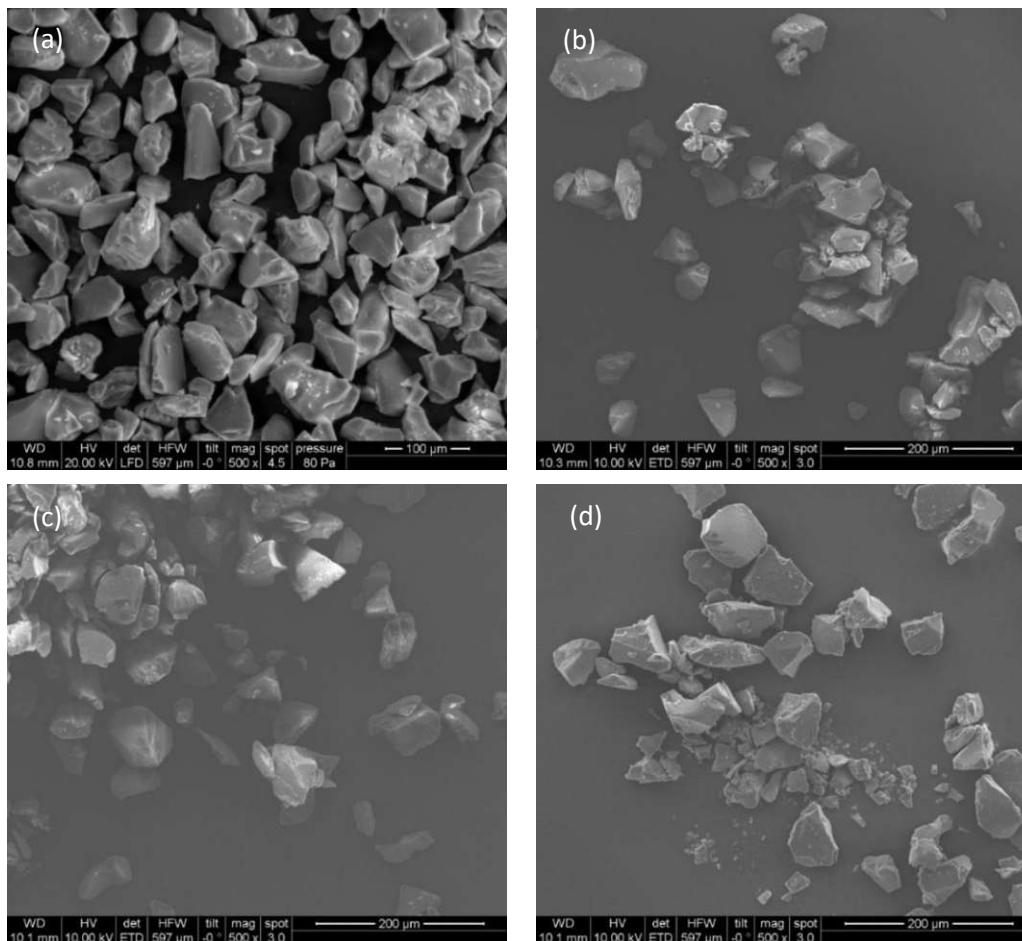


**Figure 95.** SEM image of polySILP with a loading of 20% (w/w), (a) pure, (b) after retention of PGM-rich acidic solution, (c) after 1<sup>st</sup> stripping and (d) after 2<sup>nd</sup> stripping.

### 6.6.3.4 BET analysis

The mesoporous character of the supported IL materials, which has been determined via BET analysis, is responsible for their higher surface area as opposed to other conventionally employed solid sorbent materials (Figure 96).

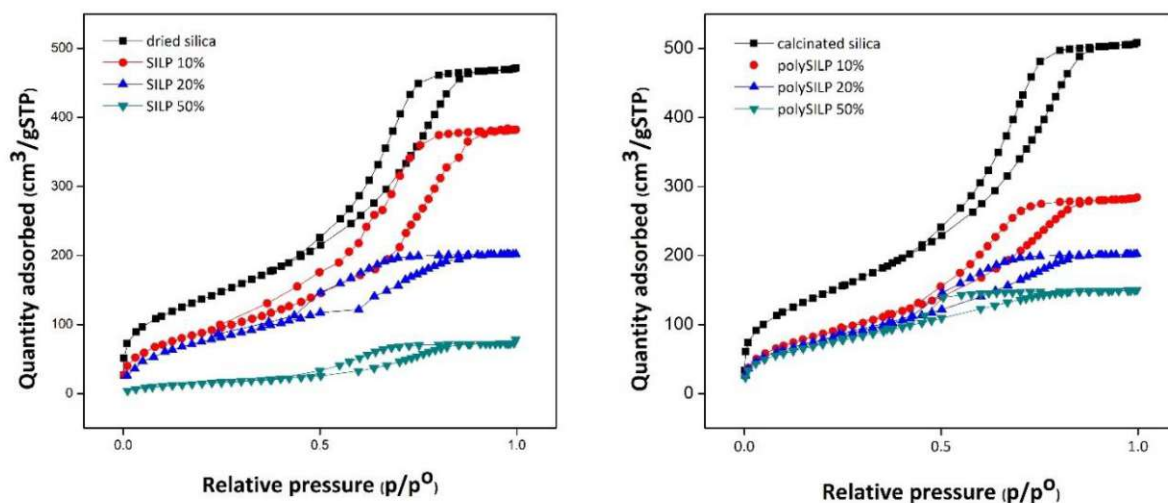


**Figure 96.** BET curve for dried silica and SILP (left) and calcinated silica and polySILP (right) with different loadings.

It is evident by the obtained BET data (Table 17) that increasing IL loading on the solid material decreases its specific surface area, as indicated by the decreasing size of the average pore diameter. The suitable loading for the target application should be selected in a way that both the mesoporous character of the material and the IL properties are effectively exploited.

**Table 17.** Structural parameters calculated for the N<sub>2</sub> absorption/desorption isotherms.

Sample	BET Surface Area (m <sup>2</sup> /g) <sup>a</sup>	Pore Volume (cm <sup>3</sup> /g) <sup>b</sup>	Average Pore Diameter (nm) <sup>c</sup>
Pure silica	496.08	0.76	5.9
Calcinated silica	525.61	0.81	6.0
SILP 10%	326.22	0.61	5.9
SILP 20%	243.63	0.42	5.4
SILP 50%	58.37	0.11	4.4
polySILP 10%	323.06	0.46	5.1
polySILP 20%	289.63	0.30	4.2
polySILP 50%	263.43	0.20	3.3

<sup>a</sup> Calculated by the BET equation. <sup>b</sup> BJH pore desorption volume. <sup>c</sup> Desorption average pore diameter.

The introduction of IL on the silica surface leads to a considerable decrease in the specific surface area, both in the case of SILPs and polySILPs, as well as a small decrease in the average pore size. Blocking of the micropores within the silica by formation of a thin IL coating in the interior of the mesopore surface could explain this observation.

Additionally, increasing IL loading leads to further decrease in the surface area, which is considerable in the case of the SILP, while in the case of the polySILP a drastic decrease in the pore diameter is observed. Our hypothesis is that in the case of SILPs, the IL does not only form uniform coatings on the silica substrate, but probably starts filling the pores instead, which does not have an effect on the pore diameter but rather a drastic effect on the surface area. In contrast, the IL in polySILPs is further deposited on the internal coating, thus decreasing the pore diameter. All samples show type IV isotherms with type

H2(b) hysteresis, which is indicative of the presence of mesopores and minor pore blocking with wide size distribution of pore and neck widths, which is typical of mesocellular silica foams.<sup>307</sup> The hysteresis curves of the SILPs indicate partially filled pores, whereas the polySILP curves indicate that the pores are uniformly coated with the exception of entrance and exit points, where thicker coatings form bottle necks.

Overall, in the case of SILPs a thin IL layer is formed which eventually starts filling up the pores instead of further contributing to the coating. The IL in the case of polySILPs adds to the interior coating in a layer-type fashion, but eventually the coating becomes non-uniform and thicker on the entrance and exit points, thus forming a bottle neck.

## 6.6.4 Evaluation of solid sorbent materials in solid-liquid separation experiments

### 6.6.4.1 Acidic leaching of car catalyst material

While different protocols for the leaching of PGMs from spent car catalysts exist in literature, the combination of HCl and H<sub>2</sub>O<sub>2</sub> as oxidant provides particularly attractive and, by way of comparison, benign conditions. A protocol developed by Harjanto et al.<sup>308</sup> was employed for the leaching process. The milled car catalyst was mixed with 1% H<sub>2</sub>O<sub>2</sub> in HCl on a solid:liquid ratio 1:5 and extracted at 65 °C for 3 h. The mixture was subsequently centrifuged for the sedimentation and separation of the solid car catalyst material and the recovered leachate was diluted prior to PGM quantification. As expected, the leaching efficiencies of Pt and Rh are proportional to the HCl concentration and a concentration of 8 M is required to obtain the maximum extraction efficiency under the employed experimental conditions (Figure 97).

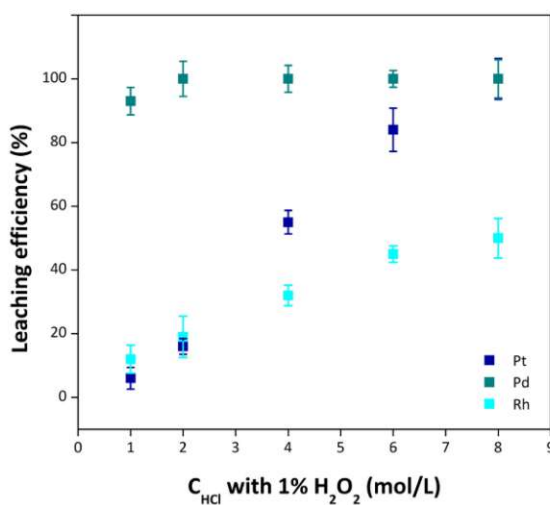


Figure 97. Effect of HCl concentration on PGM leaching efficiency (%).

On the contrary, the extraction of Pd is almost independent of the HCl concentration, since any HCl concentration over 2 M yields quantitative extraction of Pd. Additional experiments were performed at higher temperatures (80 °C, 120 °C) and longer reaction times (4 h, 6 h) in order to enhance the extraction of Rh; however, there was no observed effect on its extraction efficiency.

### 6.6.4.2 Solid-liquid separation process

The S-L separation with SILP and polySILP materials was originally investigated with a PGM model solution to study the retention of PGMs on the supported ILs. According to the results obtained from the leaching of the car catalyst material, model PGM solutions were prepared reflecting the PGM concentration levels of the actual leachate. An acidic solution with 194 ppm Pt, 318 ppm Pd and 34 ppm Rh (to which we refer as the model solution in this section) was used and the PGM retention behavior was investigated under a variety of different parameters.



## 6.6.5 Optimization of solid-liquid separation parameters

### 6.6.5.1 Effect of PGM solution acidity

The effect of different HCl concentrations of the model solution (while the PGM concentration was kept constant) on the PGM retention on the sorbent material is presented on the example of SILP 20% (w/w) and polySILP 20% (w/w) (Figure 98).

In both cases of SILP 20% and polySILP 20%, quantitative retention of Pt and Pd on the sorbent material is observed and it exhibits independency from the acidity of the model PGM solution. On the contrary, no clear trend could be established for Rh, taking into consideration the large quantification errors observed, which can be attributed to the proximity of Rh content in solution to the limit of quantification of the method.

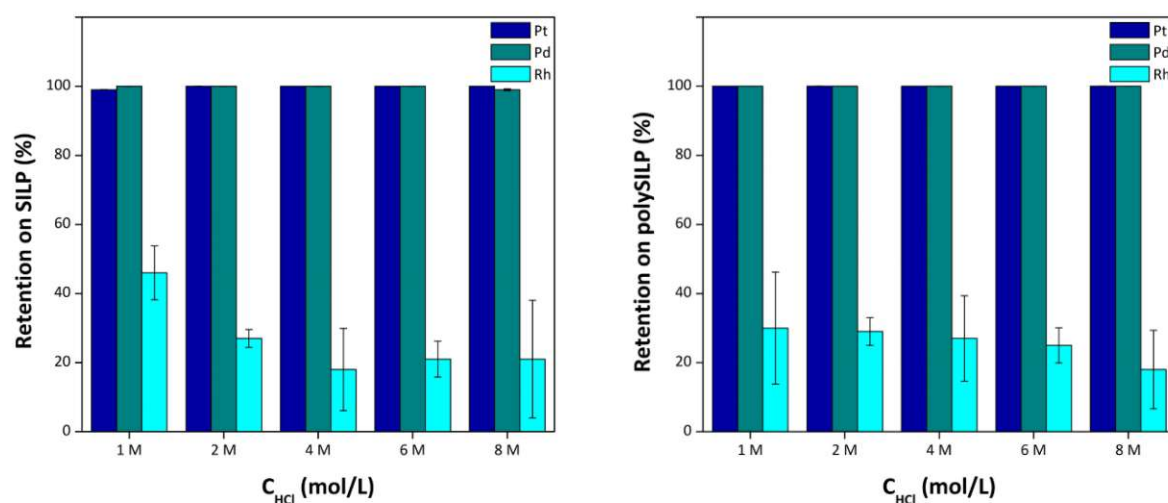


**Figure 98.** Retention behavior of PGMs from model solution of different HCl concentrations on SILP 20% (w/w) (left) and polySILP 20% (w/w) (right).

Similar behavior is observed in the case that SILPs and polySILPs with loadings of 10% (w/w) (Figure 99) and 50% (w/w) (Figure 100) are employed.

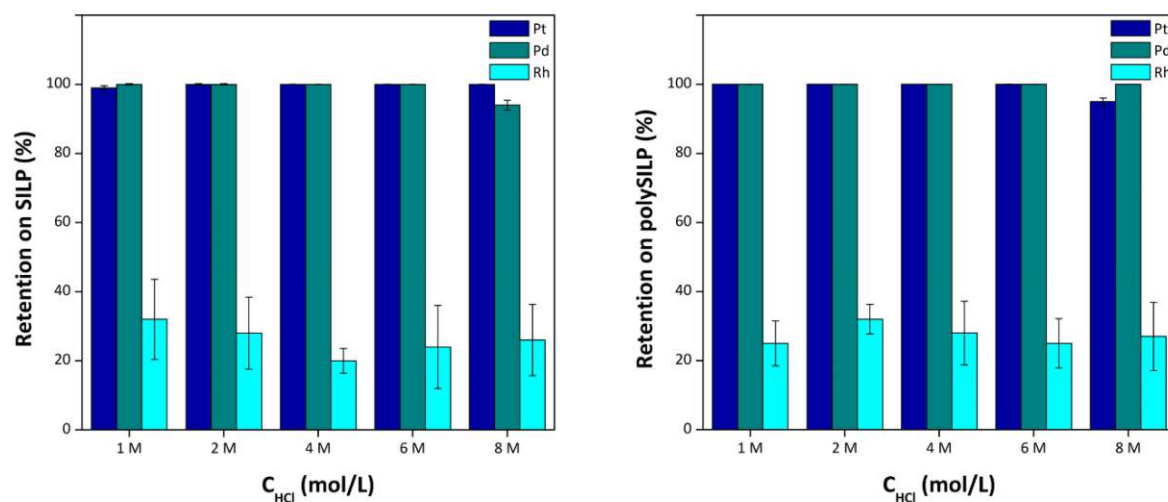


**Figure 99.** Retention behavior of PGMs from model solution of different HCl concentrations on SILP 10% (w/w) (left) and polySILP 10% (w/w) (right).

The effect of the HCl concentration on the separation of Pt and Pd from Rh in biphasic systems has been previously reported; Pt and Pd are extracted from a wide range of HCl concentrations into an amine-based extractant, whereas Rh can only be extracted when low acidic concentrations are employed.<sup>309</sup> Additionally, the dependency of Rh retention, on various anion exchangers, on the HCl acid concentration has been previously demonstrated.<sup>310,311</sup>

The dependency of Rh retention on the HCl concentration can be attributed to the presence of different Rh species at different concentrations and their respective difference in extractability. Increasing HCl concentration leads to an increase in the concentration of non-aquated Rh-chlorocomplexes, which pose higher metal ion charge densities as opposed to the aquated ones. Extraction efficiency via the anion-exchange mechanism is proportional to the metal ion charge density, while higher charge density also implies higher solvation energy of the respective complexes. At lower acidities, which implies concurrently higher amount of H<sub>2</sub>O in solution, the aquated species  $[\text{RhCl}_4(\text{H}_2\text{O})]^-$  and  $[\text{RhCl}_5(\text{H}_2\text{O})]^{2-}$  are the dominant and most probably the extractable ones, while  $\text{RhCl}_3^{6-}$  is most probably not extracted. Aside from the high charge density of the latter species, the steric demands imposed by their complexation further hinder their extraction.<sup>194,72,206,195</sup>

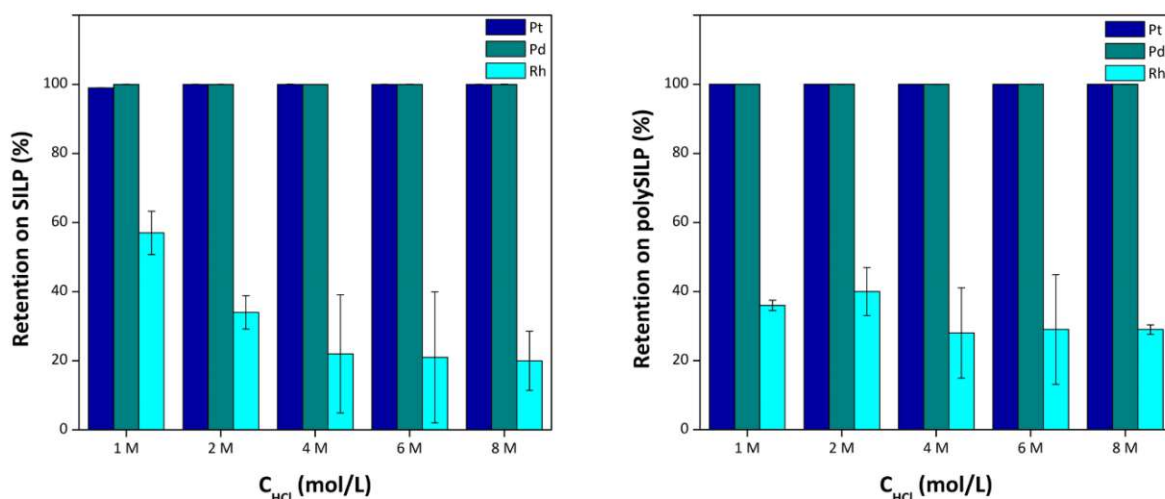


**Figure 100.** Retention behavior of PGMs from model solution of different HCl concentrations on SILP 50% (w/w) (left) and polySILP 50% (w/w) (right).

### 6.6.5.2 Effect of PGM solution dilution level

Further studies on the effect of the dilution of the 8 M HCl model PGM solution (both acidity and PGM concentration are modified via dilution) on the retention on the solid material showed that partial separation of Pt and Pd from Rh may be observed, as shown on the example of a SILP and polySILP (Figure 101) with 20% (w/w) loading. The term “undiluted” refers to the model solution (194 ppm Pt, 318 ppm Pd and 34 ppm Rh in 8 M HCl) to contrast it with the different dilution levels.

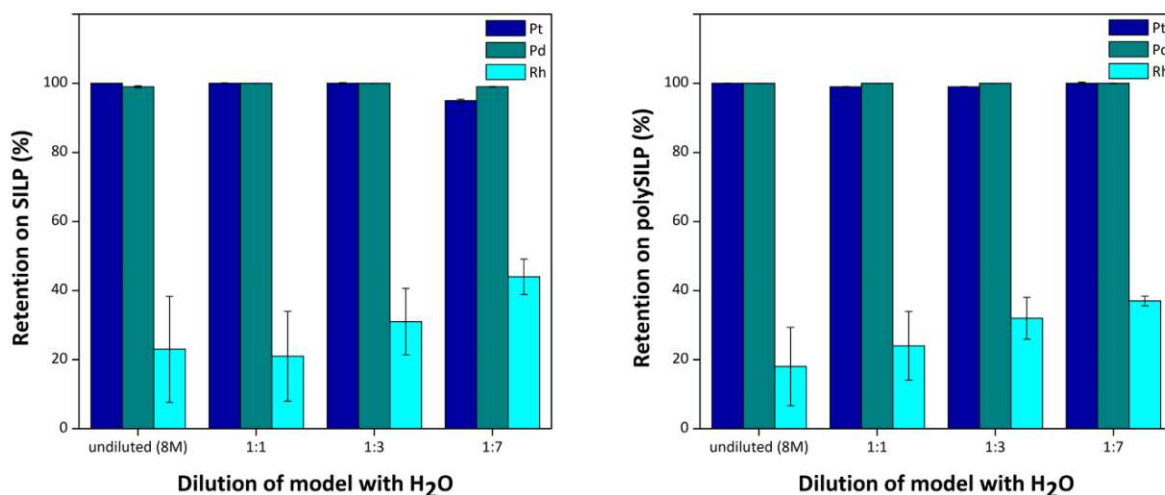


**Figure 101.** Effect of dilution on PGM retention from model solution on SILP 20% (w/w) (left) and polySILP 20% (w/w) (right).

In both cases of SILP and polySILP material, quantitative retention of Pt and Pd on the sorbent material is observed and it exhibits independency from the dilution of the model PGM solution. On the contrary, the retention of Rh is dependent on the dilution, as a lower dilution (i.e., a higher HCl concentration) yields a decrease in the retention of Rh.

Similar behavior is observed in the case that SILPs and polySILPs with loadings of 10% (w/w) (Figure 102) and 50% (w/w) (Figure 103) are employed.

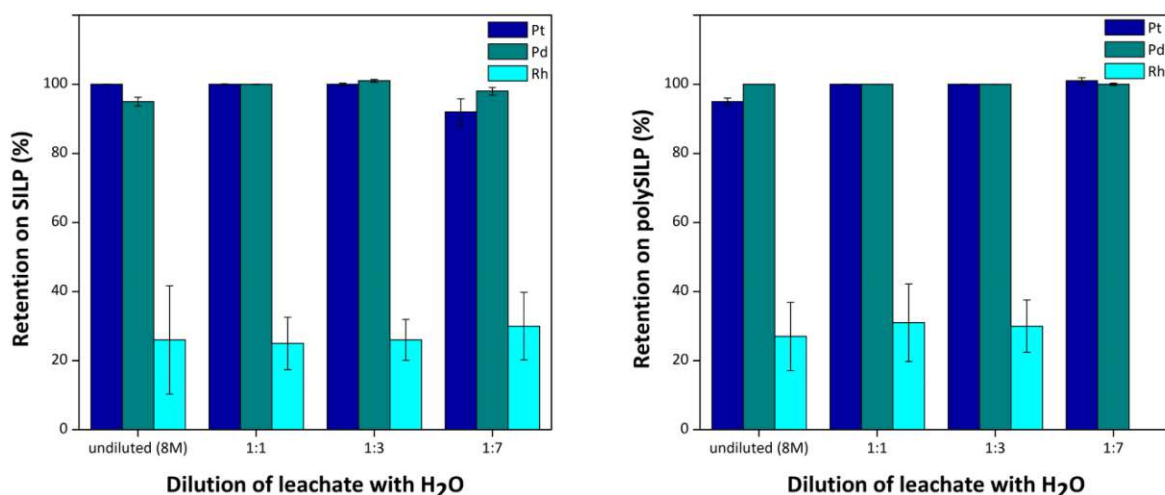


**Figure 102.** Effect of dilution on PGM retention from model solution on SILP 10% (w/w) (left) and polySILP 10% (w/w) (right).

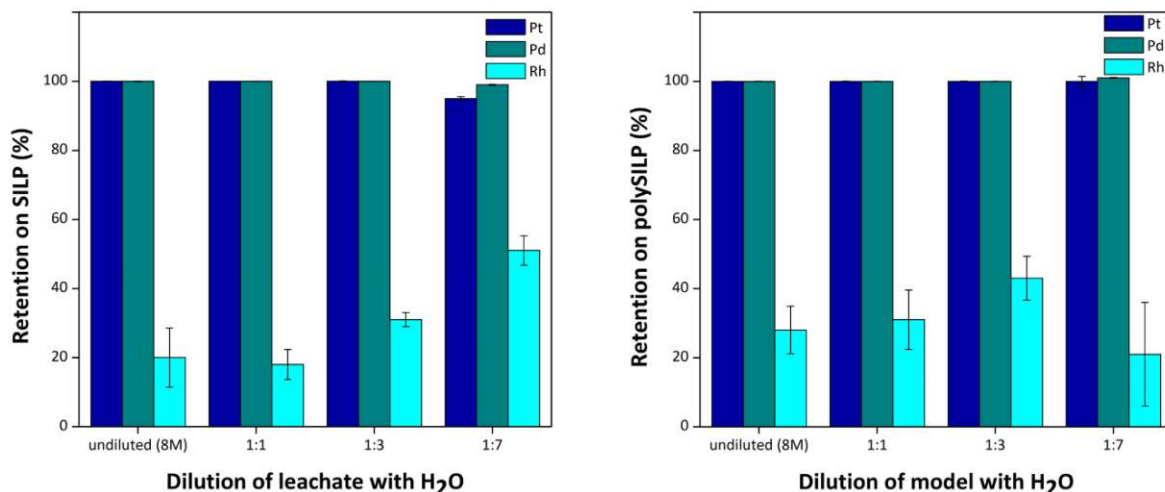


**Figure 103.** Effect of dilution on PGM retention from model solution on SILP 50% (w/w) (left) and polySILP 50% (w/w) (right).

### 6.6.5.3 Effect of IL loading on solid sorbent material

The effect of the IL loading on the sorbent material on the retention of PGMs was studied on the example of a model solution diluted on a 1:7 (w/w) ratio with H<sub>2</sub>O. In both cases of SILP and polySILP (Figure 104) material, the quantitative retention of Pt and Pd on the sorbent material is not affected by the IL loading. The retention of Rh, however, follows the trend of the increasing IL loading; increase in the loading results in higher retention of Rh on the sorbent material. The difference in the retention behavior of the PGMs might therefore be exploited in order to achieve partial separation of Pt and Pd from Rh by simply adjusting the IL loading on the sorbent material.

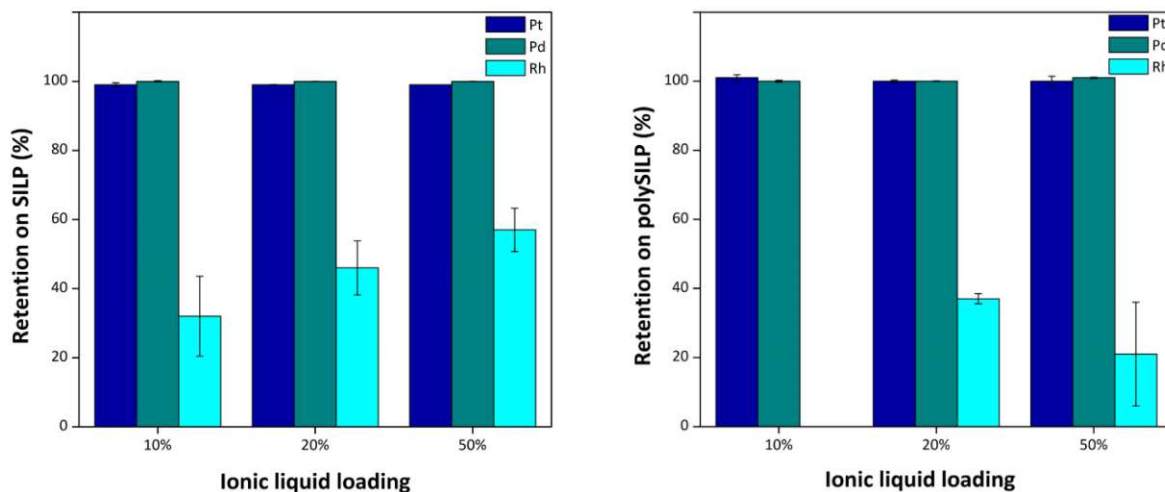


**Figure 104.** Retention behavior of PGMs from model solution diluted 1:7 (w/w), on SILP (left) and polySILP (right) with different IL loadings (w/w).

## 6.6.6 Application of optimized solid-liquid separation system to authentic car catalyst leachate

After optimization of the sorption behavior of the model solution and identification of the most suitable supported-IL phase, the development of a separation process for an authentic PGM containing solution was addressed. The effectiveness of the sorbent materials was tested on a real leachate sample in order to determine the retention behavior of PGMs as well as their recovery efficiency in the presence of other elements comprising the car catalyst matrix. For this purpose, supported-IL phases with 20% (w/w) loading were selected. The PGMs along with accompanying elements present in the catalyst matrix were leached according to the optimized conditions, and the obtained leachate was diluted with H<sub>2</sub>O on a 1:7 (w/w) ratio prior to the S-L separation.

The retention profiles of the PGMs from the leachate on the SILP 20% (w/w) and polySILP 20% (w/w) (Figure 105) are similar to the ones exhibited when model solutions are employed; quantitative retention of Pt and Pd and partial retention of Rh.

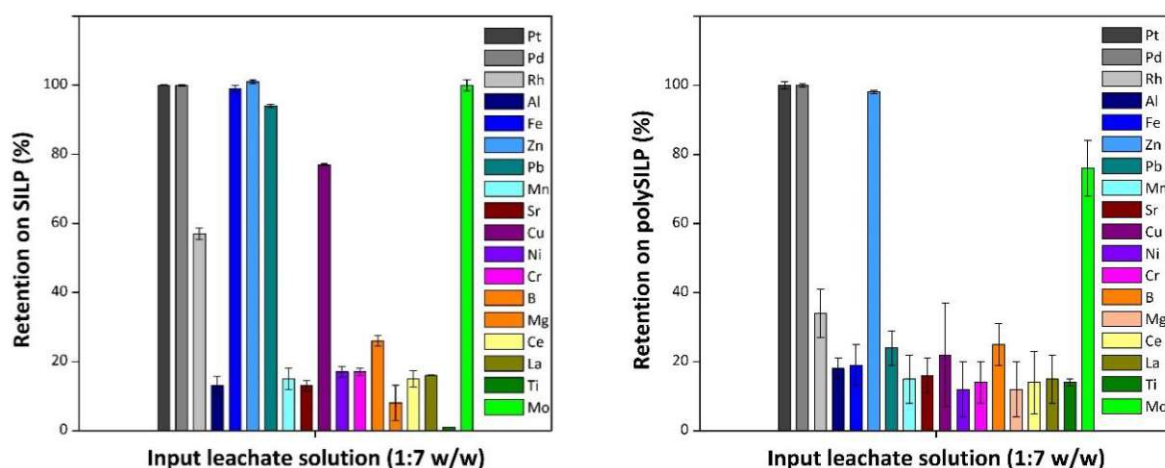


**Figure 105.** Retention behavior of PGMs and accompanying elements from automotive catalyst leachate on SILP 20% (w/w) (left) and polySILP 20% (w/w) (right).

Concerning the major interfering elements, Al, Ce, Fe and Zn, it seems that both the SILP and the polySILP have the capacity for quantitative retention of Zn. The SILP also shows high affinity for Fe, contrary to the polySILP where only partial Fe retention (20%) is observed. Furthermore, partial separation of the PGMs from Al and Ce is obtained in both cases. Overall, the polySILP 20% (w/w) is preferable to the SILP 20% (w/w) for the S-L separation process, given the fact that partial separation of the PGMs from the majority of the main interfering elements is obtained in a single separation step.

## 6.6.7 Stripping of Pt and Pd from the polySILP material

With the loading of PGMs on the sorbent material optimized, the separation of Pt and Pd from the interfering elements and their recovery was subsequently addressed. For this purpose, a stepwise stripping procedure was developed. The individual steps of the entire retention and separation process are summarized in the flowsheet presented in Figure 106.

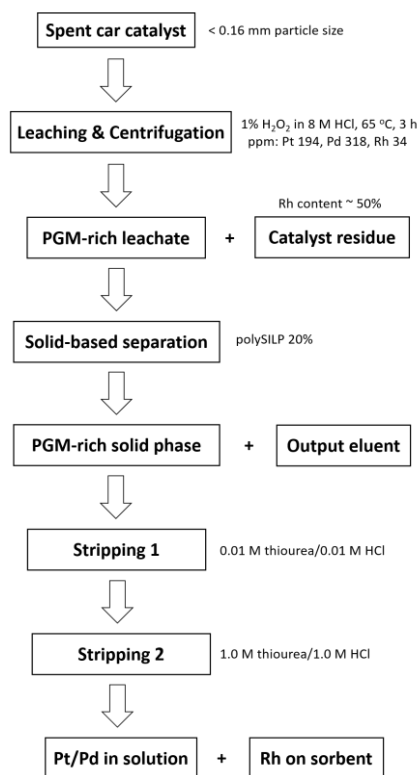


**Figure 106.** Flowsheet of PGM acidic leaching and S-L recovery process.

For the desorption of the PGMs from the sorbent material, various concentrations of the selected stripping agent were applied in a sequential order. Acidified thiourea solution (1 M thiourea/2 M HCl) has been reported as an effective stripping agent for the selective removal of Pt and Pd from a silica-based anion exchanger in the presence of Fe, Cu and Ni.<sup>312</sup> The same stripping agent (0.1 M thiourea/0.1 M HCl) has demonstrated the ability for quantitative desorption of Pt and Pd from a Dowex anion exchanger.<sup>313</sup> Employing acidified thiourea as desorption agent generates considerable matrix effects, thus all the stripped elements were quantified by a “matrix matching” approach, i.e., using acidified thiourea as a diluent for the calibration standards.

The stripping was performed in two steps with acidified thiourea solutions of different concentration levels. The 1<sup>st</sup> stripping step was performed with 0.01 M thiourea/0.01 M HCl as the stripping agent. The majority of the interfering elements was successfully removed, whereas no PGMs, except for (4 ± 2)% Pt, were desorbed from the solid sorbent material. Trace elements, Mn, Ni and Mo, were only partially removed in the 1<sup>st</sup> stripping step, while further stripping efforts with additional fractions of the stripping agent did not have any effect on stripping the PGMs or further stripping the remaining traces of interfering elements. Treatment of the loaded solids with 0.02 M thiourea/0.02 M HCl as well as 0.05 M thiourea/0.05 M HCl, generated comparable results in terms of desorption, hence the lowest concentration (0.01 M thiourea/0.01 M HCl) was selected for the 1<sup>st</sup> stripping step. For the recovery of the PGMs from the sorbent material, a 2<sup>nd</sup> stripping step was performed with a stripping solution of 1.0 M thiourea/1.0 M HCl. Pt and Pd were successfully removed from the sorbent material with a desorption of (92 ± 3)% and (100 ± 2)%, respectively. The two elements were recovered in the stripping solution with 99% purity and recoveries of 86% for Pt and 96% for Pd (Figure 107-right). The desorption of Rh was attempted with various stripping agents previously reported in the literature; 6 M HCl, 5 M NH<sub>3</sub>,<sup>235</sup> 1 M thiourea<sup>312</sup> and 1 M NaClO<sub>3</sub>/5 M HCl.<sup>311</sup> Nevertheless, none of these stripping agents was effective for the desorption of Rh from the polySILP. Rh is retained on the sorbent material along with traces of Cr, Ni and Mo.



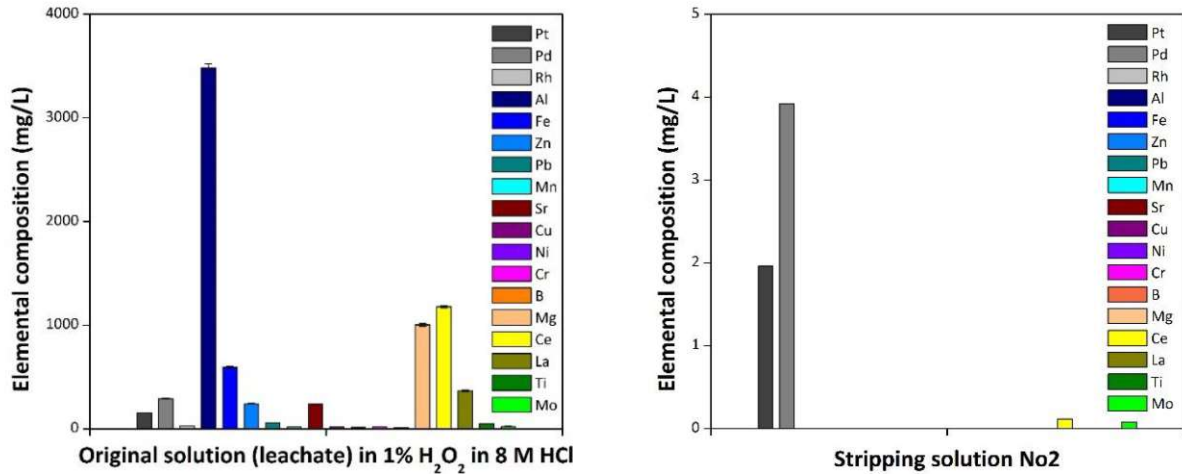


**Figure 107.** Elemental composition (mg/L) of acidic leachate solution (left) and recovered stripping solution after the 2<sup>nd</sup> stripping step (right).

### 6.6.8 Stability, capacity and recyclability of supported ionic liquid phases

The stability of the supported IL phases used for the separation is of crucial importance, since leaching of the IL out of the silica would mean decreasing capacity of the sorbent material toward PGM retention, which implies limited reuse possibility. The stability against leaching was evaluated based on the P content detected by ICP-OES measurements in the output eluents collected after the retention and stripping experiments.

The merit of polySILP materials compared to conventional SILP systems is obvious when assessing the leaching behavior of both materials, as significantly lower P contents were found in solution for the polySILP, indicating that less amount of IL is leaching out of the sorbent material in the case of the polySILPs, i.e., 10 times less than in the case of the SILPs (Table 18).

In general, PGMs have the tendency to form stable anionic chlorocomplexes in acidic chloride solutions.<sup>308,14</sup> The retention of the PGMs on the supported-IL phases can be attributed to their complexation with Cl<sup>-</sup> anions, as it has been previously reported for the L-L extraction of PGMs with ILs such as P<sub>66614</sub>Cl,<sup>205,187</sup> but also for anion-exchange resins.<sup>305</sup> The polymerized phosphonium-based salt can act as an anion exchanger,<sup>314</sup> it is thus presumed that the retention of the PGMs on the polySILP is based on the Cl<sup>-</sup> substitution by the anionic PGM-chlorocomplexes (anion-exchange mechanism).

**Table 18.** Stability of SILP and polySILP expressed in % leaching of ionic liquid.

Sorbent Material	IL Loading (%)	Retention 1:7 (w/w)	Stripping 0.01/0.01	Stripping 1.0/1.0
SILP	10	0.010	0.038	0.027
	20	0.011	0.048	0.031
	50	0.018	0.068	0.038
polySILP	10	0.002	0.003	0.004
	20	0.001	0.002	0.001
	50	0.004	0.009	0.002

In this regard, the comparison of polySILP materials with the commercially available resins that have been reported as efficient adsorbents for PGMs, such as Amberlite,<sup>235</sup> is of crucial importance. The sorbent material was loaded with leachate, the ensuing eluted fractions (5 g each) were collected and their PGM content was quantified. The sorbent loading and fraction collection was interrupted as soon as the quantification results of ten consecutive fractions were reproducible. Our studies showed a strongly increased short-term capacity of polySILP for both Pt and Pd compared to the Amberlite IRA-400 (Figure 108, left); the observed behavior implies that the polySILP retains more PGM amount *per* time unit, which can directly be translated to faster release of high PGM amounts to the market, which is highly desirable from an industrial point of view. This advantage coupled with the ability of the polySILP material to be recycled without losing any of its retention capacity, renders the polySILP a much more efficient approach for the timely satisfaction of the increasingly demanding PGM market. The complete breakthrough curves beyond the breaking point are also provided (Figure 108, right).

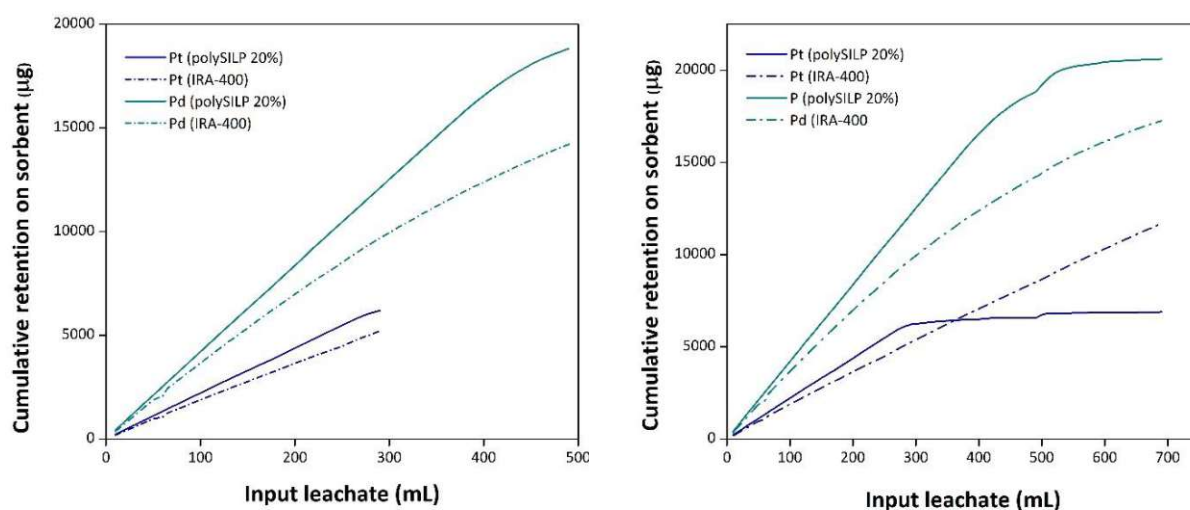


**Figure 108.** Cumulative retention capacity for Pt and Pd on polySILP 20% (w/w) versus Amberlite IRA-400, short-term (left) and complete breakthrough (right) curves.

An additional advantage of the polySILP is that it does not require equilibration prior to use, which leads to shorter experimental time and reduced generated waste. On the contrary, Amberlite can retain higher amounts of both Pt and Pd before it reaches its maximum capacity, however this is a slow process considering that it needs to be loaded with more than double the amount of leachate that the polySILP 20% (w/w) requires until it loses its retention capacity. Additionally, it has to be equilibrated and washed with solution multiple times its volume before loading.

The ease and simplicity of removing Pt and Pd should be also mentioned; in the case of polySILPs, Pt and Pd can be desorbed in a single stripping step employing acidified thiourea at RT, whereas in the case of Amberlite a two-step process with  $\text{NH}_3$  (two different  $\text{NH}_3$  concentrations consecutively applied) at elevated temperature is required for the simultaneous removal of Pt and Pd.<sup>235</sup>

Eventually, the possibility of reusing the polySILP 20% (w/w) for subsequent separation experiments was evaluated. After stripping of the PGMs and the accompanying elements from the sorbent, according to the process previously discussed in detail, the polySILP 20% (w/w) was loaded with a new fraction of acidic car catalyst leachate. The recycled column exhibited the same retention capacity for the PGMs and the accompanying elements (Figure 109). The reproducible retention behavior of the recycled sorbent material additionally verifies the stability of the IL bound on it. Nevertheless, stripping the recycled loaded sorbent with 0.01 M thiourea/0.01 M HCl did not yield comparable results to stripping fresh sorbent

material, since a considerable amount of Pt and Pd were stripped along with the interfering elements, therefore, not enabling their efficient separation and recovery.

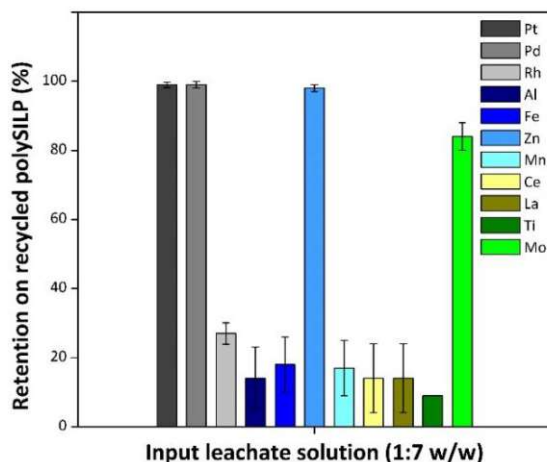


**Figure 109.** Retention behavior on recycled polySILP 20% (w/w).

It has already been demonstrated in previously published research that sufficient washing of solid sorbent materials between stripping and retention steps is necessary for regeneration of the material.<sup>239,244</sup> Therefore, the polySILP 20% (w/w) was removed from the column after completion of the 2<sup>nd</sup> stripping step and washed three times, for 8 h each, with various solvents namely H<sub>2</sub>O, 0.1 M HCl and 1.0 M HCl. Furthermore, the absence of residual thiourea after these washing steps was verified via ATR-IR (Figure 110). Nevertheless, while the retention of Pt and Pd remained excellent, the separation performance suffered with the washed and recycled sorbent material, since the majority of Pd (70%) and a considerable amount of Pt (30%) were desorbed along with the accompanying elements.

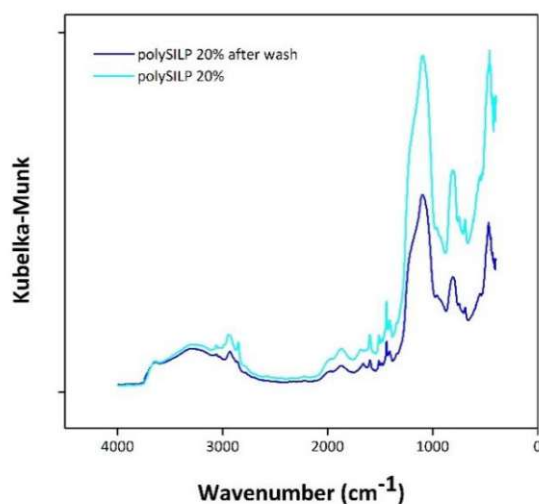


**Figure 110.** ATR-IR spectra of polySILP 20% (w/w) and stripped polySILP 20% (w/w) after washing with 0.1 M HCl.

## 7 Summary and Conclusion

A number of ILs and DESs were evaluated for their potential in extracting PGMs (Pt, Pd, Rh) from grinded car catalyst material. Several systems yielded quantitative extraction efficiencies for Pt and Pd, however, complete extraction of Rh was not possible under any conditions, a behavior which can be attributed both to the inertness of Rh as well as the presence of the hardly soluble  $\text{Rh}_2\text{O}_3$  species in the car catalyst sample. The possibility of increasing the extraction efficiency of Rh was investigated by pre-treatment (physical and chemical) of the car catalyst sample under various conditions which would allow the conversion of inert Rh species to ones that would be easier accessible to the leaching solvent. The physical pre-treatment strategies indeed affected the extraction efficiency of Rh, increasing it by approx. 25%. The leaching system choline Cl/*p*-TsOH/ $\text{HNO}_3$  yielded the maximum extraction efficiencies for the three target PGMs, while its relatively simple scalability and reasonable price are a promising aspect for industrially-relevant scales. Additionally, the developed method is an alternative to the extraction of PGMs from EOL car catalysts with an environmentally sound and more energy efficient outcome than the state-of-the-art methods, considering both the biodegradability of choline Cl and the possibility to recycle the DES, as well as the mild process parameters.

For the subsequent separation of PGMs, two strategies relying on ILs, either in liquid form or immobilized on a solid support material, were evaluated. For the L-L separation, a number of phosphonium-based ILs was evaluated for their potential in extracting PGMs from DESs as well as separating them from accompanying elements.

While several candidates yielded high extraction efficiencies for all three PGMs, only  $\text{P}_{66614}\text{Cl}$  and  $\text{P}_{66614}\text{B2EHP}$  proved suitable for complete extraction of all three target PGMs from the DES. Additionally, the phosphonium IL  $\text{P}_{66614}\text{Cl}$  is commercially available, which means reduction of time-consuming synthetic efforts. Contrary to reports on the literature, adjustment of the acidity of the PGM-containing DES phase did not lead to separation of Rh from Pt and Pd. The idea of recycling and reusing the hydrophilic IL after an entire leaching/separation cycle was investigated as a means of creating an approach that would be more financially sound and environmentally compatible in terms of generated waste. The DES proved to be equally efficient in the PGM extraction after recycling, however, the *p*-TsOH component migrated to the phosphonium IL during L-L separation, therefore, redosing of the IL before a new leaching cycle was required. The phosphonium IL remained stable during L-L separation, however, it was enriched with *p*-TsOH migrating from the DES leachate.

A novel supported IL-based method for the separation of PGMs was also developed and evaluated. PolySILPs exhibited higher efficiency than SILPs for separation of PGMs from accompanying interfering elements, as well as higher stability toward leaching of the IL out of the sorbent material. Contrary to conventionally used silica bead-based sorbent materials, polySILPs are markedly characterized by their high porosity and no requirement of pre-conditioning. Separation of Pt and Pd from Rh and other interfering elements and recovery of Pt and Pd in solution was successfully performed with successive application of acidified thiourea solutions. A recovery of Pt and Pd of 86% and 96%, respectively, in the stripping solution was obtained. While the retention efficiency for Pt and Pd was maintained in the recycled polySILP, the separation of Pt and Pd from interfering elements was no longer possible, indicating that further improvements for the recycling of the spent material are required. Overall, the developed method was highly efficient, fast and simple to implement.

In conclusion, extraction and separation methods for PGMs, characterized by speed, simplicity, mild conditions and highly satisfactory PGM recoveries, were developed in the course of this work (Figure 111). The feasibility of upscaling of the developed processes and the possibility of recycling of the

employed DES/IL are features that are compatible with industrial upscaling; however, further investigation is warranted to conclusively assess if this possibility is tangible.

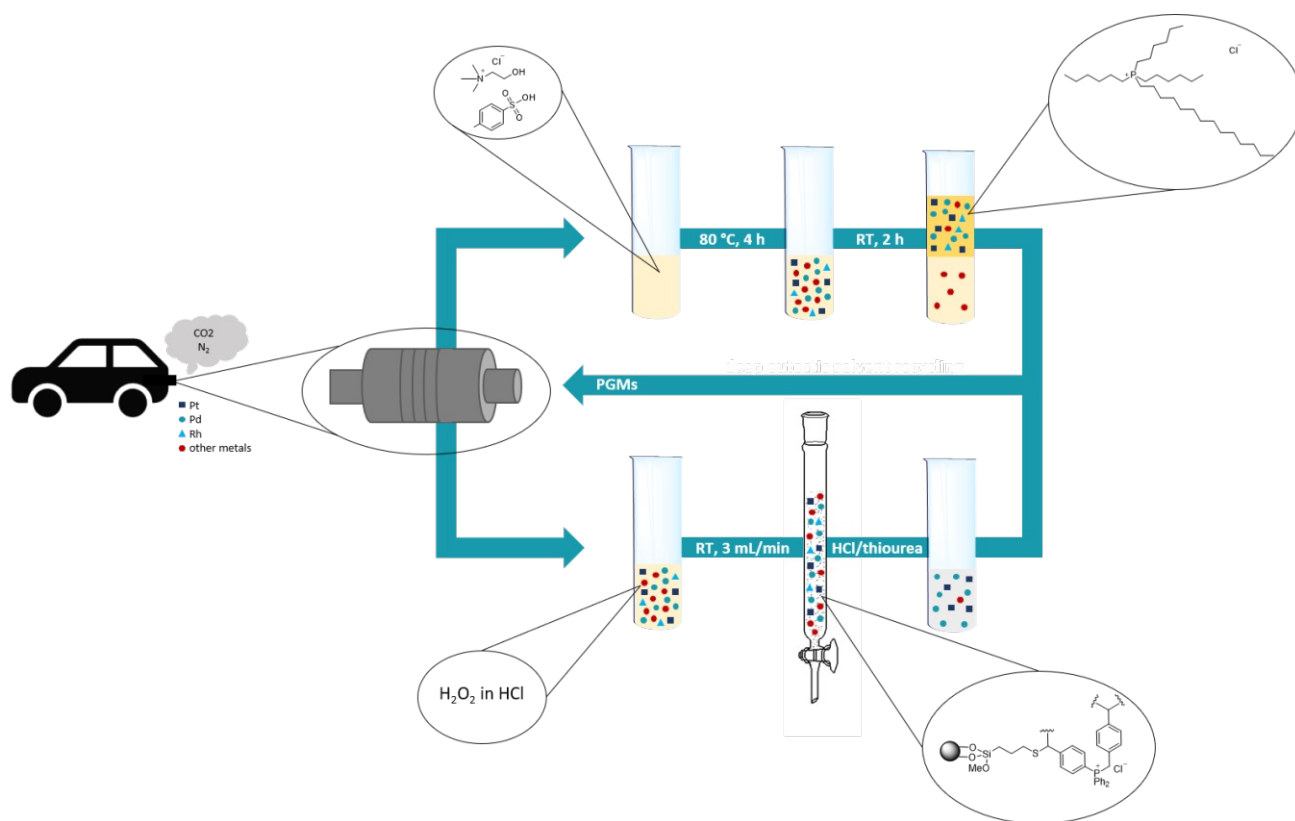


**Figure 111.** Summary of processes developed within the course of the work for PGM extraction and separation.

## 8 Outlook

Within the course of this work, the potential of ILs and DESs in the recovery process of PGMs from spent car catalysts was investigated and presented. The parameters for complete recovery of Pt and Pd and satisfactory recovery of Rh from the spent material were successfully established. Among the developed separation strategies, the liquid-liquid one managed to easily solve the challenging removal of the interfering Al from the car catalyst leachate, while the solid-liquid one demonstrated a promising outcome worthy of further investigation.

The straightforward approach and the high PGM recovery of the DES-based leaching warrants further investigation into the possibility of its application for the recovery of PGMs from different sources, such as electrical and electronic waste and slag. Obviously, optimization of the leaching parameters is expected for their adjustment to the requirements of the specific target material; nevertheless, considering the potential for upscaling of the process, there is merit in these additional investigations. At the same time, in response to any reservations regarding the viscosity of the DES and the bottlenecks it might create at larger scales, the possibility to dilute the DES with H<sub>2</sub>O with simultaneous retention of its extraction capability should be considered as a solution that could significantly facilitate its large-scale implementation.

Concerning the liquid-liquid separation, the phosphonium-based hydrophobic IL loaded with the PGMs could ideally serve as an input material for electrodeposition-based recovery. Although this task is beyond the expertise of the research group, such investigation is worth the effort in light of the importance of PGM recovery. Additionally, pursuing such a task could forge new relationships and mutually advantageous collaborations of the group with scientific experts from different fields of study.

The ease of handling and high speed of the solid-liquid separation is an undoubtedly attractive feature of this approach. While recovery of Pt and Pd with sorbent materials is quite high, the recovery of Pt can still be improved while the case of Rh definitely deserves the highest attention. The complexity of Rh, which is a well-known issue, mandates deeper research in order to understand and hopefully be able to, at least at a certain extent, control its behavior. Without deeper investigation into the type of Rh-complexes retained on the solid material, any efforts to strip it will lack proper justification and will be rather based on pure luck. Of course, the incomplete retention of Rh on the solid material is an entirely different and equally, if not more, complicated topic. Unfortunately, this separation strategy will not be beneficial for any long-term applications, since at this point, with the recycled polySILP, the separation of Pt and Pd from interfering elements is no longer possible, indicating that a closer look at the structure of the material following stripping experiments could be the answer to the change in the behavior of the material. Overcoming these issues, could probably allow consideration of this approach for a long-term and larger-scale application due to its attractive features of efficiency, speed and simplicity, while there is a clear merit in addressing different types of PGM-containing matrices with this approach.



## 9 Experimental Part

### 9.1 Materials and methods

#### 9.1.1 Chemicals and reagents

All reagents employed in the method development were of analytical grade, unless otherwise stated. Individual stock solutions of Pt, Pd and Rh, 1000 ppm in 5% HCl, were obtained from Sigma-Aldrich, Germany and used for the preparation of the model solutions and calibration standard solutions. Stock solution of In 1000 ppm in 2-3% HNO<sub>3</sub>, was also obtained from Sigma-Aldrich, Germany. Multi-element standard VIII in 2-3% HNO<sub>3</sub> was purchased from Merck, Germany. Concentrated HCl 37% and HNO<sub>3</sub> 65% were purchased from Merck, Germany. H<sub>2</sub>O<sub>2</sub> 30% was obtained from Sigma, Germany. NaCl was purchased from Sigma-Aldrich, Germany and thiourea from Merck, Germany. Choline Cl<sub>≥</sub>98% was purchased from Sigma, Germany and *p*-TsOH from Fluka, Germany. P<sub>66614</sub>Cl was purchased from Iolitec, Germany and P<sub>66614</sub>DOP from Sigma Aldrich, Germany. The rest of the ILs were synthesized in-house. The compounds used to provide the anion to the synthesized ILs were all purchased from Sigma Aldrich, Germany.

The organic solvents used for the preparation of the SILPs and polySILPs were of the highest purity. MeOH, EtOH, CH<sub>2</sub>Cl<sub>2</sub> and toluene were obtained from Merck, Germany. Silica 60 (size 40-60 μm, specific surface area 480-540 m<sup>2</sup>/g) was also obtained from Merck, Germany. The compounds (3-mercaptopropyl) trimethoxysilane >96%, 4-vinylbenzyl chloride >90%, 4-(diphenylphosphino) styrene 97% and 2,2'-azobis(2-methylproprionitrile) (AIBN) 98% were all purchased from Sigma-Aldrich, Germany.

The car catalyst material employed in this work was provided by Monolithos Ltd. (Athens, Greece). The grinding size of the provided catalyst powder was <0.16 mm. The certified reference material ERM-EB504 was also purchased from Sigma Aldrich, Germany.

High purity water was supplied by an Easipure water system (Thermo, USA, resistivity 18 MΩ·cm<sup>-1</sup>).

#### 9.1.2 Instrumentation

##### ICP-MS

The leaching efficiencies of the PGMs were quantified with the aid of an ICP-MS (Thermo iCAP-PQ, Thermo Scientific, USA) with an ESI SC-2 DX autosampler and a sample introduction kit consisting of a V-groove nebulizer (Thermo Scientific, USA), a gas cyclonic spray chamber with a riser tube and a torch injector tube with 2 mm inner diameter.

##### ICP-OES

The leaching efficiencies of the PGMs were quantified with the aid of a radial ICP-OES (Thermo iCAP 6500, Thermo Scientific, USA) with a sample introduction kit consisting of a parallel path nebulizer (PEEK Mira Mist, Thermo Scientific, Canada), a gas cyclonic spray chamber with a riser tube and a torch injector tube with 2 mm inner diameter. Background corrected emission signals in ICP-OES were recorded and processed using Qtegra 2.10 software (Thermo Scientific, USA).

## NMR

$^1\text{H}$ -,  $^{13}\text{C}$ - and  $^{31}\text{P}$ -NMR spectra were recorded from  $\text{CDCl}_3$ ,  $\text{CD}_2\text{Cl}_2$ ,  $d_4\text{-MeOD}$  or  $d_6\text{-DMSO}$  solutions on a Bruker AC 200 (200 MHz) or Bruker Avance UltraShield 400 (400 MHz) spectrometer. Chemical shifts ( $\delta$ ) are reported in ppm using tetramethylsilane as internal standard and coupling constants ( $J$ ) are given in Hertz (Hz). The following abbreviations are used to explain the multiplicities; s = singlet, d = doublet, t = triplet, q = quartet, quin = quintet, sext = sextet, m = multiplet.

## IR

DRIFT-IR spectra were recorded with a Bruker Vertex 80FT-IR spectrophotometer using a narrow band MCT (mercury-cadmium-telluride) detector measuring diffuse reflectance. 256 scans were collected for each spectrum with  $4\text{ cm}^{-1}$  resolution. All samples were dried for at least 24 h under reduced pressure (0.1 mbar) prior to measurement.

ATR-IR spectra were recorded on a Perkin Elmer Spectrum 65 ATR-FT-IR spectrometer in the region from  $4000\text{-}600\text{ cm}^{-1}$ . All samples were dried for at least 24 h under reduced pressure (0.1 mbar) prior to measurement.

## TGA

TGA analysis was performed on a Netzsch STA 449 F1 system. The temperature was increased from 25 to  $500\text{ }^\circ\text{C}$  with a rate of  $5\text{ }^\circ\text{C}/\text{min}$ . Nitrogen gas flow was set to  $40\text{ mL}/\text{min}$ . All samples were dried for at least 24 h under reduced pressure (0.1 mbar) prior to measurement.

## BET

BET curves were acquired with an ASAP 2020 from Micromeritics GmbH at 77K. All samples were dried for at least 24 h under reduced pressure (0.1 mbar). Prior to measurement, samples were degassed in vacuum at  $180\text{ }^\circ\text{C}$  for 6 h to remove moisture and adsorbed gases. For elucidation of the specific surface area and pore size distribution, the BET model and Barret-Joyner-Halenda (BJH) method were used, respectively.

## SEM

The images were recorded with a FEI Quanta 200 microscope equipped with an EDAX Octane Pro detector. Data were processed with the Team Enhanced software. All samples were dried for at least 24 h under reduced pressure (0.1 mbar) prior to measurement.

## UHPLC-MS

A Shimadzu Nexera chromatographic unit with a C4 reversed phase column (Waters Acquity UPLC protein BEH,  $300\text{ \AA}$ ,  $1.7\text{ }\mu\text{m}$ ,  $2.1\times 50\text{ mm}$ , oven T:  $40\text{ }^\circ\text{C}$ , flow rate  $1\text{ mL}/\text{min}$ , mobile phase: 1%  $\text{HCOOH}$  in  $\text{H}_2\text{O}$  and  $\text{MeOH}$ ) and an ELS (Jasco ELS-2041) detector was used. The mass spectroscopic detection was performed with a MS detector (Shimadzu LCMS-2020), with ESI in a negative (-) and positive (+) ionization mode.

## Centrifuges

The separation of the car catalyst material from the leaching solution on a small scale was performed via centrifugation in a Microstar 12 tabletop centrifuge (VWR, Germany). The separation of the car catalyst material from the leaching solution on the upscaled version was performed via centrifugation in a Heraeus Megafuge 16 centrifuge.

## Microwave

The spent car catalyst used in this study was digested with the aid of a mixture of mineral acids in a microwave oven (Multiwave 3000, Anton Paar, Germany). The following digestion programme was employed; 8:00 min at 500 W; hold 8:00 min; 15:00 min at 900 W; hold 35:00 min.

## XRD

The XRD measurements were carried out on a PANalytical X'Pert Pro diffractometer using Cu K- $\alpha$  radiation. The diffractograms were evaluated using the PANalytical program suite HighScorePlus v3.0d with background correction.

## 9.2 Experimental and analytical protocols

### 9.2.1 Leaching procedures

#### 9.2.1.1 Leaching in DES

The leaching process was performed as follows: (0.1000 ± 0.0050) g milled car catalyst were mixed with (0.5000 ± 0.0100) g DES/IL and (0.1000 ± 0.0050) g oxidizing agent. The mixture was stirred at 80 °C for 4 h. The mixture was subsequently centrifuged for 5 min at 15000 rpm (small scale) or 45 min at 15000 rpm (upscaling) for the sedimentation of the solid car catalyst material. The liquid phase was recovered and appropriately diluted prior to PGM quantification. The leaching efficiency was calculated as follows:

$$\% \text{ leaching efficiency} = \frac{\mu\text{g of } M \text{ in the leachate}}{\mu\text{g of } M \text{ in amount of catalyst powder (prior to leaching)}} * 100,$$

where M= metal.

#### 9.2.1.2 Leaching in mineral acid

The leaching process was performed as follows: (0.1000 ± 0.0050) g milled car catalyst were mixed with (0.5000 ± 0.0100) g 1% H<sub>2</sub>O<sub>2</sub>/8 M HCl. The mixture was stirred at 65 °C for 3 h. The mixture was subsequently centrifuged for 5 min at 15000 rpm for the sedimentation of the solid car catalyst material. The liquid phase was recovered and appropriately diluted prior to PGM quantification. The leaching efficiency was calculated based on the following equation:

$$\% \text{ leaching efficiency} = \frac{\mu\text{g of } M \text{ in the leachate}}{\mu\text{g of } M \text{ in amount of catalyst powder (prior to leaching)}} * 100,$$

where M= metal.

### 9.2.2 Separation procedures

#### 9.2.2.1 Liquid-liquid separation procedure

For the L-L separation, (0.2000 ± 0.0050) g model solution/DES leachate was mixed with (0.2000 ± 0.0050) g H<sub>2</sub>O to create the hydrophilic phase. For the hydrophobic phase, (0.2000 ± 0.0050) g phosphonium IL was mixed with (0.2000 ± 0.0050) g *n*-heptane. The 2 phases were mixed on a 1:1 (w/w) ratio and stirred at RT for 2 h. The mixture was subsequently centrifuged for 5 min at 15000 rpm (small scale) or 45 min at 15000 rpm (upscaling) for the separation of the 2 phases. The extraction efficiency from the hydrophilic to the hydrophobic IL was calculated based on the following equation:

$$\% \text{ extraction efficiency} = \frac{\mu\text{g of } M \text{ in input hydrophilic phase} - \mu\text{g of } M \text{ in output hydrophilic phase}}{\mu\text{g of } M \text{ in input hydrophilic phase}} * 100,$$

where M= metal.

#### 9.2.2.2 Solid-liquid separation procedure

For the S-L separation, an in-house column packed with (0.5000 ± 0.0100) g solid sorbent material (SILP or polySILP) was prepared, wherein it was immobilized by addition of glass wool. On top of the column (2.5000 ± 0.0100) g diluted leachate (1:7 w/w dilution with H<sub>2</sub>O) were pipetted and forced through it via application of constant air flow (3 mL/min). The output leachate was collected and appropriately diluted prior to PGM quantification. The retention efficiency of the metals was calculated according to the following equation:

$$\% \text{ retention} = \frac{\mu\text{g of } M \text{ in input solution} - \mu\text{g of } M \text{ in collected eluent}}{\mu\text{g of } M \text{ in input solution}} * 100,$$

where M= metal.

For the breakthrough curves, (690 ± 50) g diluted catalyst leachate 1:7 (w/w) were loaded on the polySILP 20% (w/w). An in-house column was packed with (0.5000 ± 0.0100) g Amberlite IRA-400 and (670 ± 50) g diluted catalyst leachate 1:7 (w/w) were loaded on it.

### 9.2.3 Stripping procedure

The stripping was performed in two steps with acidified thiourea solutions of different concentration levels. The 1<sup>st</sup> step was performed with 0.01 M thiourea/0.01 M HCl as the stripping agent. A total of 10 g stripping agent was required to achieve the reported desorption percentages. The 2<sup>nd</sup> step was performed with 1.0 M thiourea/1.0 M HCl as the stripping agent and a total of 30 g stripping agent was required to achieve the reported desorption percentages. The stripping efficiencies of the metals were calculated according to the following equation:

$$\% \text{ stripped} = \frac{\mu\text{g of } M \text{ retained on solid} - \mu\text{g of } M \text{ in eluted stripping agent}}{\mu\text{g of } M \text{ retained on solid}} * 100,$$

where M= metal and  $\mu\text{g of } M \text{ retained on solid} = \mu\text{g of } M \text{ in input solution} - \mu\text{g of } M \text{ in collected eluent}$ .

### 9.2.4 Measurement procedure

#### 9.2.4.1 Measurements with ICP-MS

The PGM quantification in the optimization experiments of DES-based leaching was performed with ICP-MS. Calibration curves were determined with a set of six standards in the range of 10-60 ppb. The standard and sample solutions were appropriately diluted in a 1%EtOH-5% HCl diluent.

The quantification of PGMs was conducted within a 24 h frame from the completion of the leaching process.

Five procedural replicas of each sample were prepared and each replica was measured five times. Blank solutions with composition identical to the diluent were used for the determination of limits of detection and quantification. Indium was used as internal standard and the recorded element specific signals were corrected using the <sup>115</sup>In isotope.

The following isotopes were used for the quantification of each metal: <sup>194</sup>Pt, <sup>195</sup>Pt, <sup>105</sup>Pd, <sup>106</sup>Pd, <sup>108</sup>Pd, <sup>103</sup>Rh. More than one isotopes, where applicable, were used for quality control purposes. The instrumental parameters used for quantification with ICP-MS are presented in Table 19.

**Table 19.** ICP-MS instrumental measurement parameters.

<b>Instrument</b>	iCAP-PQ (Thermo Scientific, USA)
<b>Software</b>	Qtegra 2.10 (Thermo Scientific, USA)
<b>RF Power</b>	1500 W
<b>Torch Internal Diameter</b>	2.0 mm
<b>Nebulizer</b>	V-groove nebulizer (Thermo Scientific, USA)
<b>Nebulizer Gas Flow</b>	1.0 L/min
<b>Coolant Gas Flow</b>	15 L/min
<b>Auxiliary Gas Flow</b>	0.80 L/min
<b>Collision Gas (He) Flow</b>	2.3 mL/min
<b>CCT Bias</b>	-2.00 V
<b>Sample Introduction Flow Rate</b>	0.70 mL/min
<b>Viewing Height</b>	10 mm
<b>Dwell Time</b>	0.01 sec
<b>Observation Time per Measurement</b>	5 sec
<b>Number of Replicates per Measurement</b>	5

## 9.2.4.2 Measurements with ICP-OES

### 9.2.4.2.1 Measurements of PGMs and other elements

All other quantification tasks were performed with ICP-OES. Calibration functions for ICP-OES analysis were determined using a set of six standards in the range of 500-12000 ppb for the PGMs and a set of five calibration standards in the range of 1000-30000 ppb for the other quantified elements (Al, Fe, Zn, Pb, Mn, Sr, Cu, Ni, Cr, B, Mg, Ce, La, Ti, Mo). The standard and sample solutions were appropriately diluted in a 1%EtOH-5% HCl diluent (for measurement in hydrophilic ILs and DESs) or in 5% HCl diluent (for measurements in aqueous/acidic solutions). The standard and sample solutions corresponding to the stripping experiments were diluted in a HCl/thiourea diluent, where the concentration of HCl and thiourea were accordingly adjusted to achieve “matrix matching” between standards and samples.

The quantification of PGMs in the ILs/DESs was conducted within a 24 h frame after the completion of the leaching/partition in the DES/IL. Five procedural replicas of each sample were prepared and each replica was measured five times. Blank solutions with composition identical to the diluent were used for the determination of limits of detection and quantification. Indium was used as internal standard and the recorded element specific signals were corrected using the emission line at 230.606 nm.

More than one emission lines, where applicable, were used for quality control purposes. The instrumental parameters and the emission wavelengths used for quantification with ICP-OES are presented in Tables 20 and 21.

**Table 20.** ICP-OES instrumental measurement parameters.

<b>Instrument</b>	Radial iCAP 6500 (Thermo Scientific, USA)
<b>Software</b>	Qtegra 2.10 (Thermo Scientific, USA)
<b>RF power</b>	1400 W
<b>Torch Internal Diameter</b>	2.0 mm
<b>Nebulizer</b>	Burgener PEEK Mira Mist (Thermo Scientific, Canada)
<b>Nebulizer Gas Flow</b>	0.70 L/min
<b>Coolant Gas Flow</b>	12 L/min
<b>Auxiliary Gas Flow</b>	0.80 L/min
<b>Sample Introduction Flow Rate</b>	0.70 mL/min
<b>Viewing Height</b>	10 mm
<b>Exposure Time (in Vis)</b>	10 sec
<b>Observation Time <i>per</i> Measurement</b>	5 sec
<b>Number of Replicates <i>per</i> Measurement</b>	5



**Table 21.** Selected emission wavelengths for elemental quantification.

Element	Quantification Wavelength	Quality Control Wavelength
Pt	265.945	214.423
Pd	340.458	324.270
Rh	343.489	369.236
Al	309.271	237.312
Fe	259.940	238.204
Zn	213.856	202.548
Sr	407.771	421.552
Mg	279.553	280.270
Ca	315.887	318.128
Pb	220.353	216.999
Ce	456.236	380.152
Cu	324.754	327.396
Ni	221.647	231.604
Mn	257.610	293.930
Cr	267.716	-
Ba	455.403	-
B	249.773	249.678
Mo	202.030	-
La	261.034	-
Ti	334.941	308.802

#### 9.2.4.2.2 Measurement of phosphorus

The concentration of P was measured with the aid of ICP-OES. Prior to analysis the samples were diluted (1:2 w/w) with 1% (v/v) HCl and Se was added as internal standard (5 ppm in final solution). Stock solution for P was prepared from  $\text{NaH}_2\text{PO}_4 \cdot 2\text{H}_2\text{O}$  (analytical grade). The calibration standards were prepared by appropriate dilution of the stock solution with 1% (v/v) HCl.

Samples and standards were analyzed with an ICP-OES equipped with a conventional Meinhard-type glass nebulizer and a quartz cyclone spray chamber. Background-corrected emission signals were recorded in the radial viewing mode and the emission lines 213.618 nm, 178.284 nm and 177.495 nm were used for the quantification and quality control of P. Three replicates with an integration time of 10 sec each were measured for samples as well as standard solutions. The observed signal intensities were normalized using the signal response of the internal standard (Se, emission line 196.090 nm) and converted into concentration units by means of external aqueous calibration. Derived Se signals were constant over each measurement session (RSD<5% for the whole measurement run, indicating the absence of temporal trends) and no significant difference in Se response between samples and calibration standards was observed. The instrumental parameters used for quantification of P are presented in Table 22.

**Table 22.** ICP-OES instrumental measurement parameters for phosphorus.

<b>Instrument</b>	iCAP-PQ (Thermo Scientific, USA)
<b>Software</b>	Qtegra 2.10 (Thermo Scientific, USA)
<b>RF Power</b>	1400 W
<b>Torch Internal Diameter</b>	2.0 mm
<b>Nebulizer</b>	V-groove nebulizer (Thermo Scientific, USA)
<b>Nebulizer Gas Flow</b>	0.8 L/min
<b>Coolant Gas Flow</b>	15 L/min
<b>Auxiliary Gas Flow</b>	2 L/min
<b>Viewing Height Above Load-coil</b>	9 mm
<b>Number of Replicates per Measurement</b>	5

## 9.3 Synthesis of ionic liquids and deep eutectic solvents

### 9.3.1 Choline-based deep eutectic solvents

The typical procedure for the synthesis of choline based DESs is shown on the example of choline Cl/*p*-TsOH.

A 100 mL round-bottom flask was charged with choline Cl (8.0 g, 0.057 mol) and *p*-TsOH monohydrate (19.7 g, 0.103 mol). The flask was placed on a thermostated heating block at 80 °C and the mixture was stirred with a magnetic stirring bar for 60 min until complete liquefaction of the materials. The product was obtained in quantitative yield as a dark pink viscous liquid (Figure 112).

#### Analysis

$^1\text{H-NMR}$  (400 MHz,  $\text{DMSO-d}_6$ )  $\delta$ (ppm) = 7.50 (d,  $J = 8.0$  Hz, 1H), 7.14 (d,  $J = 8.1$  Hz, 1H), 6.16 (s, 3H), 3.81 (td,  $J = 5.3, 2.9$  Hz, 1H), 3.45-3.37 (m, 1H), 3.11 (s, 3H), 2.29 (s, 1H).

$^{13}\text{C-NMR}$  (101 MHz,  $\text{DMSO-d}_6$ )  $\delta$ (ppm) = 145.45, 138.59, 128.71, 125.95, 67.37, 55.61, 53.52, 21.26.

IR  $\nu_{\text{max}}$  ( $\text{cm}^{-1}$ ): 3367 (N-H stretch), 1600, 1477 (C=C aromatic bending), 1230 (S=O), 1123, 1031, 1006.

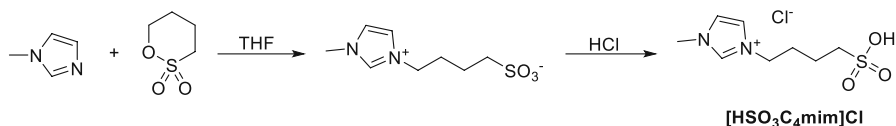


**Figure 112.** Starting materials choline Cl (front left), *p*-TsOH (front right) and the DES choline Cl/*p*-TsOH (back).

Choline-based DESs tend to form crystals during their storage at RT, which can be dissolved by mildly heating and stirring the DES before use.

### 9.3.2 Brønsted acidic ionic liquids

The typical procedure for the synthesis of Brønsted acidic ILs is shown on the example of  $[\text{HSO}_3\text{C}_4\text{mim}]\text{Cl}$ .



Step 1:

In a 100 mL round-bottom flask equipped with septum and reflux condenser, 1-methylimidazole (10.09 g, 0.122 mol) was dissolved on anhydrous THF (50 mL) under Ar atmosphere. 1,4-butansultone (16.59 g, 0.1225 mol) was added slowly to the mixture via syringe. The mixture reacted at 80 °C with magnetic stirring for 17 h. The solid material produced was collected via filtration and washed with  $\text{Et}_2\text{O}$

(100 mL). The crude product (20 g) was pre-dried for 2 h (40 °C, 20 mbar). Remaining volatile traces were removed under high vacuum (0.1 mbar) to obtain the intermediate zwitterion as colorless solid in 72% yield.

#### Step 2:

The crude zwitterion obtained in step 1 (5.05 g, 0.0321 mol) was dissolved in a mixture of H<sub>2</sub>O (20 mL) and EtOH (20 mL) in a 100 mL round-bottom flask. Subsequently, concentrated hydrochloric acid (2.32 g, 0.0229 mol) was slowly added to the mixture. The mixture was vigorously stirred for 20 min at RT and the solvent was evaporated at reduced pressure. The mixture was then dried for 24 h under high vacuum (0.1 mbar) at 50 °C with stirring. The pure Brønsted acidic IL was isolated as a colorless viscous liquid in 95% yield.

#### Analysis

<sup>1</sup>H-NMR (400 MHz, Deuterium Oxide) δ(ppm) = 8.65 (s, 1H), 7.38 (d, J = 23.8 Hz, 2H), 4.71 (s, 4H), 4.16 (t, J = 7.0 Hz, 2H), 3.80 (d, J = 1.5 Hz, 2H), 2.93-2.76 (m, 2H), 1.93 (p, J = 7.2 Hz, 2H), 1.71-1.59 (m, 2H).

<sup>13</sup>C-NMR (101 MHz, Deuterium Oxide) δ(ppm) = 135.95, 123.63, 122.14, 50.03, 48.89, 35.64, 28.07, 20.90.

IR ν<sub>max</sub> (cm<sup>-1</sup>): 3151 (N-H stretch), 3093, 2942, 2878, 1567, 1464 (C=C aromatic bending), 1158, 1035.

### 9.3.3 Protic ionic liquids

The typical procedure for the synthesis of protic ILs is shown on the example of [EtNH<sub>3</sub>][NO<sub>3</sub>-Cl].

A round-bottom flask equipped with a dropping funnel and a stirring bar was charged with a solution of EtNH<sub>2</sub> in H<sub>2</sub>O (9.47 g, 0.21 mol) and cooled to 0 °C in an ice bath. Concentrated HNO<sub>3</sub> (6.62 g, 0.11 mol) and concentrated HCl (3.82 g, 0.11 mol) were added dropwise, and the reaction mixture was stirred for 2 h, at 0 °C. Volatile materials were evaporated (40 °C, 20 mbar) to obtain the protic IL as colorless viscous liquid in quantitative yield.

#### Analysis

<sup>1</sup>H-NMR (400 MHz, Deuterium Oxide) δ(ppm) = 8.65 (s, 1H), 7.38 (d, J = 23.8 Hz, 2H), 4.71 (s, 4H), 4.16 (t, J = 7.0 Hz, 2H), 3.80 (d, J = 1.5 Hz, 2H), 2.93-2.76 (m, 2H), 1.93 (p, J = 7.2 Hz, 2H), 1.71-1.59 (m, 2H).

<sup>13</sup>C-NMR (101 MHz, Deuterium Oxide) δ(ppm) = 135.95, 123.63, 122.14, 50.03, 48.89, 35.64, 28.07, 20.90.

IR ν<sub>max</sub> (cm<sup>-1</sup>): 2987 (N-H stretch), 1616 (N-H), 1512 (N-H), 1312 (C-H), 1043.

### 9.3.4 Hydrophobic ionic liquids

A typical procedure for the synthesis of hydrophobic ILs is shown on the example of P<sub>66614</sub>Cl·HSO<sub>4</sub>.

A 100 mL round-bottom flask was charged with P<sub>66614</sub>Cl (21.3 g, 0.04 mol) and H<sub>2</sub>SO<sub>4</sub> (4.2 g, 0.04 mol) was added dropwise. The reaction mixture was connected to a trap filled with NaOH pellets and evacuated (0.1 mbar) with stirring for 24 h. The resulting mixture was dissolved in CH<sub>2</sub>Cl<sub>2</sub> (100 mL) and H<sub>2</sub>O (100 mL) was added to the mixture. The formed phases were separated and the organic phase was washed with H<sub>2</sub>O (six times, 100 mL each). The organic phase was dried over Na<sub>2</sub>SO<sub>4</sub>, evaporated, and the residue was placed under vacuum for 3 h (40 °C, 20 mbar). The resulting IL was obtained as a colorless viscous liquid.

### Analysis

$^1\text{H-NMR}$  (400 MHz, Deuterium Oxide)  $\delta(\text{ppm}) = 2.17$  (d,  $J = 13.8$  Hz, 1H), 1.54-1.13 (m, 5H), 0.85 (d,  $J = 4.3$  Hz, 2H).

$^{13}\text{C-NMR}$  (101 MHz, Deuterium Oxide)  $\delta(\text{ppm}) = 31.26, 30.39, 29.89, 29.59, 29.01, 28.68, 28.10, 22.05, 21.78, 20.56$

IR  $\nu_{\text{max}}$  ( $\text{cm}^{-1}$ ): 2954, 2923, 2854, 1466, 1232, 1163.

## 9.4 Synthesis of supported ionic liquid phases

### 9.4.1 Synthesis of SILP P<sub>66614</sub>Cl 10% (w/w)

Silica-60 (Merck, size 40-60  $\mu\text{m}$ , specific surface area 480-540  $\text{m}^2/\text{g}$ ) was pre-dried in vacuum oven at 50  $^{\circ}\text{C}$ , for 24 h. A 250 mL round-bottom flask was charged with 23.0 g silica-60 and 2.3 g P<sub>66614</sub>Cl. The mixture was suspended in 100 mL  $\text{CH}_2\text{Cl}_2$  and shaken at RT until the complete amount of IL was dissolved. The solvent was removed carefully by reduced pressure (40  $^{\circ}\text{C}$ , 20 mbar). Remaining solvent traces were removed via high vacuum (0.1 mbar) for 24 h. The procedure was accordingly adapted for the preparation of SILPs with 20% (w/w) and 50% (w/w) loadings.

### 9.4.2 Synthesis of polySILP 10% (w/w)

Silica-60 (Merck, size 40-60  $\mu\text{m}$ , specific surface area 480-540  $\text{m}^2/\text{g}$ ) was pre-dried in the oven at 400  $^{\circ}\text{C}$ , for 16 h and stored under Ar atmosphere. Silica-60 ( $10.0 \pm 0.10$ ) g was refluxed in toluene (150 mL) with 15 mL of (3-mercaptopropyl) trimethoxysilane under Ar atmosphere for 24 h. The reaction mixture was cooled down to RT and filtered. The solid was subsequently washed with MeOH and dried under high vacuum (0.1 mbar) for 24 h. The loading of the obtained product was 0.9 mmol/g. (3-Mercaptopropyl) trimethoxysilane grafted silica-60 ( $5.0 \pm 0.1$ ) g was mixed with dry EtOH (30 mL), diphenyl(4-vinylbenzyl)(4-vinylphenyl)phosphonium chloride (0.5 g, 1.12 mmol, 10%wt) and AIBN (16 mol% w.r.t. the double bonds). The mixture was stirred at RT, for 2 h. The EtOH was evaporated (40  $^{\circ}\text{C}$ , 20 mbar) and the solid was dried under high vacuum (0.1 mbar). Degassed dry EtOH (50 mL) was added to the recovered physisorbed solid under Ar atmosphere. The suspension was stirred at 78  $^{\circ}\text{C}$ , for 20 h. The solvent was evaporated (40  $^{\circ}\text{C}$ , 20 mbar) and the solid was extracted with MeOH via Soxhlet extraction. In the final step, the solid was dried under high vacuum (0.1 mbar). The polymer was obtained with a loading of 70 mg/g. The procedure was accordingly adapted for the preparation of 20% (w/w) and 50% (w/w) polySILPs and loadings of 138 mg/g and 387 mg/g, respectively, were obtained (Figure 113).

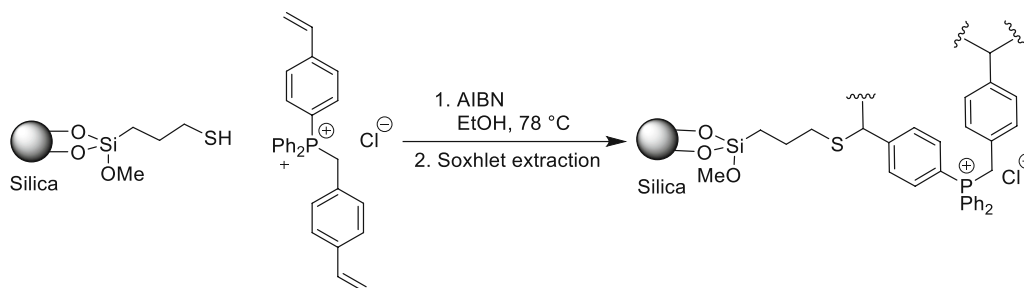


Figure 113. Polymerization of the monomer on the silica surface.

## 9.5 Characterization of solid supported phases

### 9.5.1 DRIFT-IR spectra of SILPs

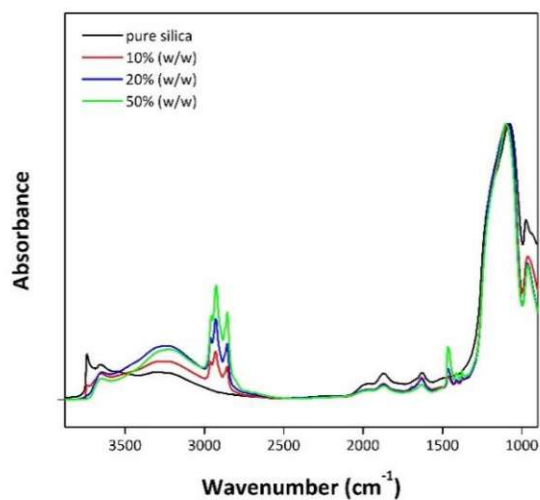


Figure 114. DRIFT-IR spectra of pure silica and SILPs with P<sub>66614</sub>Cl loadings of 10, 20 and 50% (w/w).

### 9.5.2 SEM images of SILPs

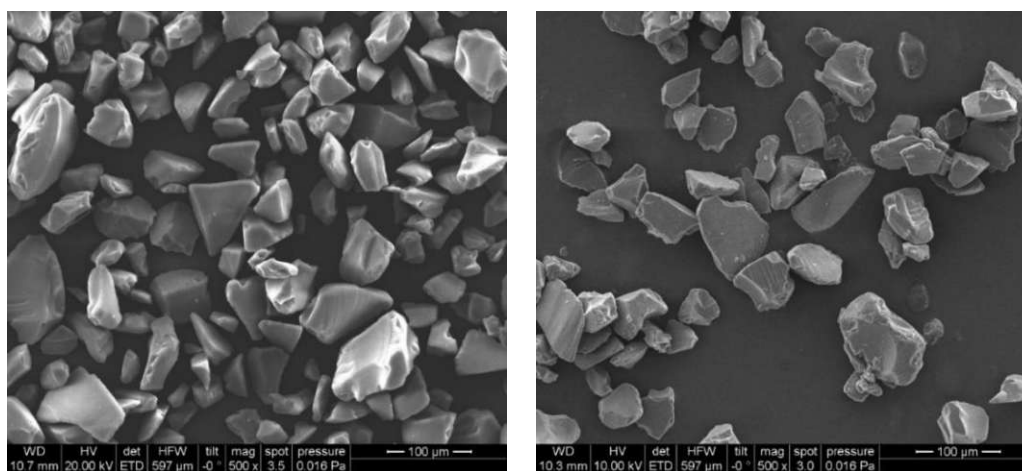


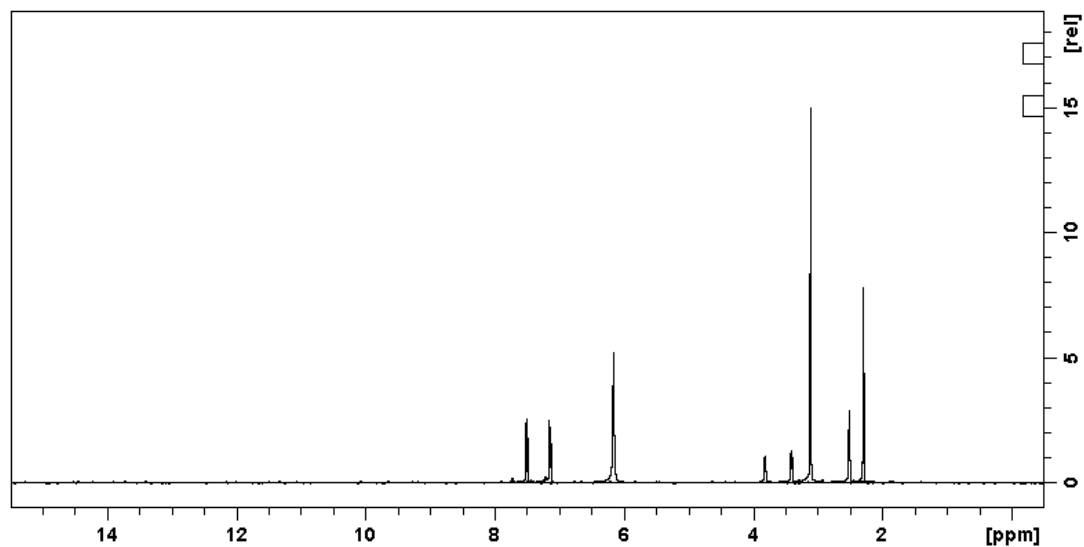
Figure 115. SEM images of SILP with P<sub>66614</sub>Cl 20% (w/w) pure (left) and loaded with PGMs (right).

## 10 Appendix

### 10.1 Characterization of deep eutectic solvents and ionic liquids

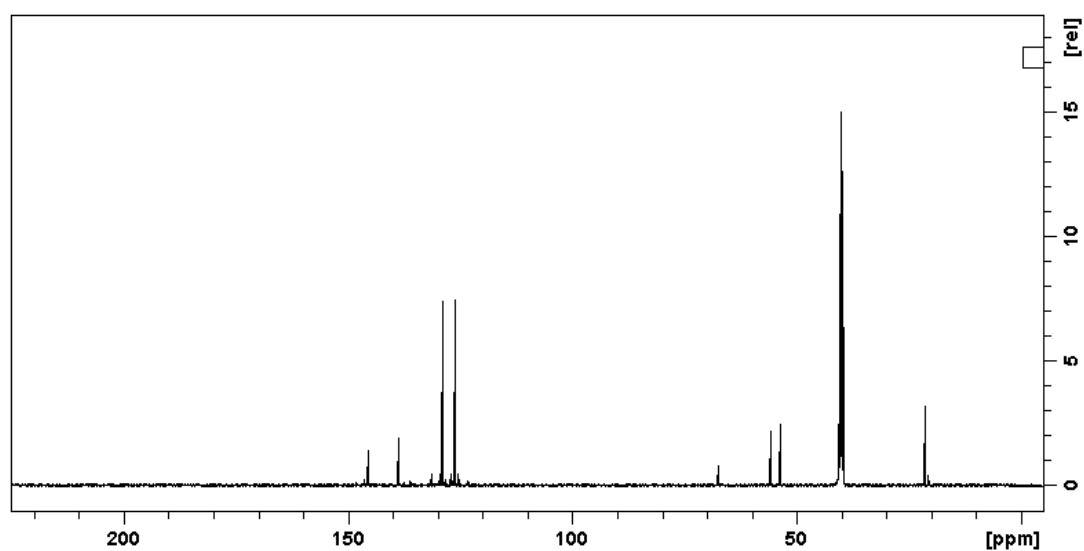
#### 10.1.1 NMR spectra of deep eutectic solvents and ionic liquids

##### 10.1.1.1 Deep eutectic solvents used in leaching



$^1\text{H-NMR}$  (400 MHz,  $\text{DMSO-}d_6$ )  $\delta(\text{ppm}) = 7.50$  (d,  $J = 8.0$  Hz, 1H),  $7.14$  (d,  $J = 8.1$  Hz, 1H),  $6.16$  (s, 3H),  $3.81$  (td,  $J = 5.3, 2.9$  Hz, 1H),  $3.45\text{-}3.37$  (m, 1H),  $3.11$  (s, 3H),  $2.29$  (s, 1H).

Figure 116.  $^1\text{H-NMR}$  of choline Cl/ $p$ -TsOH.

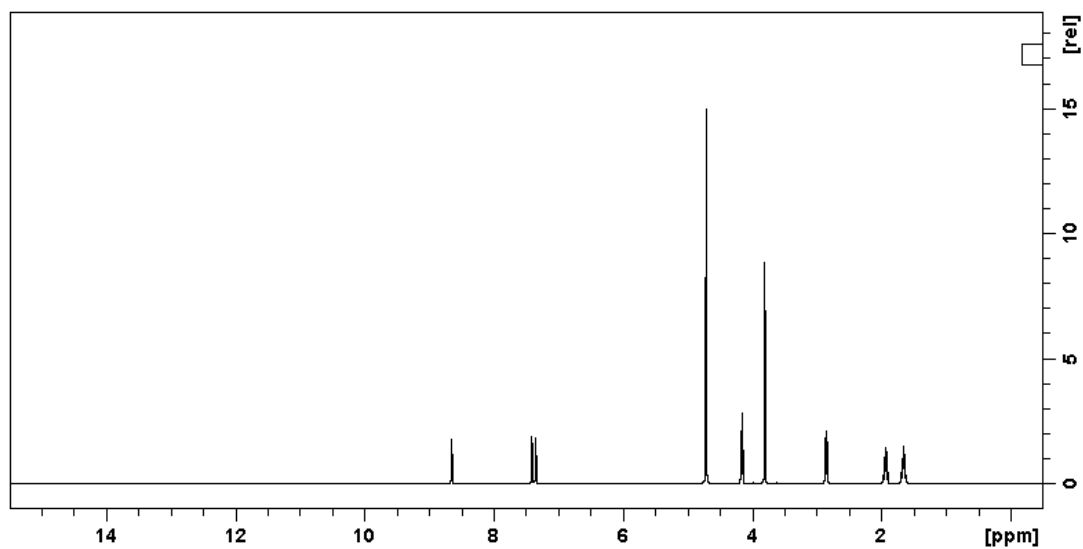


$^{13}\text{C-NMR}$  (101 MHz,  $\text{DMSO-}d_6$ )  $\delta(\text{ppm}) = 145.45, 138.59, 128.71, 125.95, 67.37, 55.61, 53.52, 21.26$ .

Figure 117.  $^{13}\text{C-NMR}$  of choline Cl/ $p$ -TsOH.

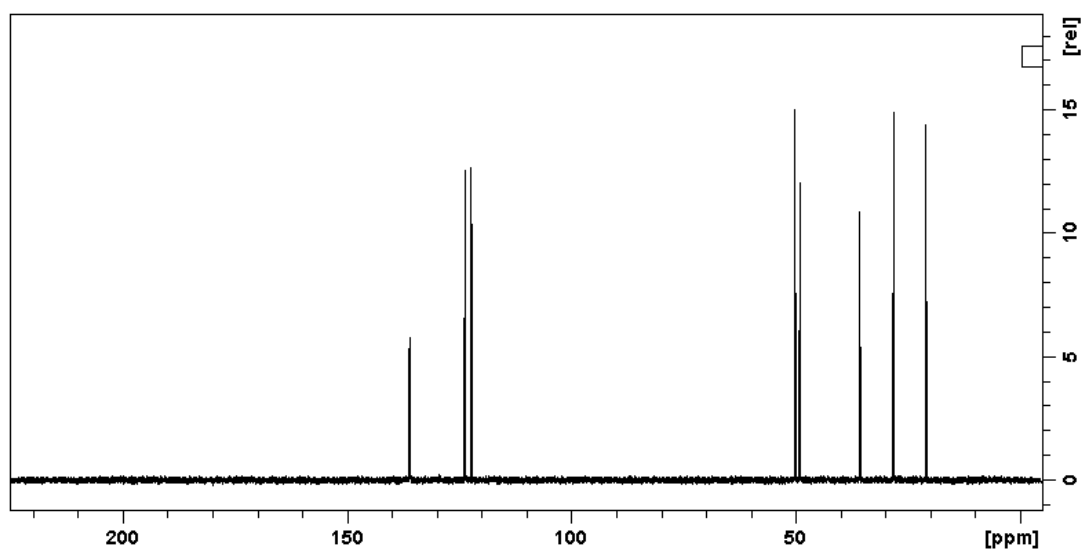


### 10.1.1.2 Ionic liquids used in leaching



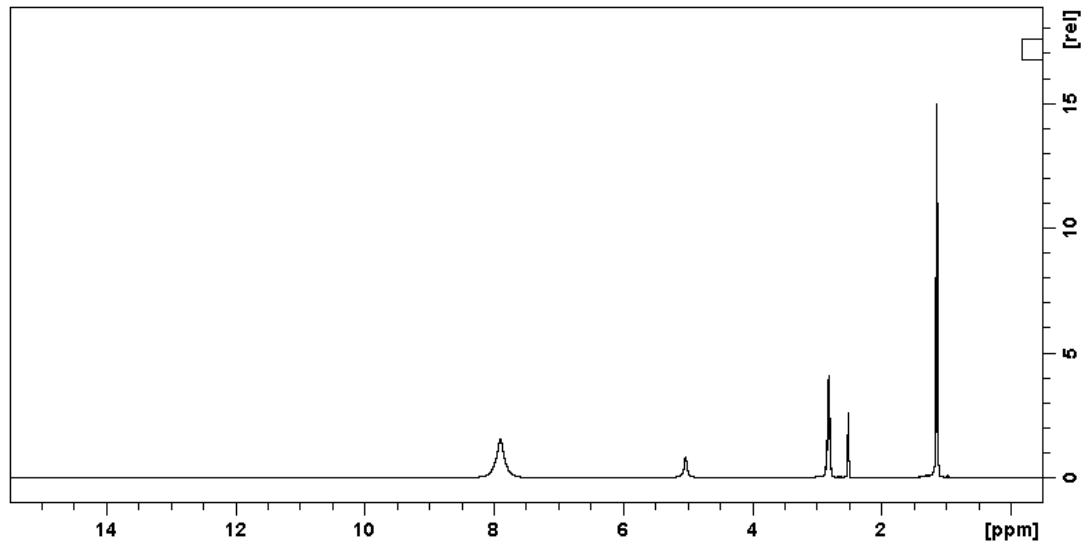
$^1\text{H-NMR}$  (400 MHz, Deuterium Oxide)  $\delta(\text{ppm}) = 8.65$  (s, 1H), 7.38 (d,  $J = 23.8$  Hz, 2H), 4.71 (s, 4H), 4.16 (t,  $J = 7.0$  Hz, 2H), 3.80 (d,  $J = 1.5$  Hz, 2H), 2.93-2.76 (m, 2H), 1.93 (p,  $J = 7.2$  Hz, 2H), 1.71-1.59 (m, 2H).

Figure 118.  $^1\text{H-NMR}$  of  $[\text{HSO}_3\text{C}_4\text{mim}]\text{Cl}$ .



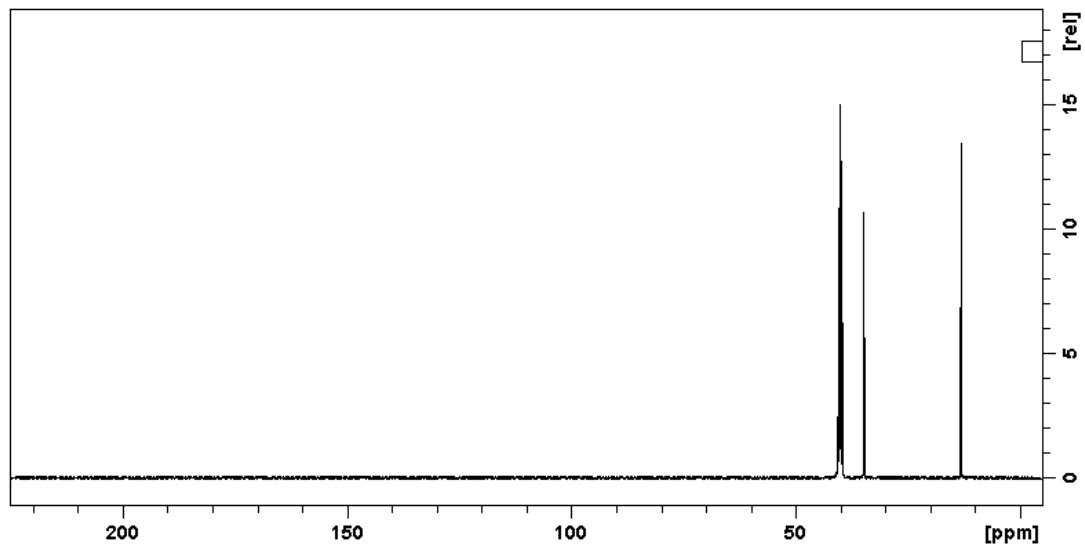
$^{13}\text{C-NMR}$  (101 MHz, Deuterium Oxide)  $\delta(\text{ppm}) = 135.95, 123.63, 122.14, 50.03, 48.89, 35.64, 28.07, 20.90$ .

Figure 119.  $^{13}\text{C-NMR}$  of  $[\text{HSO}_3\text{C}_4\text{mim}]\text{Cl}$ .



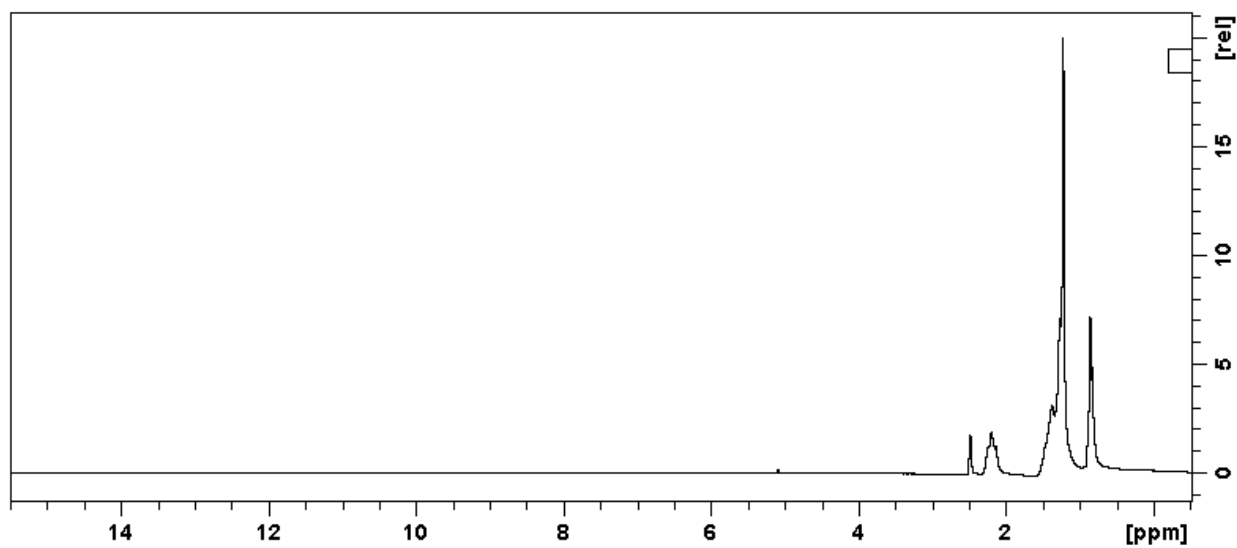
$^1\text{H-NMR}$  (400 MHz, Deuterium Oxide)  $\delta(\text{ppm}) = 8.65$  (s, 1H), 7.38 (d,  $J = 23.8$  Hz, 2H), 4.71 (s, 4H), 4.16 (t,  $J = 7.0$  Hz, 2H), 3.80 (d,  $J = 1.5$  Hz, 2H), 2.93-2.76 (m, 2H), 1.93 (p,  $J = 7.2$  Hz, 2H), 1.71-1.59 (m, 2H).

**Figure 120.**  $^1\text{H-NMR}$  of  $[\text{EtNH}_3][\text{NO}_3\text{-Cl}]$ .



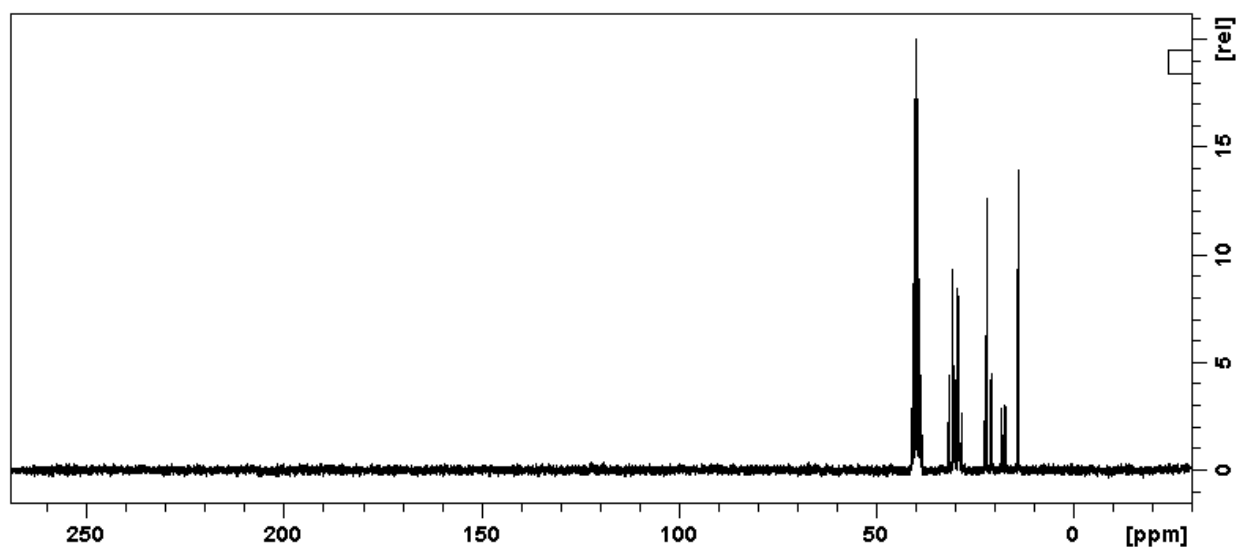
$^{13}\text{C-NMR}$  (101 MHz, Deuterium Oxide)  $\delta(\text{ppm}) = 135.95, 123.63, 122.14, 50.03, 48.89, 35.64, 28.07, 20.90$ .

**Figure 121.**  $^{13}\text{C-NMR}$  of  $[\text{EtNH}_3][\text{NO}_3\text{-Cl}]$ .



$^1\text{H-NMR}$  (400 MHz, Deuterium Oxide)  $\delta(\text{ppm}) = 2.17$  (d,  $J = 13.8$  Hz, 1H), 1.54-1.13 (m, 5H), 0.85 (d,  $J = 4.3$  Hz, 2H).

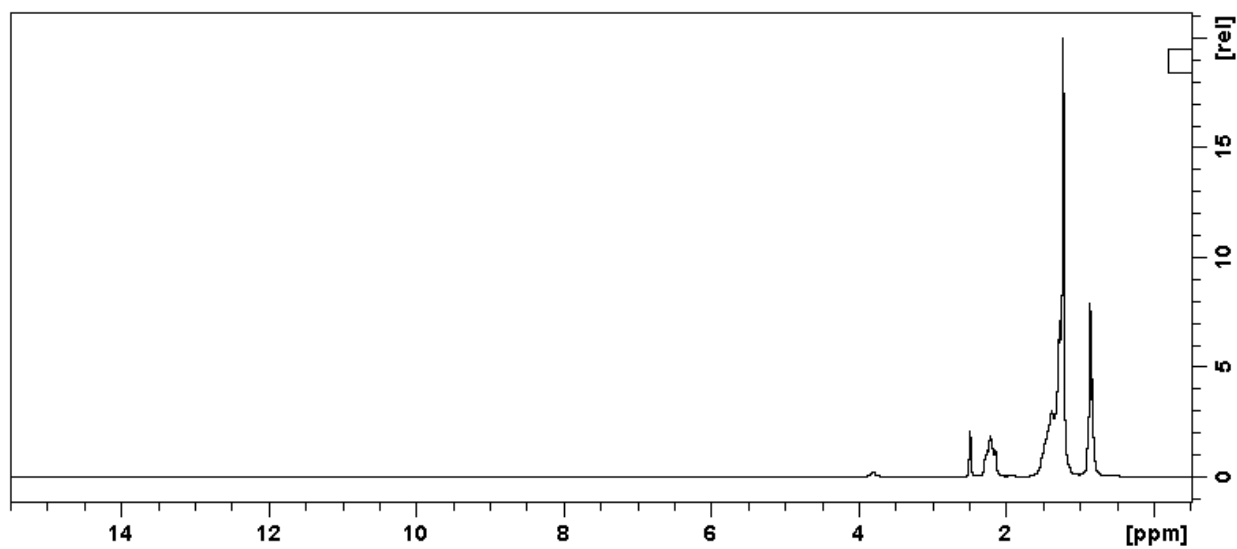
**Figure 122.**  $^1\text{H-NMR}$  of  $\text{P}_{66614}\cdot\text{HSO}_4$ .



$^{13}\text{C-NMR}$  (101 MHz, Deuterium Oxide)  $\delta(\text{ppm}) = 31.26, 30.39, 29.89, 29.59, 29.01, 28.68, 28.10, 22.05, 21.78, 20.56$ .

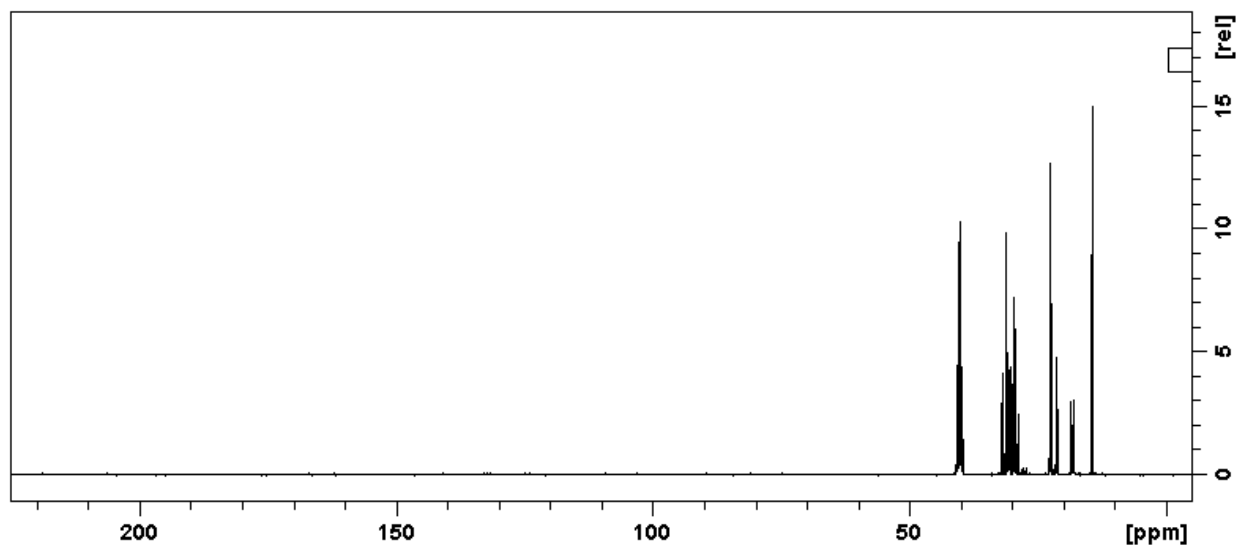
**Figure 123.**  $^{13}\text{C-NMR}$  of  $\text{P}_{66614}\text{Cl}\cdot\text{HSO}_4$ .

### 10.1.1.3 Ionic liquids used in liquid-liquid separation



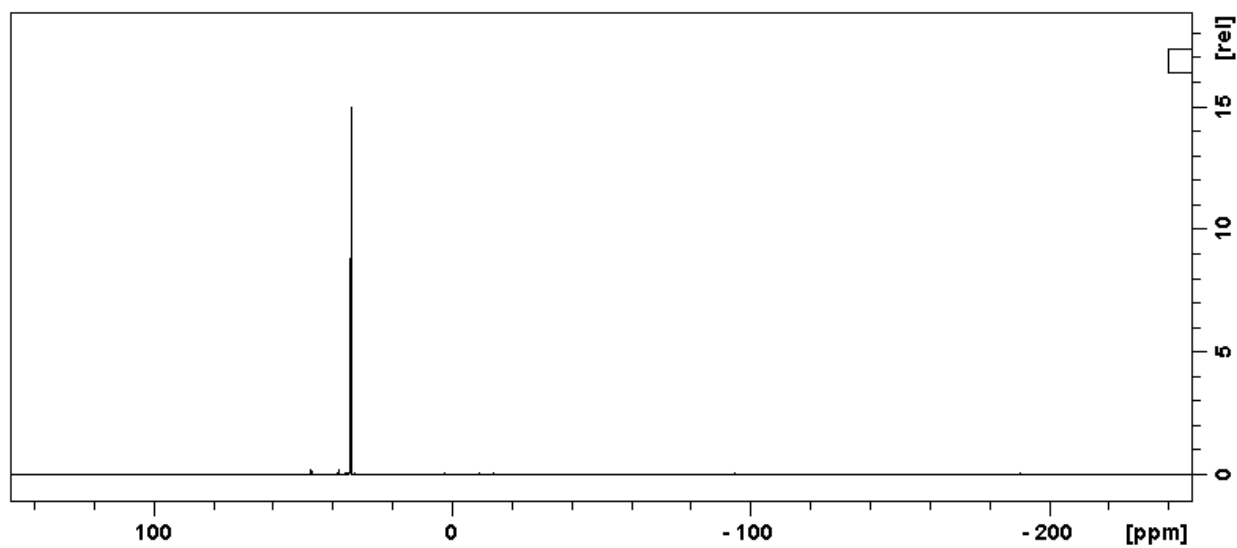
$^1\text{H-NMR}$  (400 MHz, Chloroform- $d$ )  $\delta$  (ppm) = 2.20 (m, 8H), 1.67-1.10 (m, 48H), 0.94-0.80 (m, 12H).

Figure 124.  $^1\text{H-NMR}$  of  $\text{P}_{66614}\text{Cl}$ .



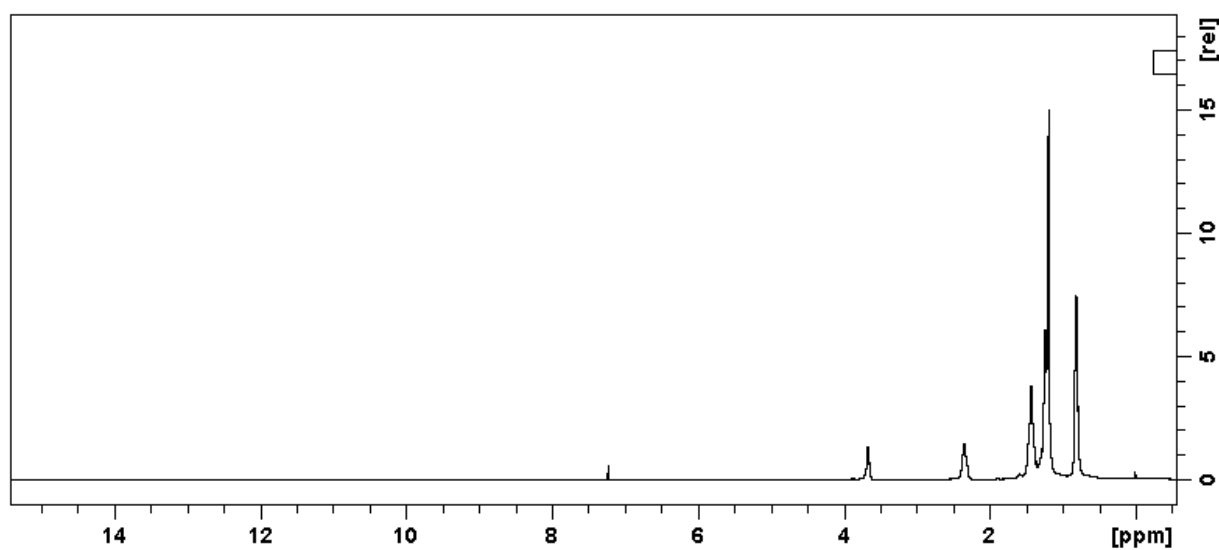
$^{13}\text{C-NMR}$  (101 MHz, DMSO- $d_6$ )  $\delta$  (ppm) = 31.26, 30.77, 30.39, 30.0 (d,  $J_{\text{P-H}} = 15.28$  Hz) 29.75 ( $J_{\text{P-H}} = 15.06$  Hz), 29.02-28.95, 28.68, 28.13, 22.04, 21.86, 21.78, 20.62-20.54, 17.60 (d,  $J_{\text{P-H}} = 47.41$  Hz), 17.52 (d,  $J_{\text{P-H}} = 47.07$  Hz), 13.76, 13.70.

Figure 125.  $^{13}\text{C-NMR}$  of  $\text{P}_{66614}\text{Cl}$ .



$^{31}\text{P}$ -NMR (162 MHz,  $\text{DMSO-}d_6$ )  $\delta$  = (ppm) 33.73.

**Figure 126.**  $^{31}\text{P}$ -NMR of  $\text{P}_{66614}\text{Cl}$ .



$^1\text{H}$ -NMR (400 MHz,  $\text{Chloroform-}d$ ):  $\delta$  (ppm) = 3.70 (dd, 4H), 2.39 m (8H), 1.47 (m, 20 H), 1.27-1.21 (m, 46H), 0.85 (m, 24H).

**Figure 127.**  $^1\text{H}$ -NMR of  $\text{P}_{66614}\text{B2EHP}$ .

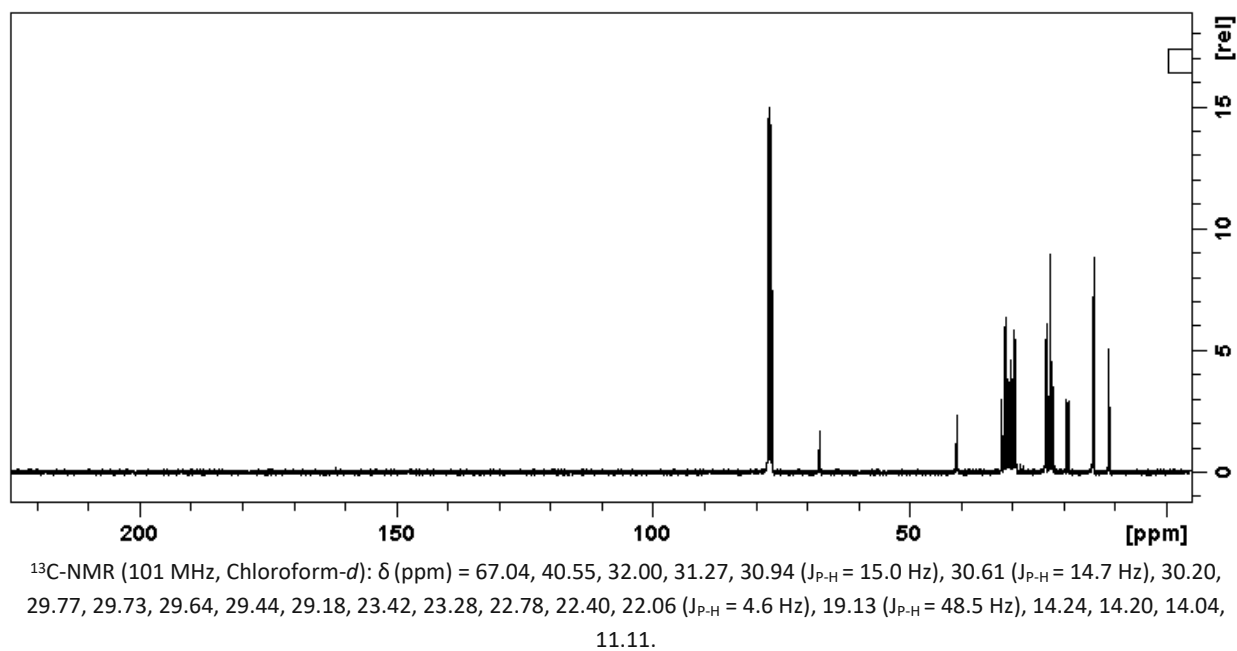


Figure 128.  $^{13}\text{C-NMR}$  of P<sub>66614</sub>B2EHP.

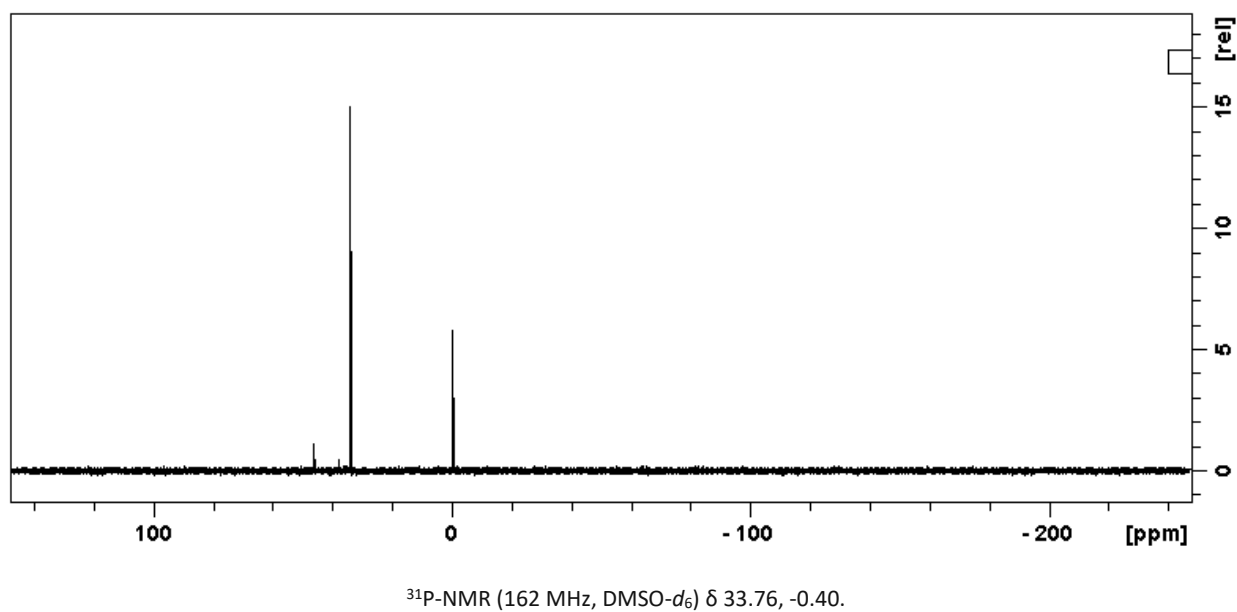
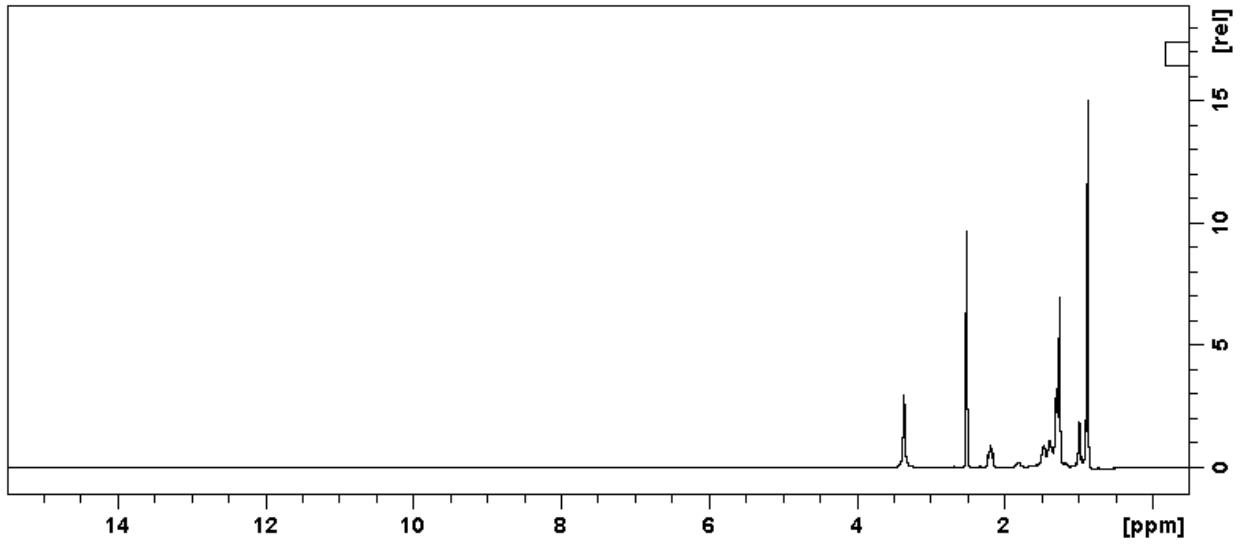
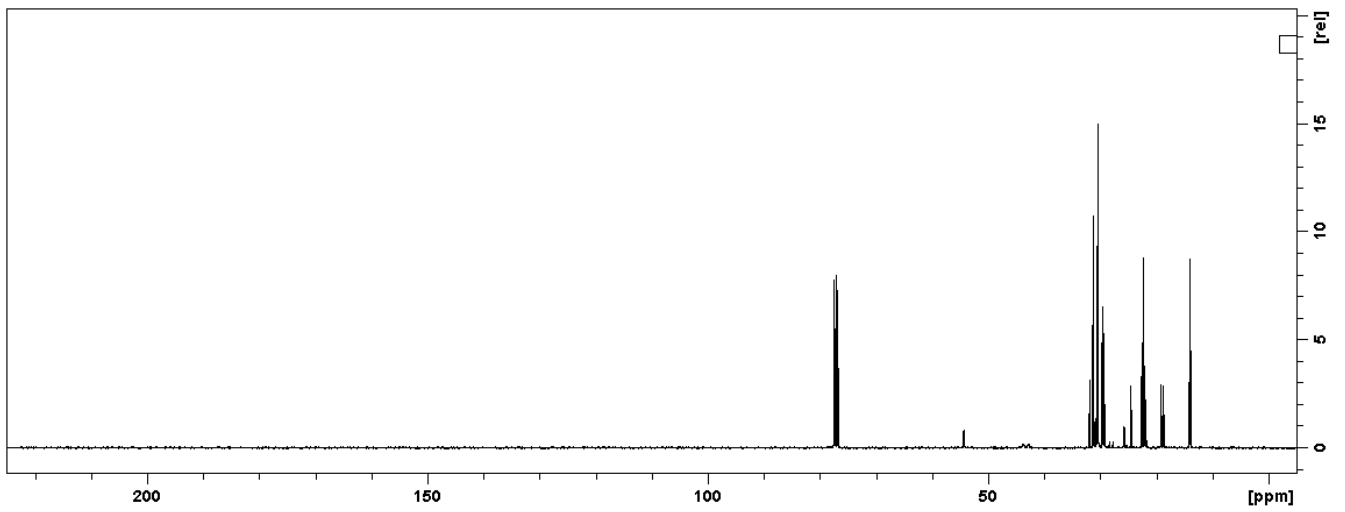


Figure 129.  $^{31}\text{P-NMR}$  of P<sub>66614</sub>B2EHP.



$^1\text{H-NMR}$  (400 MHz,  $\text{DMSO-}d_6$ )  $\delta$  (ppm) = 2.18 (m, 8H), 2.02 (m, 2H), 1.53-1.18 (m, 52 H), 1.04-0.79 (m, 40H).

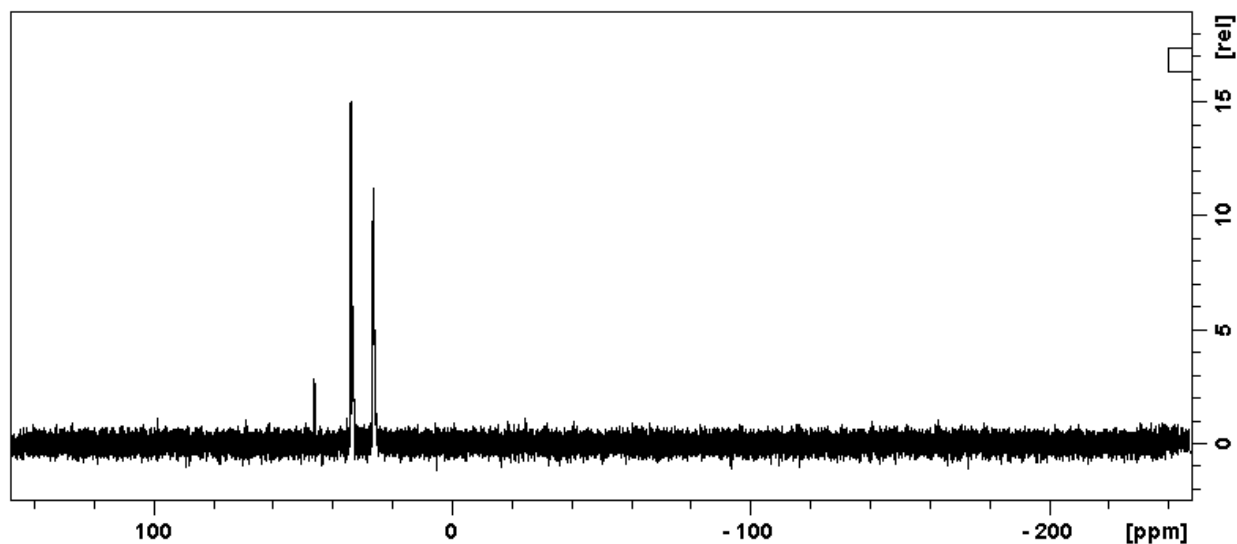
**Figure 130.**  $^1\text{H-NMR}$  of  $\text{P}_{66614}\text{DOP}$ .



$^{13}\text{C-NMR}$  (100 MHz,  $\text{Chloroform-}d$ )  $\delta$  (ppm) = 54.40, 31.80, 31.30, 30.90 ( $J_{\text{P-H}} = 14.9$  Hz), 30.39, 29.67, 29.64, 29.53, 29.34, 29.11, 25.78 ( $J_{\text{P-H}} = 10.0$  Hz), 24.52, 22.68, 22.40, 22.07 ( $J_{\text{P-H}} = 5.0$  Hz), 18.97 ( $J_{\text{P-H}} = 46.0$  Hz), 14.10, 14.00.

**Figure 131.**  $^{13}\text{C-NMR}$  of  $\text{P}_{66614}\text{DOP}$ .



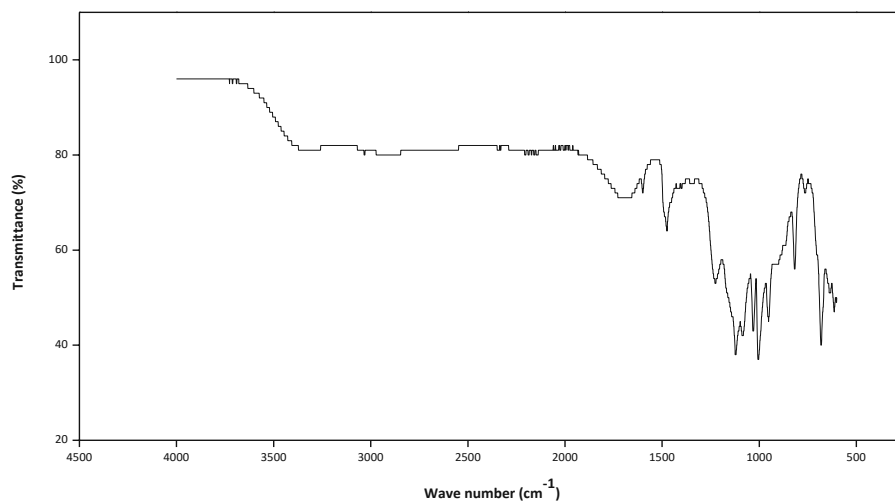


$^{31}\text{P}$ -NMR (162 MHz,  $\text{DMSO-}d_6$ )  $\delta$  (ppm) = 33.75, 26.21.

**Figure 132.**  $^{31}\text{P}$ -NMR of  $\text{P}_{66614}\text{DOP}$ .

## 10.1.2 IR spectra of deep eutectic solvents and ionic liquids

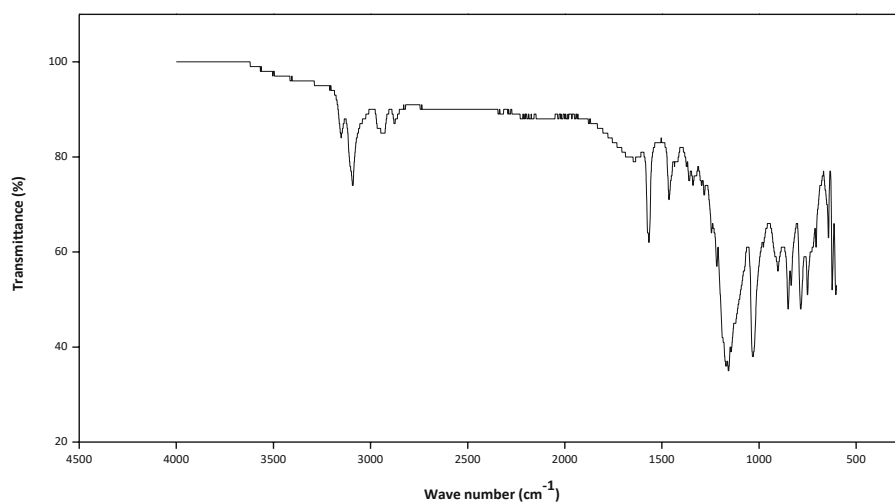
### 10.1.2.1 Deep eutectic solvents used in leaching



ATR-IR  $\nu_{\text{max}}$  ( $\text{cm}^{-1}$ ): 3367 (N-H stretch), 1600, 1477 (C=C aromatic bending), 1230 (S=O), 1123, 1031, 1006.

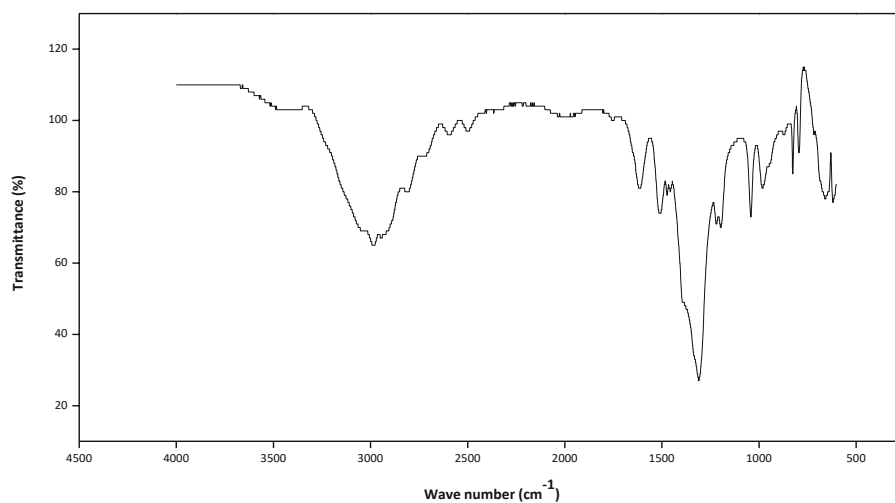
**Figure 133.** ATR-IR spectrum of choline Cl/*p*-TsOH.

### 10.1.2.2 Ionic liquids used in leaching



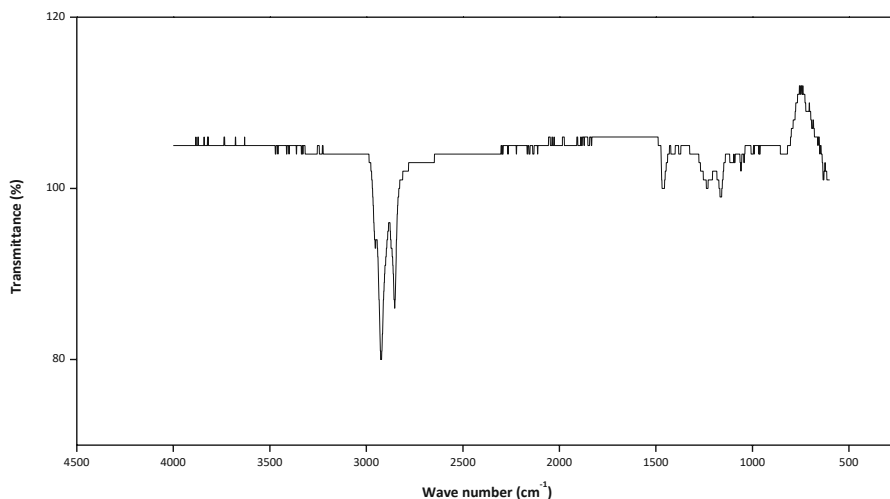
ATR-IR  $\nu_{\max}$  ( $\text{cm}^{-1}$ ): 3151 (N-H stretch), 3093, 2942, 2878, 1567, 1464 (C=C aromatic bending), 1158, 1035.

**Figure 134.** ATR-IR spectrum of  $[\text{HSO}_3\text{C}_4\text{mim}]\text{Cl}$ .



ATR-IR  $\nu_{\max}$  ( $\text{cm}^{-1}$ ): 2987 (N-H stretch), 1616 (N-H), 1512 (N-H), 1312 (C-H), 1043.

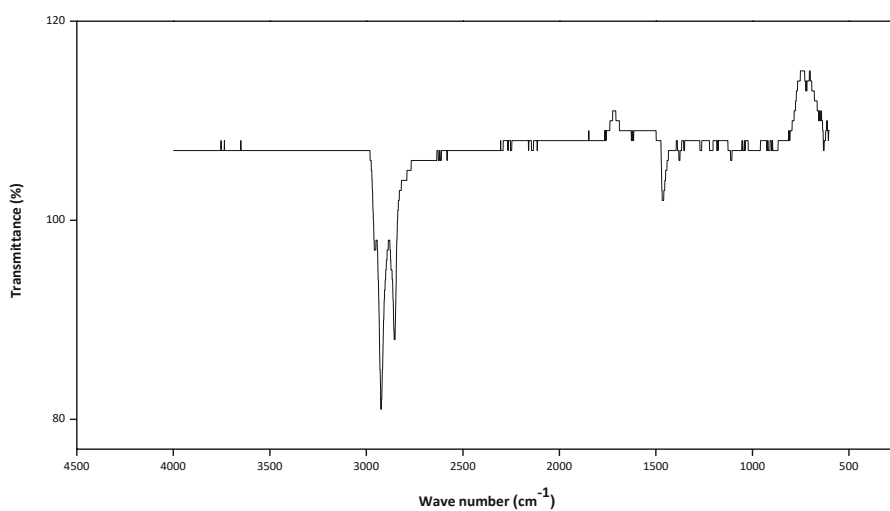
**Figure 135.** ATR-IR spectrum of  $[\text{EtNH}_3][\text{NO}_3\text{-Cl}]$ .



ATR-IR  $\nu_{\max}$  ( $\text{cm}^{-1}$ ): 2954, 2923, 2854, 1466, 1232, 1163.

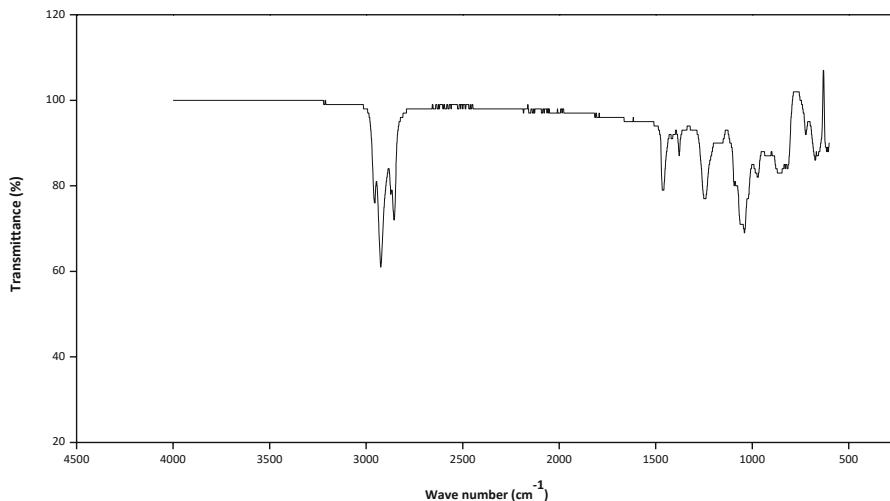
**Figure 136.** ATR-IR spectrum of  $\text{P}_{66614}\cdot\text{HSO}_4$ .

### 10.1.2.3 Ionic liquids used in liquid-liquid separation



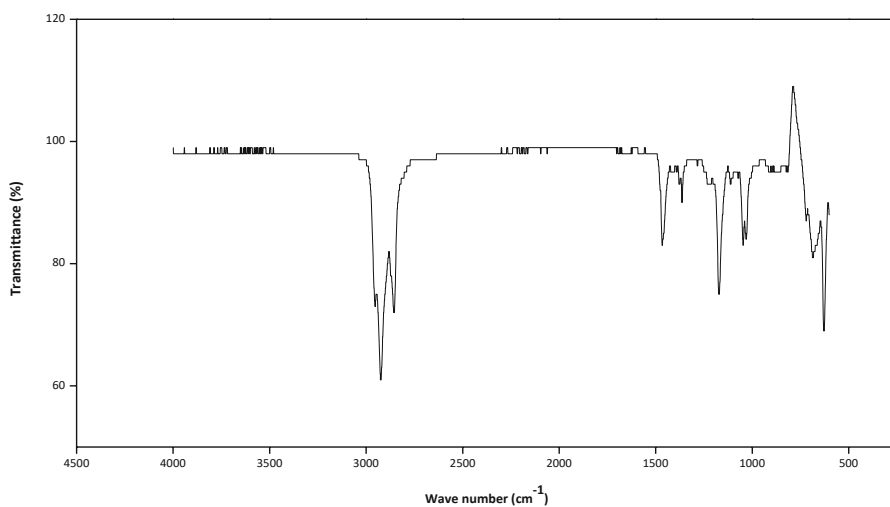
ATR-IR  $\nu_{\max}$  ( $\text{cm}^{-1}$ ): 2952 (C-H stretch), 2923 (C-H stretch), 2854 (C-H stretch), 1378 (P-C stretch).

**Figure 137.** ATR-IR spectrum of  $\text{P}_{66614}\text{Cl}$ .



ATR-IR  $\nu_{\max}$  (cm<sup>-1</sup>): 2955 (C-H stretch), 2923 (C-H stretch), 2854 (C-H stretch), 1467, 1379 (P=O stretch), 1246 (C-H bend), 1059 (C-H bend).

**Figure 138.** ATR-IR spectrum of P<sub>66614</sub>B2EHP.



ATR-IR  $\nu_{\max}$  (cm<sup>-1</sup>): 2955 (C-H stretch), 2952 (C-H stretch), 2857 (C-H stretch), 1466, 1362 (P=O stretch), 1172 (P=O stretch), 1050 (C-H bend), 1032 (P-O stretch).

**Figure 139.** ATR-IR spectrum of P<sub>66614</sub>DOP.

## 10.2 Characterization data of supported ionic liquid phases

### 10.2.1 DRIFT-IR spectra of supported ionic liquid phases

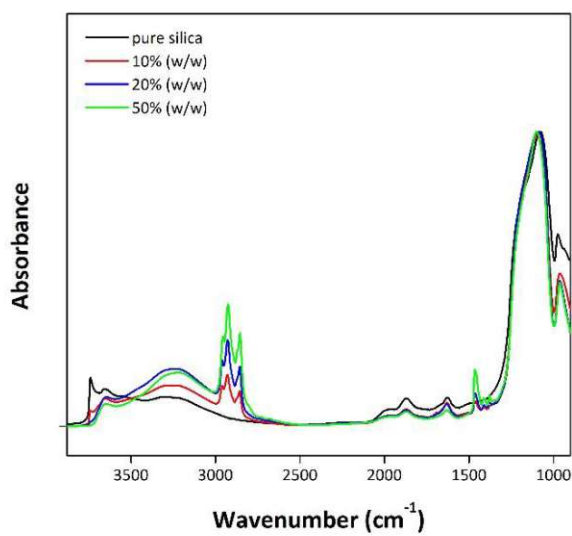


**Figure 140.** DRIFT-IR spectra of pure silica and SILPs with P<sub>66614</sub>Cl loadings of 10, 20 and 50% (w/w).

### 10.3 References

1. H. B. Trinh, J. C. Lee, Y. J. Suh and J. Lee, *Waste Management*, 2020, **114**, 148-165.
2. H. Renner, G. Schlamp, I. Kleinwächter, E. Drost, H. M. Lüschow, P. Tews, P. Panster, M. Diehl, J. Lang, T. Kreuzer, A. Knödler, K. A. Starz, K. Dermann, J. Rothaut, R. Drieselmann, C. Peter and R. Schiele, in *Ullmann's Encyclopedia of Industrial Chemistry*, Wiley-VCH Verlag GmbH & Co. KGaA, Weinheim, Germany, 2nd edn., 2012, vol. 28, pp. 317-388.
3. F. Reith, S. G. Campbell, A. S. Ball, A. Pring and G. Southam, *Earth-Science Reviews*, 2014, **131**, 1-21.
4. J. E. Mungall and A. J. Naldrett, *Elements*, 2008, **4**, 253-258.
5. B. Godel, S.-J. Barnes and W. D. Maier, *Journal of Petrology*, 2007, **48**, 1569-1604.
6. T. Naldrett, J. Kinnaird, A. Wilson and G. Chunnnett, *Earth Science Frontiers*, 2008, **15**, 264-297.
7. G. M. Mudd, *Ore Geology Reviews*, 2012, **46**, 106-117.
8. C. R. M. Rao and G. S. Reddi, *TrAC Trends in Analytical Chemistry*, 2000, **19**, 565-586.
9. R. M. Heck and R. J. Farrauto, *Applied Catalysis A: General*, 2001, **221**, 443-457.
10. M. V. Twigg, *Catalysis Today*, 2011, **163**, 33-41.
11. T. Zheng, J. He, Y. Zhao, W. Xia and J. He, *Journal of Rare Earths*, 2014, **32**, 97-107.
12. L. Bloxham, L. Cole, A. Cowley, M. Fujita, N. Girardot, J. Jiang, R. Raithatha, M. Ryan, E. Shao, B. Tang, A. Wang and F. Xiaoyan, *Johnson Matthey-PGM Market Report-February 2021*, 2021.
13. M. Shelef and G. W. Graham, *Catalysis Reviews*, 1994, **36**, 433-457.
14. D. Jimenez de Aberasturi, R. Pinedo, I. Ruiz de Larramendi, J. I. Ruiz de Larramendi and T. Rojo, *Minerals Engineering*, 2011, **24**, 505-513.
15. I. P. G. M. Association, <https://ipa-news.net/index/pgm-applications/automotive/catalytic-converters/what-is-an-autocatalyst.html> (last visit, March 2020).
16. T. Watling, <https://de.mathworks.com/company/newsletters/articles/modeling-and-simulating-advanced-catalysts-to-reduce-non-road-vehicle-emissions.html>, 2012 (last visit, October 2020).
17. D. R. Wilburn and D. I. Bleiwas, U.S. Geological Survey Open-File Report 2004-1224, 2005.
18. Bloomberg NEF, <https://about.bnef.com/electric-vehicle-outlook/>, 2020 (last visit, August 2020).
19. L. Bloxham, L. Cole, A. Cowley, M. Fujita, N. Girardot, J. Jiang, R. Raithatha, M. Ryan, E. Shao and F. Xiaoyan, *Johnson Matthey-PGM Market Report*, 2020.
20. European Commission, COM/2017/0490, 2017.
21. M. Buchert, D. Schüler and D. Bleher, *United Nations Environment Programme*, 2009.
22. C.-J. Yang, *Energy Policy*, 2009, **37**, 1805-1808.
23. F. Kapteijn, S. Stegenga, N. J. J. Dekker, J. W. Bijsterbosch and J. A. Moulijn, *Catalysis Today*, 1993, **16**, 273-287.
24. G. Qi and W. Li, *Catalysis Today*, 2012, **184**, 72-77.
25. M. E. Gálvez, S. Ascaso, I. Tobias, R. Moliner and M. J. Lázaro, *Catalysis Today*, 2012, **191**, 96-105.
26. U. Bardi and S. Caporali, *Minerals*, 2014, **4**, 388-398.
27. P. Ferro and F. Bonollo, *Materials & Design*, 2019, **177**, 107848.
28. B. J. Glaister and G. M. Mudd, *Minerals Engineering*, 2010, **23**, 438-450.
29. I. Jordaan, R. Pieters, L. P. Quinn, J. P. Giesy, P. D. Jones, M. B. Murphy and H. Bouwman, *Minerals Engineering*, 2007, **20**, 191-193.
30. U. Chemicals, *United Nations Environment Programme*, 2003, 234.
31. M. G.M., *Platinum Metals Review*, 2012, **56**, 2-19.
32. W. L. S. C. Zereini Fathi, *Platinum Metals in the Environment*, Springer-Verlag Berlin Heidelberg, 2015.
33. K. Ravindra, L. Bencs and R. Van Grieken, *Science of the Total Environment*, 2004, **318**, 1-43.
34. J.-L. Parrot, R. Hébert, A. Saindelle and F. Ruff, *Archives of Environmental Health: An International Journal*, 1969, **19**, 685-691.
35. K. Eckerman, J. Harrison, H-G. Menzel, C.H. Clement, *Annals of the ICPR*, 2012, **41**, 1-130.
36. World Health Organization, Environmental Health Criteria 125, 1991.
37. M. Buchert, C. Merz and E. van der Voet, *United Nations Environment Programme*, 2013.
38. United Nations, <https://www.un.org/sustainabledevelopment/sustainable-development-goals/> (last visit, April 2020).

39. S.-i. Sakai, H. Yoshida, J. Hiratsuka, C. Vandecasteele, R. Kohlmeyer, V. S. Rotter, F. Passarini, A. Santini, M. Peeler, J. Li, G.-J. Oh, N. K. Chi, L. Bastian, S. Moore, N. Kajiwara, H. Takigami, T. Itai, S. Takahashi, S. Tanabe, K. Tomoda, T. Hirakawa, Y. Hirai, M. Asari and J. Yano, *Journal of Material Cycles and Waste Management*, 2014, **16**, 1-20.
40. T. E. Graedel, J. Allwood, J.-P. Birat, B. K. Reck, S. F. Sibley, G. Sonnemann, M. Buchert and C. Hagelüken, *United Nations Environment Programme; International Resource Panel*, 2011.
41. N. Ferronato and V. Torretta, *International Journal of Environmental Research and Public Health*, 2019, **16**, 1060-1088.
42. D. Hoornweg and P. Bhada-Tata, *World Bank-Open Knowledge Repository*, Urban Development Series-Knowledge Paper Number 15, 2012.
43. S. A. Numfor, G. B. Omosa, Z. Zhang and K. Matsubae, *Sustainability*, 2021, **13**, 4918-4942.
44. R. Rumpold and J. Antrekowitsch, *Proceedings of the 51st Annual Conference of Metallurgists of CIM (COM 2012)*, 2012.
45. M. K. Jha, J.-c. Lee, M.-s. Kim, J. Jeong, B.-S. Kim and V. Kumar, *Hydrometallurgy*, 2013, **133**, 23-32.
46. H. Dong, J. Zhao, J. Chen, Y. Wu and B. Li, *International Journal of Mineral Processing*, 2015, **145**, 108-113.
47. C. Hagelüken, European Metallurgical Conference, 2009, **2**, 473-486.
48. L. Bloxham, L. Cole, A. Cowley, M. Fujita, N. Girardot, J. Jiang, R. Raithatha, M. Ryan, E. Shao and F. Xiaoyan, *Johnson Matthey-PGM Market Report-May 2021*, 2021.
49. C. Liu, S. Sun, X. Zhu and G. Tu, *Waste Management and Research*, 2021, **39**, 43-52.
50. S. Karim and Y.-P. Ting, *Resources, Conservation and Recycling*, 2021, **170**, Article Number 105588.
51. Z. Peng, Z. Li, X. Lin, H. Tang, L. Ye, Y. Ma, M. Rao, Y. Zhang and G. Li, *Journal of the Minerals, Metals & Materials Society*, 2017, **69**, 1553-1562.
52. R. Rumpold and J. Antrekowitsch, *The Southern African Institute of Mining and Metallurgy*, 2012.
53. R. Panda, M. Jha and D. D. Pathak, in *Rare Metal Technology 2018*, 2018, pp. 119-130.
54. S. K. Padamata, A. S. Yasinskiy, P. V. Polyakov, E. A. Pavlov and D. Y. Varyukhin, *Metallurgical and Materials Transactions B*, 2020, **51**, 2413-2435.
55. J. S. Yoo, *Catalysis Today*, 1998, **44**, 27-46.
56. I. Iavicoli and V. Leso, in *Handbook on the Toxicology of Metals*, eds. G. F. Nordberg, B. A. Fowler and M. Nordberg, Academic Press, San Diego, 4th edn., 2015, pp. 1143-1174.
57. S. Chen, S. Shen, Y. Cheng, H. Wang, B. Lv and F. Wang, *Hydrometallurgy*, 2014, **144**, 69-76.
58. J. E. Hoffmann, *Journal of the Minerals, Metals & Materials Society*, 1988, **40**, 40-44.
59. I. Yakoumis, A. Moschovi, M. Panou and D. Panias, *Journal of Sustainable Metallurgy*, 2020, **6**, 259-268.
60. E. A. Devyatykh, T. O. Devyatykh and A. N. Boyarsky, *KnE Engineering*, 2018, **3**, 154-160.
61. T. N. Angelidis, *Topics in Catalysis*, 2001, **16**, 419-423.
62. C. Hagelüken, in *Handbook of Heterogeneous Catalysis*, ed. Wiley, 2008, pp. 1846-1863.
63. M. Benson, C. R. Bennett, J. E. Harry, M. K. Patel and M. Cross, *Resources, Conservation and Recycling*, 2000, **31**, 1-7.
64. S. Steinlechner and J. Antrekowitsch, *Journal of the Minerals, Metals & Materials Society*, 2015, **67**, 406-411.
65. A. Dawson, in *Modern Earth Buildings*, eds. M. R. Hall, R. Lindsay and M. Krayenhoff, Woodhead Publishing, 2012, pp. 172-203.
66. R. Dhir, J. Brito, G. Ghataora and C. Lye, in *Sustainable Construction Materials*, Springer, 2018, pp. 327-387.
67. M. Saternus, A. Fornalczyk, W. Gąsior, A. Dębski and S. Terlicka, *Catalysts*, 2020, **10**, 880-897.
68. R. I. Edwards, *Journal of the Minerals, Metals & Materials Society*, 1976, **28**, 4-9.
69. M. J. Cleare, P. Charlesworth and D. J. Bryson, *Journal of Chemical Technology and Biotechnology*, 1979, **29**, 210-224.
70. B. W. Mountain and S. A. Wood, in *Geo-Platinum 87*, eds. H. M. Prichard, P. J. Potts, J. F. W. Bowles and S. J. Cribb, Springer Netherlands, Dordrecht, 1988, pp. 57-82.



71. Y. D. Scherson, S. J. Aboud, J. Wilcox and B. J. Cantwell, *The Journal of Physical Chemistry C*, 2011, **115**, 11036-11044.
72. E. Benguerel, G. P. Demopoulos and G. B. Harris, *Hydrometallurgy*, 1996, **40**, 135-152.
73. F. K. Crundwell, M. S. Moats, V. Ramachandran, T. G. Robinson and W. G. Davenport, in *Extractive Metallurgy of Nickel, Cobalt and Platinum Group Metals*, eds. F. K. Crundwell, M. S. Moats, V. Ramachandran, T. G. Robinson and W. G. Davenport, Elsevier, Oxford, 2011, pp. 489-534.
74. B. M. Thethwayo, in *Noble and Precious Metals - Properties, Nanoscale Effects and Applications*, Elsevier, 2018, pp. 393-403.
75. G. J. Bernfeld, R. I. Edwards, H. Köpf, P. Köpf-Maier, C. J. Raub, W. A. M. te Riele, F. Simon and W. Westwood, *Gmelin Handbook in Inorganic and Organometallic Chemistry*, Springer-Verlag, Berlin, 8th edn., 1986.
76. Y. A. El-Nadi, *Separation & Purification Reviews*, 2017, **46**, 195-215.
77. F. F. Cantwell and M. Losier, in *Comprehensive Analytical Chemistry*, Elsevier, 2002, vol. 37, pp. 297-340.
78. R. Granados-Fernández, M. A. Montiel, S. Díaz-Abad, M. A. Rodrigo and J. Lobato, *Catalysts*, 2021, **11**, 937-953.
79. K. N. G. S. Das, Y.P. Ting, *16th International Waste Management and Landfill Symposium, Sardinia*, 2017.
80. D. Shin, J. Park, J. Jeong and B.-s. Kim, *Hydrometallurgy*, 2015, **158**, 10-18.
81. S. Karim and Y.-P. Ting, *Journal of Cleaner Production*, 2020, **255**, Article Number 120199.
82. F. Lin, D. Liu, S. Maiti Das, N. Prempeh, Y. Hua and J. Lu, *Industrial & Engineering Chemistry Research*, 2014, **53**, 1866-1877.
83. M. Faisal, Y. Atsuta, H. Daimon and K. Fujie, *Asia-Pacific Journal of Chemical Engineering*, 2008, **3**, 364-367.
84. A. Ruiu, B. Bauer-Siebenlist, M. Senila, T. Jänisch, D. Foix, K. Seauudeau-Pirouley and P. Lacroix-Desmazes, *Journal of CO<sub>2</sub> Utilization*, 2020, **41**, Article Number 101232.
85. Y.-k. Taninouchi, T. Watanabe and T. H. Okabe, *Materials Transactions*, 2017, **58**, 410-419.
86. Y.-k. Taninouchi and T. H. Okabe, *Materials Transactions*, 2018, **59**, 88-97.
87. Y.-k. Taninouchi and T. H. Okabe, *Metallurgical and Materials Transactions B*, 2018, **49**, 1781-1793.
88. D. O. Abranches, M. A. R. Martins, L. P. Silva, N. Schaeffer, S. P. Pinho and J. A. P. Coutinho, *Chemical Communications*, 2019, **55**, 10253-10256.
89. N. Schaeffer, J. H. F. Conceição, M. A. R. Martins, M. C. Neves, G. Pérez-Sánchez, J. R. B. Gomes, N. Papaiconomou and J. A. P. Coutinho, *Green Chemistry*, 2020, **22**, 2810-2820.
90. R. Javed, M. Zia, S. Naz, S. O. Aisida, N. u. Ain and Q. Ao, *Journal of Nanobiotechnology*, 2020, **18**, Article Number 172.
91. K. Binnemans and P. T. Jones, *Journal of Sustainable Metallurgy*, 2017, **3**, 570-600.
92. A. P. Abbott, G. Frisch, S. J. Gurman, A. R. Hillman, J. Hartley, F. Holyoak and K. S. Ryder, *Chemical Communications*, 2011, **47**, 10031-10033.
93. A. Abbott and G. Frisch, in *Element Recovery and Sustainability*, ed. A. Hunt, RSC Publishing, 2013, pp. 59-79.
94. M. Freemantle, in *An Introduction to Ionic Liquids*, RSC Publishing, Cambridge, UK, 1st edn., 2010, pp. 12-16.
95. R. S. Kenneth, S. Annegret and T. María-José, *Pure and Applied Chemistry*, 2000, **72**, 2275-2287.
96. J. S. Wilkes, *Green Chemistry*, 2002, **4**, 73-80.
97. R. D. Rogers and K. R. Seddon, *Science*, 2003, **302**, 792-793.
98. I. Krossing, J. M. Slattery, C. Daguinet, P. J. Dyson, A. Oleinikova and H. Weingärtner, *Journal of the American Chemical Society*, 2006, **128**, 13427-13434.
99. J. N. A. Canongia Lopes and A. A. H. Pádua, *The Journal of Physical Chemistry B*, 2006, **110**, 3330-3335.
100. R. Hayes, G. G. Warr and R. Atkin, *Chemical Reviews*, 2015, **115**, 6357-6426.
101. A. I. Siriwardana, in *Electrochemistry in Ionic Liquids: Volume 2: Applications*, ed. A. A. J. Torriero, Springer International Publishing, Cham, 2015, pp. 563-603.
102. R. Shi and Y. Wang, *Scientific Reports*, 2016, **6**, Article Number 19644.

103. G. Cevasco and C. Chiappe, *Green Chemistry*, 2014, **16**, 2375-2385.
104. K. R. Seddon, *Journal of Chemical Technology & Biotechnology*, 1997, **68**, 351-356.
105. M. J. Earle and K. R. Seddon, *Pure and Applied Chemistry*, 2000, **72**, 1391-1398.
106. J. J. H. Davis, *Chemistry Letters*, 2004, **33**, 1072-1077.
107. D. Han and K. Row, *Molecules*, 2010, **15**, 2405-2426.
108. J. D. Holbrey and K. R. Seddon, *Clean Products and Processes*, 1999, **1**, 223-236.
109. J. Park, Y. Jung, P. Kusumah, J. Lee, K. Kwon and C. K. Lee, *International Journal of Molecular Sciences*, 2014, **15**, 15320-15343.
110. M. J. Earle, J. M. S. S. Esperança, M. A. Gilea, J. N. Canongia Lopes, L. P. N. Rebelo, J. W. Magee, K. R. Seddon and J. A. Widegren, *Nature*, 2006, **439**, 831-834.
111. R. P. Swatloski, J. D. Holbrey and R. D. Rogers, *Green Chemistry*, 2003, **5**, 361-363.
112. M. Smiglak, W. M. Reichert, J. D. Holbrey, J. S. Wilkes, L. Sun, J. S. Thrasher, K. Kirichenko, S. Singh, A. R. Katritzky and R. D. Rogers, *Chemical Communications*, 2006, **42**, 2554-2556.
113. A. Stojanovic and B. K. Keppler, *Separation Science and Technology*, 2012, **47**, 189-203.
114. M. L. Dietz, *Separation Science and Technology*, 2006, **41**, 2047-2063.
115. E. L. Smith, A. P. Abbott and K. S. Ryder, *Chemical Reviews*, 2014, **114**, 11060-11082.
116. A. Mannu, M. Blangetti, S. Baldino and C. Prandi, *Materials*, 2021, **14**, 2494-2520.
117. Y. Dai, J. van Spronsen, G.-J. Witkamp, R. Verpoorte and Y. H. Choi, *Analytica Chimica Acta*, 2013, **766**, 61-68.
118. M. A. R. Martins, S. P. Pinho and J. A. P. Coutinho, *Journal of Solution Chemistry*, 2019, **48**, 962-982.
119. A. P. Abbott, D. Boothby, G. Capper, D. L. Davies and R. K. Rasheed, *Journal of the American Chemical Society*, 2004, **126**, 9142-9147.
120. O. S. Hammond, D. T. Bowron and K. J. Edler, *Angewandte Chemie International Edition*, 2017, **56**, 9782-9785.
121. M. Jablonsky, A. Skulcova, A. Haz, J. Sima and V. Majova, *BioResources*, 2018, **13**, 7545-7559.
122. D. Rengstl, V. Fischer and W. Kunz, *Physical Chemistry Chemical Physics*, 2014, **16**, 22815-22822.
123. S. Riaño, M. Petrániková, B. Onghena, T. V. Hoogerstraete, D. Banerjee, M. Foreman, C. Ekberg and K. Binnemans, *RSC Advances*, 2017, **7**, 32100-32113.
124. A. P. Abbott, G. Capper, D. L. Davies, R. K. Rasheed and P. Shikotra, *Inorganic Chemistry*, 2005, **44**, 6497-6499.
125. N. Osowska and L. Ruzik, *Food Analytical Methods*, 2019, **12**, 926-935.
126. N. Rodriguez Rodriguez, L. Machiels and K. Binnemans, *ACS Sustainable Chemistry & Engineering*, 2019, **7**, 3940-3948.
127. Y. Liu, J. B. Friesen, J. B. McAlpine, D. C. Lankin, S.-N. Chen and G. F. Pauli, *Journal of Natural Products*, 2018, **81**, 679-690.
128. J. Płotka-Wasyłka, M. de la Guardia, V. Andruch and M. Vilková, *Microchemical Journal*, 2020, **159**, Article Number 105539.
129. P. Wasserscheid and W. Keim, *Angewandte Chemie International Edition*, 2000, **39**, 3772-3789.
130. Q. Zhang, K. De Oliveira Vigier, S. Royer and F. Jérôme, *Chemical Society Reviews*, 2012, **41**, 7108-7146.
131. T. Zhang, T. Doert, H. Wang, S. Zhang and M. Ruck, *Angewandte Chemie International Edition*, 2021, **60**, 22148-22165.
132. A. Jarosik, S. R. Krajewski, A. Lewandowski and P. Radzimski, *Journal of Molecular Liquids*, 2006, **123**, 43-50.
133. M. Francisco, A. van den Bruinhorst and M. C. Kroon, *Angewandte Chemie International Edition*, 2013, **52**, 3074-3085.
134. I. Khan, K. A. Kurnia, F. Mutelet, S. P. Pinho and J. A. P. Coutinho, *Journal of Physical Chemistry B*, 2014, **118**, 1848-1860.
135. J. E. S. J. Reid, A. J. Walker and S. Shimizu, *Physical Chemistry Chemical Physics*, 2015, **17**, 14710-14718.
136. J. Park, Y. Jung, P. Kusumah, J. Lee, K. Kwon and C. K. Lee, *International Journal of Molecular Sciences*, 2014, **15**, 15320-15343.

137. M. Gras, N. Papaiconomou, N. Schaeffer, E. Chainet, F. Tedjar, J. A. P. Coutinho and I. Billard, *Angewandte Chemie International Edition*, 2018, **57**, 1563-1566.
138. C. H. C. Janssen, N. A. Macías-Ruvalcaba, M. Aguilar-Martínez and M. N. KobraK, *International Reviews in Physical Chemistry*, 2015, **34**, 591-622.
139. Z. Chen and S. Zhang, in *Encyclopedia of Ionic Liquids*, ed. S. Zhang, Springer Singapore, Singapore, 2019, pp. 1-8.
140. M. L. Dietz, J. A. Dzielawa, M. P. Jensen, J. V. Beitz and M. Borkowski, in *Ionic Liquids IIIB: Fundamentals, Progress, Challenges, and Opportunities*, American Chemical Society, 2005, vol. 902, pp. 2-18.
141. T. L. Greaves and C. J. Drummond, *Chemical Society Reviews*, 2013, **42**, 1096-1120.
142. V. A. Cocalia, M. P. Jensen, J. D. Holbrey, S. K. Spear, D. C. Stepinski and R. D. Rogers, *Dalton Transactions*, 2005, **34**, 1966-1971.
143. S. L. Garvey, C. A. Hawkins and M. L. Dietz, *Talanta*, 2012, **95**, 25-30.
144. M. L. Dietz and J. A. Dzielawa, *Chemical Communications*, 2001, **37**, 2124-2125.
145. M. L. Dietz, J. A. Dzielawa, I. Laszak, B. A. Young and M. P. Jensen, *Green Chemistry*, 2003, **5**, 682-685.
146. M. P. Jensen, J. A. Dzielawa, P. Rickert and M. L. Dietz, *Journal of the American Chemical Society*, 2002, **124**, 10664-10665.
147. M. P. Jensen, J. Neuefeind, J. V. Beitz, S. Skanthakumar and L. Soderholm, *Journal of the American Chemical Society*, 2003, **125**, 15466-15473.
148. A. E. Visser, R. P. Swatloski, S. T. Griffin, D. H. Hartman and R. D. Rogers, *Separation Science and Technology*, 2001, **36**, 785-804.
149. A. E. Visser, M. P. Jensen, I. Laszak, K. L. Nash, G. R. Choppin and R. D. Rogers, *Inorganic Chemistry*, 2003, **42**, 2197-2199.
150. C. H. C. Janssen, A. Sánchez, G.-J. Witkamp and M. N. KobraK, *ChemPhysChem*, 2013, **14**, 3806-3813.
151. C. H. C. Janssen, A. Sánchez and M. N. KobraK, *ChemPhysChem*, 2014, **15**, 3536-3543.
152. M. N. KobraK, *Solvent Extraction and Ion Exchange*, 2008, **26**, 735-748.
153. R. E. Clement and C. Hao, in *Comprehensive Sampling and Sample Preparation*, ed. J. Pawliszyn, Academic Press, Oxford, 2012, pp. 51-63.
154. A. P. Daso and O. J. Okonkwo, in *Analytical Separation Science*, 2015, pp. 1437-1468.
155. Y.-C. Hoh, W.-S. Chuang and P.-S. Yueh, *Journal of Chemical Technology and Biotechnology*, 1985, **35**, 41-47.
156. C. Fontàs, V. Salvadó and M. Hidalgo, *Solvent Extraction and Ion Exchange*, 1999, **17**, 149-162.
157. M. H. Campbell, *Analytical Chemistry*, 1968, **40**, 6-9.
158. Q. Rong and H. Preiser, *Solvent Extraction and Ion Exchange*, 1987, **5**, 923-937.
159. C. Foulon, D. Pareau and G. Durand, *Hydrometallurgy*, 1999, **51**, 139-153.
160. N. M. Sundaramurthi and V. M. Shinde, *Bulletin of the Chemical Society of Japan*, 1990, **63**, 1508-1511.
161. G. Levitin and G. Schmuckler, *Reactive and Functional Polymers*, 2003, **54**, 149-154.
162. W. Wei, C.-W. Cho, S. Kim, M.-H. Song, J. K. Bediako and Y.-S. Yun, *Journal of Molecular Liquids*, 2016, **216**, 18-24.
163. C.-Y. Peng and T.-H. Tsai, *Desalination and Water Treatment*, 2014, **52**, 1101-1121.
164. P. Giridhar, K. A. Venkatesan, T. G. Srinivasan and P. R. Vasudeva Rao, *Hydrometallurgy*, 2006, **81**, 30-39.
165. J.-Y. Lee, J. R. Kumar, J.-S. Kim, D.-J. Kim and H.-S. Yoon, *Journal of Industrial and Engineering Chemistry*, 2009, **15**, 359-364.
166. J. Y. Lee, B. Raju, B. N. Kumar, J. R. Kumar, H. K. Park and B. R. Reddy, *Separation and Purification Technology*, 2010, **73**, 213-218.
167. B. Raju, J. R. Kumar, J.-Y. Lee, H.-S. Kwonc, M. L. Kantam and B. R. Reddy, *Journal of Hazardous Materials*, 2012, **227-228**, 142-147.
168. R. S. Marinho, J. C. Afonso and J. W. S. D. da Cunha, *Journal of Hazardous Materials*, 2010, **179**, 488-494.

169. S. Boudesocque, A. Mohamadou, A. Conreux, B. Marin and L. Dupont, *Separation and Purification Technology*, 2019, **210**, 824-834.
170. S. Katsuta, Y. Yoshimoto, M. Okai, Y. Takeda and K. Bessho, *Industrial & Engineering Chemistry Research*, 2011, **50**, 12735-12740.
171. S. Katsuta and J. Tamura, *Journal of Solution Chemistry*, 2018, **47**, 1293-1308.
172. T. J. Bell and Y. Ikeda, *Dalton Transactions*, 2012, **41**, 4303-4305.
173. J. R. Kumar, I.-H. Choi and J.-Y. Lee, *Korean Chemical Engineering Research*, 2017, **55**, 503-509.
174. V. T. Nguyen, S. Riaño and K. Binnemans, *Green Chemistry*, 2020, **22**, 8375-8388.
175. G. J. Suppes and T. S. Storvick, in *Sustainable Nuclear Power*, Academic Press, Burlington, 2007, pp. 283-317.
176. E. A. Mezhev, V. A. Kuchumov and V. V. Druzhnikov, *Radiochemistry*, 2002, **44**, 135-140.
177. W. Liu, Q. Wang, Y. Zheng, S. Wang, Y. Yan and Y. Yang, *Dalton Transactions*, 2017, **46**, 7210-7218.
178. N. Papaiconomou, S. Génand-Pinaz, J.-M. Leveque and S. Guittonneau, *Dalton Transactions*, 2013, **42**, 1979-1982.
179. S. Génand-Pinaz, N. Papaiconomou and J.-M. Leveque, *Green Chemistry*, 2013, **15**, 2493-2501.
180. N. Papaiconomou, L. Svecova, C. Bonnaud, L. Cathelin, I. Billard and E. Chainet, *Dalton Transactions*, 2015, **44**, 20131-20138.
181. O. Sha, X.-S. Zhu and Y.-H. Gu, *Asian Journal of Chemistry*, 2013, **25**, 1434-1436.
182. Y. Tong, C. Wang, Y. Huang and Y. Yang, *Industrial & Engineering Chemistry Research*, 2015, **54**, 705-711.
183. Y. Yan, Q. Wang, Z. Xiang and Y. Yang, *Separation Science and Technology*, 2018, **53**, 2064-2073.
184. M. Chen, S. Li, C. Jin, M. Shao and Z. Huang, *Separation and Purification Technology*, 2021, **259**, Article Number 118204.
185. J. Yang, F. Kubota, Y. Baba, N. Kamiya and M. Goto, *Solvent Extraction Research and Development, Japan*, 2014, **21**, 89-94.
186. J. Yang, F. Kubota, Y. Baba, N. Kamiya and M. Goto, *Solvent Extraction Research and Development, Japan*, 2014, **21**, 129-135.
187. F. Kubota, E. Shigyo, W. Yoshida and M. Goto, *Solvent Extraction Research and Development, Japan*, 2017, **24**, 97-104.
188. C. Wang, W. Lu, Y. Tong, Y. Zheng and Y. Yang, *RSC Advances*, 2014, **4**, 57009-57015.
189. C. Wang, Y. Tong, Y. Huang, H. Zhang and Y. Yang, *RSC Advances*, 2015, **5**, 63087-63094.
190. T. Kakoi, M. Kawagoe and M. Goto, *Journal of Chemical Engineering of Japan*, 2014, **47**, 666-670.
191. S. Ma, K. Funaki, A. Miyazaki, A. Muramatsu and K. Kanie, *Chemistry Letters*, 2017, **46**, 1422-1425.
192. C. Zhang, K. Huang, P. Yu and H. Liu, *Separation and Purification Technology*, 2013, **108**, 166-173.
193. N. Papaiconomou, L. Cointeaux, E. Chainet, C. Iojoiu and I. Billard, *Chemistry Select*, 2016, **1**, 3892-3900.
194. L. Svecova, N. Papaiconomou and I. Billard, *Dalton Transactions*, 2016, **45**, 15162-15169.
195. L. Svecova, N. Papaiconomou and I. Billard, *Molecules*, 2019, **24**, 1391-1491.
196. M. Rzelewska, M. Baczyńska, M. Regel-Rosocka and M. Wiśniewski, *Chemical Papers*, 2016, **70**, 454-460.
197. M. Rzelewska, M. Wiśniewski and M. Regel-Rosocka, *Separation Science and Technology*, 2018, **53**, 1249-1260.
198. A. Cieszyńska, M. Regel-Rosocka and M. Wiśniewski, *Polish Journal of Chemical Technology*, 2007, **2**, 99-101.
199. A. Cieszyńska and M. Wisniewski, *Separation and Purification Technology*, 2010, **73**, 202-207.
200. A. Cieszyńska and M. Wisniewski, *Separation and Purification Technology*, 2011, **80**, 385-389.
201. M. Regel-Rosocka, M. Rzelewska, M. Baczyńska, M. Janus and M. Wiśniewski, *Physicochemical Problems of Mineral Processing*, 2015, **51**, 621-631.
202. A. Cieszyńska and M. Wiśniewski, *Hydrometallurgy*, 2012, **113-114**, 79-85.
203. M. Rzelewska, M. Janiszewska and M. Regel-Rosocka, *Chemik*, 2016, **70**, 515-520.
204. M. Rzelewska-Piekut and M. Regel-Rosocka, *Separation and Purification Technology*, 2019, **212**, 791-801.
205. V. T. Nguyen, J.-c. Lee, A. Chagnes, M.-s. Kim, J. Jeong and G. Cote, *RSC Advances*, 2016, **6**, 62717-62728.



206. M. L. Firmansyah, F. Kubota and M. Goto, *Journal of Chemical Technology and Biotechnology*, 2018, **93**, 1714-1721.
207. M. L. Firmansyah, F. Kubota, W. Yoshida and M. Goto, *Industrial & Engineering Chemistry Research*, 2019, **58**, 3845-3852.
208. M. L. Firmansyah, F. Kubota and M. Goto, *Journal of Chemical Engineering of Japan*, 2019, **52**, 835-842.
209. V. T. Nguyen, J.-c. Lee, M.-s. Kim, S.-k. Kim, A. Chagnes and G. Cote, *Hydrometallurgy*, 2017, **171**, 344-354.
210. Y. Tong, C. Wang, J. Li and Y. Yang, *Hydrometallurgy*, 2014, **147-148**, 164-169.
211. N. Wang, Q. Wang, W. Lu, M. Ru and Y. Yang, *Journal of Molecular Liquids*, 2019, **293**, Article Number 111040.
212. N. Papaiconomou, J.-M. Lee, J. Salminen, M. von Stosch and J. M. Prausnitz, *Industrial & Engineering Chemistry Research*, 2008, **47**, 5080-5086.
213. J.-M. Lee, *Fluid Phase Equilibria*, 2012, **319**, 30-36.
214. K. Chayama, Y. Sano and S. Iwatsuki, *Analytical Sciences*, 2015, **31**, 1115-1117.
215. H. Zhang, C. Wang, Y. Zheng, S. Wang, Z. Liu and Y. Yang, *RSC Advances*, 2016, **6**, 63006-63012.
216. K. Funaki, S. Ma, S. Kawamura, A. Miyazaki, A. Sugie, A. Mori, A. Muramatsu and K. Kanie, *Chemistry Letters*, 2017, **46**, 434-437.
217. V. G. Torgov, V. V. Tatarchuk, I. A. Druzhinina, T. M. Korda, A. N. Tatarchuk and É. V. Renard, *Atomic Energy*, 1994, **76**, 442-448.
218. L. V. Arseenkov, B. S. Zakharkin, K. P. Lunichkina, É. V. Renard, V. Y. Rogozhkin and N. A. Shorokhov, *Atomic Energy*, 1992, **72**, 411-420.
219. E. V. R. Zdenek Kolarik and É. V. Renard, *Platinum Metals Review*, 2003, **47**, 74-87.
220. N. Hirokazu, T. Mikiya, M. Kazuko and A. Tsutomu, *Chemistry Letters*, 2004, **33**, 1144-1145.
221. H. Narita, K. Morisaku, K. Tamura, M. Tanaka, H. Shiwaku, Y. Okamoto, S. Suzuki and T. Yaita, *Industrial & Engineering Chemistry Research*, 2014, **53**, 3636-3640.
222. P. Nockemann, B. Thijs, S. Pittois, J. Thoen, C. Glorieux, K. Van Hecke, L. Van Meervelt, B. Kirchner and K. Binnemans, *Journal of Physical Chemistry B*, 2006, **110**, 20978-20992.
223. K. Sasaki, K. Takao, T. Suzuki, T. Mori, T. Arai and Y. Ikeda, *Dalton Transactions*, 2014, **43**, 5648-5651.
224. S. Ikeda, T. Mori, Y. Ikeda and K. Takao, *ACS Sustainable Chemistry & Engineering*, 2016, **4**, 2459-2463.
225. S. Kono, H. Kazama, T. Mori, T. Arai and K. Takao, *ACS Sustainable Chemistry & Engineering*, 2018, **6**, 1555-1559.
226. J. Lemus, J. Palomar, M. A. Gilarranz and J. J. Rodriguez, *Adsorption*, 2011, **17**, 561-571.
227. L. Zhu, L. Guo, Z. Zhang, J. Chen and S. Zhang, *Science China Chemistry*, 2012, **55**, 1479-1487.
228. L. J. Lozano, C. Godínez, A. P. de los Ríos, F. J. Hernández-Fernández, S. Sánchez-Segado and F. J. Alguacil, *Journal of Membrane Science*, 2011, **376**, 1-14.
229. J.-c. Lee, Kurniawan, H.-J. Hong, K. W. Chung and S. Kim, *Separation and Purification Technology*, 2020, **246**, Article Number 116896.
230. Z. Hubicki, M. Wawrzekiewicz, G. Wójcik, D. Kołodyńska and A. Wołowicz, in *Ion Exchange - Studies and Applications*, IntechOpen, 2015, pp. 1-35.
231. A. N. Nikoloski and K.-L. Ang, *Mineral Processing and Extractive Metallurgy Review*, 2014, **35**, 369-389.
232. W. M. MacNevin and W. B. Crummett, *Analytical Chemistry*, 1953, **25**, 1628-1630.
233. I. Jarvis, M. M. Totland and K. E. Jarvis, *Analyst*, 1997, **122**, 19-26.
234. S. S. Berman and W. A. E. McBryde, *Canadian Journal of Chemistry*, 1958, **36**, 835-844.
235. R. Gaita and S. J. Al-Bazi, *Talanta*, 1995, **42**, 249-255.
236. P. Cyganowski, *Solvent Extraction and Ion Exchange*, 2020, **38**, 143-165.
237. R. Navarro, E. Garcia, I. Saucedo and E. Guibal, *Separation Science and Technology*, 2012, **47**, 2199-2210.
238. A. Arias, I. Saucedo, R. Navarro, V. Gallardo, M. Martinez and E. Guibal, *Reactive and Functional Polymers*, 2011, **71**, 1059-1070.

239. R. Navarro, I. Saucedo, C. Gonzalez and E. Guibal, *Chemical Engineering Journal*, 2012, **185-186**, 226-235.
240. R. Navarro, M. A. Lira, I. Saucedo, A. Alatorre and E. Guibal, *Gold Bulletin*, 2017, **50**, 7-23.
241. Z. Xu, Y. Zhao, P. Wang, X. Yan, M. Cai and Y. Yang, *Industrial & Engineering Chemistry Research*, 2019, **58**, 1779-1786.
242. O. Lanaridi, A. R. Sahoo, A. Limbeck, S. Naghdi, D. Eder, E. Eitenberger, Z. Csendes, M. Schnürch and K. Bica-Schröder, *ACS Sustainable Chemistry & Engineering*, 2020, **9**, 375-386.
243. T. Vincent, A. Parodi and E. Guibal, *Separation and Purification Technology*, 2008, **62**, 470-479.
244. T. Vincent, A. Parodi and E. Guibal, *Reactive and Functional Polymers*, 2008, **68**, 1159-1169.
245. S. D. Kolev, Y. Sakai, R. W. Cattrall, R. Paimin and I. D. Potter, *Analytica Chimica Acta*, 2000, **413**, 241-246.
246. C. Fontàs, E. Anticó, V. Salvadó, M. Valiente and M. Hidalgo, *Analytica Chimica Acta*, 1997, **346**, 199-206.
247. C. Fontàs, C. Palet, V. Salvadó and M. Hidalgo, *Journal of Membrane Science*, 2000, **178**, 131-139.
248. C. Fontàs, V. Salvadó and M. Hidalgo, *Industrial & Engineering Chemistry Research*, 2002, **41**, 1616-1620.
249. T. Kakoi, K. Muranaga and M. Goto, *Journal of Chemical Engineering of Japan*, 2018, **51**, 917-920.
250. S. Zhou, N. Song, X. Lv and Q. Jia, *Microchimica Acta*, 2017, **184**, 3497-3504.
251. O. Mokhodoeva, V. Shkinev, V. Maksimova, R. Dzhenloda and B. Spivakov, *Separation and Purification Technology*, 2020, **248**, Article Number 117049.
252. C. M. Rydberg Jan, Musikas Claude, Choppin R. Gregory, *Solvent Extraction Principles and Practice, Revised and Expanded*, Taylor & Francis, 2nd edn., 2004.
253. A. Wołowicz and Z. Hubicki, *Hydrometallurgy*, 2009, **98**, 206-212.
254. R. A. Silva, K. Hawboldt and Y. Zhang, *Mineral Processing and Extractive Metallurgy Review*, 2018, **39**, 395-413.
255. R.M. Freer and A. Curzons, in *Green Industrial Applications of Ionic Liquids*, eds. R. D. Rogers, K. R. Seddon and S. Volkov, Springer, Netherlands, 1st edn., 2002, pp. 129-136.
256. J. Brennecke, R. Rogers and K. Seddon, *Ionic Liquids IV: Not Just Solvents Anymore*, 2007.
257. S. P. Ventura, A. M. Gonçalves, T. Sintra, J. L. Pereira, F. Gonçalves and J. A. Coutinho, *Ecotoxicology*, 2013, **22**, 1-12.
258. X. Wang, C. A. Ohlin, Q. Lu, Z. Fei, J. Hu and P. J. Dyson, *Green Chemistry*, 2007, **9**, 1191-1197.
259. P. Stepnowski, A. C. Składanowski, A. Ludwiczak and E. Laczyńska, *Human & Experimental Toxicology*, 2004, **23**, 513-517.
260. R. F. M. Frade, A. Matias, L. C. Branco, C. A. M. Afonso and C. M. M. Duarte, *Green Chemistry*, 2007, **9**, 873-877.
261. A. Mehrkesh and A. Karunanithi, Life Cycle Perspectives on Human Health Impacts of Ionic Liquids, *bioRxiv*, 2016.
262. R. J. Bernot, E. E. Kennedy and G. A. Lamberti, *Environmental Toxicology and Chemistry*, 2005, **24**, 1759-1765.
263. C. Pretti, C. Chiappe, D. Pieraccini, M. Gregori, F. Abramo, G. Monni and L. Intorre, *Green Chemistry*, 2006, **8**, 238-240.
264. T. P. Thuy Pham, C.-W. Cho and Y.-S. Yun, *Water Research*, 2010, **44**, 352-372.
265. J. Flieger and M. Flieger, *International Journal of Molecular Sciences* 2020, **21**, 6267-6308.
266. M. Cvjetko Bubalo, K. Radošević, I. Radojčić Redovniković, J. Halambek and V. Gaurina Srček, *Ecotoxicology and Environmental Safety*, 2014, **99**, 1-12.
267. J. G. Huddleston, A. E. Visser, W. M. Reichert, H. D. Willauer, G. A. Broker and R. D. Rogers, *Green Chemistry*, 2001, **3**, 156-164.
268. A. E. Visser, R. P. Swatloski, W. M. Reichert, S. T. Griffin and R. D. Rogers, *Industrial & Engineering Chemistry Research*, 2000, **39**, 3596-3604.
269. E. Kim, S. Yoo, H.-Y. Ro, H.-J. Han, Y.-W. Baek, I.-C. Eom, H.-M. Kim, P. Kim and K. Choi, *Environmental Analysis Health and Toxicology*, 2013, **28**, Article ID e2013002.
270. S. Stolte, M. Matzke, J. Arning, A. Bösch, W.-R. Pitner, U. Welz-Biermann, B. Jastorff and J. Ranke, *Green Chemistry*, 2007, **9**, 1170-1179.
271. P. G. Jessop, *Faraday Discussions*, 2018, **206**, 587-601.

272. V. G. Maciel, D. J. Wales, M. Seferin, C. M. L. Ugaya and V. Sans, *Journal of Cleaner Production*, 2019, **217**, 844-858.
273. N. V. Plechkova and K. R. Seddon, *Chemical Society Reviews*, 2008, **37**, 123-150.
274. H. Passos, M. G. Freire and J. A. P. Coutinho, *Green Chemistry*, 2014, **16**, 4786-4815.
275. K. Katsu, K. Yoko, S. Haiying and T. Robert, *Spectroscopy*, 2004, **19**, 14-23.
276. R. Thomas, *Practical Guide to ICP-MS: A Tutorial for Beginners*, Taylor and Francis, Boca Raton, 3rd edn., 2013.
277. J. Nölte, *ICP Emission Spectrometry: A Practical Guide*, Wiley-VCH, Weinheim, 2003.
278. N. Yamada, *Spectrochimica Acta Part B: Atomic Spectroscopy*, 2015, **110**, 31-44.
279. G.-c. Tian, J. Li and Y.-x. Hua, *Transactions of Nonferrous Metals Society of China*, 2010, **20**, 513-520.
280. J. A. Whitehead, G. A. Lawrance and A. McCluskey, *Green Chemistry*, 2004, **6**, 313-315.
281. H. Mehdi, K. Binnemans, K. Van Hecke, L. Van Meervelt and P. Nockemann, *Chemical Communications*, 2010, **46**, 234-236.
282. S. Wellens, R. Goovaerts, C. Möller, J. Luyten, B. Thijs and K. Binnemans, *Green Chemistry*, 2013, **15**, 3160-3164.
283. A. Rout, S. Wellens and K. Binnemans, *RSC Advances*, 2014, **4**, 5753-5758.
284. G. R. T. Jenkin, A. Z. M. Al-Bassam, R. C. Harris, A. P. Abbott, D. J. Smith, D. A. Holwell, R. J. Chapman and C. J. Stanley, *Minerals Engineering*, 2016, **87**, 18-24.
285. T. L. Greaves and C. J. Drummond, *Chemical Reviews*, 2008, **108**, 206-237.
286. S. Wellens, T. Vander Hoogerstraete, C. Möller, B. Thijs, J. Luyten and K. Binnemans, *Hydrometallurgy*, 2014, **144-145**, 27-33.
287. L. Fischer, T. Falta, G. Koellensperger, A. Stojanovic, D. Kogelnig, M. Galanski, R. Krachler, B. K. Keppler and S. Hann, *Water Research*, 2011, **45**, 4601-4614.
288. Y. Kayanuma, T. H. Okabe, Y. Mitsuda and M. Maeda, *Journal of Alloys and Compounds*, 2004, **365**, 211-220.
289. H. B. Trinh, J.-c. Lee, R. R. Srivastava, S. Kim and S. Ilyas, *ACS Sustainable Chemistry & Engineering*, 2017, **5**, 7302-7309.
290. G. A. Bezuidenhout, J. J. Eksteen, G. Akdogan, S. M. Bradshaw and J. P. R. De Villiers, *Minerals Engineering*, 2013, **53**, 228-240.
291. Y. Dai, P. Lu, Z. Cao, C. T. Campbell and Y. Xia, *Chemical Society Reviews*, 2018, **47**, 4314-4331.
292. M. H. H. Mahmoud, *Journal of the Minerals, Metals and Materials Society*, 2003, **55**, 37-40.
293. J.-Y. Lee, J. Rajesh Kumar, J.-S. Kim, H.-K. Park and H.-S. Yoon, *Journal of Hazardous Materials*, 2009, **168**, 424-429.
294. T. H. Nguyen, C. H. Sonu and M. S. Lee, *Hydrometallurgy*, 2016, **164**, 71-77.
295. C. P. Mehnert, R. A. Cook, N. C. Dispenziere and M. Afeworki, *Journal of the American Chemical Society*, 2002, **124**, 12932-12933.
296. A. Riisager, B. Jørgensen, P. Wasserscheid and R. Fehrmann, *Chemical Communications*, 2006, **42**, 994-996.
297. R. Kukawka, A. Pawlowska-Zygarowicz, J. Dzialkowska, M. Pietrowski, H. Maciejewski, K. Bica and M. Smiglak, *ACS Sustainable Chemistry & Engineering*, 2019, **7**, 4699-4706.
298. Y. Liu, L. Zhu, X. Sun, J. Chen and F. Luo, *Industrial & Engineering Chemistry Research*, 2009, **48**, 7308-7313.
299. X. Sun, Y. Ji, J. Chen and J. Ma, *Journal of Rare Earths*, 2009, **27**, 932-936.
300. S. Van Rosendael, M. Regadío, J. Roosen and K. Binnemans, *Separation and Purification Technology*, 2019, **212**, 843-853.
301. A. Riisager, R. Fehrmann, M. Haumann and P. Wasserscheid, *European Journal of Inorganic Chemistry*, 2006, **2006**, 695-706.
302. Y. Zhou, S. Boudesocque, A. Mohamadou and L. Dupont, *Separation Science and Technology*, 2015, **50**, 38-44.
303. A. C. Barsanti, C. Chiappe, T. Ghilardi and C. S. Pomelli, *RSC Advances*, 2014, **4**, 38848-38854.
304. K. J. Fraser and D. R. MacFarlane, *Australian Journal of Chemistry*, 2009, **62**, 309-321.
305. M. Gruttadauria, L. F. Liotta, A. M. P. Salvo, F. Giacalone, V. La Parola, C. Aprile and R. Noto, *Advanced Synthesis & Catalysis*, 2011, **353**, 2119-2130.



306. L. A. Bivona, F. Giacalone, L. Vaccaro, C. Aprile and M. Gruttadauria, *ChemCatChem*, 2015, **7**, 2526-2533.
307. M. Thommes, K. Kaneko, A. V. Neimark, J. P. Olivier, F. Rodriguez-Reinoso, J. Rouquerol and K. S. W. Sing, *Pure and Applied Chemistry*, 2015, **87**, 1051-1069.
308. S. Harjanto, Y. Cao, A. Shibayama, I. Naitoh, T. Nanami, K. Kasahara, Y. Okumura, K. Liu and T. Fujita, *Materials Transactions*, 2006, **47**, 129-135.
309. M. A. Khattak and R. J. Magee, *Analytica Chimica Acta*, 1969, **45**, 297-304.
310. C. Fontàs, M. Hidalgo and V. Salvadó, *Solvent Extraction and Ion Exchange*, 2009, **27**, 83-96.
311. M. S. Alam, K. Inoue and K. Yoshizuka, *Hydrometallurgy*, 1998, **49**, 213-227.
312. J. Kramer, W. L. Driessen, K. R. Koch and J. Reedijk, *Separation Science and Technology*, 2005, **39**, 63-75.
313. P. Kovacheva and R. Djingova, *Analytica Chimica Acta*, 2002, **464**, 7-13.
314. Q. Sun, S. Ma, Z. Dai, X. Meng and F.-S. Xiao, *Journal of Materials Chemistry A*, 2015, **3**, 23871-23875.

## 10.4 Curriculum Vitae

### Olga Lanaridi

**Address:** Hetzgasse 11/1, 1030, Vienna, Austria  
**Contact:** +43 664 393 1607, olga.lanaridi@tuwien.ac.at

#### Education

<b>Aug 2017-Dec 2021</b>	<b>PhD in Technical Chemistry</b> Technische Universität Wien, Vienna, Austria Department of Applied Synthetic Chemistry Thesis title: <i>“Extraction and Separation of Platinum Group Metals from Spent Car Catalysts with the Aid of Ionic Liquids and Deep Eutectic Solvents”</i> supervisor: Prof. Katharina Schröder
<b>Oct 2010-Oct 2012</b>	<b>MSc in Chemical Analysis-Quality Control</b> National Kapodistrian University, Athens, Greece Department of Analytical Chemistry Thesis title: <i>“Study of One- and Two- Dimensional High-Performance Liquid Chromatography for the Separation of Polyphenols”</i> , conducted at TU Wien supervisors: Prof. Erwin Rosenberg (Vienna), Prof. Thomaidis Nikolaos (Athens)
<b>Oct 2000-Oct 2009</b>	<b>BSc in Chemistry</b> National Kapodistrian University, Athens, Greece

#### Professional Experience

<b>Apr 2017-Jul 2017</b>	<b>Lab Analyst in Quality Control</b> British Petroleum (BP), Wiener Neudorf, Austria
<b>Nov 2015-Jan 2017</b>	<b>Technical Assistant in Quality Control</b> Valneva, Vienna, Austria
<b>Apr 2013-Oct 2015</b>	<b>Lab and On-site Chemist</b> Seibold Wasser GmbH, Klosterneuburg, Austria

#### Technical Skills

<b>Analytical</b>	ICP-OES, ICP-MS, LA-ICP-MS, 1D- & 2D-HPLC-UV, HPLC-ESI-MS, GC-MS, FT-IR, UV-Vis, Karl Fischer titration
<b>Bio-assays</b>	ELISA, PRNT, SDS-PAGE, cell culture

#### Languages

<b>Greek</b>	Mother tongue
<b>English</b>	C2 - Certificate of Proficiency in English, University of Cambridge
<b>Spanish</b>	B2 - Diploma Básico de Español como Lengua Extranjera, Instituto Cervantes
<b>German</b>	B2 - no Certificate

